N 72 - 25 8 4 5

Report No. 16568-6014-R000   March 1972

STUDY OF ADVANCED TECHNIQUES
FOR DETERMINING
THE LONG TERM PERFORMANCE OF COMPONENTS

INTERIM REPORT

CASE FILE
COPY

Prepared for

THE JET PROPULSION LABORATORY
PASADENA, CALIFORNIA 91103

Under

NATIONAL AERONAUTICS AND SPACE ADMINISTRATION
CONTRACT NAS 7-782

TRW
SYSTEMS GROUP

ONE SPACE PARK • REDONDO BEACH • CALIFORNIA

STUDY OF ADVANCED TECHNIQUES
FOR DETERMINING
THE LONG TERM PERFORMANCE OF COMPONENTS

INTERIM REPORT

TRW

SYSTEMS GROUP

ONE SPACE PARK • REDONDO BEACH • CALIFORNIA

FOREWORD

CONTENTS

CONTENTS (CONTINUED)

CONTENTS (CONTINUED)

1.0 INTRODUCTION

1.1 GENERAL

Future spacecraft missions will require that propulsion components perform for long mission durations in the space and planetary environments. The components must be able to function satisfactorily after continuous long-term exposure to reactive propellants and the environments of space. It is imperative that spacecraft designers be provided with data which can be used to predict component performance reliably for long mission durations. Mission durations for future space flight are projected up to 2, 5, 10 and 15 years. In many cases, performance criteria cannot be established by real time testing. For example, it becomes obvious that full duration compatibility testing would be insufficient even if begun now, to meet the ten-year spaceflights to the outer planets planned to be launched in 1977 (Grand Tour). At the same time, rapid technology advances in materials and processes might provide more reliable components than presently known. It is important, then, that techniques for qualifying components be developed having the capability of determining performance and reliability of components for spaceflight liquid propulsion system applications for long-term missions.

Two major approaches can be taken to advance the art of testing techniques for qualifying propulsion components: 1) improvement in the existing technology and 2) the evolution of new technology. This program is directed to both approaches. Of the various spacecraft propulsion system components, primary emphasis is placed on testing techniques and methods which can be applied to valve components. Techniques developed must be based on limited or short term testing which can generate information that could be used in the design of components for long-term duration. At present, determining the operational life of liquid propellant feed systems and components is extremely complicated because of the lack of meaningful long-term testing. There is no detailed documented information relating to the performance of liquid propulsion system components for long-term storage. There is, however, limited data on specific components over short periods of time. Through qualification testing and storage (Minuteman) in silos, some closely attended monitoring of missile systems for periods as long as seven years was obtained.

The most needed advances lie in the area of surfaces and surface interfaces and materials compatibility, especially for cases involving the use of the reactive propellants being considered for long-term missions. The long-duration performance of materials and surfaces in propellants and space environments has not been substantiated by test. Also, classical failure analyses are not sufficient for the long-duration prediction of specific component items since classical analyses are based upon test data accumulated from a large sampling to evaluate behavior in terms of probabilities. Qualification testing is normally restricted to similar hardware using referee fluids, and, in many cases, tests are run without consideration to environments. In general, adequate design data does not exist which can be used to support decisions made in the component design stage, such as those impacting valve leakage.

The techniques and methods necessary to establish performance criteria include: 1) identifying fundamental mechanisms causing component failure; 2) identifying interactive and/or synergistic effects; 3) component evaluation; 4) failure analysis; and 5) laboratory testing as performed by the research community.

The effects of propellant aging on surfaces should be evaluated through experimental studies in which: 1) decomposition products are identified; 2) soluble impurities formed on aging are characterized; and 3) the effect of contaminants on the stability of the propellant is determined.

On the basis of short term laboratory test data it is possible, but not necessarily always reliable, to predict the extent of metal loss under long-term exposure. The reliability of the prediction depends largely on how closely laboratory experimental conditions simulate operating environments and how precisely the corrosion rate law constants are determined from experimental data.

The corrosion rate results, expressed in $mg/cm^2/day$, at best only enable one to compute the rate at which a component corroded away materially. It does not provide the answer to the one important question: At what time will the component still mechanically function?

The choice of materials for the long-term mission requirements cannot be made without detailed study of the mechanisms involved in component degradation. Of particular interest is the identification of chemical or mechanical reactivity on the surface of materials by microanalytical techniques, such as electron microprobe analysis, scanning electron microscopy and analysis of the propellant and compatibility specimen. The influence of physicochemical processes of absorption and protective film formation on the mechanical destruction and wear of metals must also be established.

In many of the system components, nonmetals are employed which cause different types of failures than those experienced with metals. The particular mode of failure with nonmetallic materials is usually determined by change in their physical properties and by change in their physical dimensions. To permit improved interpretation of the failure mode, it is desirable to correlate the degradation of the nonmetallic materials with changes in the chemical structure. Studies of this type would permit the designer to establish limits or material requirements necessary for successful operation of the component.

Dynamic test evaluation is another area that is necessary for improved understanding of failure mechanisms. A system under dynamic load usually will react to a much greater extent than one under static load or at rest. The more complex the dynamic test setup is, the greater the possibility of extraneous reaction. However, if planned well, effective tests can be devised which simulate the functional use operation.

In evaluating the results of storage experiments, not only should the examination of stored samples be considered, but the propellants and

nonvolatile materials in the propellants should be analyzed by sensitive techniques such as infrared and atomic absorption, x-ray and mass spectrometry, gas chromatography, x-ray diffraction and radioactive tracers. The latter technique is currently being investigated by the Boeing Company under NASA Contract NAS7-789.

One approach would be to determine whether accelerated aging through the use of elevated temperature is valid. The principal problem with this technique is that as one increases the temperature, new reactions can be initiated that do not occur at the lower operational use temperature. For this reason, it is essential that the mode of failure reaction is determined at elevated temperature and confirmed to be the identical mechanism which occurs at lower temperature. The difficulty with determining the mode of failure at low temperature is that the reactions often never proceed to a degree necessary for failure in the test duration. The rates of degradation mechanisms should be determined, however, by the evolution of new technology which can determine whether the failure is due to the same mechanism at both temperature levels.

1.2 PURPOSE AND SCOPE

The purpose of this program is to advance the art of techniques for determining the performance and reliability of components for spacecraft liquid propulsion system applications for missions of long durations. The investigation should provide a better understanding of the problems associated with performance verification measurement techniques and correlation necessary for qualifying liquid propulsion components. The criteria established and methods evolved are to be applicable to valve components. Primary emphasis was placed on the propellants oxygen difluoride and diborane combination. Consideration was also given to the use of propellants MMH, N_2H_4 and/or N_2H_4 mixes, N_2O_4 and LF_2. The scope of the work included analysis, fabrication, and test of experimental equipment to provide data and performance criteria applicable to meet the program objectives.

1.3 SUMMARY OF SPECIFIC TASKS

- Perform a survey of the existing technology of methods, measurement and testing techniques for qualifying liquid propulsion components for spacecraft applications which as currently practiced would contribute and provide meaningful results toward determining component performance and reliability for long-mission durations in the space and planetary environments.

- Based on the results of Task I, determine if any existing techniques can be made to meet the requirements. Identify, analyze and present necessary changes or specific areas of refinement. Engineering documentation of concepts shall be made and technical feasibility demonstrated.

- New concepts consistent with the objectives should be evolved. Experimental demonstrations of new concepts should be accomplished using laboratory models. This effort will include:

  A. Investigation of feasibility and advantages of developing new technology to achieve significant improvements over existing techniques.

  B. Investigation of feasibility and advantages of developing new technology which potentially could yield significant improvements over existing techniques.

- Generate and conduct a test program that will provide a complete technical demonstration of one or more of the techniques falling within Task II and III to obtain results that are directly related to the following:

  A. Reliable evidence that the information generated is directly correlatable with extended periods of time such as two, five, ten and fifteen years.

  B. Reliable evidence that basic and subtle requirements have been clearly met and satisfactory service in spacecraft application can be assured.

1-5

●   Provide documentation of the investigations and analysis. Include
    recommendations for future investigations of those concepts or
    problem areas which the contractor feels worthy of more extensive
    investigation.

A detailed summary of specific tasks in outline form is presented
in Table 1-1.

TABLE 1-1

STUDY OF THE ADVANCED TECHNIQUES FOR
DETERMINING THE LONG TERM PERFORMANCE OF COMPONENTS

SUMMARY OF SPECIFIC TASKS

PERIOD May 14, 1970 to August 14, 1971

I. SURVEY AND REVIEW OF TECHNOLOGIES

A. Agency Review

B. Minuteman Aging Program

 1. Identify Age Sensitive Component Parts

 2. Identify Failure Modes

 3. Predict Preventative Repair

C. Accelerated Testing Techniques

 1. Overstress Cumulative Damage

 2. Step Stress Time Compressed Testing

D. Aging

 1. Relativistic Mechanics

 2. Thermodynamics

 3. Aging Analysis Chart

Mechanical	Physical
Wear	Polymorphism
Fatigue	Radiation
Creep	
Friction	

Chemical
Corrosion
Oxidation
Reduction

E. Test Methods and Signature Analysis

 1. Bulk Signatures

  a. Leak Rate

  b. Wear Particle Measurements

  c. Acousto-Optical Imaging

  d. Acoustic Propagation

  e. Electromagnetic Interaction

  f. Thermal Imaging

  g. Interferometric Holograms

  h. Neutron Radiography

 2. Microsignatures

  a. Holographic Surface Topology

  b. Scanning Electron Microscopy

  c. Electron Microprobe Analysis

  d. Plasma Emission Analysis

II. MECHANISM EFFECTS AND ANALYSIS STUDY

A. Leakage

 1. True Contact Area

 2. Wear

 3. Wear Particle Generation

 4. Fatigue

 5. Corrosion

B. Analysis

 1. Scaling Analysis

 2. Derivation of Leakage Area

 3. Dimensional Analysis

III. DIFFUSION COUPLE

Electrolized Inconel/BeCu-Seat/Poppet Diffusion Tests:

 500°C

 Vacuum - 10^{-9} Torr

 300 Hours

IV. ACOUSTIC SIGNATURES STUDY

Low and High Frequency Testing:

Steel/BeCu Seat/Poppet Couple

 1 KHz to 50 KHz

 4 MHz to 12 MHz

 Continuous and Pulsed Transmission

V. LEAKAGE - CYCLE TEST

A. Electrolized Inconel Seat

 1. Unpolished

 2. Polished

B. BeCu Poppet

C. Surface Topology Characterization

D. Cycles Vs. Topology Changes

E. Correlation

VI. CONCEPTUAL STUDIES

A. Valve Seat Surface Compatibility

 1. Surface Energy Studies

  a. Aging

  b. Propellant Compatibility

B. Leakage Measurement - Technology Refinement

 1. Mass Spectrometer Calibration

C. Propellant Gauging in Zero Gravity

 1. Tracer Gas Technique

 2. Nuclear Tracer Technique

2.0 STUDY AND REVIEW OF TECHNOLOGIES

This task was designed to include the general study of components and their performance for long term mission durations in space and planetary environments. Although this study was general, the major effort of this program was directed toward the critical performance function of valve seat leakage.

A portion of the study included a survey of the industrial agencies and NASA centers to determine current practice in testing components for performance and life. Emphasis was placed on methods used to accelerate testing.

Agencies contacted during the study were:

- NASA Ames Research Center
- NASA Goddard Space Flight Center
- NASA Langley Research Center
- NASA Lewis Research Center
- NASA Manned Spacecraft Center
- NASA Marshall Space Flight Center
- General Electric (Research and Development Center)
- Philco-Ford (Aeronutronic Division)
- TRW Systems Group

2.1 AGING TEST PROGRAM

The most comprehensive aging effects program within the industrial agencies interviewed is the Minuteman aging program. This program involves predicting, on a statistical basis, the probable aging-out of component parts of operational Minuteman missiles. Every age-sensitive part is evaluated using available data on the aging properties of the materials of construction under the expected environment. Each aging failure mode is related to time-sensitive parameters so that the margin for reliable operation is expressed as a function of time. Mean and 3σ values are calculated to occurrence of zero margin (failure).

Aging-out commences when the lower 3σ limit reaches the critical parameter value. Storage tests of actual hardware supply data which are intended to supplement and corroborate the statistical analysis. No accelerated testing is used. So far, there are no positive results since the predicted aging-out points have not been reached.

In addition, industry engineers in current engine and spacecraft programs were interviewed. These active flight projects include LMDE, Intelsat III, Pioneer, and classified military satellites. Most of the components involved were solenoid-operated on-off valves. The accelerated test techniques currently in use are limited to overstressing. Increased temperature or loads are imposed and the assumption made that there is some continuous relation between temperature or load and rate of degradation which allows extrapolation and interpolation. In most cases, life expectancy is demonstrated by simply mechanically cycling the parts. These cycle tests are run at an arbitrarily chosen temperature. In some cases, particularly where previously qualified designs are used, the majority of cycles are accomplished during subassembly testing. Qualification-level vibration, shock, etc., are imposed at the subassembly level (e.g., propellant valves are tested on thruster assemblies or clusters).

Essentially the same information was obtained from NASA personnel. Long-life tests apparently are the exception and no one interviewed expressed faith in presently available accelerated testing methods. Repetitive cycling and imposition of environments representative of flight are the general rule. Few of the people interviewed were involved with long-life missions; therefore, most testing was accomplished over periods amounting to the actual mission durations or longer. Several mentioned that JPL was the center of such work.

2.2 ACCELERATED LIFE TESTING

Contact was made with R. W. Bricker at MSC, who also has completed a survey of accelerated testing techniques; he included commercial as well as government-sponsored work in his survey. Mr. Bricker suggested these sources for information on effects of aging, test methods, and investigations into physical causes of degradation:

- USAF Desert Storage Facility (Tucson, Arizona) - for effects of long storage periods on aircraft fluid systems.

- USAF Rome Development Center (Griffin Air Force Base, New York) - for aging and environmental effects on smaller mechanisms (and electronics equipment).

- Ford Motor Company (Grosse Point, Michigan)- for cycle life testing.

- Charles Lipson (Professor of Mechanical Engineering, University of Michigan, Ann Arbor, Michigan) - consultant to Ford Motor Company on development of theory of degradation and test methods.

In addition, Mr. Bricker suggested that extensive work on accelerated testing of aerospace equipment was performed by Hughes Aircraft Company (Fullerton, California).

Accelerated test techniques have been used by several investigators in both the aerospace and commercial industry. Accelerated life testing as currently practiced usually consists of either overstressing or repetitive (cyclic) operation of the component at a rate higher than required during its normal operational life. Repetitious or cycling operations have been classified as time-compressed testing. The most often used accelerated testing techniques used are briefly described in the following:

- Over Stress

    This technique has been applied by investigators in accelerated testing of both mechanical and electronic components. The component or materials are overstressed mechanically, or through the application of contact loads, temperature, thermal shock, acceleration, voltage, power, etc., usually to beyond the endurance limit of the material. The stresses are applied to the level of component failure. If temperature is the accelerating stress, the Arrhenius relationship is normally used to accelerate processes in real time. The Weibull distribution analysis is also used to estimate the failure parameters.

2-3

● <u>Step Stress</u>

Mechanical, thermal and electrical stresses are applied in
step increases. The components are stressed to failure and
the distribution of failure as a function of stress is plotted.
A statistical method of analysis is used to predict the number
and rate of failures which may occur at the design stress level.

● <u>Cumulative Damage</u>

Each sample in a representative batch of components is stressed
to different levels. This method is based on the assumption that
the life of the component can be predicted by the cumulation of
the damage induced by each stress cycle. This method has been
investigated for fatigue-type failure prediction.

● <u>Time-Compressed Testing</u>

This method is based on the assumption that the component per-
formance is independent of time-related mechanisms. Cycles to
failure or increased cycle rate is assumed to represent the
actual performance of the components. This test is widely
used in test programs, however, time-dependent phenomena are
usually present (e.g., corrosion, reactivity with
environments).

A serious restriction in the application of the above test methods is the
limited correlation of test results to the real-time results. This is
probably due to the limited knowledge of the mechanisms responsible for
the failure.

2.3 TEST PHILOSOPHIES AND CONSTRAINTS

The major differences in opinions concerning test philosophy center about
the degree to which time-dependent degradation can be measured separately
from cycle-dependent effects. At one extreme is the belief that aging
cannot be reliably evaluated so testing should be concentrated on cycle
effects. Usually the severity of cycle testing is increased to compensate

for lack of aging influences on degradation; sometimes cycle tests are carried to failure but usually the number of cycles is fixed at two to four times the estimated maximum in real-life. Where aging effects cannot be duplicated, there is a tendency to estimate them and to design-out as many age-sensitive parts as possible. Such preventive design is, of course, easiest where actual environments are well characterized and/or mild. High vacuum and radiation effects, typical of space missions, appear to present more uncertainty than the more fully characterized earth environment presents to aircraft and missiles. Radiation environments, especially, are not well defined or well simulated during test.

The opposite extreme is where empirical aging information is of great concern as are mutual interactions between cycle and age-dependent mechanisms. An example of the latter would be wear rates which are increased by corrosion. Present accelerated testing methods are regarded as untrustworthy by most engineers interviewed, but many feel it is the only technique available. Increasing the rates of chemical reactions (corrosion, polymerization, decomposition, etc.) is the most commonly used accelerated test. In most cases, this is done by simply increasing the ambient temperature. Questions of the validity have been frequently raised.

In some cases, cycle tests are carried on over the real time period so accelerated testing would be advantageous but not necessary; short lived (3 to 6 months) satellite systems are tested in this manner.

Where accelerated testing is not feasible or considered insufficient, sometimes there are attempts to either predict aging effects or to monitor it in real-time during the life of the actual item so as to provide data to be used in judging the merits of alternative operations. Two examples were cited. One engineer (not at JPL) supported the JPL procedure for maintaining a duplicate spacecraft "operational" on the ground while the flight progressed so the grounded spacecraft's condition could be monitored for changes in performance which might make alterations in the flight sequence advisable.

The second example, a large-scale program, based on the premise that most aging effects are predictable, is the Minuteman Age-Sensitive Components and Failure Criteria Program. This is a TRW-directed program being carried out by the subsystem contractors, North American Rockwell (Autonetics Division) and Bell Aerosystems. It's purpose is to identify all age-sensitive component parts and the resulting failure modes, and to predict when preventive repair would be necessary to keep the fielded missiles operational at a high level of reliability.

There appears to be several different testing philosophies current at the moment:

- Test-as-you-go
- Qualify by similarity
- Requalification of "off-the-shelf" designs

Most noticeably absent from all the approaches described were the once popular ideas of limit testing, combined environment testing, and other carefully planned, comprehensive, and costly testing sequences (e.g., References 1, 2 and 3). Economics dominate essentially all cases discussed with engineers on current programs so even though a half dozen or more combined environment facilities exist, they are seldom used for this purpose.

"Test-as-you-go" programs develop as testing proceeds. Simple, fundamental tests are initiated and further testing scheduled only if cognizant personnel see evidence in early performance of possible trouble developing. In some cases, there is no qualification test, per se, at any stage prior to flight.

"Qualify by similarity" is economic because duplication is avoided. Only those parts of the assembly which have been changed since previous qualification for the same or very similar mission, are considered in planning the tests. In other words, if cycle life would not be adversely effected by the design changes, then cycle life testing would not be repeated. The hazard here is the possibility that combined effects might cause unsuspected problems.

"Re-qualification of off-the-shelf designs" is similar to the previous case but applies when no changes have been made. Re-testing is limited to revealing what effects result from any differences in application (i.e., mission environment, duration, etc.).

"Qualify at the assembly level" tests several devices simultaneously and is justified in terms of the combined interactions which occur essentially as in the spacecraft, rather than being bracketed or exceeded by the test conditions imposed by test fixtures. Assembly level testing often coincidentally results in less knowledge of the precise conditions which cause failure, however, because of the interactions.

There is a technical and budgetary incentive to reduce the criticality of testing by improving the inherent reliability and durability of component designs. Several engineers interviewed felt that emphasis on proving design validity was detrimental since it tended to induce a relaxed attitude toward design improvement and satisfaction with present designs because test results are depended upon to prove that present designs are adequate. Improved design, in their view, is the best approach to reducing the costs of testing and rectification of failures. In other words, testing is after-the-fact; failures are caused by poor design, and merely confirmed by test.

2.4 REVIEW OF CURRENT COMPONENT TEST METHODS

Chief concern of those engaged in testing is the significance of the tests, rather than the problems of mechanizing the procedures. This probably reflects the growing availability of sophisticated facilities such as space simulators where combined thermal-vacuum testing can be readily carried out. Nevertheless it is still rare to find the imposition of pressures as low as experienced in space.

In the design of experiments, there are several factors which determine the quality of the test. Sample size, accuracy of simulation, and measurement methods are the most important. In practically all cases, the sample sizes are too small to be statistically meaningful. One or two samples are typical. Where assemblies are tested (as in a cluster of small thrusters) there may be two to six sample shutoff valves being tested simultaneously; this exposes all samples to the same test conditions. Only pyrotechnic (one-shot) devices are believed tested in numbers approaching the statistically-meaningful sample. Production runs offer the chance for data to be collected from large numbers of samples during acceptance

tests but these are conducted under milder conditions since one objective here is to avoid test-induced failure. At TRW, for example, relatively large numbers (dozens to hundreds) of solenoid valves, filters, regulators, fill valves, and tubing assemblies have passed through acceptance test. Results have not been too meaningful for the present purpose since neither cycle life degradation nor aging tests were included.

Accuracy of simulation involves proper choice of conditions to be imposed, the levels attained during test, and the test durations. The most complete tests involve determining performance (leakage, response, filtration level, etc.) variations as various environments are imposed and operational cycles are completed. For space applications* the environments and what they simulate are:

- Acceleration (launch, propulsion maneuver, or low-g in space)
- Vibration (launch or propulsion maneuver)
- Shock (transportation, stage-separation, propellant sloshing, water hammer, etc.)
- Temperature cycle (uniform if internal, local if sun or exhaust jet or heat soak source)
- Humidity and salt atmosphere (launch pad)
- Fluid contamination (total mission)
- Vacuum (space)
- Radiation (space)

Test simulation accuracies are estimated in the following paragraphs.

2.4.1 Acceleration

Axial acceleration is difficult to simulate in the laboratory at low 'g's for periods greater than 10 seconds; and even these periods are available only in drop towers. The g'-level can be controlled within a few hundredths of a "g" or so. Aircraft tests which provide tens of seconds of "free-fall" have been carried out for few components because of the expense and instrumentation difficulties. Test periods of up to one or

---

*MIL Specification requirements for salt spray, sand and dust, and fungus are seldom used for space equipment.

two earth orbits are available onboard upper stages of boosters. Only tests onboard satellites offer periods long enough to measure performance degradation with time under low-g.

High-g tests (up to 30 g's or more) have been relatively numerous. Centrifuges are in operation for this purpose, and the military also uses high speed sleds on test tracks. Centrifuge tests last longer than launch acceleration periods but the tracks allow only a limited test period (from less than 1 second to less than 20 seconds). The accuracy to which centrifuges can control acceleration varies from about ± 10 percent for the ordinary rocket test centrifuge to ± a few thousandths of one percent in inertial guidance test centrifuges. Sled accelerations are controlled to about ± five percent.

2.4.2 Vibration

Vibration tests are almost inevitably carried out on large electromotive transducers ("shakers"). Size of test articles is limited so assemblies cannot always be tested at extreme levels but individual components can be handled with ease. Test periods can be much longer than the in-flight vibration period. Complex wave-forms are possible as well as frequency sweeps, dwells at resonance, random combinations, etc. Problems arise only in the combined effects of test item and test fixture; local amplitudes can vary from a true simulation by several "g's" due to amplification factors unless special care is taken. Combining vibration with other environments has been attempted but the equipment is expensive. Shakers within pressure or thermal conditioners and on centrifuges have been used. During a development program sponsored by the USAF and directed by TRW Systems, a missile vent-relief valve failed under such a combined environment despite the fact that it had passed tests in the separate environments imposed individually at the same levels.

Vibration amplitudes are controlled to better than ± 5 percent at frequencies controlled to better than ± 2 percent.

2.4.3 Shock

Shock tests are carried out on a shaker, by a controlled drop onto a surface of a specific compliance or by impacting the test item with a moving mass.

System induced shocks usually occur during the early part of a spacecraft's life and therefore these shocks do not interact with aging effects unless the shock causes damage. Exceptions are shocks caused by meteorite impacts, separations of bus and payload, pyrotechnic valve actuations, engine firings, and landings. Here there is ample opportunity for shocks to cause secondary damage if they dislodge corrosion or deform parts that have been weakened by an aging mechanism. Test shock levels should be repeatable within ± 10%.

2.4.4 Temperature Cycle

Temperature simulation has received much attention, particularly simulation inside of space simulators of radiant energy from the sun using high-powered lamps and lenses or mirrors; accuracy is reasonable (accurate to 7%, at best,when spectral distribution is not important). Heating by exhaust jet plume has been simulated with hot gas jets. Heat loads conducted to parts are often duplicated by electrical resistance heater elements; these permit very accurate adjustment of the heat load and temperature. Components handling hot or cold fluids are tested with the actual fluid (or a referee, for reasons of safety) at temperature. Temperatures from hot gas reactors should be within ± 100°F or closer from test-to-test. Cold gas tests can be fairly accurate if heat exchangers and mixers are available (± 10°F), but otherwise may vary considerably. Cryogenic liquids at their boiling points are very accurate thermal sinks (± 1°F). But most common is the use of thermally conditioned chambers used to heat or chill the test item uniformly and either cycle the temperature with time or hold temperature steady; good equipment can keep an average test component temperature at ± 2°F within the range of -300°F to +300°F.

2.4.5 Humidity and Salt Atmosphere

Humidity chambers are used to expose parts to moist atmospheres. Control is probably not better than ± 5%.

2.4.6 Fluid Contamination

Contamination testing is a developing art. Size and shape distribution of particulate matter and the uniformity of its distribution throughout the carrier fluid are significant variables. Spherical particles are generally

used because they are easily obtainable and gradable. Maximum and average diameter can be controlled within about 5 microns. Propellants can be chemically contaminated with great accuracy but so far the resultant products are difficult to identify when the fluid is a reactive (propellant) compound which contains nitrogen or hydrogen. The colloids or gels are just recently being characterized.

2.4.7 Vacuum

Ambient pressure level for testing is usually one atmosphere (to simulate the earth's surface conditions) or the best available vacuum (to simulate space). The former is no problem. Small chambers can be reduced to near space pressures (10^{-12} or $^{-13}$ torr) but larger space simulators and ordinary vacuum chambers operate at much higher pressures (10^{-5} to 10^{-7} torr). For a given test, the engineer cannot expect to know in advance how well the chamber will hold vacuum to closer than one-half an order of magnitude. The level actually achieved can be measured, however, much more accurately than necessary for his purposes. To levels of 10^{-9} torr, the standard accuracy is ± 20 percent.

2.4.8 Radiation

Radiation effects in spacecraft components will vary greatly depending upon the kind and energy level of the particles, the dose received, and the materials' susceptibility to degradation; to a lesser degree the effects will depend upon the temperature, stress state of the materials, etc., while being irradiated. Three important sources produce the radiation to which a spacecraft is subjected during flight:

1) On-board nuclear devices such as RTG's which radiate fast neutrons and gamma rays

2) Fields of electrons and protons trapped in the magnetic fields of the planets (Van Allen belts)

3) The sun which produces "winds" of low energy protons and "flares" which release high energy protons.

Two types of damage mechanisms must be considered: bulk (which is due to atomic displacement), and ionization (which is due to electron loss

or gain). The potential for causing bulk damage can be expressed in terms of Equivalent 1-MeV Electrons/cm^2 (DENI's)[*]. Potential for causing ionization can be expressed in ergs of ionization energy (100 ergs/gram equals one rad); it must be cautioned however that the amount of energy absorbed depends upon the energy level of the incident particles.

Since different materials vary considerably in their tolerance to radiation, the usual procedure is to estimate the potential dose to be absorbed during the functional life of the components and then to examine in more detail only those parts which may approach the threshold of degradation (i.e., an arbitrary data specifying cumulative damage sufficient to impair integrity or function within allowable tolerances). This estimation is a complex process which must account for the number, direction and energy content of particles, their ability to penetrate, and the shielding present. The last two named factors may be used to define a "damage profile." A "hard" design is one which is very resistant to radiation damage (Reference 4).

Results of the estimate may indicate no problem exists, or that further analysis, redesign and/or testing will be required. Usually metals are sufficiently immune to obviate further analysis. Polymers tend to be degraded. Semiconductors are prone to damage. Hence, the major potentials for damage in rocket components are to polymeric seals, potting compounds, insulations, and diodes or other semiconductor devices. The reader is directed to Reference 5 for a short summary of test results. Increased shielding often is the quick/easy way to solve problems of marginal dose. New materials present a problem due to lack of effects information. Synergistic effects caused by combined radiation components and environments may be impossible to predict. Lack of basic data and synergistic effects are two strong reasons for conducting tests in cases where high reliability must be demonstrated in the presence of high doses.

Basically there are two methods of radiation testing in current use: (1) using the test item as the target in a particle accelerator, and (2) exposing the test item to radiation from nuclear fission. Method (1) is essentially

---

[*]Damage-Equivalent Normally-Incident, 1-MeV Electrons/cm^2

2-12

limited to materials testing. Method (2) can be used to test materials or mechanisms; both nuclear reactors and portable sources (powered by disintegrating radioactive materials) are used. Both methods are limited in the maximum particle energy available -- some "cosmic rays", for example, cannot be simulated. Safety precautions impose considerable handicaps during testing, and to a large extent dictate the test procedures.

Experiments to measure the changes in materials caused by irradiation contain errors arising from the effect of radiation on measuring devices, changes and gradients in the radiation fields, changes in specimen configuration, and inaccuracies in dose measurement. Environmental conditions in the test chamber may induce significant effects. Examples are temperature and the gas atmosphere. Contaminants may be present even in a vacuum chamber as in the case where the breakdown of organic insulation on solenoid coils may release gaseous products into the chamber (Reference 6).

Complete characterization of the pre- and post-radiation properties of the material under test is necessary to detect all effects since some changes caused by irradiation are not ordinarily measured. Examples are the variations of mechanical properties with strain rate or temperature.

The fundamental measurements in radiation testing are the dose and fluence. Measurement accuracy varies with the type of radiation being measured and whether or not several components (e.g., protons and neutrons) are present. Typical measurement accuracies are $\pm$ 10 percent for dose, $\pm$ 3 percent for electron and proton fluence, and $\pm$ 10 percent for neutron fluence.

2.5 REVIEW OF MEASUREMENT METHODS

Measurements of component performance must resolve significant difference or changes if test results are to be extrapolated to longer periods. Measurements cannot be made with uniform accuracy so it is important to recognize the individual properties of the measurements in planning tests and interpreting data. Fluid component performance is normally characterized by measurements of:

- Leakage
- Actuation response
- Pressure set point
- Flow rate vs pressure loss
- Force output
- Power consumption
- Filtration level

2.5.1 Leakage

Conservation of the fluid, avoidance of reactions, and over pressurization of isolated components with displaced fluid make leakage of prime importance. Several comprehensive surveys of leakage measurement techniques have been published which may be consulted for details.

It is sufficient to indicate here that the most sensitive methods have a measurement threshold of between 10^{-9} and 10^{-8} scc/sec of helium. Component specifications usually allow seat (internal) leakages in the range of 10^{-4} to 10^{-6} scc/sec of helium. External leakage specification is most commonly "zero", which has been defined (Reference 7) in the range of 10^{-6} to 10^{-8} scc/sec or less. Liquid leakage rates are seldom measured. This raises the perennial problem of correlating gas and liquid leak rates; no generalized solution has been found that has been supported by test. Reference 7 presents a method and a criterion for "zero" liquid leakage.

2.5.2 Actuation Response

Actuation response is often a prime parameter when evaluating valves. The definition of response usually determines how it is to be measured. Flow response requires the transient flow rate to be measured accurately; this is very difficult except with hot wire or small ΔP devices (orifice plates, etc.). Electrical response permits the valving mechanism motion to be implied from the variation in current flow. Mechanical response requires some signal to be generated in response to motion of the valving mechanism itself; potentiometers are usually used as continuous indicators of position but sometimes proximity devices or directly-actuated switches are used to indicate the start and end of motion. In general, it seems difficult to resolve valve response to closer than 2 milliseconds in small valves; since

this is approximately the apparent repeatibility of such valves, the measurement techniques are only marginally adequate for characterizing valve response.

2.5.3 Pressure Set Point

Pressure set point is a parameter used in evaluating regulators, relief devices and check valves. As in response, it is necessary to measure flow rate in order to fully characterize this property of the component. The problem is that most devices (perhaps the only exception is the burst disc) exhibit a gradual opening rather than snap-action. Also, the pressure at which opening starts and at which closure is complete must both be determined to fully characterize performance. Resolution of set-point is, therefore, not very precise except for burst discs and regulators at rated flow. Usually time-average pressure is measured with electrical transducers to within $\pm$ 1/10 to 1/2%, which is adequate for almost all aerospace applications.

Initiation and termination flows cannot be measured with precision. Relief and check valves for most applications, however, do not need to be precisely calibrated except for steady-state flow vs. pressure drop. Such data might prove valuable in assessing wear or other changes in the components if it were available.

2.5.4 Flow Rate Vs. Pressure Loss

Flow rate vs. pressure loss measurement is used to calibrate components which individually or collectively control flow rates. Pressure differentials can be measured with transducers to within 1/4 to 3/4%. Steady-state flow rates can be measured within 1/4% with carefully calibrated and used turbine meters but most flow measurements made in the rocket industry are accurate to between 3/4 and 1-1/4%. Special laboratories are equipped to calibrate components with water to 0.1%. A new, commercial meter is claimed to provide $\pm$ 0.05 percent accuracy. Changes in propellant flow rate with age or cycle life is not likely except in response to erosion of orifices, corrosion, formation of gels, or swelling of polymer seals.

2.5.5 Force Output

Reliable force output from actuators is very important so its measurement vs life is of interest. Load cells or strain gauges on calibrated load-transmitting parts of the actuator are used to measure force. Their accuracy is excellent (better than 1%).

2.5.6 Power Consumption

Power input is easily measured if it is electrical but difficult if it is fluid power. Electrical measurements should be to better than 1%. Fluid power probably can be measured best by simultaneously recording stroke and pressure within the actuator and the temperature of the fluid; the combined error of these measurements is probably on the order of 2 to 10% depending upon whether the fluid is liquid or gaseous, and upon the rate of temperature change. Comparing power input to power output may reveal changes in friction, fluid leakage, or electrical breakdown.

2.5.7 Filtration Level

Filter performance measurement methods are currently undergoing development. Usually the filter is characterized as to pore size by a test such as the bubble point in alcohol. This may be related to theoretical minimum size particle removal capability. More realistically, the filter is used to remove particles from a certain quantity of fluid and the distribution of particle sizes in the filter cake is measured. The drawback is sensitivity to the character of the particles; usually spheres are used in testing which do not realistically simulate real contamination. Alternately, arbitrary samples of contaminated fluid from working systems may be filtered and the removed particles measured in terms of three dimensions. This method is not reproducible since the particles in the contaminated fluid are not standardized. Therefore, none of the presently available methods appear to be an accurate measurement of filter performance.

2.5.8 Other Tests

In addition to performance measurements, there are measurements made solely for detecting changes due to aging or cycling of the components. Dimensional, weight and surface profile changes for wear detection, mechanical properties for fatigue or chemical changes, etc., are used. These are almost limitless in variety and method.

2.6 RESULTS OBTAINED AND RECOMMENDATIONS

A number of engineers interviewed expressed opinions concerning the present state of the art and recommended improvements. Generally speaking there are two schools of thought: (1) test the component thoroughly under the simulated mission conditions and determine how it fails, and (2) analyze the design to determine what physical mechanisms are likely to be the causes of failure, then measure their rate, so they may be extrapolated for prediction purposes.

The test-to-failure school depends upon uniformity between the test item and the examples to be flown, and upon the accuracy of the environmental/cycle simulation. A common problem stated by engineers was sample variability, especially among solenoid valves. TRW has experienced a number of failures due to variations between units; i.e., production quality control acceptance test problems at suppliers shops. Hence, it appears that special checks must be made by the testing agency to fully characterize the test items in terms of configuration, materials, etc.

The design of the tests are influenced by the opinions of the designers. Often the tests are not comprehensive enough to assure successful detection of all design shortcomings. For example, it may be thought that leakage is purely a function of cycle history, not aging. In this case, the testing will emphasize correlating leak rate with number of cycles. In one case, the cognizant engineer was convinced that contamination and improper assembly accounted for essentially all failures, so he designed his tests to reveal sensitivity to those factors while ignoring time-related factors.

Testing also tends to be centered on new conditions not previously encountered, such as effects of heat sterilization.

The test-to-failure school have few recommendations for improvements except more careful design, assembly and test.

The physical mechanism school feels that the whole subject is just beginning to be explored. Here too, there are some engineers who feel that effects can be divided a priori into the two cases: those caused by cycle history and those caused by aging. Part of the evidence they cite is the relatively good correlation obtained in cycle tests versus the poor correlation in aging tests, especially the accelerated aging tests.

An argument against the isolation of one cause from another is that wear theories are not well enough developed to exclude aging influences. A common case of direct interaction between cycle life and aging is corrosion effects on wear.

Several engineers mentioned the difficulties inherent in the physical mechanism approach. Corrosion, for example, is a very localized phenomenon. Uniform corrosion seldom occurs or, if it does, it poses little hazard to reliability. Local pitting and generation of salt crystals, on the other hand, are direct causes of component failure. Local phenomena, occurring due to micro-size variations appears to be hard to predict.

Fatigue models appear to be used with some success, as are models for purely mechanical wear (adhesive or abrasive wear), when the loads and structures are well defined.

Aging effects are complex. Real time tests, such as are done by the Navy, plastics and rubber formulators, etc., have proven fairly successful provided the environment is reasonably consistent. Accelerated tests have, in general, been unsuccessful. One of the larger efforts to use available data is the Minuteman program referred to in an earlier section. In this case, each part is analyzed for possible malfunction modes. Each mode is related to a specific material property (tensile strength, hardness, etc.). Then for each case a critical value for that property is established which is defined as being the failure point of the part. Next the rate at which each material property deteriorates is estimated based on laboratory and field data. From these rates, a predicted time of failure is calculated. This is done using statistics so there are 3σ limits, at the lower of which field repairs are made to prevent actual failures. Correlation with field experience is interpolated into the program to improve the prediction accuracy.

2.7 AGING

Aging is used frequently to describe a time dependent change in a material or measured performance. No rigid definition of aging has been found in the literature dealing with life testing. Aging mechanisms are not well understood mainly because of the interactions of several mechanisms acting synergistically. One could postulate that at absolute zero temperature no aging occurs.

The thermodynamist might describe aging as the process of continually increasing entropy since all processes are irreversible. Aging may at least in part be defined as an irreversible process. This definition then relates aging to the second law of thermodynamics which provides a technical description of the process. The second law restricts the direction of a process.

A relationship involving the time related process is given by

$$\Delta t = \frac{\Delta t'}{\sqrt{1 - v^2/c^2}}$$

where: Δt is the elapsed time measured by the stationary observer

$\Delta t'$ is the elapsed time measured by the observer moving at velocity v

C is the speed of light

v is the velocity of the object relative to the stationary observer

This equation is based on the laws of relativity.

All processes slow down as viewed by the stationary observer according to the above equation. When v is small or zero, $\Delta t = \Delta t'$ as would be expected for ordinary situations.

It may be of interest to pursue the disciplines of relativistic mechanics. However, at this time no simple experiment is obvious which can be implemented to accelerate an object close to the velocity of light relative to

the observer. Yet, for long term missions (relative to the observer on earth) all processes are slowed down depending on the velocity and, if our laboratory is in space, the future reliability predictions may indeed be based on relativity.

For example, assume a spacecraft traveling to the star Sirius at 99.98% the velocity of light. Sirius is approximately nine light years distant. According to the relativity equation it would be sufficient to test the components only one day under simulated conditions to verify the nine year mission. All processes on the spacecraft including wear, corrosion and valve leakage would be slowed down. To the earth observer one day aging on earth would represent nine years aging of the spacecraft.

Aging then may be defined as any process resulting in increased entropy in the time frame of the observer relative to the time frame of the process.

This definition does not restrict aging to material changes alone, but includes any process: mechanical, physical or chemical. For example, the mechanical process of wear is by the above definition an aging process.

For most of all aging processes, which concern us here, the relativistic part of the above definition may be dropped and stated simply:

> Aging is defined as any process resulting in increasing entropy.

2.7.1 Aging Analysis Chart

A preliminary aging analysis chart, Table 2-1, was constructed in order to assess the aging parameters against the components with regard to their long term performance. The format is essentially the one utilized in the Advanced Valve Technology Program[8]* since the listed components are representative of almost any type of a liquid propulsion assembly.

---

*Numbers in parentheses refer to the references listed at the end of the section.

Table 2-1. Aging Analysis Chart

Functionality	Component	Mechanical					Physical			Chemical		
		Wear	Fatigue	Creep	Friction		Polymorphism	Radiation		Corrosion	Oxidation	Reduction
Valve Closure	Ball (Polymeric Seat)	1	2-3	1	1		2-3	1-2		1	U	U
	Poppet	1	1	1-2	3		2-3	3		1	U	1-2
	Butterfly						2-3	3		1	U	1-2
	Burst Diaphragm	3	1-2	1-2	3		2-3	3		1	U	3
Polymeric Seals	Static Seals	3	3	1	3		2-3	1		1	U	U
	Dynamic Seals	1	1-2	1	1		1-2	1		1	U	U
Metal Seals	Static Seals	3	3	2-3	3		2-3	3		2-3	U	U
	Dynamic Seals	1	1	1-2	1		1-2	3		1	U	1-2
Actuators	Solenoid	2-3	2-3	3	2-3		2-3	3		1-2	3	3
	Pneumatic	1-2	2-3	2-3	1-2		2-3	3		2-3	U	U
	Hydraulic [a]	1-2	2-3	2-3	1-2		2-3	3		1-2	1-2	1-2
	Electric Motor	1-2	2-3	3	1-2		2-3	2-3		2-3	U	U
	Squib	3	3	2-3	3		3	1-2		2-3	U	U
Drive Mechanisms	Screw Drives	1	1-2	3	1		2-3	3		1	1-2	1-2
	Ball Screw Drives	1	1-2	3	1		2-3	3		1	1-2	1-2
	Linear Ball Drives	1	1-2	3	1		2-3	3		1	1-2	1-2
	Geared	1	1-2	3	1		2-3	3		1	1-2	1-2
	Piston	1	2-3	3	1		2-3	3		1	1-2	1-2
Bearings and Bushings	Ball-Rotary	1	1-2	1-2	1		1-2	3		1	1-2	1-2
	Polymeric	1	2-3	1	1		1-2	2-3		1	1	1
	Metal	1	1-2	1-2	1		1-2	3		1	1-2	1-2
	Flexure Pivots	1	1-2	1-2	2-3		1-2	3		1	1-2	1-2
Hermetic Seals	Bellows	3	1	1	3		1	3		1	1-2	1-2
	Diaphragms Metals	3	1	1	3		1	3		1	1-2	1-2
Lubes	Dry Film	1	3	1-2	1		1-2	2-3		1	1	1
	Liquid	1	3	1	1		1-2	2-3		1	1	1
Springs	Coil	3	1	1	3		1-2	3		1	U	U
	Belleville	3	1	1	3		1-2	3		1	U	U
	Liquid	3	1	1	3		1-2	3		1	U	U
Fittings and Fasteners	AN Flare and MS Flareless	3	3	2-3	3		1-2	3		1	U	U
	Welded	3	3	3	3		1	3		1	U	U
	Bolts and Screws	3	3	2-3	3		1	3		1	U	U
	Filters	3	3	3	3		3	3		1	1	1
	Tanks	3	1-2	1-2	3		2	3		1	1-2	1-2

[a] Propellant used as fluid

Influencing Factors:
- 1: Major
- 2: Moderate
- 3: Minor
- U: Unknown

2.8 TEST METHODS AND SIGNATURE ANALYSIS

Test methods have been identified including those methods now in use and where technology refinement is necessary or where new methods must be developed. Signature techniques may provide the means for determining experimentally the changes in a component function due to a perturbation of some physical quality. Signatures are a characterization of a component or element that is obtained before and after application of a stimuli.
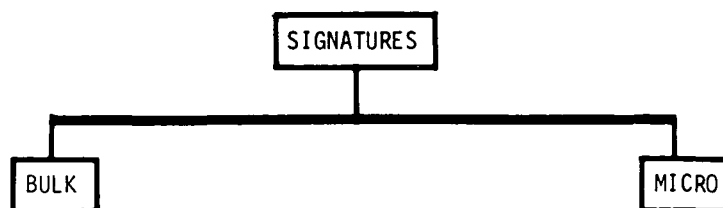
A number of advanced testing techniques were examined in order to determine their applicability in evaluating the long term reliability of components. The criteria for selection of these methods were as follows:

a. The test should have the potential of obtaining a general signature which, in turn, could be related to any degradation mechanisms or functional changes occurring to the component.

b. The test should be able to be performed without component disassembly, although the component may have to be removed from the propellant system.

c. The test may be conceptual at this time, although it should relate to a mechanism affecting long term performance.

The signatures have been grouped into two types. A bulk signature is defined here as a measurement of a performance function (such as leakage) which does not necessarily distinguish between or identify what variables affect the performance function. A microsignature is defined as the measurement of a single or related variable which can be identified and which affects and causes a change in measurement.

Table 2-2 lists the grouping of the signatures, the first level mechanism which may affect the component function, and a generic listing of the applicability of the signatures to components. Where possible, the terms and definitions as defined by NASA[9] and the Research Group on Wear of Engineering Materials, Organization for Economic Cooperation and Development, Paris[10] have been used to describe the mechanisms which may affect component function.

2-22

Table 2-2. List of Component Signatures, Mechanisms, and Generic Applicability

```
                    ┌─────────────┐
                    │ SIGNATURES  │
                    └──────┬──────┘
              ┌────────────┴────────────┐
         ┌────┴────┐               ┌────┴────┐
         │  BULK   │               │  MICRO  │
         └─────────┘               └─────────┘
```

1. Leak Rate (G)[a]
   valve seat surface changes
   cyclic life variation

2. Wear Particle Measurements (G)
   particulate contamination
   surface changes

3. Acousto-Optical Imaging (C)
   valve seat surface changes
   internal deformation of
   components

4. Acoustic Propagation (C, I)
   valve seat surface changes

5. Electromagnetic Interactions (C)
   general and specific function-
   ality changes

6. Thermal Imaging (G)
   leakage
   incorrect operation producing
   friction

7. Interferometric Holograms (G)
   cyclic life variations
   stress variations
   pressure variations

8. Neutron Radiography
   pyrotechnics
   material defects
   propellant characterization

1. Holographic Surface Topology (I)[a]
   wear
   valve seat surface changes

2. Scanning Electron Microscopic
   Topology (I)
   wear
   valve seat surface changes

3. Electron Microprobe Analyses (I)
   corrosion products and profiles

4. Plasma Emission Analyses (I)
   corrosion products

a

G = General signature which can be applied to all components
C = Class signatures which may only apply to certain types of components
I = Individual signature which may require disassembly of the component

2-23

2.8.1 Bulk Signatures

2.8.1.1 Leak Rate

The measurement of the leak rate of a valve is perhaps one of the most sensitive and rapid tests that can be performed. Examination of the types of instruments commercially available for leak detectors indicates that the equipment based on mass spectrometer detection techniques[11] are the most sensitive. This technique entails the bombardment of the gas molecules by an electron beam. The resulting charged particles are then accelerated into a magnetic field, and separated according to their mass number (M/e). The measurement of the relative intensity of the mass number of the leak gas in question is accomplished by the current flow and is converted into an electrical output. The primary detection gas is helium, however, some leak detectors offer a detection mass range of 2 to 200. This range includes the propellants of interest, but a technological difficulty arises with respect to a standardized leak source. None of the leak sources are traceable to a primary NBS standard, although secondary standards are available for helium (diffusion through glass and for hydrogen diffusion through palladium). Thus, for the leak detection to be completely correlatible to the propellant and valve of interest, standardized leak sources for each propellant must be developed, and the corresponding leak detection hardware must be compatible to the reactive propellants of interest. ABLEAK[8] developed under NASA contract, may provide a method of establishing standardized leak sources for the various propellants.

The leak rate of a valve may be directly related to changes in the valve seat surfaces and variations in the cycle life. Changes in the valve seat surfaces are due to four main types of wear: adhesive wear, abrasive wear, corrosive wear and surface fatigue wear. Cyclic life is influenced by the wear of the valve seat, fatigue of the springs, bellows, etc., and variations in the valve actuator.

This signature is general, in that any valve configuration can be leak checked. Sensitivities of 5×10^{-13} std cc/sec helium (corresponding to a virtual leak of 1.6×10^{-4} std cc in 10 years) are claimed by some manufacturers, but experience at TRW Systems under normal laboratory conditions indicate

2-24

that a sensitivity of 3×10^{-9} std cc/sec (helium) is a more realistic figure (corresponding to a virtual leak of 1 std cc in 10 years).

The operation and description of the mass spectrometer leak detector is as follows:

Mass Spectrometer Leak Detector

Specificity: Gases (primarily helium).

Output: Panel meter, audio alarm.

Sensitivity: Maximum = 5×10^{-14} std cc/sec;
realistic = 3×10^{-9} std cc/sec.

Mass Detection Range: 2 - 200 (necessity for standardized leak source)

Operation: Device to be measured is connected to leak detector. A vacuum is pulled on one side of the device. After the appropriate vacuum level is established (less than 10^{-4} torr), the mass spectrometer isolation valve is opened and a stream of helium gas is sprayed around the device. If the device leaks, the helium (plus any other gases present) are pulled into the mass spectrometer, and the gases are bombarded by an electron beam. The resulting charged particles are then accelerated into a magnetic field, and separated according to their mass number. The measurement of the relative intensity of the mass number of the leak gas is accomplished by the current flow and is converted into an electrical output. Figure 2-1 is a block diagram of a helium mass spectrometer leak detector, and Figure 2-2 schematically illustrates the operation of the mass spectrometer.
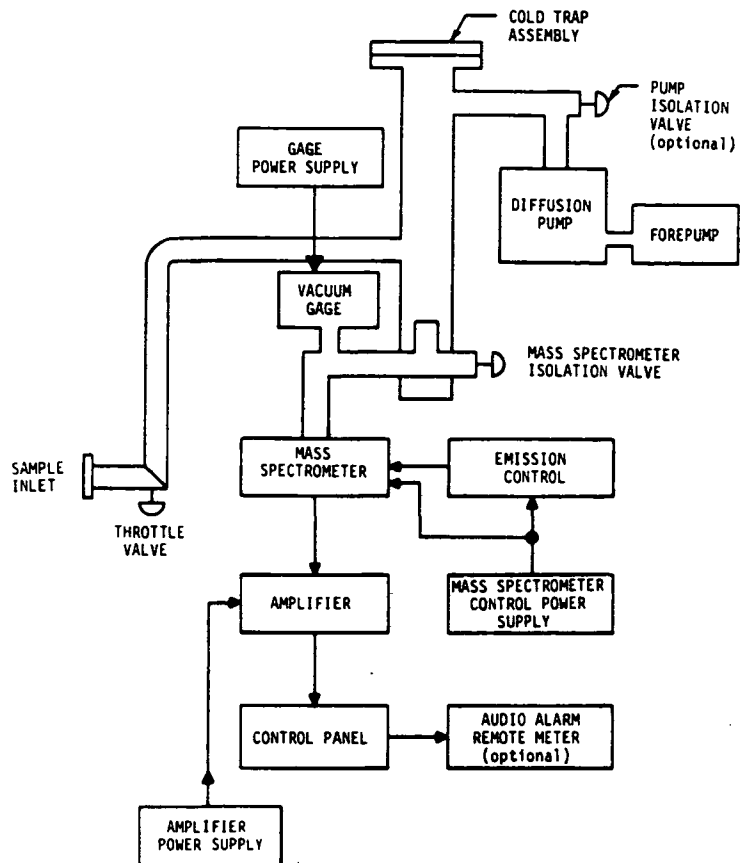
Figure 2-1. Typical Block Diagram for Mass
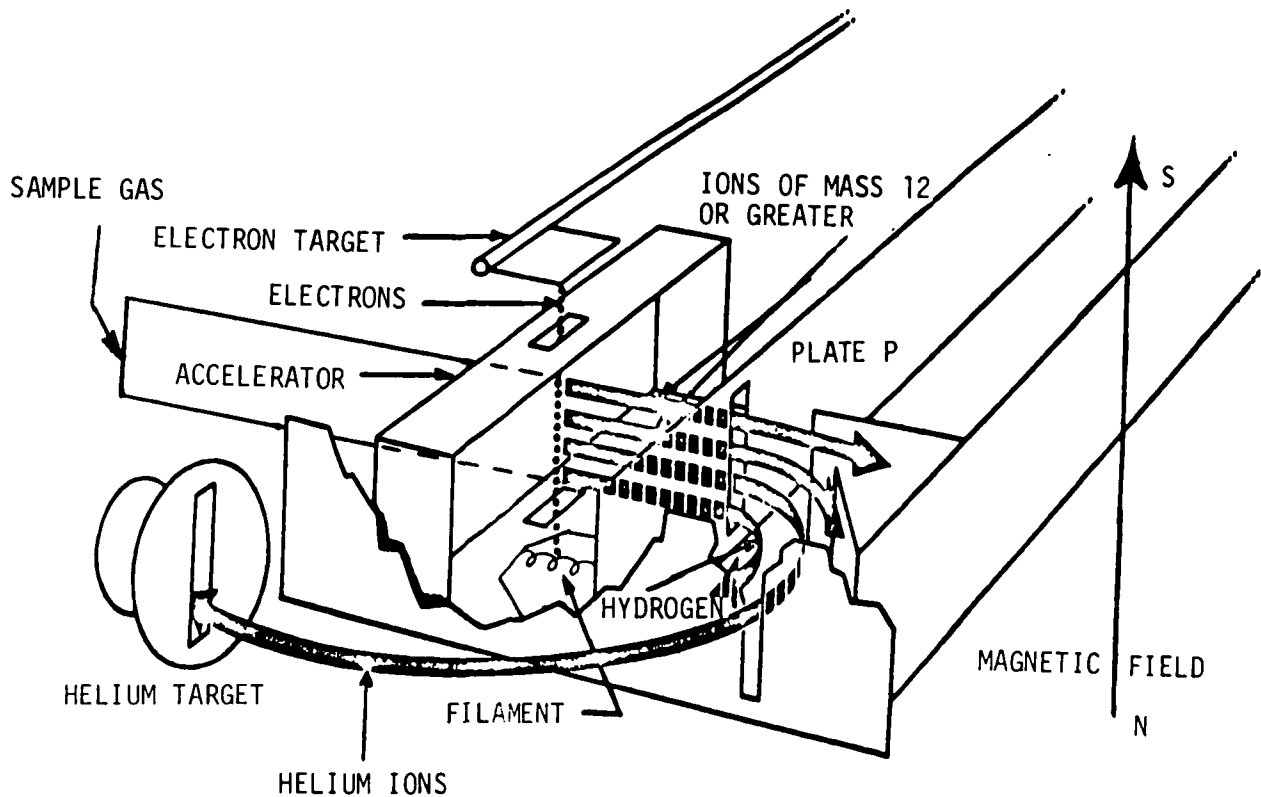Spectrometer Helium Leak Detector

Figure 2-2. Helium Mass Spectrometer Operating Diagram

2.8.1.2 Wear Particle Measurements

There are two main sources of particulate material which can contribute to component degradation: "built-in" and system generated. The built-in particulate source is caused during the manufacturing and handling of the parts and at installation of the components in the system. Also, particulate material may be introduced by the propellants and pressurants. It is important to know the source and type of particles since these particles can interact with the components having sliding surfaces and interfere with valve seating. Millipore Corporation has developed the πMC particle measurement computer system which can measure and record individual particles, total particles, and statistically average the entire particle population with a particle range of 0 to 300 micrometers.

Rabinowicz[12] has shown that the volume dV of surface material swept out by particles sliding dX along a surface is:

$$\frac{dV}{dX} = \frac{L \ (\overline{\tan \theta})}{\pi P}$$

where: L   = total load

$\overline{\tan \theta}$ = weighed average of the tangents of all the roughness angles of the particles

P   = hardness of the surface

In addition, he has also determined that as wear particles are generated, (e.g., during valve actuation) an equilibrium wear particle diameter, d is formed, corresponding to d = 60,000 Wab/P.

where: Wab = work of adhesion of the contacting materials

P   = hardness of the softest contacting material

which is correlatible to the maximum wear coefficient. Thus, by measuring the particulate contamination shape and concentration in the propellant before and after valve actuation, the amount of wear, the wear rate, and the seat removal rate can be estimated and correlated with the other

signatures. In addition, it may be possible that a study of this phenomenon of particle production could result in the following:

- Determination of a relationship between leakage and materials used in metal-to-metal seats including poppet, ball and spool configurations.

- Prediction of the optimum filter size for use in valves or in valve-controlled systems.

- Determination of the minimum clearance between moving parts before seizure can occur, or determination of the optimum materials for close-fitted parts in sliding contact.

- Determination of the final surface finish that can be expected for sliding surfaces given a long period of time, or determination of the materials that will develop the best finish after wear-in.

- Determination of the minimum normal load materials will sustain before wear takes place or when loose wear particles will not be formed.

This signature is general, in that particulate contamination and generation is common to all components having sliding surfaces and the materials properties necessary for calculation of wear rate and surface removal are known.

A detailed description including a block diagram, Figure 2-3, of a particle counter follows:

Particle Counter

Specificity:	Filterable particles
Output:	TV monitor display, digital readout
Sensitivity:	Detects particles from 0 to 300 micrometers with provisions for selective "oversize" particle count.

Operation: TV camera scans particles from microscope stage
by utilizing a raster scan pattern. Threshold circuits sense
the difference in particle intensity from the background inten-
sity as the sweep passes over both leading and trailing particle
boundaries. On the following raster sweep, the instrument scans
in advance of the boundaries. During sweep traverse, digital
data stores the information in the memory for conversion to
desired data format. Particle characterization includes indivi-
dual particles, longest linear dimension, area, volume, average
diameter, distribution, and concentration. Figure 2-3 is a
block diagram of the Millipore Corporation πMC particle counter
and its operation.
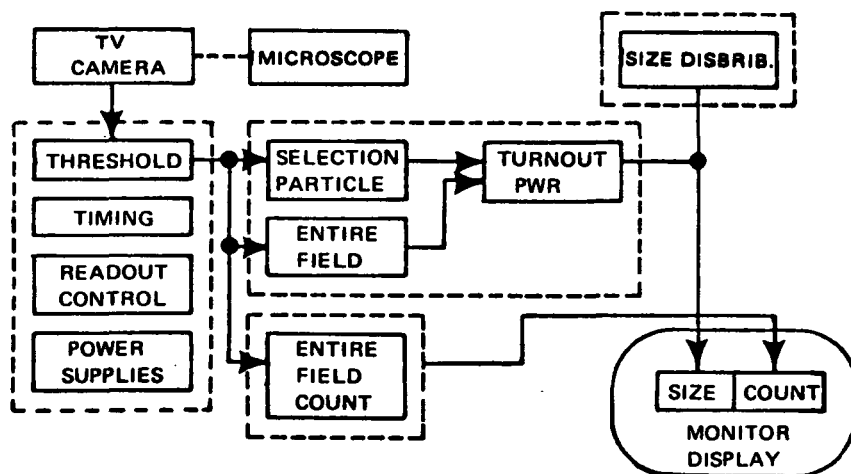
Figure 2-3. Block Diagram of Particle Counter Analyzer

2.8.1.3 Acousto-Optical Imaging

Acousto-optical imaging consists of an acoustic wave coupler or Bragg cell,
an acoustic transducer attached to the bottom of the cell, and a monochro-
matic light source (e.g., a laser). A two-dimensional image of the object
is visually displayed on a viewing screen. By using proper orifices, one
may view the object by focusing on various planes of the image and also
induce desired magnifications or demagnifications. The resolution of the
acousto-optical images is on the order of the wavelength of the sound in
the medium in which the light and sound interact. Thus, it is advantageous

to use high frequency ultrasonic waves for best resolution.

The advantages of this type of signature are:

- Ability to produce visual images of the interior of optically opaque bodies

- Operates in real time

- Signatures or traces from known flaws are not requires

- Quantitative information is obtained from the images

- Insensitive to material thickness

As with other ultrasonic imaging techniques, acousto-optical imaging is application dependent, thus it must be categorized as a class signature, since it may be necessary to use shaped and/or focusing transducers depending on the component configuration.

The operation and schematic illustration, Figure 2-4, of the acousto-optical image technique is described as follows:

Acousto-Optical Imaging

Specificity: Solid objects

Output: Photographic or visual images

Sensitivity: Variable, depends on geometry of object and type of image desired. Flaw detection in flat metal specimens has shown 0.001" crack width resolution.

Operation: The object to be viewed is placed in an acoustic wave coupler (Bragg cell) with an acoustic transducer attached to the bottom of the cell. A monochromatic light source (e.g., a laser) is focused perpendicular to the Bragg cell above the object. The acoustic transducer generates acoustic waves, which pass through the object and "excites" every point within the object. These points in turn act as sound sources. Thus, sound

waves which are a superposition of all the point sound sources
within the object are emitted from the object. These emitted
sound sources interact with the monochromatic light and induce
Bragg reflection from each of these sources thereby obtaining
an image of every point of the object. Thus, visual images of
flaws or objects within the interior of optically opaque bodies
can be produced. In addition, the technique operates in real
time, signatures or traces from known flaws are not required,
quantitative information is obtained and it is insensitive to
material thickness. Figure 2-4 schematically illustrates the
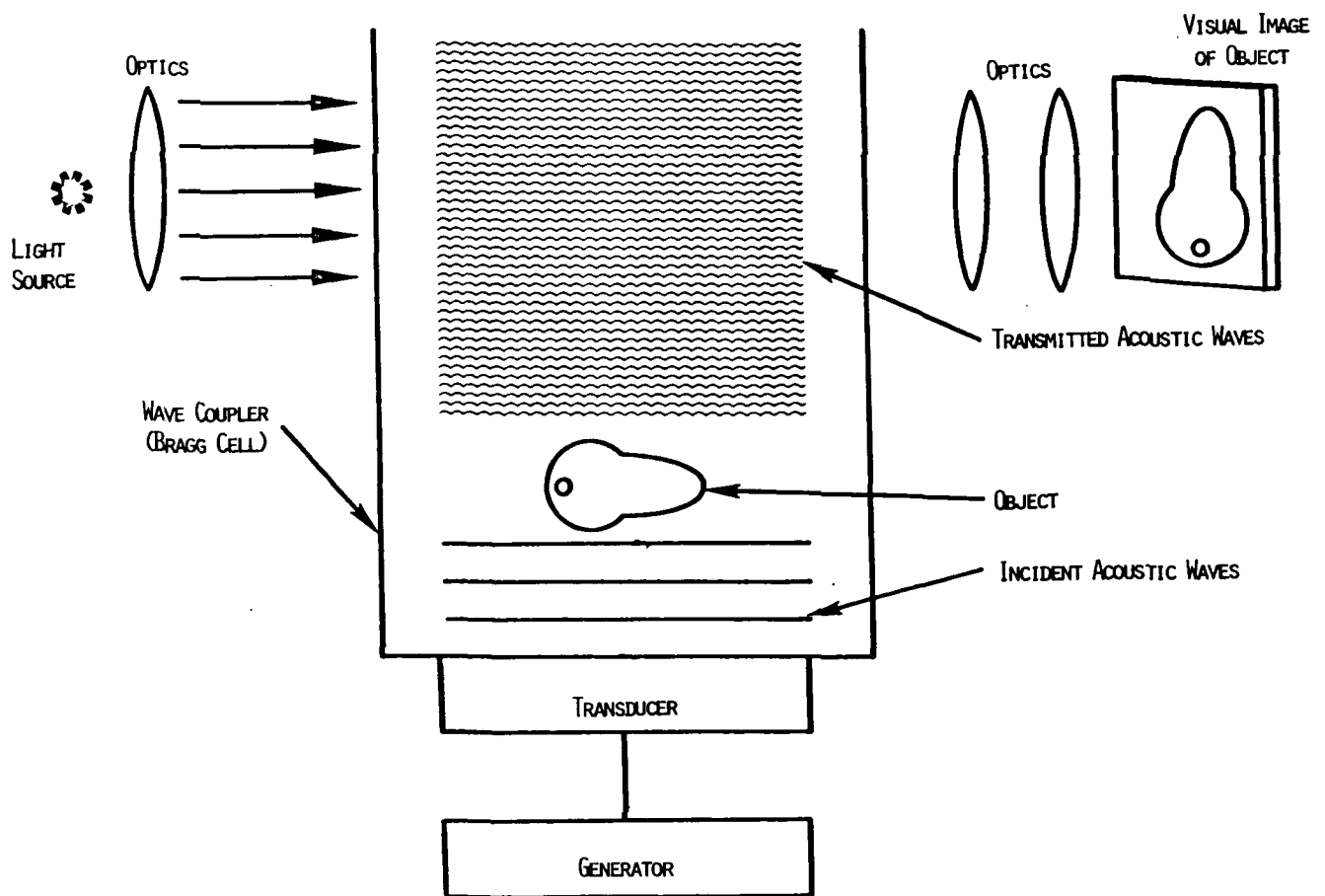acousto-optical imaging device.

Figure 2-4. Schematic Illustration of the
Acousto-Optic Imaging Device

2.8.1.4 Acoustic Propagation

As an acoustic wave is propagated through a medium, its velocity and phase remain the same. When the wave impinges on an interface, such as the junction between a poppet and the valve seat, both the velocity and the phase of the acoustic wave changes. Since the propagation and phase change of an acoustic wave can be precisely measured for any combination and spacing of materials, this technique can be a very sensitive test of changes occurring in the valve seating as a function of operation. This technique must be grouped as a class-individual signature, since the placement of the transmission and receiving acoustic transducers will depend on the component geometry and initial signature of the components.

Acoustic Propagation

Specificity: General, can be used in any medium.

Output: Variable, although usually recorded photographically from an oscilloscope showing velocity, phase changes, and/or delay times.

Sensitivity: Variable, depending on application. For flow or interfacial detection, sensitivity is limited to natural inhomogeneities of the materials (e.g., grain size in metals). For thickness measurements, sensitivity is limited to frequency and propagation stability of transducer.

Operation: Two modes of operation are commonly used: acoustic propagation by a transmitter which is detected by a receiver, and acoustic propagation in a pulse mode where the transducer is both the transmitter and receiver. As an acoustic wave is propagated through a medium, its velocity and phase remain the same. When the wave impinges at a flaw or an interface, the wave front is scattered, and in the case of a flaw, the signal is picked up as a reflection or loss in signal strength. In the case of an interface, the velocity and phase of the acoustic wave changes. Since the propagation and phase change of an acoustic wave can be precisely measured for any combination and spacing of materials, the technique can be highly selective for any operational test. Figures 2-5 and 2-6 schematically illustrate the various methods of acoustic propagation and detection.
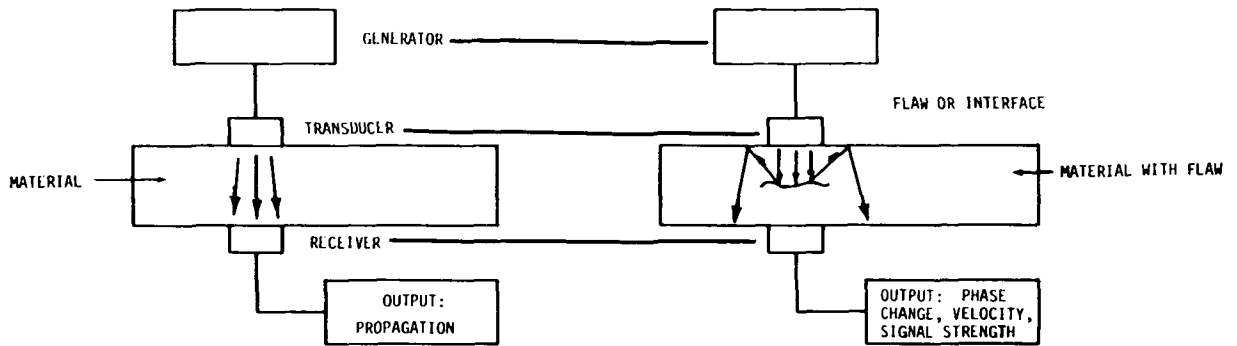
Figure 2-5. Schematic Illustration of Transducer-
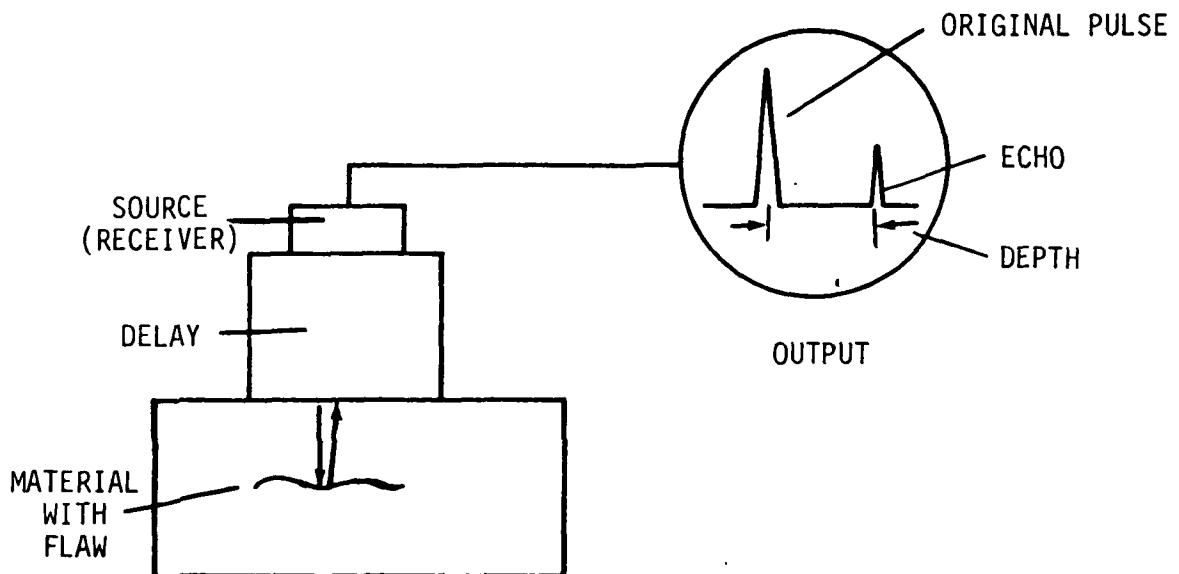Receiver Flaw Detection Mode

Figure 2-6. Schematic Illustration of Pulse-Echo
Method of Flaw Detection

2.8.1.5 Electromagnetic Interactions

This signature analysis groups electrical (resistance and capacitance), magnetic and x-ray measurements on the component. The rationale for this decision is that although all the techniques utilize electromagnetic interactions between the component and the measurement, they are not completely defined at this time. Thus, they will require further investigation to ascertain their value for inclusion in this signature group.

Of the three types of measurement, the x-ray measurements are probably the best defined at this time. The use of high intensity x-rays to examine the interior of moving components has been demonstrated, and successive time lapse x-ray photographs can reveal anomalies which could be difficult to obtain and/or interpret using other methods.

These techniques are grouped as class signatures, since the geometry of the component will determine the techniques to be utilized.

Electromagnetic Interactions

Specificity: General, depending on measurement. For capacitance and resistance measurements, corrosion rate on surfaces and true contact area. For magnetic measurements, changes in component materials as a function of operating life. For x-ray measurements, functionality of moving parts in the interior of components, and flaws or malfunctions in components.

Output: Variable, depending on measurement. For the electrical and magnetic measurements, the output will be in the form of a meter reading. For the x-ray measurements, the output will be photographic images.

Sensitivity: Since these signatures are geometry dependent, the sensitivity will necessarily depend on the component and its configuration. Capacitance measurements can detect changes as low as 5 - 10 picofarads corresponding to a lineal change of approximately 10^{-3} μm per square meter of surface area. Resistance

measurements can detect as little as a 10^{-3} ohm change corresponding to a lineal change of approximately 10^{-3} μm per square centimeter of surface area. Magnetic measurements can detect changes of 0.2 gammas in the component if Helmholtz coils are used to cancel out the earth's magnetic field. This corresponds to a magnetic field intensity change of approximately 10^{-6} oersted per unit area. This change can be equated to a metal transfer or material transformation if the metal is specified. X-ray measurements can detect flaws as small as 0.01 inch in any dimension, depending on the material, its thickness, and the component geometry. One to one photographic resolution of the component interior can be made using x-rays, depending on beam collimation, intensity, and component geometry.

Operation: a. Electrical Measurements

Most of the electrical measurements are made using a null bridge balance technique. This method measures the difference between the unknown capacitance or resistance against a known variable reference and the error signal is displayed on a meter. The reference capacitor or resistor is varied and when the reference value matches the unknown, the meter is nulled and the value of the unknown is equal to the reference.

b. Magnetic Measurements

The component is placed inside a Helmholtz coil arrangement which cancels the earth's magnetic field. The magnetic remnance of the component is detected by magnetometers in various directions depending on the component geometry.

c. X-ray Measurements

High intensity x-ray machines are normally used to examine the interior of components. By the use of a chopper synchronized with a moving piece of film, x-ray movies of the interior of the component can be made during its operation.

2.8.1.6 Thermal Imaging

The technique of thermal imaging has been utilized as a means to provide an indication of a component's thermal performance. Incorrect operation of any dynamic mechanical device tends to produce excessive friction. This, in turn, generates heat and manifests itself as an increase in material temperature. In addition, small leaks through the valve seat will produce heat paths which are detectable using infrared radiometry. Experimental investigations by Hughes Aircraft[13] using infrared radiometry have shown the following advantages:

- The sensor is not in contact with the surface under examination and thus there can be no contamination or damage.

- Equally applicable to metals and nonmetals.

- The contour of the part under examination is not critical as long as it is possible to focus optically on the part's surfaces.

- It is easy to determine temperature profiles.

Thus, the measurements can be made under actual working conditions to give accurate thermal trends. The technique is grouped as a general signature, since it is not dependent upon the component geometry.

Thermal Imaging

Specificity: Solid objects having thermal profiles.

Output: Panel meter or thermograms (photographic images where temperature produces the contrast or color variable).

Sensitivity: $\pm$ 0.3°C, instantaneous field of view 1.77 milliradian (0.1°).

Operation: All objects have a thermal photon self-emission, with the photon wavelength corresponding to the temperature of the object. These photons are too weak to be recorded directly on a photographic film, but can be sensed by an infrared radiometer (i.e., bolometer, pyroelectric crystals, etc.). The thermal

imaging device optically scans the object with a small area radio-
meter in a raster pattern, while simultaneously a light source,
amplitude modulated by the radiometer, is caused to scan a similar
raster to produce a visible image on film. The temperature distri-
bution of the object in the scene is indicated by the brightness
of the resulting visible image. By using a continuously variable
color wheel, color thermograms having excellent resolution can be
produced. The advantages of this type of thermal sensing are:
non-contact with the object being viewed, equally applicable to
metals and non-metals and the contour of the object under examina-
tion is not critical as long as it is possible to focus optically
on its surface. Figure 2-7 is a block diagram of a thermal imaging
device.

2.8.1.7 Interferometric Holograms

Holography which may be described as the science of wavefront reconstruction
has made practical the art of three-dimensional, lensless photography. A
hologram contains both amplitude and phase information, while a conventional
photograph contains only the amplitude information. The phase information
stored in the hologram is recorded by combining a scene wavefront with a
reference wavefront to produce an interference pattern having a very fine
spacing (>20,000 lines per inch). The interference pattern may be recorded
by a conventional photo-sensitive plate. When the developed holographic plate
is reilluminated with the reference wavefront only, the scene wavefront is
reconstructed by diffraction by the interference pattern. The scene wave-
front reconstruction allows an investigator at any convenient time to make
all the optical observations and measurements on the holographic image just
as if it were the original object. Physically viewing a hologram is like
looking out of a window with the recorded scene having both the proper
parallax and binocular effects as the original subject.

Holography has made practical a new type of interferometry for deformation
measurements which is not dependent on precise optical equipment and align-
ment which is normally required for interferometry. A holographic inter-
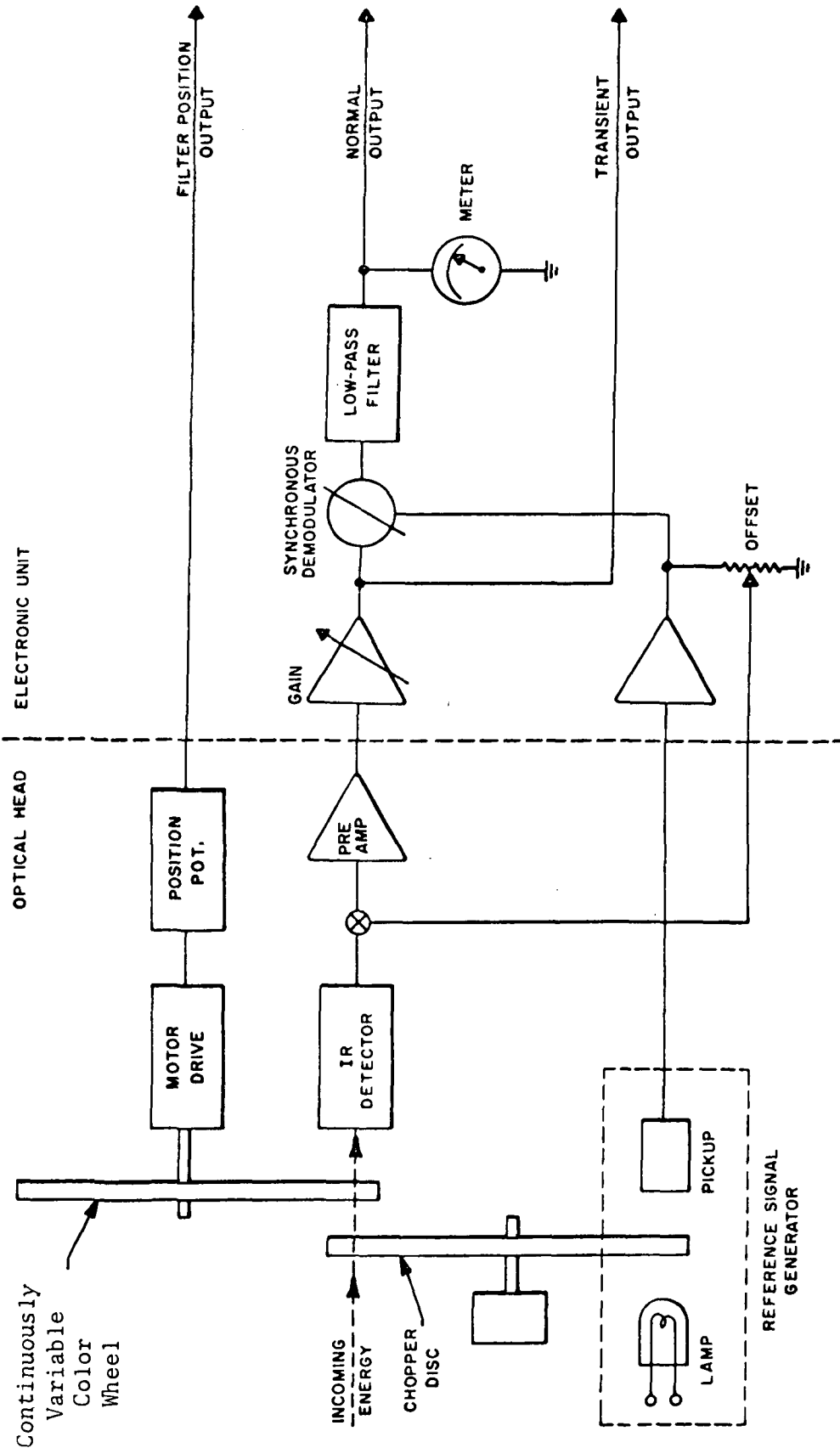ferogram can be produced by recording sequentially on the same hologram

Figure 2-7. Block Diagram of Thermal Imaging Device

plate the image of an object in the free state and subsequently in a
disturbed state. The resultant interferogram contains a quantitative
comparison of the free and strained states of the object in terms of a
contour fringe pattern. This pattern revleals minute distortions occurring
between the multiple exposures, of the order of 0.1 wavelengths of the
illuminating light.

There are a variety of different lasers and holographic techniques that
an investigator may apply to interferometric measurement techniques. Recent
developments in holography have made possible the application of a pulsed
ruby laser to holographic interferometry. Major improvements in the quality
of reflected flight holograms have resulted from technological breakthroughs
in the design of the laser equipment and holographic apparatus. The poor
coherence property of the pulsed ruby laser has heretofore limited the depth
of field of reflected light holograms to a few centimeters, usually with
unimpressive resolution. However, new equipment permits holographing in
fine detail objects which occopy several hundred cubic feet in volume.
Stop action exposure times of a few nanoseconds are possible using the
intense illumination from the pulsed ruby laser. The apparatus permits
interferometry of large objects in hostile environments under dynamic
conditions.

The basic capability may be applied to a variety of materials testing
situations involving both interferometry and microscopy. This unique tool
may permit major advances in instrumentation for activities such as mechani-
cal property testing, environmental and nondestructive testing. Potentially,
one of the most economically rewarding applications of reflected light
holographic interferometry using the pulsed ruby laser will be in the field
of nondestructive testing. Preliminary laboratory tests have demonstrated
the feasibility of applying these techniques under a variety of conditions
in both the laboratory and in the field, ranging from coupon-type samples
to full-scale structures. When a body containing a flaw or imhomogeneity is
loaded nondestructively, either thermally or mechanically, the localized
distortions due to force redistribution around the flaw will be seen inter-
ferometrically even though the flaw is not visible. (Holographic non-
destructive testing in the past has been accomplished with the continuous

wave laser (CW) which is lacking with respect to the intensity of illumination needed for stop action and large depth of fields. Existing CW techniques lack versatility and require elaborate vibration free installations to insure mechanical stability during long exposures). Interferograms have been made of distortions occurring in impulsively loaded specimens as a means for studying materials and component response at high strain rates.[14]

Since interferograms can record the cyclic life, stress wave, and pressure variations of the valve as a whole, the information recorded gives a more precise indication of valve performance than that recorded with strain gauges, since these are single point sources.

This signature is general, in that an interferometric hologram can be made of any component configuration, due to the large depth of field, under its normal environmental operating conditions.

Interferometric Holograms

Specificity: Photographic images and interferograms.

Output: Variable depending on measurement. For large areas interferometric holograms, pressure differentials of closed containers ± 0.1 psia and surface deformations of ± 20 micrometers are possible to be measured.

Operation: A holographic interferogram is produced by recording sequentially on the same hologram plate an image of a component in a free and subsequently disturbed state. The resultant interferogram contains a comparison of the two states in terms of a contour fringe pattern which represents minute distortions occurring between the multiple exposures. Interferometric holography in fine detail can now be performed on objects which occupy several hundred cubic feet in volume. Stop action exposure times of a few nanoseconds are possible using the intense illumination from the pulsed ruby laser. This technique permits interferometry of large objects in hostile environments with dynamic response. Figure 2-8 is a schematic representation of hologram recording and image reconstruction.

LASER

PHOTOGRAPHIC
PLATE
(HOLOGRAM)

REFERENCE BEAM

SCENE BEAM

MIRROR

OBJECT

LIGHT SCATTER
FROM THE OBJECT
BACK TO THE
PHOTOGRAPHIC PLATE
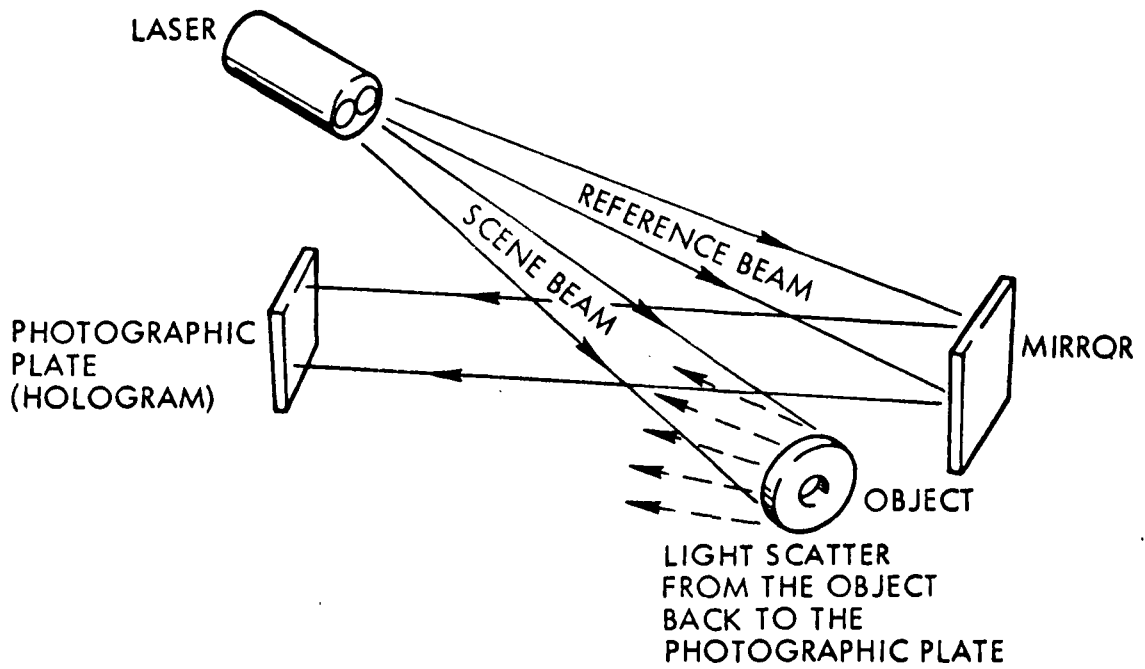
a. Hologram Recording System

OBSERVER

HOLOGRAM

D.C. TERM

REFERENCE BEAM

REAL IMAGE
(REVERSED FOCUSING)

VIRTUAL IMAGE
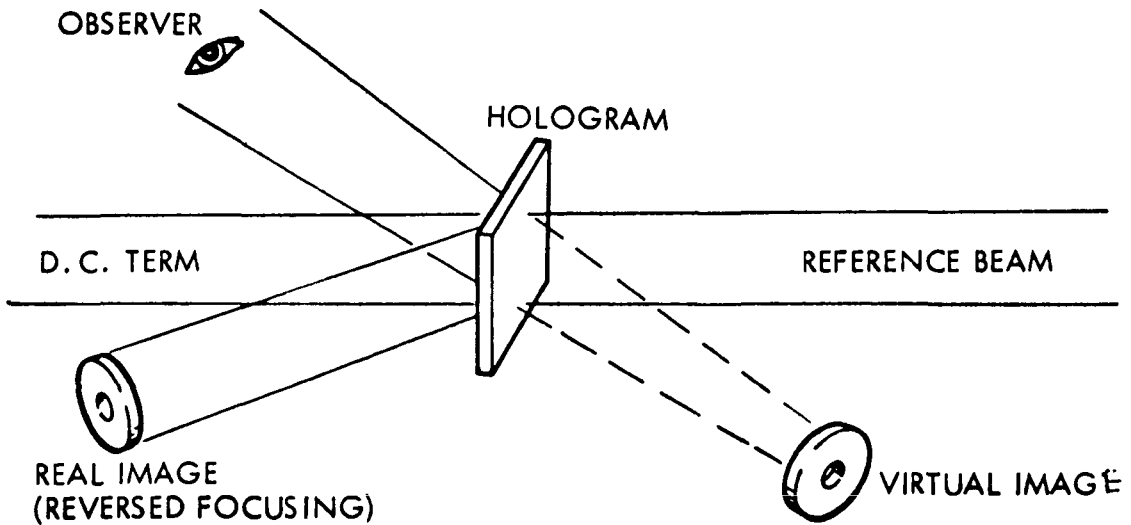
b. Reconstruction of Images from the Hologram

Figure 2-8. Schematic Representation of Hologram
Recording and Image Reconstruction

2.8.1.8 Neutron Radiography (References 15-24)

Neutron radiography is dependent upon the effects of a stream of neutrons passing through the test object. The results obtained differ greatly from X-ray or gamma ray radiograms because neutrons are most readily absorbed by molecules containing the low molecular weight elements such as hydrogen, lithium, beryllium and boron. High atomic weight elements such as lead, tungsten, palladium, etc. do not absorb a significant quantity of neutrons. X-rays and gamma rays are absorbed by the high molecular weight materials and transmitted by low molecular weight materials. Neutrons can thus penetrate a lead shield containing organic or light metal interior components and provide a good "picture" of the interior components; this result is unobtainable with X-ray or gamma ray radiography. Neutron radiography can thus give detail in material com- binations not shown in gamma or X-rays and vice versa.

Neutron radiography requires a collimated neutron source. A choice of three types of neutron sources may be used depending upon the application, (1) collimated neutron accelerator neutron generator, (2) collimated filtered neutrons from reactor sources, and (3) collimated neutrons from a radioisotope source (californium 252 is the most powerful and expensive neutron emitting radioisotope).

The collimated neutron accelerator is presently most practical for general use for many requirements. The nuclear reactor is the most powerful neutron source for applications requiring high resolution and short exposures. The isotope sources can be portable but, because of their lower and less energetic neutron output, are not suitable for short exposures or high resolution because a high resolution collimator incurs a large loss of neutrons which would be available for test sample exposure.

Neutron radiography supplements rather than replacing X-ray and gamma ray radiography. For example, collimated neutrons (N-rays) will not detect a void in a casting unless occlusions of light elements, i.e., water, exist in the void as they cannot be as easily imaged remotely as X-rays in common usage. Although an image intensifier may solve this problem, the resolution

is not as good as high quality X-rays. Neutron sources are not compact and readily portable; in contrast, excellent gamma radiographs are taken with very simple portable equipment. All that is required for a stationary gamma radiograph is a protected source of γ emitting radioisotope, a holding fixture for the test and an opaque envelope containing a suitable size of X-ray film to cover the desired object X-ray shadow area.

Neutron radiography is a routine nondestructive testing (NDT) tool in the aerospace industry. NASA specifies the technique for man rated Apollo hardware. Detonating devices are neutron radiographed for effective quality checks without damage or hazard. Castings and welds are checked for hydrogen embrittlement and honeycomb panels are checked for defects. The N-radiography technique is especially useful for checking composite matrices containing high strength fibers such as boron and carbon. Boron fibers in an aluminum matrix are effectively checked for alignment and dispersion with N-radiography. Electronic components have been inspected to ensure they are properly assembled and free of contamination. Hydraulic systems are checked for proper assembly of seals and absence of contaminants. N-rays are the only nondestructive method known for checking nuclear fuel cells.

Conventional N-radiography can detect 1500 ppm of hydrogen and improved techniques detect 150 ppm. The improved methods are very useful for checking hydrogen embrittlement and hydriding in critical structural parts and welds.

N-radiography will find increasing use to identify and measure materials. The technique could be used for real time imaging in fluid flow analyses, flow patterns, turbulence and cavitation. Chemical reactions including explosions can be studied as they occur. Diffusion of solids and gases are discernable with N-rays. It is apparent N-rays can be a valuable aid in corrosion and clogging investigations.

Neutron Ray Facilities

The basic facility concept for N-radiography is simple, yet it is large and expensive. A basic N-radiography system is shown in Figure 2-9.

```
        ┌─────────────┐
        │             │
        │   NEUTRON   │
        │   SOURCE    │
        │             │
        └─────────────┘

        ┌─────────────┐
        │  ╲       ╱  │
        │ COLLIMATOR  │
        │  ╱       ╲  │
        └─────────────┘

        ┌─────────────┐
        │   OBJECT    │
        └─────────────┘

      ┌─────────────────┐
      │ CONVERSION SCREEN │
      └─────────────────┘

        ┌─────────────┐
        │IMAGE RECORDER│
        └─────────────┘
```
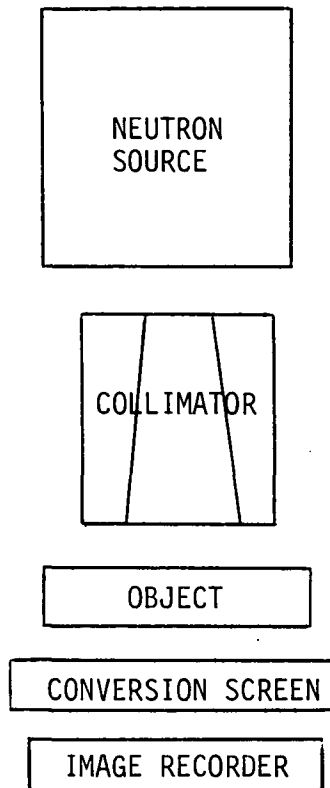
Figure 2-9. N-Radiography System

The basic facility involves a source of neutrons, a neutron collimator, an object volume and a conversion screen for converting the neutron beam into a more readily observed or detectable source of radiation and an image recorder. Neutron sources are obtained directly from radioisotopes, nuclear fission reactors and neutron generator accelerators which are usually dependent upon the deuterium-tritium nuclear reaction.

Neutron sources are generally nearly isotropic and the collimator and shield structure must absorb all except a narrow pencil of neutrons which exit through the collimator window. Lead filters can absorb the undesired X-radiation without affecting the N-radiation. The collimated N beam passes through the test object and activates the conversion screen. The test object spatially modulates the N beam according to the distribution of its N absorbing materials. The image conversion screen is exposed to X-ray film or some image intensifying amplifying observation or recording device. A commercially sealed tube N generator claims push button operation and outputs of 10" 14 Mev N/sec output. Table 2-3 lists typical characteristics of established neutron sources.

Table 2-3. Neutron Source Characteristics

Source	Output N/sec	Advantages	Disadvantages
Isotopic	$10^5 - 10^9$	Small size, ease of operation, portability	Low flux level, decay of intensity, continuous output
Accelerator	$10^7 - 10^{10}$	Good flux capability, amenable to intermittent operation, portability	Target life may be poor, moderately complex to operate
Reactor	$10^{10} - 10^{15}$	High flux capability	High cost, complex to operate, not portable

Imaging Methods

Two imaging methods are commonly used in N-radiography, the direct exposure method and the transfer method. The conversion screen and the image recorder are exposed simultaneously to the N-beam in the direct exposure method. The conversion screen emits detectable radiation promptly upon neutron exposure. The conversion screen only is exposed to the N-beam in the transfer method and the screen builds a persistent radioactive image during N-exposure. The transfer screen is then transferred to make a separate autoradiograph of the screen activity image on X-ray film. A third real time imaging device provides a TV display of the modulated N-beam image. These devices use a fast, direct exposure screen and an electronic tube image intensifier and a TV camera pickup with display. A summary of imaging methods is given in Table 2-4.

Real time imaging is the most useful in applications of N-radiography, however, the resolution is impaired when a standard 525 line TV system is used. Improvements of commercial instruments in this respect is expected.

Table 2-4. Neutron Beam Imaging Methods

Imaging Method	Converter Type	Typical Converter Materials	Detachable Radiator	Image Recorder
Direct Exposure	Neutron scintillators Prompt-emission materials Potentially radio-active materials Fissionable materials	Li^6 or B^{10} loaded phosphor Gd,B^{10},Li^6,Cd,Sm Rh,Dy,In,Ag,Au U^{235}	Visible light α, β, γ β, γ Fission fragments	Photo film X-ray film X-ray film Plastic (track etch)
Transfer	Potentially radio-active materials Thermoluminescent	Dy, In, Au Li^6F	β, γ Visible light	X-ray film Photo film
Real time	Neutron scintillators	Li^6 or B^{10} loaded phosphor	Visible light	Vidicon or orthicon

Applications of Neutron Radiography

A general characterization and examples of useful neutron radiography are helpful in considering possible new applications. N-radiography is especially useful when it is able to produce results which are not possible with X-rays. Neutron radiography can indicate the difference between materials of similar density and atomic number but different neutron cross sections, the location of light materials within heavy materials and examine radioactive materials. Table 2-5 gives a partial summary of application categories.

Neutron radiography application is more complicated than many other NDT methods. In many cases special treatment and methods are used to sensitize the components and areas to be examined with N-rays. Neutron radiography can provide the only known satisfactory method of NDT for many components. The details of application and use are extensive and the reader is referred to references 8 through 17 listed at the end of this section for further information.

Table 2-5. Applications of Neutron Radiography

Neutron Radiation Can Be Used To	Specific Applications Include
Differentiate between materials of similar density but different neutron cross section	Inspection of braze joints; determination of plutonium distribution in uranium/plutonium mixtures; determination of hydrogen content in metals and organics; determination of moisture content in ceramics; inspection of turbine blades and other mechanical-type metal joints; inspection of castings for voids or occlusions; inspection of cladding uniformity; inspection of electronic devices; inspection of welds.
Locate low density parts in high density containers	Inspection of metal-jacketed explosive devices; inspection of expoxy-bonded metal honeycomb; location of fluids and lubricants in metal systems; inspection of elastomers in metal structures; inspection of adhesive bonds in metal parts; location of liquid metals in certain metal containers; inspection of boron-filament composites; studies of fluid migration in sealed metal systems; inspection of uniformity of boron distribution in nuclear-reactor control rods.
Examine radioactive specimens	Inspection of irradiation test capsules; inspection of fuel rods and plates; determination of nuclear fuel distribution in assemblies; weld and braze inspection in irradiated parts.

2.8.2 Microsignatures

2.8.2.1 Holographic Surface Topology

The integrity of the poppet-valve seat interface is one of the critical areas for long term valve performance. Since there are many variables which affect this interface integrity, it is important to characterize the interface before and after actuation in order to ascertain the functional changes occurring during valve operation.

One of the inherent advantages of the pulsed ruby holographic technique is that holograms may be obtained in hostile environments, with 2 to 4 orders of magnitude signal to noise advantage over competing techniques. Thus, holograms may be taken with the original environment present in order to prevent change in surface structure due to environmental effects not associated with the valve actuation. Since the hologram contains information of the original object in microscopic detail, viewing the hologram at a later time with microscopic apparatus could provide valuable information related to surface effects. Excellent resolving power would be obtained in almost any environmental situation. At present, detail 20 micrometers in diameter can be observed. Microscopy at approximately 150X magnification appears feasible with existing apparatus using special techniques and procedures. Thus, holographic microscopy offers the important advantage of examining the surface topology of components at greater depths of field than conventional techniques, and can be utilized in hostile environments.

Holographic Surface Topology

Specificity: Surfaces

Output: Photographic Images and Interferograms

Sensitivity: Variable depending on measurement. For inter-ferometric topological recordings, variations of one to ten microinches can be resolved. For holographic surface topological studies, objects of ± 20 micrometers can be measured.

Operation: The technique of measuring the topology of
surfaces by holographic methods is identical to that utilized
in making regular or interferometric holograms. The only
difference is that the hologram is viewed through a special
microscope attachment. Figure 2-8 illustrating the hologram
recording and image reconstruction for interferometric measure-
ments is the same for topological recordings, with the exception
that the microscope is used for viewing.

2.8.2.2 Scanning Electron Microscope Topology

The scanning electron microscope (SEM) has an advantage over most
topographic scanning equipment in that it has a higher resolution
(continuously variable from 20X to 100,000X), greater depth of field
(200 to 500 times that of an optical light microscope), and can produce
stereographic micrographs (stereopairs) which can be used to measure
surface asperities[25]. Most surface analyzers (profilometers) have,
at best, an 0.5 micrometer arithmetic average vertical displacement
capability. The SEM can resolve to approximately 100 $\overset{\circ}{A}$ (0.01 micrometer),
which is important in calculating the asperity heights and radii of
curvatures of surfaces. The ability to follow the topological changes
of the poppet-valve seat surfaces should help elucidate the mechanisms
occurring during the life of the valve.

Scanning Electron Microscope Topology

Specificity: Multipurpose machine, primarily used for surface
topology studies by secondary electron emission.

Output: TV display, photomicrographs.

Sensitivity: Resolution: approximately 200 $\overset{\circ}{A}$ (0.02 micro-
meter); depth of field 300 to 500 times that of an optical
light microscope.

Operation: Surface to be examined is placed in scanning
electron microscope (SEM). The electron beam is accelerated
past two or more condensing lenses that reduce the beam to a
small diameter for use as a probe in scanning the specimen.
Deflection coils are placed between the last two lenses to
provide x-y scanning of the surface in a rectangular raster.
The scanning generator produces a sweep signal to the deflec-
tion coils and to two (or more) cathode ray tubes (CRT) for
one-to-one correspondence between the position of the beam
on the specimen and the spot on the CRTs. The brightness of
the spot on the face of the CRTs is controlled by the amount
of secondary electron emission generated at the surface by the
primary probe and collected by the secondary electron detec-
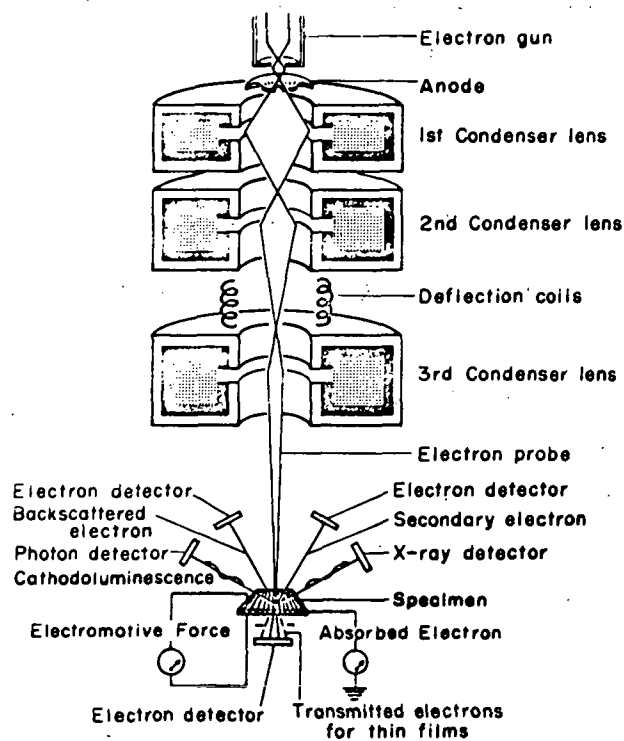tion unit. Figure 2-10 is a schematic diagram of the scanning
electron microscope.

Figure 2-10. Schematic Diagram of Scanning
Electron Microscope (SEM)

2.8.2.3 Electron Microprobe Analysis

Since one of the wear mechanisms is corrosive wear, it is necessary to obtain information on the corrosion products that accumulate on the valve surfaces. The electron microprobe is suited to identify localized surface reaction products and quantitatively determine the chemical elements which penetrated or reacted on the metal surface.

In the electron microprobe technique, an electron beam is focused on the specimen to a diameter of about one micrometer and the x-ray excitation lines in this limited volume of the specimen are analyzed for the wavelength and intensity of the characteristic lines. In the case of the unknown elements, the spectrometers are set to scan the complete spectrum for a selected area on the specimens. The results are then recorded by digital or analog methods. X-ray images can also be obtained of the area under observation showing distribution of various elements of the reaction zone. Both quantitative and qualitative data reduction is accomplished through the use of on-line computer programs, and a computer console which is connected directly to the electron microprobe system.

Electron Microprobe Analyses

Specificity: Elemental analysis of surfaces.

Output: Element X-ray emission spectra, photographic images.

Sensitivity: Variable depending on the element. Sensitivity decreases with decrease in atomic number, and elements below boron cannot be detected. With comparators, sensitivity is in the parts per million range.

Operation: A primary beam of electrons, approximately 0.5 micrometer in diameter, impinges on the specimen, causing electron excitation within the specimen to a depth of 1 to 2 micrometers. The excited electrons relax to their respective ground state and emit x-rays. The emitted x-ray spectrum is analyzed by crystal dispersion techniques and pulse-height analyzers. For qualitative

analysis, only the wavelength locations are used. For quantitative
analysis, both the wavelength location and peak heights are measured.
These are compared to a sample of known composition and the ratio
of intensities gives the quantitative amount of element in the
specimen. Three operating modes can be utilized: single spot
analyses, movement of the specimen, continuously or step-wise,
under a stationary incident electron beam or the electron beam can
scan the specimen in a raster mode.

In the third mode, single elements can be analyzed and displayed
as a photographic image showing where the element is concentrated.
Magnifications of 250 to 8,000X are accomplished with the use of
either x-ray excitation, or with backscattered electrons. The
latter are electrons which are elastically backscattered from
the specimen surface. These photographic images are referred
to as beam-scanning images. Figure 2-11 schematically illustrates
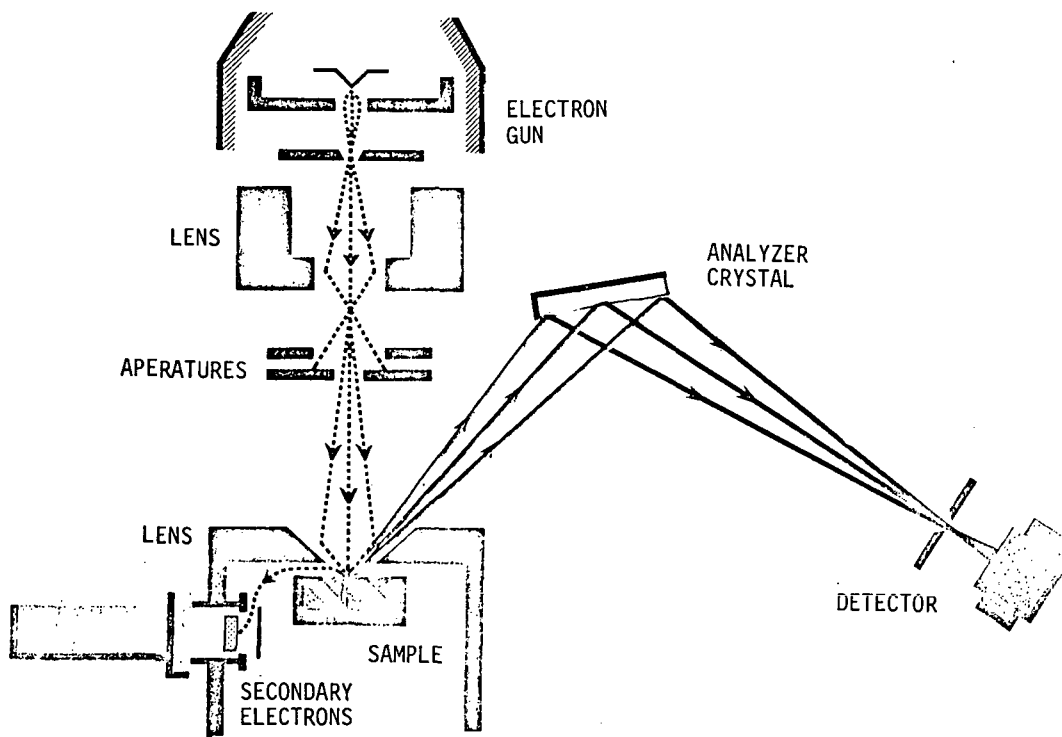the electron beam microprobe.

Figure 2-11. Schematic Diagram of an Electron Beam Microanalyzer

2.8.2.4 Plasma Emission Analysis

The analysis of surfaces and surface contamination by the electron beam
microprobe, as mentioned previously, utilizes the emission of x-rays from
the electron beam excitation of the material. The plasma emission analyzer
(sometimes called the laser microprobe, [26]), utilizes the intense energy
from a focused laser beam to volatilize the material to be analyzed,
which is then excited by an electrical spark and the excited gas is then
analyzed by an emission spectrograph. The advantages of this method are
that every element can be analyzed, and no special preparation of the
sample is required. A potential disadvantage is that it produces a crater
25-40 micrometers in diameter and approximately half the diameter deep;
however, if large corrosion deposits are encountered, the depth and com-
position of the layer can be accurately determined, since the microprobe
is coupled with a microscope for accurate positioning of the beam.

Plasma Emission Analysis

Specificity: Elemental analysis of surface contaminants.

Output: Emission spectra of the elements.

Sensitivity: Variable depending on the element. Sensitivity
decreases with decrease in atomic number, but is usually within
the parts per million range.

Operation: A ruby laser beam is passed through a conventional
microscope, and the concentrated beam is focused upon the sample
surface to be analyzed. The intense energy spot (25-40 micrometers
in diameter) vaporizes the surface, which is then converted to a
plasma by an electrical spark discharge. This spark excites the
gas, which produces a spectrum which is recorded by an emission
spectrograph analyzer. The advantage of this type of analysis
is that the area to be studied can be located by the microscope,
and the surface does not have to be polished or conductive, as
is the case with the scanning electron microscope or the electron
microprobe. Figure 2-12 schematically illustrates the plasma
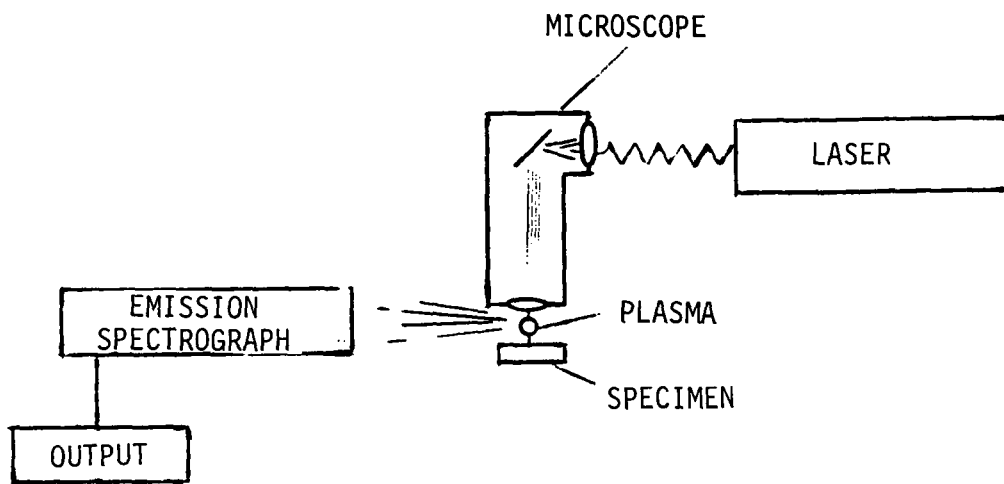emission analyzer.

Figure 2-12.   Schematic Representation of the
Plasma Emission Analyzer

REFERENCES

1. Anonymous, "Evaluation Test Program Environmental Limit and Combined Environmental Tests of Titan Three Way Solenoid Valve Martin P/N PD 475100002-9," Report AFBMD-TR-61-2, Stellardyne Laboratories, Inc., Air Force Ballistic Missile Division, Los Angeles, January 1961.

2. Anonymous, "Evaluation Test Program Acceptance, Limit and Combined Environmental Tests of Titan Nitrogen Start Check Valve AGC P/N 1-233080-A," Report AFBMD-TR-60-158, Stellardyne Laboratories, Inc., Air Force Ballistic Missile Division, Inglewood, August 1960.

3. Kirchman, E. J., "Loads Testing in Combined Environments," 1970 Proceedings of the Institute of Environmental Sciences, Mount Prospect, 1970.

4. West, W. S., et al, "Subsystem Radiation Susceptibility Analysis for Deep-Space Missions," NASA TR-R-371, National Aeronautics and Space Administration, Washington, November 1971.

5. Anonymous, "Nuclear and Space Radiation Effects on Materials," NASA SP-8053, National Aeronautics and Space Administration, June 1970.

6. Wilson, J. C., "Experimental Approaches to Radiation Effects," in the Effects of Radiation on Materials, J. J. Harwood, et al, Reinhold Publishing Corp., New York, 1958.

7. Weiner, R. S., "Basic Criteria and Definitions for Zero Fluid Leakage," Technical Report No. 32-926, Jet Propulsion Laboratory, Pasadena, 15 December 1966.

8. "Advanced Valve Technology," TRW Systems Interim Report No. 06641-6004-R000, Contract NAS 7-436, November 1966.

9. "Friction and Wear Interdisciplinary Workshop", NASA TMS-52748, NASA Lewis Research Center, Cleveland, Ohio, November 19-21, 1968.

10. "Friction, Wear and Lubrication, Terms and Definitions", Organization for Economic Cooperation and Development, Paris. Published by: American Gear Manufacturers Association, 1330 Massachusetts Ave., N.W., Washington, D. C. 20005.

11. A. J. Biolous, "Characteristics and Sources of Commercially Available Leak Detectors", Contract NAS 7-396, June 1967, General Electric Co., Report No. S-67-1013.

12. E. Rabinowicz, "Surface Energy Effects in Sliding Phenomena", Contract DA-31-124-ARO (D)-143, MIT Project No. 9889, 12 Sept. 1966.

13. W. J. Quinn, "Dynamic Mechanical Components Evaluated with Infrared Optics", Space Aeronautics, Sept. 1968, p. 88.

14. W. G. Gottenberg, "Some Applications of Holographic Interferometry", TRW Systems, EM 17-13, 99900-6305-R000, August 1967.

15. "Neutron Radiography Methods, Capabilities and Applications," by Harold Berger, Elsevier Publishing Co., New York, N.Y., 1965.

16. Publications, conferences and journals of the American Society for Nondestructive Testing, including "Materials Applications 'and former' Nondestructive Testing," (Monthly).

17. "Neutron Radiography a Solution In Search of Problems," by Joseph W. Ray, Research/Development, July 1969.

18. "Neutron Radiography With a Cockroft-Walton Accelerator," by Frank A. Iddings and Normal A. Bostrom, Materials Evaluation, Oct. 1969.

19. "Proceedings of the International Conference for 1965, Modern Trends in Activation Analysis," College Station, Texas, 1965.

20. "Neutron Radiography-Utilization of Neutrons from a Cockroft-Walton Accelerator," by Barry E. Chernick, Louisiana State University, January 1966.

21. "Neutron Radiography - Why and How," Proceedings of the Technical Session on Neutron Radiography, 24rh National Convention, Society for Nondestructive Testing, October 1964.

22. "Neutron Radiographic Inspection of Heavy Metals and Hydrogenous Materials," by H. Berger and I. R. Kraska, Materials Evaluation, p. 22, vol. XXII, July 1964.

23. "Utilization of a Low Voltage Accelerator for Neutron Radiography," by F. A. Iddings and N. A. Baxter, 7th Symposium of Nondestructive Evaluation of Components and Materials in Aerospace, Weapons Systems and Nuclear Applications, San Antonio, Texas, 1969.

24. "Problems in Precision Activation Analyses with Fast Neutrons," Kaman Nuclear, 1700 Garden of the Gods Road, Colorado Springs, Colorado 80907.

25. J. T. Black, "SEM: Scanning Electron Microscope", Photographic Applications in Science, Technology and Medicine, March 1970, p. 29.

26. J. R. Ryan and J. L. Cunningham, "Laser Microprobe Helps Identify Inclusions", Metal Progress, Dec. 1966, p. 100.

3.0 MECHANISM EFFECTS AND ANALYSIS STUDY

3.1 INTRODUCTION

The purpose of this study is to identify the mechanisms which may cause component failure and to perform a study of analytical methods directed toward predicting the long term performance of the component. Emphasis is placed on the long term performance of metal valve seats.

3.2 MECHANISM EFFECTS: LEAKAGE

The operational performance of valve leakage was evaluated with respect to the mechanisms that effect valve seat degradation. Figure 3-1 delineates these mechanisms in the form of a chart (tree) and in terms of their effects on the leakage limitations, which is the maximum allowable leak that the valve can sustain and still perform satisfactorily during the life of the mission.

The rationale for assigning the various mechanisms in the tree of Figure 3-1 is as follows: The primary factors that determine the leakage limitation are the leakage area and the type of leak. The type of leak can be further delineated in terms of the characteristics of the propellant and the operational requirements imposed by the mission. The leakage area is directly effected by the approach or effective closure between the valve seat and poppet, and the amount of waviness that is inherent in their mating surfaces. The approach is in turn governed by the load or force exerted when the valve is closed, the surface finish of the mating valve seat/poppet combination and particulate contamination which would not allow the surface to properly seat. The contamination can be generated elsewhere in the system, or it can be introduced either during assembly or from the propellant. Finally, the mechanism of corrosion, diffusion or wear during the operational life of the valve can affect the surface finish of the valve seat poppet interface by altering the finish itself or by introducing additional particulate contamination which again would interfere with the closure of the valve.

The effects on leakage (Figure 3-1) are expressed statically in that the mechanisms which effect leakage are defined in terms of the number of cycles or the total time that the valve has been operated. By redefining the leakage area, approach, surface finish and wear as a function of time, the leakage limitation can be expressed dynamically.

The number of molecules per unit time which can leak through a metal valve seat interface is within a three dimension domain; namely, length, breadth and depth. The length and breadth of the leak probably does not vary significantly compared to the depth. The depth is defined as the approach and is a function of surface geometry, yield stress and load. The length and breadth, however, are a function of the amount of material that is not in true contact. It is obvious that 100% true contact area would give zero leakage since all leak paths (depth) would be closed. This is a limiting case, however, an interesting one in that welded or fusion valve seats would offer such a solution. For the more practical valve seat geometries the true contact area is, for a given design and material, a strong function of load. Given a fixed load the true contact area does not affect leakage significantly, as does the closeness of approach.

What does affect leakage significantly is the closeness of approach at interface. This is a function of the initial surface topology (finish and waviness). However, the topology of the surface of hard metal seats will change significantly only in the wear of the surface asperities since these make up the contact points. The waviness affects the initial leakage rate but will not change to any extent due to wear. It should be noted, however, that reorientation of the poppet or seat may indeed change the approach. For example: waviness of the two surfaces may be of the same period and interlock, minimizing leakage while in the worst case the maximum amplitude of each wave may be additive.

3.3 TRUE CONTACT AREA

There are three valve seat contact areas that are interrelated: (1) apparent contact area, which is the geometrically measured area of the poppet and valve seat, (2) contour contact area, which is a function of the machining and surface waviness and the applied load, and (3) the real contact area, which is a function of the surface asperities and the contour contact area. It is convenient to express these contact areas in terms of dimensionless quantities as:[1]*

$$\eta_1 = \frac{A_r}{A_c}, \quad \eta_2 = \frac{A_c}{A_a}, \quad \eta_3 = \frac{A_r}{A_a}$$

where: A_r = real contact area

A_c = contour contact area

A_a = apparent contact area

Usually, the real area of contact is a relatively small portion of the contour area. For valves, the real contact area determines the relative ease of sealing although the applied load, the differential pressure across the valve seat and the viscosity of the gas or liquid and surface tension of the liquid also influence sealing. To a first approximation, the ratio η_1 may be expressed as

$$\eta_1 = b\, \varepsilon^\upsilon = b\left(\frac{a}{h_m}\right)^\upsilon$$

where: b, υ = constants determined by the surface finish, υ is usually 3, b is usually 5 to 10 with 10 representing the finest finish possible

ε = relative approach

a = true approach

h_m = maximum asperity height

For complex surface topologies, the contour area must be determined experimentally. In normal machining of fine finishes, the contour area usually assumes a hemispherical or semi-cylindrical surface waviness, and the contour area can be calculated from the Hertz relationship as follows:

---

*Numbers in parenthesis refer to the references listed at the end of this section.

(a) Hemispherical Waviness

$$A_c = \frac{C_1 R^{2/3} A_a^{1/3} L^{2/3}}{\ell^{2/3}}$$

where: C_1 = constant in the Hertz relationship
         R = radius of the wave
         L = applied load
         ℓ = distance between waves (wavelength)
         A_a = apparent contact area

(b) Semi-Cylindrical Waviness

$$A_c = \frac{C_2 R^{1/2} A_a^{1/2} L^{1/2}}{\ell^{1/3}}$$

where: C_2 = constant in the Hertz relationship

Thus, in the case of semi-cylindrical waviness, the contour area is less dependent on the distance between the peaks of the waves.

These results then allow the area of contact between two "rough" surfaces to be calculated. If the probability of contact between individual asperities is taken into account, then the relative area of contact is:

$$\eta_1 = \frac{K_1 b_1 b_2 (h_{m_1} + h_{m_2})}{\left(h_{m_1}\right)^{\upsilon_1} \left(h_{m_2}\right)^{\upsilon_2}} \cdot \epsilon^{\upsilon_1 + \upsilon_2}$$

where: h_{m_1}, h_{m_2} = maximum asperity height of surface 1 and 2, respectively

         k_1 = constant depending on υ_1 and υ_2, usually 0.05 for fine finishes

         $\upsilon_1, \upsilon_2, b_1, b_2$ = constants depending on the finish of the machined surface. υ usually equals 3, b usually equals 5-10, with 10 for finest finish

         ϵ = relative approach

3-5

These equations illustrate the necessity of machining the poppet and valve seat surfaces to the finest finish possible, in order to increase the real area of contact and provide maximum sealing capability.

3.4 CREEP

The equation for the total strain of a material under axial loading is:

$$\varepsilon = \varepsilon_E + \varepsilon_P + \varepsilon_T$$

where: $\quad \varepsilon_E = \dfrac{\sigma}{E} =$ elastic strain

$\quad\quad\quad \varepsilon_P = f(\tau, t) =$ plastic strain

$\quad\quad\quad \varepsilon_T = (\alpha \Delta T) =$ thermal strain

and $\quad\quad \sigma =$ axial (normal) stress

$\quad\quad\quad \tau =$ shear stress

$\quad\quad\quad E =$ Young's Modulus

$\quad\quad\quad t =$ time

$\quad\quad\quad \alpha =$ coefficient of linear expansion

$\quad\quad \Delta T =$ temperature change

The elastic and thermal strain can be considered to be reversible, so long as the thermal strain is not constrained to produce a significant stress. The plastic strain contains two functions; a time independent plastic strain which is irreversible and a time dependent plastic creep which is continuous. Thus, ε_P may be expressed as:

$$\varepsilon_P = C_1 \sigma^{n_1} + C_2 \sigma^{n_2}$$

where: $\quad C, n =$ constants from creep curve

$\quad\quad\quad \sigma =$ axial (normal) stress

The time independent function, $C_1\sigma^{n_1}$, is a function of the flaws and irregularities in atomic arrangement and, as such, is an approximate "probability function" of the amount of irreversible slip that occurs when a stress is applied. The time dependent function, $C_2\sigma^{n_2}$, is a function of the stress, temperature and time. Thus, depending on the stress level, the time under load and the temperature, either of the functions can dominate.

Kragelskii[1] has shown that the effect of creep, depending on the duration of static contact on a valve seat, can be a dominant function upon the real contact area and the frictional forces involved. Thus, the effect of creep on the large mechanical parts of the valve must be expanded to include the effect on the seat. For calculating the relative approach (or deformation) between two surfaces under a normal load:

$$\mu_t = \left[\mu_\infty^{\upsilon+1} - \left(\mu_\infty^{\upsilon+1} - \mu_0^{\upsilon+1}\right)e^{-t[r(\upsilon+1)]/[r/u+\upsilon]}\right]^{\frac{1}{\upsilon+1}}$$

where: μ_t = approach of surfaces at time t

μ_∞ = approach of surfaces after infinite long time

μ_0 = initial approach of two surfaces

r = relaxation time

υ = constant for surface finish (usually 3)

u = anelastic behavior of the metal

and

$$\mu_\infty = \frac{L(\upsilon+\omega)}{A_c bH}^{1/(\upsilon+\omega)}$$

where: b = constant for surface finish (usually 10)

ω = coefficient of work-hardening

L = normal load

H = plastic deformation

---

*Numbers in parenthesis refer to the references listed at the end of this section.

Then the relationship between the real contact area and the approach is

$$A_r = A_c b \mu_t{}^\upsilon$$

where: A_r = real contact area
          A_c = contour area

Thus, the real contact area is affected by the duration of contact, the separate physical and mechanical properties, and the geometric aspects of the machined surfaces. Since the force required to open and close the valve is dependent partially upon the surfaces, long durations when the valve is closed can have a deleterious effect from both an actuation time lag and increased frictional load if the seat materials and surface finish are not carefully considered.

3.5 WEAR

There are three main types of surface wear of valves during operation: (1) wear during elastic contact, (2) wear during plastic contact, and (3) wear during microcutting. If the contact is elastic, the surfaces will continue to operate in the elastic regime, and with no other processes occurring, the true contact area will remain essentially the same during the cycle life of the valve. If the contact is plastic, the repeated plastic contact between the surfaces will plastically deform the asperities and reduce their height and increase the radius. In the absence of any other process, the trend will continue until the contact becomes elastic, after which no further change will occur and the "worn-in" surfaces will continue to operate in the elastic regime. If the contact produces wear because of microcutting, the surfaces become damaged when an asperity penetrates into the bulk material, and the wear is considered to be catastrophic, since the operational cycle life diminishes rapidly (usually one cycle).

In both elastic and plastic contact, however, extraneous particles can be trapped between the surfaces and deform them sufficiently to change the contact mode. If the wrong choice of seat materials is made, this can also affect the wear characteristics.

The three equations which govern the type of wear, and the cycle life, are as follows:

(a) Wear during elastic contact

$$J_M = \frac{1.1\ (1-\mu^2)\ L\upsilon^{1/2}\rho}{K_2\ (\upsilon+1)\ En}$$

where: J_M = mass wear

μ = Poisson's ratio

L = load

υ = constant for surface finish (usually 3)

K_2 = constant for surface finish (usually 0.12)

E = elastic modulus of strongest surface

n = cycle life

ρ = average density of contacting materials

(b) Wear during plastic contact

$$J_M = \frac{\tan\theta\ L\rho\ (\varepsilon_t)^2}{2(\upsilon+1)\ H\ (2\varepsilon_{fail})^2} = \frac{\tan\theta\ L\rho}{2(\upsilon+1)Hn}$$

where: $\tan\theta$ = slope of asperities

L = load

ε_t = elongation for failure of weakest material after n cycles of loading

ε_{fail} = elongation for failure of weakest material after one cycle

$\left(\dfrac{2\varepsilon_{fail}}{\varepsilon_t}\right)^2$ = number of cycles

H = plastic deformation

(c) Wear during microcutting (n=1)

$$J_M = \frac{\tan\theta\ L\rho}{2(\upsilon+1)H}$$

3-9

Thus, by calculating the wear and wear particle generation, the operational life of the valve can be estimated.

Conversely, by knowing the load and the number of cycles the valve must operate, the amount of wear, from operation only, can be calculated. Since other extraneous factors and failure mechanisms are present, this estimation of operational life must be utilized with other calculations.

3.6 WEAR PARTICLE GENERATION

Wear particle generation in valves can be caused by particulate contamination on the seat surfaces, or by plastic contact of the surfaces. Rabinowicz[2] has shown that when the contact is plastic, wear particles can be generated due to asperity removal, and that these particles can cause additional damage.

The relationship between particle size and adhesive energy has been developed by E. Rabinowicz[3] at MIT and is given by the following equation:

$$d = 60 \ E \ W_{ab}/\delta_{yp}^{2}$$

where: d = the average diameter of the wear particle

E = Young's modulus

δ_{yp} = yield stress of the material in compression

W_{ab} = the work of adhesion of the materials a & b in contact and is further defined as:

$$W_{ab} = \gamma_a + \gamma_b - \gamma_{ab}$$

where: γ_a = surface free energy of material a per unit area

γ_b = surface free energy of material b per unit area

γ_{ab} = interface free energy per unit area.

It has been found that δ_{yp} is about one-third the hardness P and that $\delta_{yp/E}$ is about 3×10^{-3} for many materials, then:

$$d = 60,000 \ W_{ab}/P$$

Experimental results showing the relation between material and the average wear particle diameter obtained by E. Rabinowicz[3] are presented in Table 3-1.

Table 3-1. Average Wear Particle Size Under Ambient Atmosphere for Different Materials

Metal	$P \frac{dynes}{cm^2}$	$W \frac{ergs}{cm^2}$	d cm
Lead	4×10^8	440	270×10^{-4}
Tin	6	540	120 "
Bismuth	12	375	50 "
Cadmium	23	600	320 "
Aluminum	30	900	140 "
Zinc	30	750	440 "
Copper	60	1100	250 "
Brass	120	700?	180 "
Mild Steel	200	1000	60 "
Iron (Oxide)	2000?	600?	1 "
Aluminum (Oxide)	2000	900	1 "
Teflon	4	15?	90 "
Nylon	20	30?	? "
Silver	80	920	330 "
Nickel	260	1650	35 "
Glass	550	200?	1 "

Another assumption made is that the wear particle size generated at any given cycle is equal to the surface finish or mean asperity height characterized by the surface of the softer seat. The wear particle size d given by the above equation is the equilibrium size. That is, the particle tends to a certain size and remains at that size. Also the surface finish will generate to a finish equal to the equilibrium size. This equilibrium surface is then the final surface characterized after "wear in", independent

of the initial surface condition. In most cases, a valve seat finish is very fine, ranging about 2 rms or greater. If we assume an initial surface finish of .05 microns (2 rms) and using an iron oxide surface model it can be seen the average wear particle will eventually "wear in" to 1.0 micron. The corresponding finish will be 40 rms. For a valve seat this is a severely rough surface and leakage would be considered gross.

What needs to be known is the generation of wear particle diameter as a function of cycles. Using the above example the 40 rms finish may require a cycle "wear in" of an unrealistic number considering the life usefulness of the valve.

It is important to consider the effect of the reactivity of the environment on the wear particle size. The more reactive the environment the smaller the wear particle. This effect is illustrated in Table 3-2 using copper-copper surfaces in various environments. In vacuum the wear particle would be quite large. For a reactive propellant such as fluorine or oxygen difluoride the wear particle should be smaller than those listed in Table 3-1. However, for the fuels such as diborane the wear particle size should be greater indicating a better leakage performance characteristic of metal valve seats for the oxidizer over the seats used with the fuel.

The design implications of the foregoing analysis are apparent. The use of harder seat materials will result in smaller wear particles and subsequently the wear process will result in finer surface finishes. This has previously been reported in Reference 4. By selecting a seat material with a characteristic small wear particle size it should be possible to predict the final surface finish after N cycles. If the surface finish is approximately equal to the wear particle size for a given seat material combination then prediction is easily obtained. However, it appears that surface roughness can be much smaller than the average wear particle size reported in Table 3-1. Therefore, the initial performance of the valve seal should be better than at "wear-in." It remains to develop a relation between wear particle size as a function of cycle life. In addition, the equilibrium wear particle size of a material exposed to the propellant needs to be determined.

Table 3-2. Effect of Environment on the
Average Wear Particle Size

Environment	Average Particle Diameter Copper-Copper Surfaces Micrometers
Nitrogen	480
Helium	380
Carbon Dioxide	300
Dry Air	224
Oxygen	201
Laboratory Air	177
Wet Air	144
Cetane	12
Silicone DC 200-100 cst.	9.5
Ucon Fluid LB-70X	9.5
Palmitic Acid in Cetane	8.0

Surface roughness and wear particle generation criteria can be used for the leakage model only by assuming that the surfaces at the interface conform in curvature (or flatness) within the dimensions of the minimum surface roughness. If the conformity is larger than the surface roughness the dominant leakage area will be the gaps produced by waviness of the surfaces and will undoubtedly be much higher. This design implication favors the use of flat surface geometry for thick seats which can be most easily fabricated with present day fabrication techniques. The use of thin elastic seats such as the lip seal can be made to conform to the poppet, however, the conformity on a micro level is not well known.

Wear fragments can also be transferred from one material to the other contacting element. Adhesive fragments take the form of semiellipsoids of dimensions approximately 1.0×10^{-3} to 4.0×10^{-3} cm wide. The proportion of length and height will be 1.7 and 0.5 times its width[5] The amount of adhesive wear is generally proportional to the normal load at the interface. Adherent wear fragments can be important since surfaces can be roughened by this process.

An example of the analysis that may be applicable to predicting cycle life vs. surface roughness is given in the following:

Assuming a spherical wear particle is removed for each junction on the valve seat surface, the volume removed is:

$$V_i = \frac{N_i}{6} \pi D_i^3$$

where N_i is the number of junctions and D_i is the diameter of the wear particle generated during the first cycle.

In the same manner:

$$V_e = \frac{N_e}{6} \pi D_e^3$$

where N_e is the number of junctions and D_e the wear particle diameter generated at equilibrium.

Also, $N = \frac{4L}{\pi p D^2}$ where L is the normal load, p the penetration hardness and D is taken here to equal the diameter of the junction interface and equal to the wear particle size at any given cycle.

Further assuming that each cycle removes an equal volume (or mass) of material (not verified), then:

$$C_e = \frac{V_e - V_i}{V_i} \quad \text{cycles to equilibrium or}$$

$$C_e = \frac{V_e}{V_i} - 1 \quad \text{or}$$

$$C_e = \frac{D_e}{D_i} - 1$$

Taking the initial finish at $.05\mu$ and using the aluminum oxide average wear particle to be 1μ

$$C_e = \frac{1}{.05} - 1 = 19 \text{ cycles}$$

Another expression of the number of cycles to equilibrium would relate the number of junctions which must be destroyed (or created) to equal one junction of the same area. This assumes the real area of contact is always constant.

$$A_r = \frac{\pi d_i^2}{4} N_i = \frac{\pi d_e^2}{4} N_e$$

$$N_i = \frac{d_e^2}{d_i^2} N_e$$

where N is the number of junctions and d is the diameter of the loose particle generated. The subscripts i and e are representative of the first cycle and at equilibrium.

The total adhesive energy for a given set of junctions is:

$$W = \frac{d \, P}{60,000} N$$

The adhesive energy required to change N_i junctions of average diameter d_i to N_e junctions of average diameter d_e is:

$$\Delta W = \frac{d_i P}{60,000} \frac{d_e^2}{d_i^2} N_e - \frac{d_e P}{60,000} N_e$$

Assuming only one junction at equilibrium, then:

$$\Delta W = \frac{P}{60,000} \frac{d_e}{d_i} (d_e - d_i)$$

(8)

Further assuming that an equal adhesive energy is used to create a wear particle per cycle, then:

$$C_e = \frac{\frac{d_e}{d_i} (d_e - d_i)}{d_i} = \frac{d_e}{d_i} \left(\frac{d_e}{d_i} - 1\right)$$

(9)

Taking d_e to be 1.0μ and d_i to be .05μ

(10)

$$C_e = 20(19) = 380 \text{ cycles}$$

The above analyses are presented as illustrative only and should not be taken as accurate. The assumptions made in the analyses were not verified by test or documented by others.

3.7 WEAR PARTICLE GROOVING

As wear particles are generated or when particle contaminants from other parts of the system are introduced at the contacting surfaces, the volume dV swept out by particles sliding dx along a surface is[6]:

$$\frac{dV}{dx} = L \frac{\overline{(\tan \theta)}}{P}$$

where: L = total load

$\overline{\tan \theta}$ = weighted average of the tangents of all the roughness angles of the particles

P = penetration hardness of the surface

By measuring particles, as they are generated as a function of cycle life, the amount of grooving that is occurring on the contacting surfaces can be estimated and correlated with the actual grooving that has occurred in the component.

3.8 ASPERITY INTERACTIONS

The above variables can be summarized in another manner[7] by the following table which illustrates the main types of events which can occur between asperities in contact.

Table 3-3. Main Types of Asperity Interactions

Nature of Deformation	Elastic Displacement	Plastic Displacement (Repeated Deformations)	Cutting of the Material (Grooving)	Destruction of Surface Films	Destruction of Bulk Material
Number of cycles, n, leading to failure of base material	$n = \infty$	$1 < n < \infty$	$n \rightarrow 1$	$n \rightarrow 1$	$n = 1$
Conditions	$\frac{h}{R}^{a}$ <0.01 (ferrous metals) $\frac{h}{R}$ <0.0001 (non-ferrous metals)	$\frac{h}{R}$ <0.1	$\frac{h}{R}$ <0.1	$\frac{d\tau}{dh}^{b}$ >0	$\frac{d\tau}{dh}$ < 0

a $\frac{h}{R}$ = ratio of asperity height h to radius of curvature R

b $\frac{d\tau}{dh}$ = variation of shear strength, τ, with depth, h, below the surface

3-17

3.9 FATIGUE

The mechanism by which cracks form and grow during cyclic loading has been the subject of much investigation and many theories. The theory which seems to satisfactorily explain many fatigue phenomena is unbonding as a result of reversed slip[8].

The basic assumption of the theory is that some atoms must become unbonded when slip occurs at a free surface. During the next cycle, more atoms become unbonded, and under cyclic loading progressive unbonding occurs along a slip plane. After a number of cycles, N, at a cyclic strain loading $\pm \sigma$, a critical crack of depth h_o develops and fatigue failure occurs.

Then
$$h_o = NC\sigma^x$$

where: h_o = critical crack depth
          C = constant
          N = total number of cycles
          x = slope of S-N curve on log-log paper

Rearranging:
$$\sigma = \frac{B'}{N^{1/x}}$$

where: $B' = \dfrac{h_o}{C}$ = stress intercept at N=1 (ultimate stress)

Thus, for a given stress-cycle fatigue curve (S-N curve), the design parameters for predicting the fatigue life of the component are available.

There are some components, however, that are subjected to loadings of variable amplitude. It is possible to utilize results obtained from constant stress amplitude tests by determining an equivalent stress (reduced stress) σ_r, which would have the same overall effect as the variable loading. Thus, the stress σ_r, applied at constant amplitude, would cause failure at the same number of cycles N.

To develop this concept, represent the stress loading by a spectrum of certain stresses σ_i which will be applied N_i times during the service life of the component. It is assumed that the stress loadings are randomly applied; i.e., the loading will not consist of σ_1 applied N_1 times, followed by σ_2 for N_2 times, etc. Thus, under phase random conditions the amount of crack growth contributed by each stress level σ_i will be assumed to be governed by the rate of crack growth at that level and for N_i loadings.

The rate of crack growth per cycle is:

$$\frac{dh}{dn} = C\sigma^X$$

and the total crack growth is:

$$h = \Sigma \, C\sigma_i^X \, n_i$$

The equivalent stress will give the same crack depth if applied the same total number of times, thus:

$$h = C\sigma_r^X \, \Sigma n_i$$

Solving for σ_r gives:

$$\sigma_r = \left(\frac{\Sigma \, \sigma_i^X \, n_i}{\Sigma \, n_i} \right)^{1/x}$$

If there is a definite endurance limit, all values of stress below this value should be neglected.

An alternative method of predicting fatigue failure is based on life (N) rather than stress. If the equation $h = \Sigma C\sigma_i^X \, n_i$ is expanded, then

$$h_o = C\sigma_1^X \, n_1 + C\sigma_2^X \, n_2 + \ldots$$

If any one of these stresses were to be applied at constant amplitude, the same crack depth at failure would be reached when: $C_{\sigma_i}{}^X N_1 = h_o$, $C_{\sigma_2}{}^X N_2 = h_o$, etc. By dividing the two equations by h_o and substituting,

$$\frac{n_1}{N_1} + \frac{n_2}{N_2} + \frac{n_3}{N_3} + \ldots = 1 \text{ or } \Sigma_n{}^i = \sum_{n=o}^{i} \frac{n_i}{N_i} = 1$$

Therefore, the fractions of life used up at any given stress amplitude will add up to unity at failure.

These methods of predicting fatigue failure (fatigue life) are best utilized by specifying the required life, and then predicting an allowable stress with the aid of the S-N fatigue curves. Then, by utilizing the interferometric holographic signature to determine that the actual stress levels are within the predicted limits, the service life can be verified.

Although the above mechanism by which cracks form is currently accepted theory, the results of other investigators show that modified mechanisms relative to the fatigue limit should not be ignored. Tests conducted in vacuum have shown that the cyclic life of parts are greatly improved compared to cyclic testing in atmosphere. These results led to the theory that oxidation of the atoms at small cracks and openings causes further crack growth. The oxides tend to create stresses at the crack during that cycle which tends to close the crack. That is, the crack cannot close because of the oxides and leverage is exerted against the crack causing further openings which in turn become oxidized during subsequent cycling. This theory may have importance in developing accelerated test methods for determining the long term performance of components and elements subject to fatigue failure. The recommended approach would include the use of reactive fluids (oxidizers) to cyclic elements to accelerate the mechanism. The mechanism of chemical reactivity can also be accelerated by increasing temperature. In the case of reducing agents (fuels) similar chemical reactivity testing could be accomplished to determine what effects fuels have on cyclic fatigue. Vacuum or inert fluids could be used as the test environment to establish a base for comparison.

3.10 CORROSION

Although corrosion is primarily a function of the materials and the
environment in which they are placed, the effect of corrosion can be
critical to the functionality of the components. In particular, leakage,
structural integrity, and contamination buildup may be directly
relatible to corrosion.

Corrosion and/or film formation in general (in terms of thickness y as a
function of time t) can be expressed by one of three general equations[7].

$$\text{(a)} \quad \text{Linear} \qquad y = k_1 t + k_2$$

$$\text{(b)} \quad \text{Logarithmic} \qquad y = k_3 \log k_4 t + k_5$$

$$\text{(c)} \quad \text{Parabolic} \qquad y^2 = k_6 t + k_7$$

where: y = corrosion thickness

t = time

k_{1-7} = constants for a particular reaction

Depending upon the corrosion mechanism, the formation of corrosion products
or films can lead to different types of failures. In linear corrosion, the
layer formed presents no barrier to further growth, and can continue to
become thicker. Since the adhesion of the corrosion layer to a metal surface
decreases as its thickness increases, the layer will be removed when it
reaches a critical thickness. Thus, if the layer is between the contacting
surfaces of the valve, the corrosion layer will be removed after it has
reached the critical thickness. Regrowth will occur, with subsequent
sloughing of the layer and generate wear debris which either remains on
the valve seat or is transported downstream and becomes a source of con-
tamination and a potential failure mode.

In the other two cases, the initial film slows the solid/corrodent inter-
action. Interaction of the substrate with the corrodent must take place
by migration of corrodent through the corrosion layer to the metal interface,
or by migration of metal species through the corrosion layer to the corrodent-
layer interface. Both mechanisms can operate simultaneously.

In these cases, either wear particle or debris generation can occur, or the mating surfaces of the poppet/valve seat can become mismatched due to deposit buildup and cause the valve to leak.

These mechanisms have been treated in great detail either in general terms or as applied to specific systems. In some instances, theory and experiment are in agreement; however, many questions remain unsettled. It is of particular interest, for example, to know the role of the initial stages of film formation in the subsequent film growth corrosion. Some of the microsignature techniques can be applied to this problem.

An equation exists which can give qualitative results on long term corrosion rates using measurements which are carried out over a period of hours. This equation expresses corrosion rates in mils per year as a function of weight loss in hours, as follows:

$$\text{mil/year} = \frac{3.449 \times 10^6 W}{DAT}$$

where:

W = weight loss of substrate in grams
D = specific gravity of substrate
A = area of substrate in cm^2
T = duration of test in hours

Thus, by making several measurements, a general idea of the corrosion behavior of the component can be made, and the effect on its functionality can be estimated. It must be emphasized that this equation gives an over-all corrosion rate and does not differentiate between the various types of corrosion (e.g., general surface as opposed to pitting corrosion). Thus, specific measurements of the component surface must be made to ascertain the type of corrosion occurring.

3.11 ANALYSIS

The objective of this analysis is to investigate the effect of varying the controlling variables affecting valve leakage which may be used to develop accelerated test procedures. Leakage rate is first introduced followed by the development of a leakage model. A scaling investigation was performed to determine the scaling laws which may govern certain modes of valve seat degradation.

The scaling investigation was performed by applying the theory of dimensional analysis. This results in the computation of a set of nondimensional "numbers" or groupings of variables which are used to derive the scaling laws. A computer program was developed under this project which performs the algebra necessary to transform the set of dimensional variables to a set of non-dimensional variables or pi terms.

3.11.1 Leak Rate

The leak rate of a valve is a function of all the other surface mechanisms, and as such (except for initial gross mismatch of the poppet/valve seat) is a dependent variable. However, the operational lifetime of a valve is dependent upon its leak rate, and for this reason is included as a primary failure mechanism.

The leak rate failure mode in a valve is either by permeation leakage or leakage through an open passage. Permeation leaks are a function of both the permeable material and the fluid or gas that is leaking. Since permeation is usually specific, from the standpoint of the materials, pressure differentials, temperature, etc., the leakage is usually empirically determined from the equation

$$Q_p = \frac{DSAt \ \Delta P}{\ell}$$

where: D = diffusion coefficient
         S = solubility coefficient
         A = permeation area
         t = time
         ΔP = differential pressure
         ℓ = permeation path length

3-23

Leakage through an open passage is usually molecular or laminar. The three equations that govern these types of gas leaks are as follows[9, 10]:

(a) Molecular Flow (long circular hole)

$$Q_g = \frac{\sqrt{2\pi}}{6} \sqrt{\frac{RT}{M}} \frac{d^3}{\ell} (P_2 - P_1)$$

where: R = gas constant

           T = absolute temperature

           M = molecular weight of gas

           d = hole diameter

           ℓ = leak path

           P_2 = upstream pressure

           P_1 = downstream pressure

(b) Molecular Flow (small path entrance)

$$Q_g = \frac{1}{\sqrt{2\pi}} \sqrt{\frac{RT}{M}} A (P_2 - P_1)$$

where: A = cross sectional area of hole

(c) Laminar Flow

$$Q_g = \frac{\pi}{8} \left(\frac{d}{2}\right)^4 \frac{Pa}{\eta\ell} (P_2 - P_1)$$

where: $P_a = \dfrac{P_1 + P_2}{2}$

           η = absolute gas viscosity

To convert from one gas to another for molecular or laminar flow, the equations are as follows:

(d) Molecular Flow

$$\frac{Q_{g_1}}{Q_{g_2}} = \left(\sqrt{\frac{T_1}{T_2}}\right)\left(\sqrt{\frac{M_2}{M_1}}\right)\left(\frac{\Delta P_1}{\Delta P_2}\right)$$

where the subscripts refer to gas 1 and gas 2.

(e) Laminar Flow

$$\frac{Q_{g_1}}{Q_{g_2}} = \left(\frac{\eta_2}{\eta_1}\right)\left(\frac{P_2^2 - P_1^2}{P_4^2 - P_3^2}\right)$$

where the upper pressure term is for gas 1 and the lower pressure term is for gas 2.

It is assumed in both cases, that if a change in pressure occurs, the flow mode remains the same. If the flow mode appears to change, then the following correlations are recommended:

(1) for pressure increase, calculate as laminar flow
(2) for pressure decrease, calculate as molecular flow
(3) for change in gas, calculate as molecular flow

Modification of these equations for predicting liquid leakage is as follows:

(f) $Q_\ell = \dfrac{\eta_g}{\eta_\ell}\ \dfrac{Q_g}{P_a}$

This equation is correlatible to both laminar and molecular flow.

However, the effect of surface tension, the possibility of transition from a liquid on one side to a gas at the exit, and any viscosity changes make the interpretation and utilization of the equation difficult, and will predict a larger liquid leakage than is present for molecular flow.

3.11.2 Scaling Analysis

Initially, the dimensional analysis was applied to a simple failure/ degradation mechanism which is assumed to be essentially independent of time. This mechanism, which is plastic and/or elastic deformation of a valve seat, will be discussed in more detail later. The purpose of this section is to simply consider the important variables which pertain to this mechanism and to nondimensionalize these variables.

In order to determine the important variables which influence the leakage flow through a valve which displays elastic/plastic deformation, the mechanism must be explored. A study of this process has suggested that the valve deformation is quite sensitive to surface "waviness" which is defined as the relatively long wave length convolutions that are caused by machining of the valve face and falve seat as illustrated in Figure 3-2.

Scaling Investigation: Plastic Deformation and Valve Leakage

A preliminary scaling investigation was performed in order to derive the nondimensional groupings which govern the wear and degradation of the sealing surfaces of a simple poppet valve. These nondimensional groupings can be used to derive scaling laws which will lend some insight into the life span of the valve.

By inspection of Figure 3-2 and some intuitive reasoning, the variables given in Table 3-4 can be established as those which may influence valve leakage and the elastic or plastic deformation of the valve seat.

These variables may now be rearranged in terms of the critical dependent and independent variables. For this purpose the variables; namely, fluid viscosity, valve force and diameter are chosen since these are easily varied test parameters. All the variables can be listed in matrix form in terms of the exponents of the basic units. This matrix, given in Table 3-5, is then transformed to the diagonal form of Table 3-6.

a) VALVE CONFIGURATION

b) EFFECT OF WAVINESS

c) CLOSE UP OF CONTACT AREA
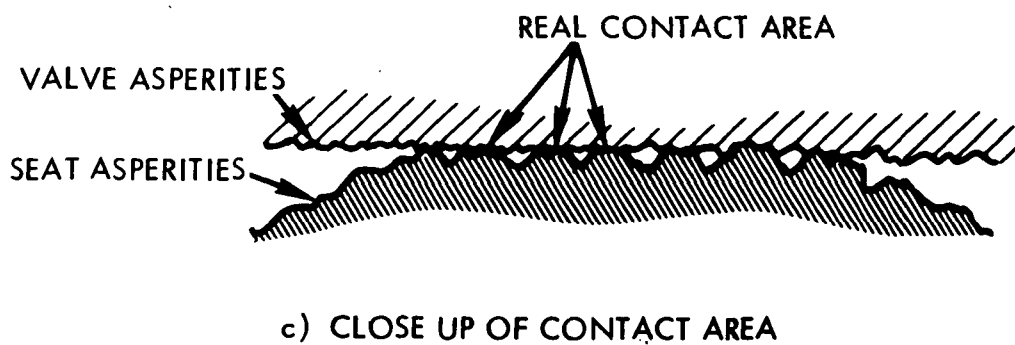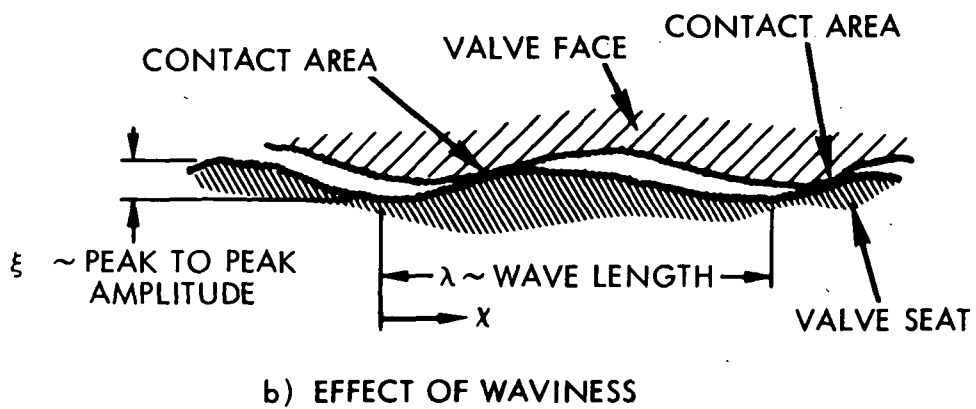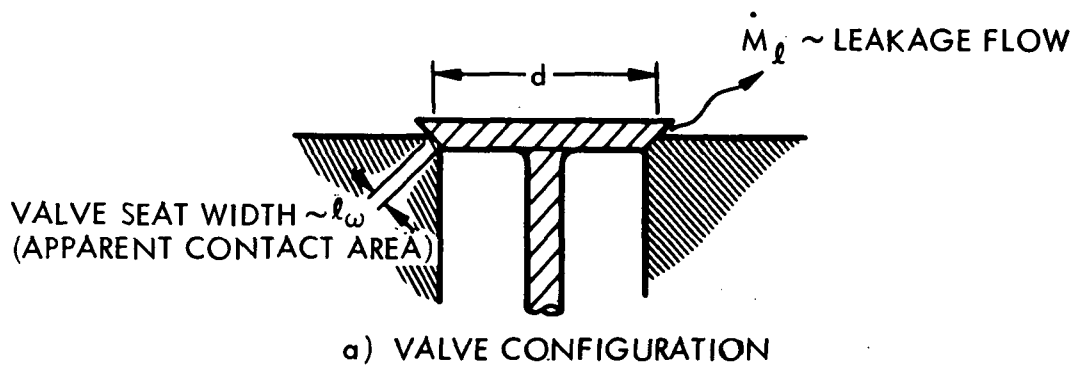
Figure 3-2. Valve Leakage Model

Table 3-4. List of Critical Variables

SYMBOL	VARIABLE	UNITS
θ	Characteristic Valve Angle (i.e., seat angle)	-
ℓ_w	Characteristic Valve Seat Width	L
A	Seating Area (apparent, contact & real)	L^2
q_b	Normal Bearing Stress (apparent, contact & real)	M/Lt^2
σ_y	Yield Strength of Softest Material	M/Lt^2
H	Surface Hardness of Softest Material	M/Lt^2
E	Elastic Modulus of Softest Material	M/Lt^2
ξ_{ms}	RMS Asperity Amplitude (Std. Deviation of Asperities)	L
η_{ms}	RMS Waviness Amplitude (Std. Deviation of Waves)	L
$\bar{\lambda}$	Mean Wavelength of Surface Waves	L
$\bar{\beta}$	Mean Radius of Curvature of Asperities	L
$\dot{m}$	Mass Flow	M/t
ρ	Density	M/L^3
υ	Fluid Kinematic Viscosity	L^2/t
μ	Fluid Absolute Viscosity	M/Lt
P	Fluid Pressure	M/Lt^2
F	Force	ML/t^2
d	Valve Diameter	L
W_{AB}	Work of Adhesion	M/t^2
Q_g	Pressure-Volume Flow	ML^2/t^3
μ	Chemical Potential	M/Tt^3
A_L	Leakage Area	L^2
E_e	Energy Input	ML^2/t^2
CL	Cycle Life	t
CR	Cycle Rate	t^{-1}

Table 3-4. List of Critical Variables
(continued)

SYMBOL	VARIABLE	UNITS
$\dot{w}$	Wear Rate per Unit Area	M/L^2t
m	Mass Removed	M
C	Corrosion Rate	L/t
S	Entropy	ML^2/Tt^2
∇	Momentum	ML/t
ε	Approach	L
σ	Surface Tension	$M\,t^2$
D_L	Equilibrium Particle Size	L
θ/v	Friction Temperature	Tt/L
T	Temperature	T

Table 3-5. Dimensional Matrix

UNITS		1	2	3	4	5	6	7	8	9	10	11	12	13	14	15	16
		ℓ_w	A	q_b	σ_y	H	E	η_{rms}	ξ_{rms}	$\bar{\lambda}$	$\bar{\beta}$	$\dot{m}$	ρ	P	μ	F	d
	M	0	0	1	1	1	1	0	0	0	0	1	1	1	1	1	0
	L	1	2	-1	-1	-1	-1	1	1	1	1	0	-3	-1	-1	1	1
	t	0	0	-2	-2	-2	-2	0	0	0	0	-1	0	-2	-1	-2	0

Table 3-6. Derivation of Nondimensional π Groups

i	1 ℓ_w	2 A	3 q_b	4 σ_y	5 H	6 E	7 η_{rms}	8 ξ_{rms}	9 $\bar{\lambda}$	10 $\bar{\beta}$	11 $\dot{m}$	12 ρ	13 P	14 μ	15 F	16 d	π_i
1	1													0	0	1	ℓ_w/d
2		1												0	0	2	A/d^2
3			1											0	-1	2	$q_b d^2/F$
4				1										0	-1	2	$\sigma_y d^2/F$
5					1									0	-1	2	Hd^2/F
6						1								0	-1	2	Ed^2/F
7							1							0	0	-1	η_{rms}/d
8								1						0	0	-1	ξ_{rms}/d
9									1					0	0	-1	$\bar{\lambda}/d$
10										1				0	0	-1	$\bar{\beta}/d$
11											1			-1	0	-1	$\dot{m}/\mu d$
12												1		-2	1	0	$\rho F/\mu^2$
13													1	0	-1	2	Pd^2/F

The pi terms can be used to derive certain scaling laws which relate the "model" (i.e., subscale) test values to the "prototype" (i.e., full scale) test values. These scaling laws are simply expressed as simple ratios of the model value to the prototype value for each variable. Thus, the scale factor for the variable x is written:

$$\Lambda_x = \frac{x_m}{x_p} = \frac{\text{model value of variable x}}{\text{prototype value of variable x}}$$

The scale factors are derived by equating the model and prototype pi terms. For example, the length scale factor is obtained by equating the model and prototype values of the pi terms π_1, π_7, π_8, π_9, and π_{10}:

$$(\pi_1)_m = (\pi_1)_p, \quad (\pi_7)_m = (\pi_7)_p, \quad (\pi_8)_m = (\pi_8)_p,$$

$$(\pi_9)_m = (\pi_9)_p, \quad (\pi_{10})_m = (\pi_{10})_p$$

Hence:

$$\Lambda_d = \Lambda_{\eta_{rms}} = \Lambda_{\zeta_{rms}} = \Lambda_{\overline{\lambda}} = \Lambda_{\overline{\beta}}$$

Therefore, the valve must be scaled in the same way as the waviness and surface asperities.

3.11.3 Derivation of Leakage Area

The objective of this section is to derive an expression for the average leakage area for a typical valve seat interface. This analysis applies to a perfectly rigid flat surface which is in contact with a deformable surface with random irregularities. Consider the sketch of the surface leakage geometry given in Figure 3-3. The total average leakage area is simply the sum of the individual leakage areas:

$$\overline{A} = \sum_{k=1}^{N} \overline{A}_k \tag{1}$$

where: $\overline{A}_k$ = average leakage area for the kth leakage segment
$\overline{A}$ = total average leakage area for entire surface

This expression is valid for both independent and dependent random variables. It is based on the statistical theorem that the sum of the mean equals the mean of the sum for any combination of stationary random variables.

The average leakage area for the kth leakage segment can be determined from the knowledge of the average gap and irregularity amplitude for the kth segment. The instantaneous leakage area is given by the following non-linear function:

$$A_i = \begin{cases} 0 & \xi_k \geq h \\ -\Delta\ell(\xi_k - \overline{h}) & \xi_k < h \end{cases} \tag{2}$$

where: $\Delta\ell$ = peripheral length of each segment

It is seen in Figure 3-4 that the leakage gap is divided into n segments of equal length $\Delta\ell$. The leakage through each segment is controlled by the surface contact variable, which is defined as follows for the kth leakage segment:

$$\xi_k(x) = \xi_k(x) - \overline{h} \tag{3}$$
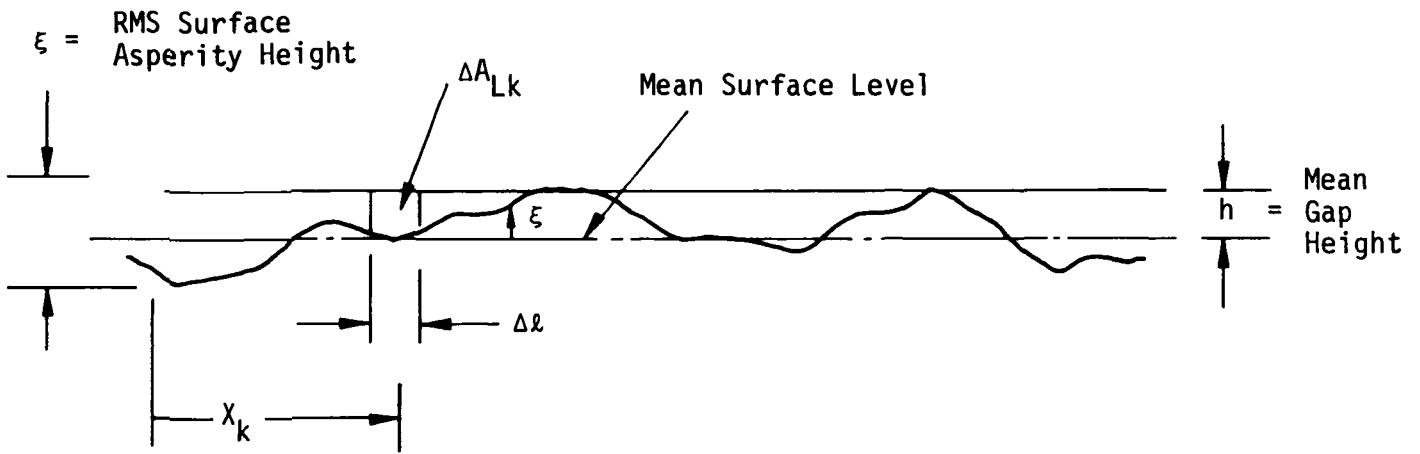
Figure 3-3. Leakage Geometry
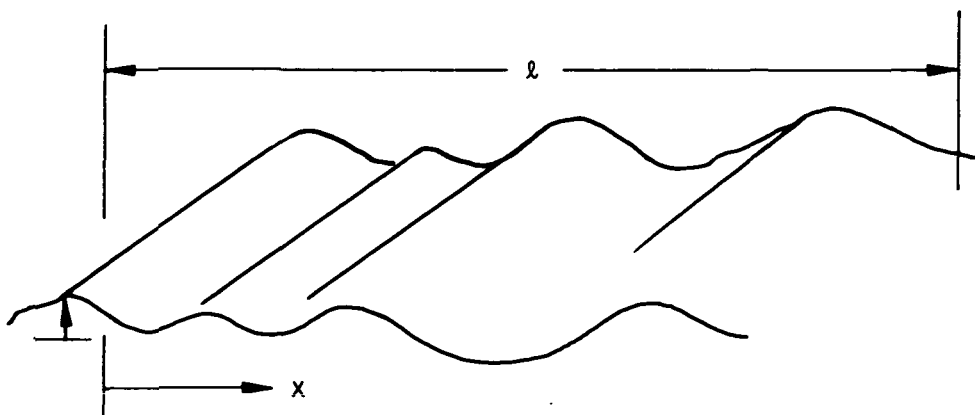
Figure 3-4. One Dimensional Random Surface

where: $\xi_k(x)$ = contact variable for k^{th} leakage segment

$\xi_k(x)$ = surface irregularity amplitude at k^{th} leakage segment

$\bar{h}$ = average leakage gap

The sign of the surface contact variable indicates the occurrence of leakage at the kth segment. Leakage occurs when the sign is negative:

$$\xi_k(x) > 0 \quad \rightarrow \quad \text{No leakage at } k^{th} \text{ leakage segment}$$

$$\xi_k(x) < 0 \quad \rightarrow \quad \text{Leakage occurs at the } k^{th} \text{ segment}$$

This statement can be written in terms of the surface irregularity amplitude at the kth segment:

$$\xi_k(t) < \bar{h} \quad \rightarrow \quad \text{Leakage occurs at } k^{th} \text{ segment}$$

In the case of random surface irregularities, the irregularities are described by the power spectral density, S_o.

Since each irregularity amplitude is assumed to be a stationary random variable with zero mean value, the root-mean-squared value is equal to the standard deviation which is obtained from the integrated spectrum:

$$(\xi_k)_{rms} = \sigma_k = \left[\int_0^\infty S_k(\Omega) \, d\Omega \right]^{1/2} \tag{4}$$

This non-linear relationship between the random irregularity amplitude, ξ_k, and the random leakage area, $\bar{A}_k$, will be used to determine the probability density function (PDF) of A_k. The PDF of the random leakage area is required so that the average value can be computed from its first moment:

$$\bar{A}_k = E(\bar{A}_k) = \int_{-\infty}^\infty g(A_k) \, A_k \, d A_k \tag{5}$$

where: $E(\bar{A}_k)$ = Expected value (i.e., mean value) of random variable A_k

$g(A_k)$ = Probability Density Function (PDF) of random variable A_k

The required PDF, $g(A_k)$, can be obtained from a non-linear transformation of the PDF of the relative motion variable, ξ_k. For a general, single valued, strictly increasing functional relationship [i.e., $A_k = \alpha(\xi_k)$], the transformation can be accomplished from the following equation as given by Reza[11]:

$$\begin{cases} g\ (A_k) & 0 & ,\ A_k \leq \alpha(-\infty) \\ g\ (A_k) & = \left| \dfrac{\partial \xi_k}{\partial A_k} \right| f\ (\xi_k),\ \alpha(-\infty) < A_k < \alpha(\infty) \\ g\ (A_k) & = 0 & ,\ A_k \geq \alpha(+\infty) \end{cases} \tag{6}$$

where: $f(\xi_k)$ = PDF of variable ξ_k

This transformation can now be applied to the normal (Gaussian) distribution with zero mean which describes ξ_k:

$$f(\xi_k) = \frac{1}{(2\pi)^{1/2}\ \sigma_k}\ e^{-\xi_k^2/2\sigma_k^2} \tag{7}$$

Applying equation (6) with $\alpha(\xi_k)$ yields the PDS of the random leakage area:

$$g\ (A_k) = \begin{cases} 0 & A_k < 0 \\ \dfrac{1}{\Delta \ell}\ f\left(\dfrac{A_k}{\Delta \ell}\right) & A_k \geq 0 \end{cases} \tag{8}$$

$$g\ (A_k) = \begin{cases} 0 & A_k < 0 \\ \dfrac{1}{(2\pi)^{1/2}\ \sigma_k\ \Delta\ell}\ e^{-1/2\sigma_k^2\left(\frac{A_k}{\Delta\ell} - \bar{h}\right)^2} & A_k \geq 0 \end{cases} \tag{9}$$

The PDF is sketched in Figure 3-5. Note that an impulse function with area $K_1(h)$ is required at the origin to insure that $\int_{-\infty}^{\infty} g(A_k)\ dA_k = 1$. This is a requirement for all probability density functions.

Non-Linear Function

Output PDF

Input PDF
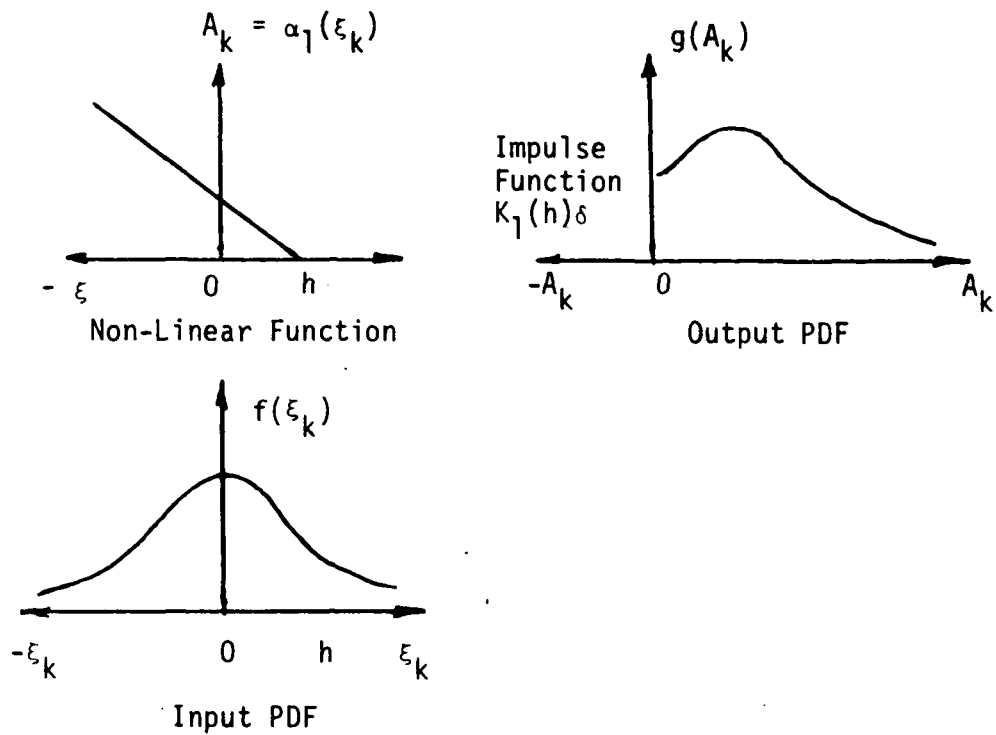
Figure 3-5. Probability Density Function for Leakage Area

The average leakage area is given by the following integral, which results from substitution of equation (9) in equation (5):

$$\bar{A}_k = \frac{\Delta \ell}{\sigma_k (2\pi)^{1/2}} e^{-\frac{1}{2} h^2 \sigma_k^{-2}} \int_0^\infty \xi_k e^{-\frac{1}{2} \xi_k^2 \sigma_k^{-2}} e^{h \xi_k \sigma_k^{-2}} d\xi_k \quad (10)$$

This definite integral can be evaluated by use of Laplace transform theory. Consider the following Laplace transform:

$$I_1 = \int_0^\infty x e^{-\alpha^2 x^2} e^{-sx} dx = L\left[x e^{-\alpha^2 x^2}\right]$$

$$I_1 = \frac{1}{2\alpha^2} - \frac{(\pi)^{1/2}}{4\alpha^3} s e^{s^2/4\alpha^2} erfc\left(\frac{s}{2\alpha}\right) \quad (11)$$

The above integral can be related to the desired integral by substituting $s = -h\sigma_k^{-2}$ and $\alpha = (1/2)^{1/2} \sigma_k^{-1}$. Therefore, the solution can be written:

$$\bar{A}_k = \frac{\Delta\ell\, e^{-\frac{1}{2}h^2\sigma_k^{-2}}}{\sigma_k(2\pi)^{1/2}} \left[\sigma_k^2 + \frac{(2\pi)^{1/2}}{2}\, \bar{h}\sigma_k\, e^{1/2h^2\sigma_k^2}\, \mathrm{erfc}\left(-\frac{\bar{h}}{\sqrt{2}\sigma_k}\right)\right] \quad (12)$$

Since the error function is an odd function, the following simplification can be written for the complimentary error function:

$$\mathrm{erfc}\left(-\frac{\bar{h}}{\sqrt{2}\sigma_k}\right) = 1 - \mathrm{erf}\left(-\frac{\bar{h}}{\sqrt{2}\sigma_k}\right) = 1 + \mathrm{erf}\left(\frac{h}{\sqrt{2}\sigma_k}\right) \quad (13)$$

Substituting equation (13) in equation (12) results in the final expression for the average leakage area:

$$\bar{A}_k = \Delta\ell\sigma_k\left\{\frac{1}{(2\pi)^{1/2}}\, e^{-\bar{h}^2/2\sigma_k^2} + \frac{\bar{h}}{2\sigma_k}\left[1 + \mathrm{erf}\left(\frac{\bar{h}}{\sqrt{2}\sigma_k}\right)\right]\right\} \quad (14)$$

It can be shown that, as the gap becomes much larger than the rms irregularity amplitude, the leakage area approaches the value which is dictated by the average gap:

$$\mathrm{Lim}\ \bar{A}_k = \Delta\ell\,\bar{h}$$
$$(\bar{h}/\sigma_k) \to \infty \quad (15)$$

Equations 1, 14 and 15 can be combined to derive the following leakage equation:

$$A_L = \xi_{ms}\ell\left\{(2\pi)^{-1/2}\, e^{-h^2/2\xi_{ms}^2} + \frac{h}{2\xi}\left[1 + \mathrm{erf}\left(\frac{h}{\sqrt{2}\,\xi}\right)\right]\right\} \quad (16)$$

where: A_L = leak area

ℓ = circumferential length of contact area

ξ_{ms} = rms surface asperity height

h = gap height between mean surface level and contacting surface

erf = error function

3-37

This equation is plotted in Figure 3-6 in terms of a dimensionless leak area as a function of a dimensionless gap.

The limiting value for $A/\Delta\ell\xi$ as h/ξ approaches zero is due to the constraint of assumption that the approach and contact cannot exceed the mean surface level of the machined surface. Figure 3-7 is a plot of the leak rate of helium as a function of the differential pressure across the two surfaces for a given surface finish and gap height. The valve seat diameter was chosen as 0.050 inch as representative of valves used on small engines. Molecular flow with a small path entrance (Equation (b), Page 3-24) was assumed as the dominating leak mechanism.

The calculated leak rates are within the range of actual values of valve leak rates (uncycled), therefore, this model and assumptions will be utilized for further investigation.
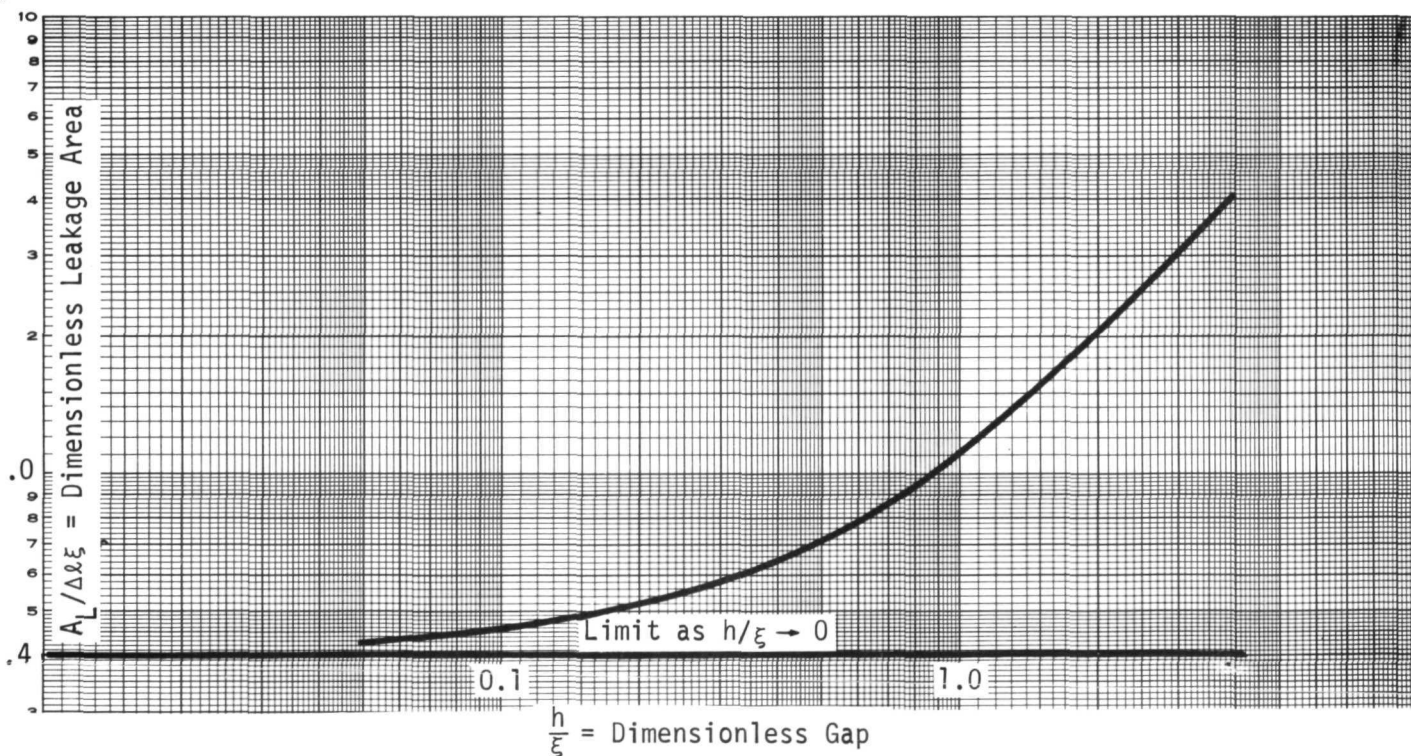
Figure 3-6. Dimensionless Area Vs. Gap

3-38
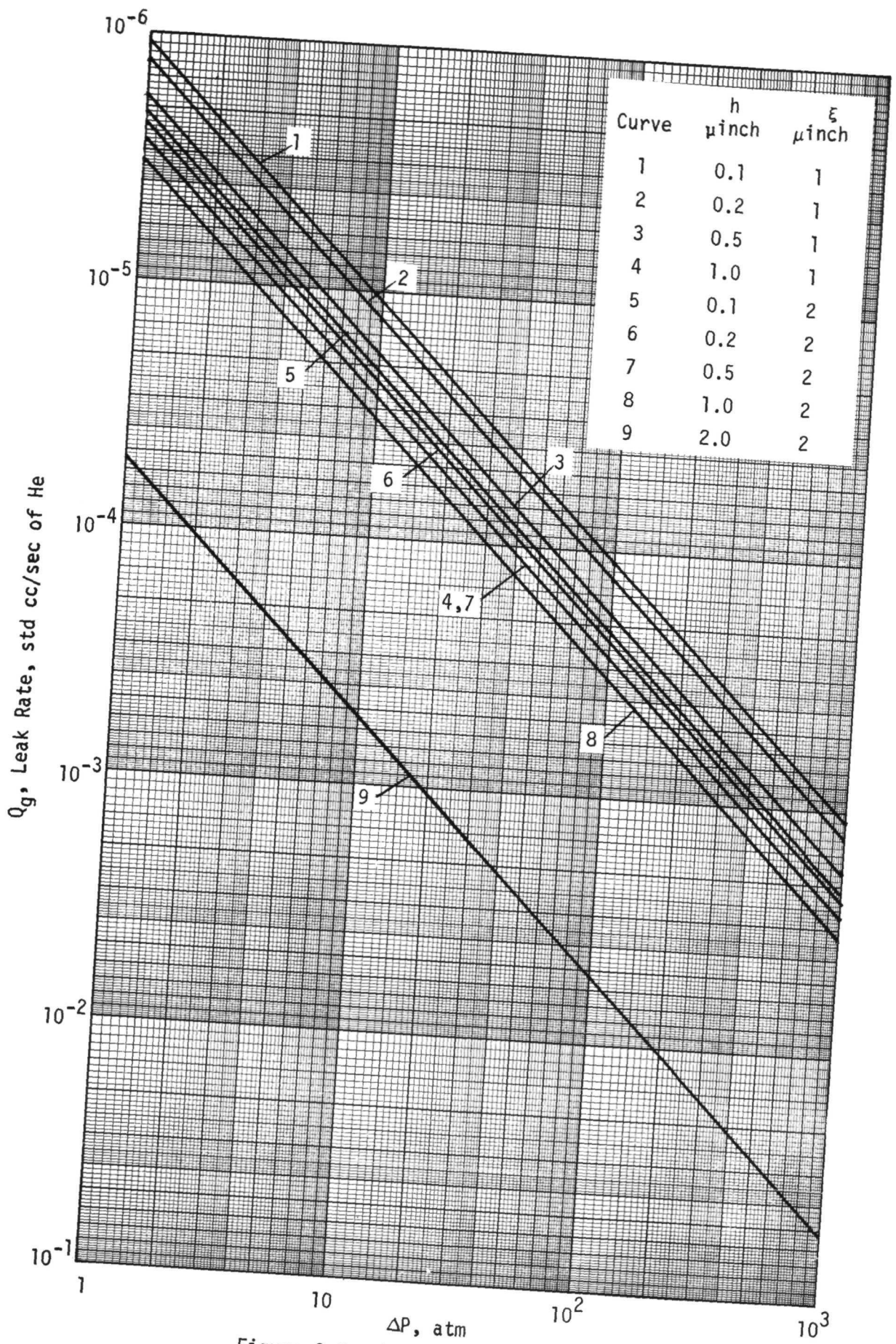
Figure 3-7. Leak Rate Vs. ΔP

3-39

3.11.4 Cycle Life and Cycle Rate

A preliminary scaling investigation was performed in order to examine a set of non-dimensional groups which may govern the cycle life of a poppet valve. Some of these non-dimensional groupings were used to derive scaling laws which were dependent upon the leakage area and the cycle rate to determine the cycle life of the valve. The independent variables were chosen as mass, length and time and pi terms were derived on the basis of cycle rate and cycle life.

The cycle life was assumed to be a function of bearing stress, leak rate, leak area, rms asperity height and average wear particle diameter. Thus, cycle life, $CL = f(q_b, Q_g, A_L, \xi, D_L)$.

Then the pi terms are:

$$\pi_1 = \frac{(q_b)^{2/3} A_L}{(CL)^{2/3} (Q_g)^{2/3}} \; ; \quad \pi_2 = \frac{(q_b)^{1/3} (\xi)}{(CL)^{1/3} (Q_g)^{1/3}} \; ; \quad \pi_3 = \frac{(q_b)^{1/3} (D_L)}{(CL)^{1/3} (Q_g)^{1/3}}$$

The cycle rate (CR) was also assumed to be a function of the same parameters. In this case, the pi terms are as follows:

$$\pi_1 = \frac{(CR)^{2/3} (q_b)^{2/3} (A_L)}{(Q_g)^{2/3}} \; ; \quad \pi_2 = \frac{(CR)^{1/3} (q_b)^{1/3} (\xi)}{(Q_g)^{1/3}} \; ; \quad \pi_3 = \frac{(CR)^{1/3} (q_b)^{1/3} (D_L)}{(Q_g)^{1/3}}$$

The scale factors for determining the cycle life are derived as outlined in 4.1. Thus, the scale factor for cycle life is:

$$\lambda_{CL} = \frac{\lambda_{q_b} \lambda_{A_L}^{3/2}}{\lambda_{Q_g}}$$

From 4.1, the asperities in the model must be scaled the same way as the prototype, thus:

$$\lambda_\xi = \frac{\lambda_{Q_g}^{1/3}}{\lambda_{CR}^{1/3} \lambda_{q_b}^{1/3}} = 1 \quad \text{or} \quad \frac{\lambda_{Q_g}}{\lambda_{CR} \lambda_{q_b}} = 1$$

Then: $\dfrac{\lambda_{Q_g}}{\lambda_{q_b} \lambda_{A_L}^{3/2}} = \dfrac{\lambda_{CR}}{\lambda_{A_L}^{3/2}}$ and $\lambda_{CL} = \dfrac{\lambda^{3/2}_{A_L}}{\lambda_{CR}} = \dfrac{(CR)_p}{(CR)_m} \cdot \dfrac{(A_L)_m^{3/2}}{(A_L)_p^{3/2}}$

If the cycle life was to be accelerated by a factor of 100, $\lambda_{CL} = 1/100$. Then the cycle rate of the model must be 100 times the prototype, for the same leakage area, or the leakage area of the model must be approximately .048 of that of the prototype valve, for the same cycle rate. Alternatively, both the cycle rate and the leakage area of the model may be varied to obtain the accelerated cycle life.

3.11.5 Dimensional Analysis of Valve Parameters

A general investigation of the parameters which may govern the mechanisms affecting the time dependency of valve leakage was performed. A number of parameters were utilized in order to obtain non-dimensional pi terms for analysis. The objective of this analysis was to investigate the effect of varying the controlling variables and which may give insight to developing accelerated test methods.

Not all of the variables listed in Table 3-1 were used, since there are a number of them that have the same dimensions, and the pi terms generated for one such variable can be utilized for any other variable having the same dimensional grouping.

The non-dimensional pi terms generated as a result of the computer program are tabulated in Table 3-7, along with the independent variables used to obtain them. The analyses of these terms are not complete, but two relationships have been noted which may be of potential use.

The pi terms $\dfrac{(Qg)}{(CR)\,(Ee)}$ and $\dfrac{(CL)\,(Qg)}{(Ee)}$ are power and energy terms, respectively. Since they involve pressure-volume flow, energy input, cycle rate and cycle life, these are ratios of mechanical power or energy to the power or energy involved in the leakage of a valve. When these terms are coupled with those involving wear, leak area, rms surface finish and approach, they may provide a basis for deriving scaling laws which will lend some insight into the life span of the valve.

Table 3-7. Tabulation of Non-Dimensional Pi Terms As A Function of Their Independent Variables

Independent Variables   Pi Terms

$\dot{m}$, $\dot{w}$, q_b

$$\pi_1 = \frac{(A_L)(\dot{w})}{(\dot{m})} \qquad \pi_5 = \frac{(Q_g)(\dot{w})^2}{(q_b)^2(\dot{m})}$$

$$\pi_2 = \frac{(\zeta_{ms})(\dot{w})^{1/2}}{(\dot{m})^{1/2}} \qquad \pi_6 = \frac{(CL)(q_b)}{(\dot{m})^{1/2}(\dot{w})^{1/2}}$$

$$\pi_3 = \frac{(E_e)(\dot{w})^{3/2}}{(q_b)(\dot{m})^{3/2}} \qquad \pi_7 = \frac{(CR)(\dot{m})^{1/2}(\dot{w})^{1/2}}{(q_b)}$$

$$\pi_4 = \frac{(W_{AB})(\dot{w})^{1/2}}{(q_b)(\dot{m})^{1/2}}$$

CR, E_e, q_b

$$\pi_1 = \frac{(A_L)(q_b)^{2/3}}{(E_e)^{2/3}} \qquad \pi_5 = \frac{(Q_g)}{(CR)(E_e)}$$

$$\pi_2 = \frac{(C)(q_b)^{1/3}}{(CR)(E_e)^{1/3}} \qquad \pi_6 = \frac{(m)(CR)^2}{(E_e)^{1/3}(q_b)^{2/3}}$$

$$\pi_3 = \frac{(D_L)(q_b)^{1/3}}{(E_e)^{1/3}} \qquad \pi_7 = \frac{(\dot{m})(CR)}{(E_e)^{1/3}(q_b)^{2/3}}$$

$$\pi_4 = \frac{(W_{AB})}{(E_e)^{1/3}(q_b)^{1/3}} \qquad \pi_8 = \frac{(\dot{w})(CR)(E_e)^{1/3}}{(q_b)^{4/3}}$$

Q_g, E_e, q_b

$$\pi_1 = \frac{(A_L)(q_b)^{2/3}}{(E_e)^{2/3}} \qquad \pi_6 = \frac{(C_L)(Q_g)}{(E_e)}$$

$$\pi_2 = \frac{(C)(E_e)^{2/3}(q_b)^{1/3}}{(Q_g)} \qquad \pi_7 = \frac{(m)(Q_g)^2}{(E_e)^{7/3}(q_b)^{2/3}}$$

$$\pi_3 = \frac{(D_L)(q_b)^{1/3)}}{(E_e)^{1/3}} \qquad \pi_8 = \frac{(\dot{m})(Q_g)}{(E_e)^{4/3}(q_b)^{2/3}}$$

$$\pi_4 = \frac{(W_{AB})}{(E_e)^{1/3}(q_b)^{2/3}} \qquad \pi_9 = \frac{(\dot{w})(Q_g)}{(E_e)^{2/3}(q_b)^{4/3}}$$

$$\pi_5 = \frac{(CR)(E_e)}{(Q_g)}$$

Table 3-7. (Con't).

Independent Variables	Pi Terms

CR, Q_g, q_b

$$\pi_1 = \frac{(A_L)(CR)^{2/3}(q_b)^{2/3}}{(Q_g)^{2/3}} \qquad \pi_5 = \frac{(CR)(E_e)}{(Q_g)}$$

$$\pi_2 = \frac{(C)(q_b)^{1/3}}{(CR)^{2/3}(Q_g)^{1/3}} \qquad \pi_6 = \frac{(m)(CR)^{7/3}}{(Q_g)^{1/3}(q_b)^{2/3}}$$

$$\pi_3 = \frac{(D_L)(CR)^{1/3}(q_b)^{1/3}}{(Q_g)^{1/3}} \qquad \pi_7 = \frac{(\dot{m})(CR)^{4/3}}{(Q_g)^{1/3}(q_b)^{2/3}}$$

$$\pi_4 = \frac{(W_{AB})(CR)^{1/3}}{(Q_g)^{1/3}(q_b)^{2/3}} \qquad \pi_8 = \frac{(\dot{w})(CR)^{2/3}(Q_g)^{1/3}}{(q_b)^{4/3}}$$

$\dot{w}$, Q_g, q_b

$$\pi_1 = \frac{(A_L)(q_b)^2}{(\dot{w})(Q_g)} \qquad \pi_5 = \frac{(CL)(q_b)^2}{(\dot{w})^{3/2}(Q_g)^{1/2}}$$

$$\pi_2 = \frac{(C)(\dot{w})}{(q_b)} \qquad \pi_6 = \frac{(m)(q_b)^4}{(\dot{w})^{7/2}(Q_g)^{3/2}}$$

$$\pi_3 = \frac{(D_L)(q_b)}{(\dot{w})^{1/2}(Q_g)^{1/2}} \qquad \pi_7 = \frac{(\dot{m})(q_b)^2}{(\dot{w})^2(Q_g)}$$

$$\pi_4 = \frac{(W_{AB})}{(\dot{w})^{1/2}(Q_g)^{1/2}} \qquad \pi_8 = \frac{(CR)(\dot{w})^{3/2}(Q_g)^{1/2}}{(q_b)^2}$$

$\dot{w}$, Q_g, E_e

$$\pi_1 = \frac{(A_L)(\dot{w})^{1/2}(Q_g)^{1/2}}{(E_e)} \qquad \pi_6 = \frac{(CL)(Q_g)}{(E_e)}$$

$$\pi_2 = \frac{(C)(\dot{w})^{1/4}(E_e)^{1/2}}{(Q_g)^{3/4}} \qquad \pi_7 = \frac{(m)(Q_g)^{3/2}}{(\dot{w})^{1/2}(E_e)^2}$$

$$\pi_3 = \frac{(D_L)(\dot{w})^{1/4}(Q_g)^{1/4}}{(E_e)^{1/2}} \qquad \pi_8 = \frac{(\dot{m})(Q_g)^{1/2}}{(\dot{w})^{1/2}(E_e)}$$

$$\pi_4 = \frac{(W_{AB})}{(\dot{w})^{1/2}(Q_g)^{1/2}} \qquad \pi_9 = \frac{(CR)(E_e)}{(Q_g)}$$

$$\pi_5 = \frac{(q_b)(E_e)^{1/2}}{(\dot{w})^{3/4}(Q_g)^{3/4}}$$

Table 3-7. (Con't)

Independent Variables   Pi Terms

$\dot{w}$, CR, $\dot{m}$

$$\pi_1 = \frac{(A_L)(\dot{w})}{(\dot{m})}$$

$$\pi_5 = \frac{(q_b)}{(CR)(\dot{m})^{1/2}(\dot{w})^{1/2}}$$

$$\pi_2 = \frac{(C)(\dot{w})^{1/2}}{(CR)(\dot{m})^{1/2}}$$

$$\pi_6 = \frac{(CR)(m)}{(\dot{m})}$$

$$\pi_3 = \frac{(D_L)(\dot{w})^{1/2}}{(\dot{m})^{1/2}}$$

$$\pi_7 = \frac{(Q_g)(\dot{w})}{(CR)^2(\dot{m})^2}$$

$$\pi_4 = \frac{(W_{AB})}{(CR)(\dot{m})}$$

$$\pi_8 = \frac{(E_e)(\dot{w})}{(CR)(\dot{m})^2}$$

$\dot{w}$, E_e, q_b

$$\pi_1 = \frac{(A_L)(q_b)^{2/3}}{(E_e)^{2/3}}$$

$$\pi_6 = \frac{(\nabla)(q_b)}{(\dot{w})(E_e)}$$

$$\pi_2 = \frac{(C)(\dot{w})}{(q_b)}$$

$$\pi_7 = \frac{(m)(q_b)^2}{(E_e)(\dot{w})^2}$$

$$\pi_3 = \frac{(D_L)(q_b)^{1/3}}{(E_e)^{1/3}}$$

$$\pi_8 = \frac{(\dot{m})(q_b)^{2/3}}{(\dot{w})(E_e)^{2/3}}$$

$$\pi_4 = \frac{(W_{AB})}{(E_e)^{1/3}(q_b)^{2/3}}$$

$$\pi_9 = \frac{(CR)(\dot{w})(E_e)^{1/3}}{(q_b)^{1/3}}$$

$$\pi_5 = \frac{(Q_g)(\dot{w})}{(E_e)^{2/3}(q_b)^{4/3}}$$

Table 3-7. (Con't)

Independent Variables   Pi Terms

CR, $\dot{w}$, Q_g

$$\pi_1 = \frac{(CR)(A_L)(\dot{w})^{1/2}}{(Q_g)^{1/2}}$$

$$\pi_6 = \frac{(q_b)}{(CR)^{1/2}(\dot{w})^{3/4}(Q_g)^{1/4}}$$

$$\pi_2 = \frac{(C)\,(\dot{w})^{1/4}}{(CR)^{1/2}(Q_g)^{1/4}}$$

$$\pi_7 = \frac{(CR)\,(E_e)}{(Q_g)}$$

$$\pi_3 = \frac{(CR)^{1/2}(D_L)(\dot{w})^{1/4}}{(Q_g)^{1/4}}$$

$$\pi_8 = \frac{(CR)^2\,(m)}{(\dot{w})^{1/2}(Q_g)^{1/2}}$$

$$\pi_4 = \frac{(W_{AB})}{(\dot{w})^{1/2}(Q_g)^{1/2}}$$

$$\pi_9 = \frac{(CR)\,(\dot{m})}{(\dot{w})^{1/2}(Q_g)^{1/2}}$$

$$\pi_5 = \frac{(CR)^{3/2}\,(\triangledown)}{(\dot{w})^{1/4}(Q_g)^{3/4}}$$

CR, $\dot{w}$, A_L

$$\pi_1 = \frac{Q_g}{(CR)^2(\dot{w})(A_L)^2}$$

$$\pi_5 = \frac{(q_b)}{(CR)(\dot{w})(A_L)^{1/2}}$$

$$\pi_2 = \frac{(C)}{(CR)\,(A_L)^{1/2}}$$

$$\pi_6 = \frac{(E_e)}{(CR)(\dot{w})(A_L)^2}$$

$$\pi_3 = \frac{(W_{AB})}{(CR)(\dot{w})(A_L)}$$

$$\pi_7 = \frac{(CR)\,(m)}{(\dot{w})\,(A_L)}$$

$$\pi_4 = \frac{(\triangledown)}{(\dot{w})(A_L)^{3/2}}$$

$$\pi_8 = \frac{(\dot{m})}{(\dot{w})\,(A_L)}$$

Table 3-7. (Con't.)

Independent Variables	Pi Terms	

CR, Q_g, T, C

$$\pi_1 = \frac{(CR)^2(A_L)}{(C)^2} \qquad \pi_5 = \frac{(CR)(E_e)}{(Q_g)}$$

$$\pi_2 = \frac{(CR)(D_L)}{(C)} \qquad \pi_6 = \frac{(CR)(m)(C)^2}{(Q_g)}$$

$$\pi_3 = \frac{(\mu)(T)(C)^2}{(CR)^2(Q_g)} \qquad \pi_7 = \frac{(\dot{m})(C)^2}{(Q_g)}$$

$$\pi_4 = \frac{(\theta/v)(C)}{(T)} \qquad \pi_8 = \frac{(\dot{w})(C)^4}{(CR)^2(Q_g)}$$

$\dot{q}_b$, Q_g, T, C

$$\pi_1 = \frac{(A_L)(q_b)(C)}{(Q_g)} \qquad \pi_6 = \frac{(CR)(Q_g)^{1/2}}{(q_b)^{1/2}(C)^{3/2}}$$

$$\pi_2 = \frac{(D_L)(q_b)^{1/2}(C)^{1/2}}{(Q_g)^{1/2}} \qquad \pi_7 = \frac{(CL)(q_b)^{1/2}(C)^{3/2}}{(Q_g)^{1/2}}$$

$$\pi_3 = \frac{(\mu)(T)}{(q_b)(C)} \qquad \pi_8 = \frac{(m)(q_b)^{1/2}(C)^{7/2}}{(Q_g)^{3/2}}$$

$$\pi_4 = \frac{(\theta/v)(C)}{(T)} \qquad \pi_9 = \frac{(\dot{m})(C)^2}{(Q_g)}$$

$$\pi_5 = \frac{(E_e)(q_b)^{1/2}(C)^{3/2}}{(Q_g)^{3/2}} \qquad \pi_{10} = \frac{(\dot{w})(C)}{(q_b)}$$

Table 3-7. (Con't)

Independent Variables   Pi Terms

CR, E_e, T, C

$$\pi_1 = \frac{(CR)^2 (A_L)}{(C)^2}$$

$$\pi_6 = \frac{(q_b) (C)^3}{(CR)^3 (E_e)}$$

$$\pi_2 = \frac{(CR) (D_L)}{(C)}$$

$$\pi_7 = \frac{(m) (C)^2}{(E_e)}$$

$$\pi_3 = \frac{(\mu) (T) (C)^2}{(CR)^3 (E_e)}$$

$$\pi_8 = \frac{(\dot{m}) (C)^2}{(CR) (E_e)}$$

$$\pi_4 = \frac{(\theta/v) (C)}{(T)}$$

$$\pi_9 = \frac{(\dot{w}) (C)^4}{(CR)^3 (E_e)}$$

$$\pi_5 = \frac{(Q_g)}{(CR) (E_e)}$$

μ, S, T, C

$$\pi_1 = \frac{(A_L) (\mu)^{2/3}}{(S)^{2/3}(C)^{2/3}}$$

$$\pi_6 = \frac{(q_b) (C)}{(\mu) (T)}$$

$$\pi_2 = \frac{(D_L) (\mu)^{1/3}}{(S)^{1/3} (C)^{1/3}}$$

$$\pi_7 = \frac{(CL)(\mu)^{1/3}(C)^{2/3}}{(S)^{1/3}}$$

$$\pi_3 = \frac{(E_e)}{(S)(T)}$$

$$\pi_8 = \frac{(m) (C)^2}{(S) (T)}$$

$$\pi_4 = \frac{(\theta/v) (C)}{(T)}$$

$$\pi_9 = \frac{(\dot{m}) (C)^{4/3}}{(T)(\mu)^{1/3}(S)^{2/3}}$$

$$\pi_5 = \frac{(Q_g)}{(T)(\mu)^{1/3}(S)^{2/3}(C)^{2/3}}$$

$$\pi_{10} = \frac{(\dot{w})(C)^2}{(\mu) (T)}$$

Table 3-7. (Con't)

Independent Variables   Pi Terms

μ, S, T, q_b

$$\pi_1 = \frac{(A_L)(q_b)^{2/3}}{(S)^{2/3}(T)^{2/3}}$$

$$\pi_6 = \frac{(CR)(q_b)^{2/3}(S)^{1/3}}{(\mu)\ (T)^{2/3}}$$

$$\pi_2 = \frac{(D_L)(q_b)^{1/3}}{(S)^{1/3}\ (T)^{1/3}}$$

$$\pi_7 = \frac{(E_e)}{(S)\ (T)}$$

$$\pi_3 = \frac{(\theta/v)\ (\mu)}{(q_b)}$$

$$8 = \frac{(m)\ (T)\ (\mu)^2}{(S)\ (q_b)^2}$$

$$\pi_4 = \frac{(Q_g)(q_b)^{2/3}}{(\mu)(S)^{2/3}(T)^{5/3}}$$

$$\pi_9 = \frac{(\dot{m})\ (\mu)\ (T)^{1/3}}{(S)^{2/3}(q_b)^{4/3}}$$

$$\pi_5 = \frac{(C)\ (q_b)}{(\mu)\ (T)}$$

$$\pi_{10} = \frac{(\dot{w})\ (\mu)\ (T)}{(q_b)^2}$$

REFERENCES

1. I. V. Kragelskii, "Friction and Wear," Butterworths, Washington, D.C. 1965.

2. E. Rabinowicz, "Compatibility Criteria for Sliding Materials," presented at the 1966 ASME Spring Lubrication Symposium, June 6-8, New Orleans, La.

3. E. Rabinowicz, "Compatibility Criteria for Sliding Materials," presented at the 1966 ASME Spring Lubrication Symposium, June 6-8, New Orleans, La.

4. "Advanced Spacecraft Valve Technology Compilation," Volume I, Mechanical Controls, Report No. 12411-6012,R000, TRW Systems, Contract NAS 7-717, July 1970.

5. E. Rabinowicz, "Friction and Wear of Materials," John Wiley and Sons, New York, New York. 1965.

6. E. Rabinowicz, "Surface Energy Effects in Sliding Phenomena," Contract DA-31-124-ARO (D)-143, MIT Project No. 9889, 12 Sept. 1966.

7. "Friction and Wear Interdisciplinary Workshop," NASA TMS-52748, NASA Lewis Research Center, Cleveland, Ohio, November 19-21, 1968.

8. F. R. Shanley, "Strength of Materials," McGraw-Hill Inc., New York, New York, 1957.

9. "Leakage Testing Handbook," Revised Edition, General Electric Report No. S-69-1117, Prepared for JPL, NASA under Contract NAS 7-396, July 1969.

10. R. C. Elwell and A. J. Bialous, "Study of Dynamic and Static Seals for Liquid Rocket Engines," General Electric Co., NASA Contract NAS 7-102, NASA No. CR-50662, March 1963.

4.0 POPPET AND SEAT DIFFUSION STUDY

4.1 INTRODUCTION

There are two main degradation mechanisms which can affect the functionality of valves when long-term service life is considered: (1) metallic transfer and wear, and (2) corrosion of the valve seat-poppet interface. If one considers that the intermittent usage of the valve exposes it to both vacuum and propellant contact conditions, then the leak rate is a direct function of the two degradation mechanisms.

Both of these degradation mechanisms can be simulated and tested by utilization of the diffusion block technique. This technique utilizes the materials of interest for poppet-valve seat construction which are combined to form a multi-component system. The couples, during heat treatment and concomitant diffusion, will form a wide range of alloy compositions for investigation in the specific environment of interest, and simulate metallic transfer under long duration, static loading of the poppet-valve seat interface.

The interdiffusion of materials is characterized by Fick's first and second laws which relate the functions of time, temperature, concentration gradient and diffusion distance[1]*. The diffusion coefficient D is known for many metal combinations, and can be readily calculated from the Arrhenius Equation

$$D = D_o e^{-Q/RT}$$

where: D_o = diffusion constant

Q = activation energy

R = universal gas constant

T = absolute temperature

---

*Numbers in parenthesis refer to the references listed at the end of this section.

It should be noted that the origin of the Arrhenius Equation is empirical. The Eyring Equation is not discussed here, however, is derived from physical principles of quantum mechanics. The Arrhenius Equation is considered a first approximation of the Eyring Equation and probably sufficient for use in the diffusion studies.

Fick's first law correlates the flux J_x of the diffusing species over a distance X under steady state conditions as

$$J_x = -D \frac{dc}{dx}$$

where: J_x = flux

D = diffusion coefficient

$\frac{dc}{dx}$ = change in concentration of the diffusing species with distance

If the concentration of the diffusing species changes with time, then Fick's second law defines the transient case:

$$\frac{dC_x}{dt} = \frac{d}{dx} \left[D \frac{dC_x}{dx} \right]$$

where: $\frac{dC_x}{dt}$ = change in concentration of the diffusing species at a point x with time

$\frac{dC_x}{dx}$ = change in concentration of the diffusiong species with distance

Assuming that the diffusion coefficient D does not depend on concentration (an assumption that probably is valid in this case), then the integrated equation is:

$$\frac{C_x - C_o}{C_s - C_o} = 1 - erf \left(\frac{x}{2\sqrt{Dt}} \right)$$

where: C_x = concentration of diffusion species at a distance x

C_o = original substrate concentration

C_s = original diffusing species concentration

x = diffusion path length at time to

t = diffusion time

erf = error function

In order to obtain the desired metallic transfer in a short period of time, an elevated temperature must be utilized. To insure that the mechanisms of metallic transfer, which is a surface diffusion process, will duplicate that which can occur under long duration, high contact force conditions, the diffusion temperature must be selected such that secondary processes such as grain boundary migration or volume diffusion will not occur. This can be determined by utilization of the Fick and Arrhenius equations. Thus, by clamping the materials of interest together under the conditions of intimate contact, subjecting the couple to an elevated temperature in order to reduce the time necessary for allowing material transfer, the conditions of material transfer during long duration missions can be simulated.

After material transport has been achieved, the couple can be subjected to the propellant environment of interest in order to determine the corrosion resistance of the materials. Pre-exposure photomicrographs provide detailed information of the diffusion interfaces and an indication of the material transport. The couple is then subjected to the propellant environment of interest in order to determine the corrosion resistance of the parent metals and the diffused area. The post-exposure examination is on a macroscale in that the surfaces rather than the interfaces are examined. The "hill and valley" effect is a direct result of combinations of materials which show a variation of corrosion resistance with respect to the parent materials. The "hill" areas are those points which show enhanced corrosion resistance, and are further examined by techniques such as the electron microprobe.

This technique, then, allows a comprehensive examination of the mechanisms affecting the valve seat-poppet interface under long duration missions, and may afford an interpretation of the efficacy of the materials utilized in the valve.

4.2 DIFFUSION TEST

A series of diffusion tests were performed using a simulated poppet-valve seat arrangement of beryllium copper and Inconel with an electrolized chromium plate. Figure 4-1 illustrates the design of the diffusion seat and poppet couple. The couple was clamped using an A286 steel bolt with a silver plated A286 steel nut. Before preloading the couple to the designed bearing stress to simulate a seat load in the closed position, the parts were loosely connected together and hydrogen fired at 500°C for two hours to clean the mating surfaces. After firing, the parts were placed in a plastic bag under hydrogen and clamped to prevent reoxidation of the surfaces before the diffusion tests were performed. The couples were clamped to a preset load of 900 pounds which represents a load of approximately 33,000 psi bearing stress.

The diffusion tests were performed in a Brew vacuum furnace at 500°C. This temperature was chosen to insure that surface diffusion rather than volume or grain boundary diffusion would occur, since the test was to simulate metallic transfer and wear that might take place during long term missions and affect the reliability of valves. The postulated mechanism was as follows: since there is limited solid solubility of either copper in chromium or vice versa, the chromium would have to diffuse into the Inconel enough to expose the Inconel surface, or some portion of it, to the copper. Copper diffuses rather rapidly into Inconel, and thus the two surfaces would be diffusion bonded. If the chromium did not diffuse sufficiently into the Inconel, then the high loading force on the couple might cause some of the copper to become mechanically attached to the chromium surface, simulating wear and metal transfer during valve operation. Thus the test should give some indication of mechanisms that may occur during long life operation.

Three test times were utilized: 100, 200 and 400 hours at temperature. A fourth test time of 800 hours was scheduled, but the vacuum system of the furnace became inoperative and the test was cancelled. For the three tests performed, the vacuum was maintained at 1×10^{-6} torr or better to insure minimal extraneous side effects. After 100 hours, the chromium plated Inconel and the bolt had a bluish tint on the exterior surfaces,

500 ± 010

.020 ± 002

.376 DIA $+.002 \atop -000$

.500 DIA ± 010

.415 $+000 \atop -002$

.030 ± 005

.002 R MAX.

16/
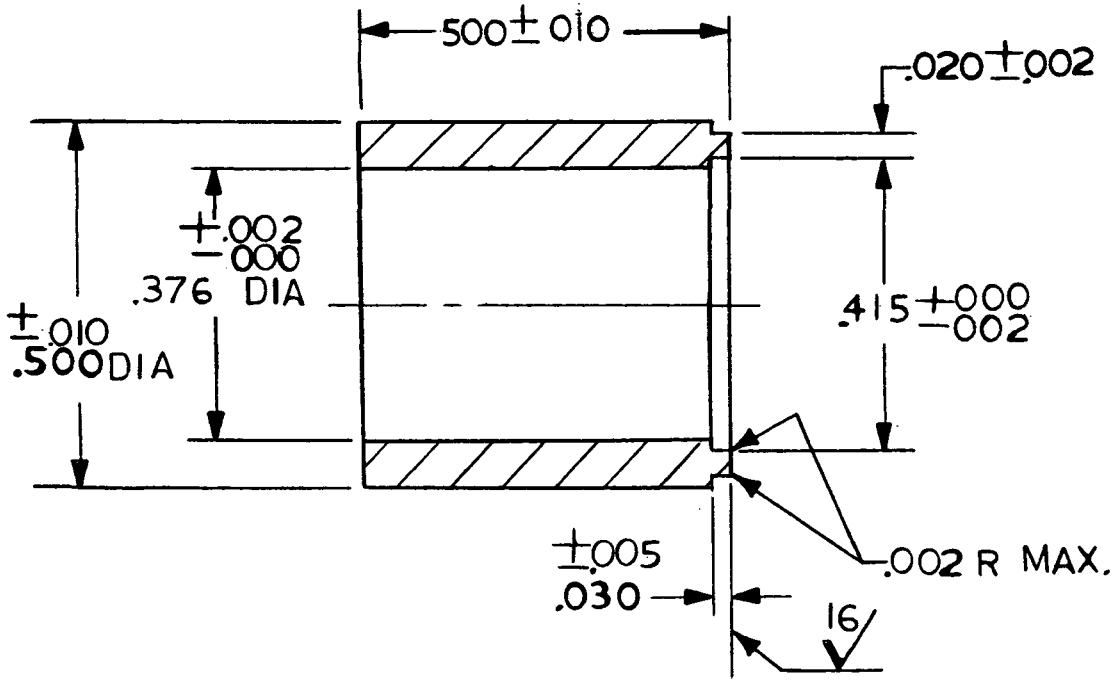
—1 POPPET   SCALE: 4/1
MATL: BERYLLIUM COPPER ALLOY 172 COND AT QQC 530

16/

ELECTROLIZED .0002 — .0003

.376 DIA $+.002 \atop -000$

.500 DIA ± 010

.375 ± 010
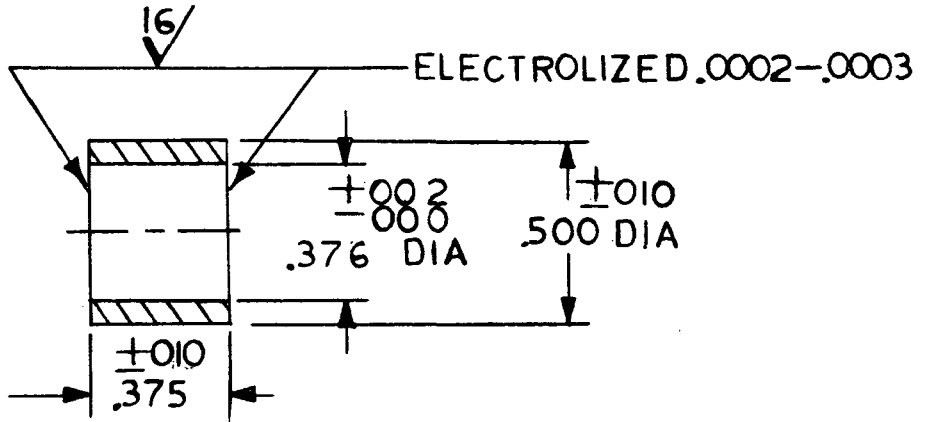
—2 SEAT   SCALE: 2/1
MATL: INCONEL NO 718 SOL'N ANNEALED AND AGE
HARDENED TO R_C 42 MIN

UNLESS OTHERWISE NOTED:
1 BREAK ALL EDGES
2 FINISH .32 RMS ALL OVER

ORIGINATOR	DATE	TITLE	ENGINEERING SKETCH
		DIFFUSION COUPLE	**TRW** SYSTEMS
			ONE SPACE PARK · REDONDO BEACH, CALIFORNIA
		Figure 4-1	
MJO			**SK** 16568
			SHEET I OF I

SYSTEMS 523A REV 9—65

4-5

but none at the contact area. The copper was unaffected, as was the nut. Refiring a sectioned piece in hydrogen did not remove the color. The reason for this effect is unknown. After each test, the couples were sectioned, polished and metallurgically examined with a Reichart Mef Metallograph.

Diffusion was not observed between the copper-chromium interface in any of the samples nor were any of the samples bonded together. It does not appear that the chromium diffused into the Inconel to any appreciable extent, but there are numerous cracks in the plated chromium where the copper contacted it. This is shown in Figure 4-2. There was adhesion between the A286 bolt and silver plated nut, however. The copper-chromium interface contact area became progressively greater, indicating that the combined load and temperature were causing the copper to conform to the surface finish of the chromium plate. Examination of the chromium surface revealed that some copper adhered to the surface, with the amounts increasing with diffusion time. The copper was unevenly adhered around the circumference of the contact area, although the 400 hour test sample had a more even deposit than the others. Figure 4-3 illustrates the progressive buildup of surface deposits on the chromium with time.

4.3 CONCLUSIONS

The tests revealed that, under relatively short diffusion times, bonding does not occur between copper-chromium plated Inconel couples under load. Mechanical adhesion of copper to chromium does occur, and increases with diffusion time. This adhesion is probably due to the deformation and closer contact with the chromium, allowing the copper to be "locked in" on the uneven surface. A similar mechanism would be expected to occur in valves either statically closed for long periods of time or frequently operated.

If the assumption is made that the diffusion rate of chromium into Inconel is increased approximately two orders of magnitude by a 500°C temperature change (a reasonable estimate for a large variety of metals), then the observations indicate that this couple should not experience diffusion

bonding for approximately five years. However, the mechanical adhesion found may provide deleterious leakage paths under the same time span.

Thus, the use of diffusion techniques for evaluating metal valve seat-poppet couples appears valid and can be expected to reveal if metallic transfer or wear occurs and be used as one criteria for predicting the compatibility of the couples for use in long term missions.

4.4 RECOMMENDATIONS

It is recommended that further diffusion tests be performed as follows:

1. Vary both time at temperature and temperature at equal times in order to verify time - temperature diffusion relationships of valve materials of interest.

2. Perform diffusion tests on other couples of proposed valve materials.

3. Perform corrosion tests on the proposed valve material couples before and after diffusion to verify if any net material transfer affects the extent of corrosion or its mechanism. These tests should be performed on both the fuels and oxidizers of interest.
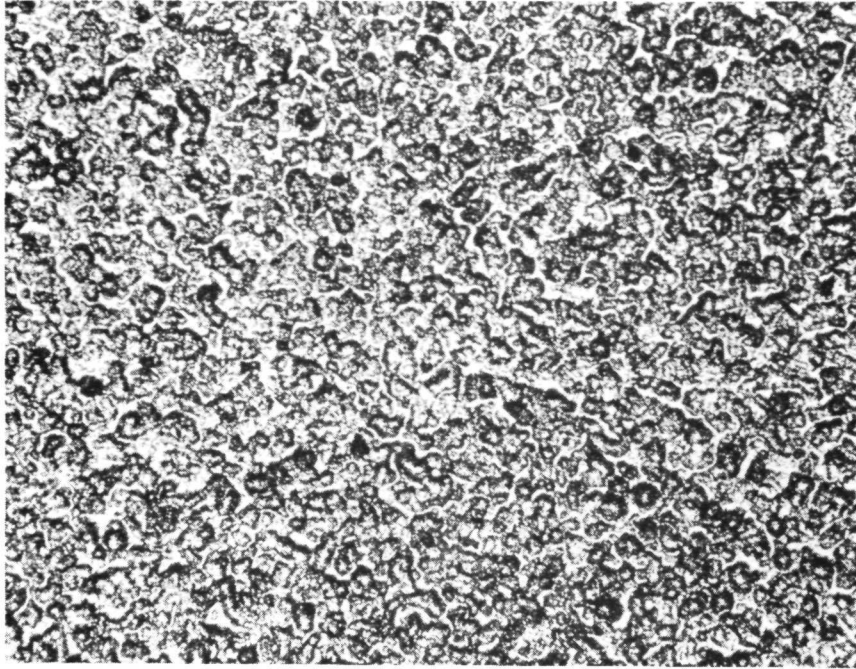
a. -2A Seat Control
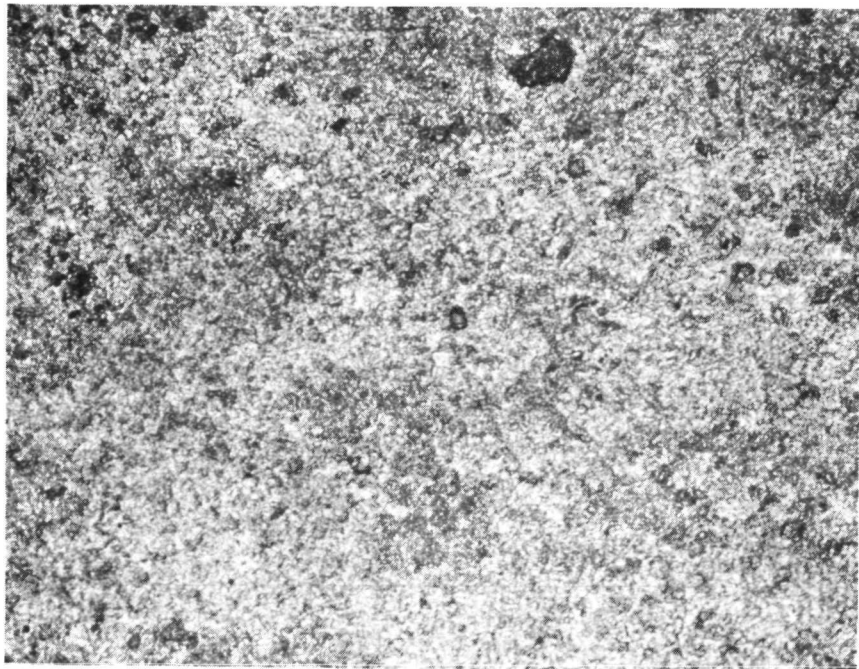
b. -2B Seat After 100 Hours

Figure 4-2. Photomicrographs of Electrolized-Inconel -2 Seat Surface
as a Function of Time. 500°C Exposure in 10^{-6} Torr.
Magnification 100X
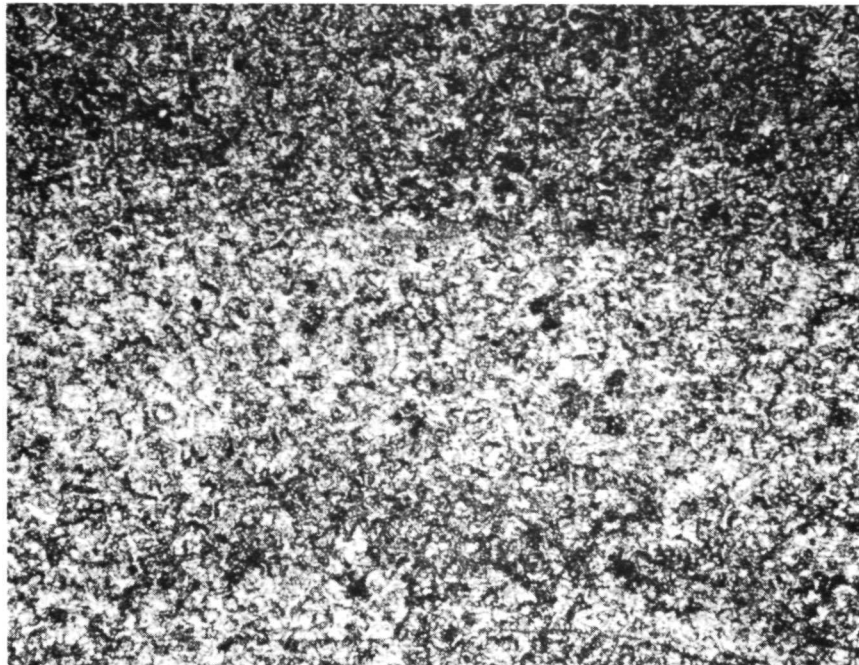
c. -2C Seat After 200 Hours
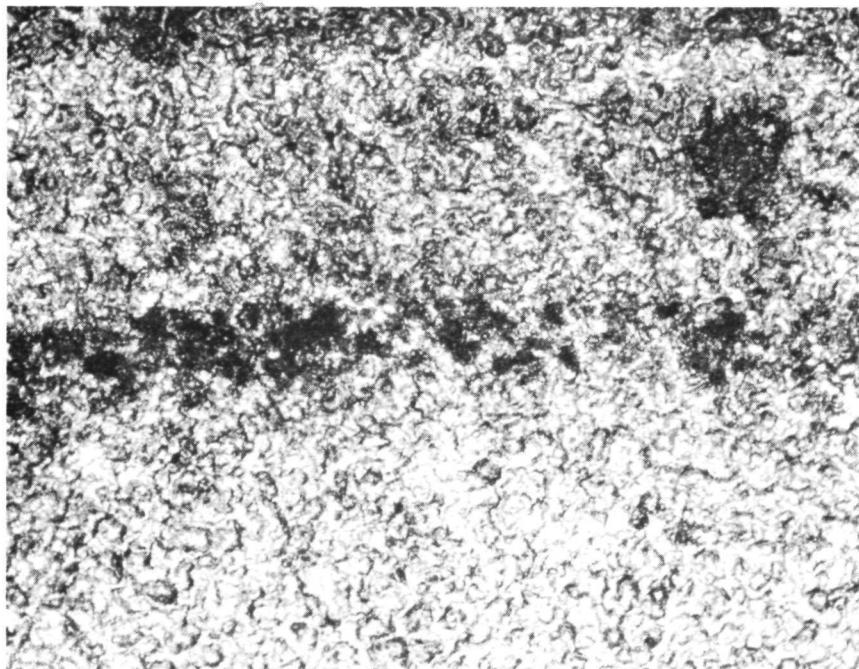
d. -2D Seat After 400 Hours

Figure 4-2 (Cont'd). Photomicrographs of Electrolized-Inconel -2 Seat Surface as a Function of Time. 500°C Exposure in 10^{-6} Torr. Magnification 100X
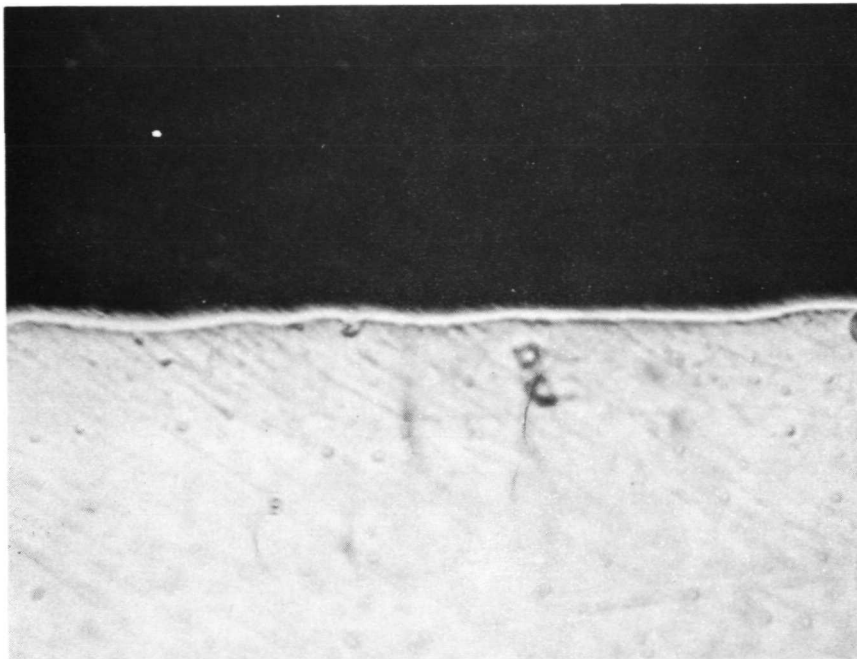
a. -1A/-2A Control
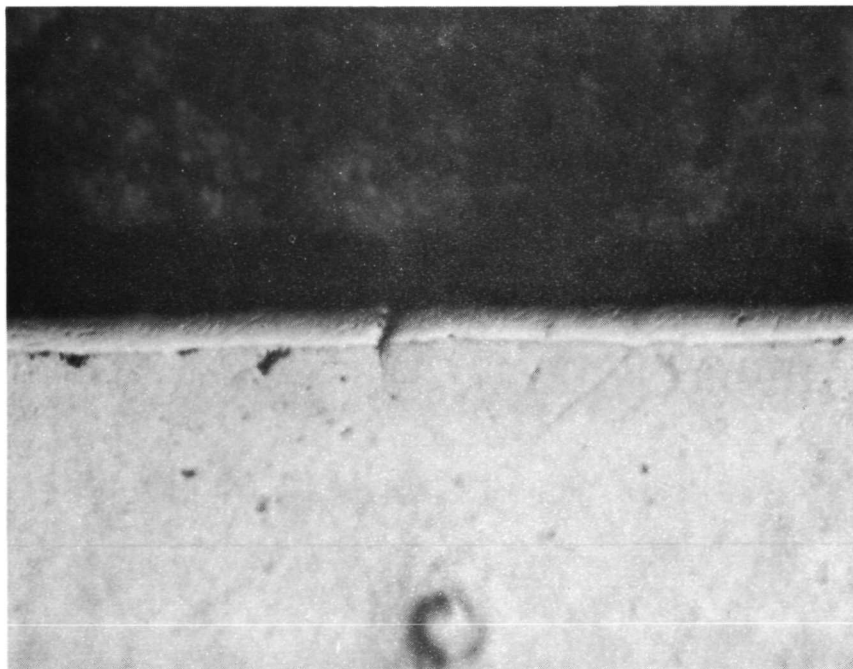
b. -1B/-2B After 100 Hours

Figure 4-3. Photomicrographs of Electrolized-Inconel -1 Poppet and -2 Seat Interface as a Function of Time. 500°C Exposure in 10^{-6} Torr. Magnification 1000X
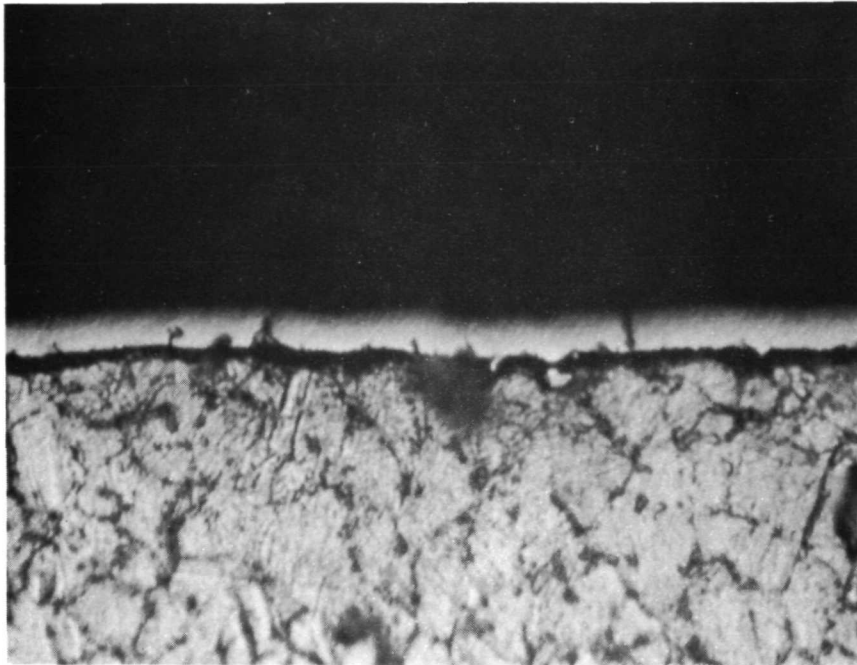
c. -1C/-2C After 200 Hours
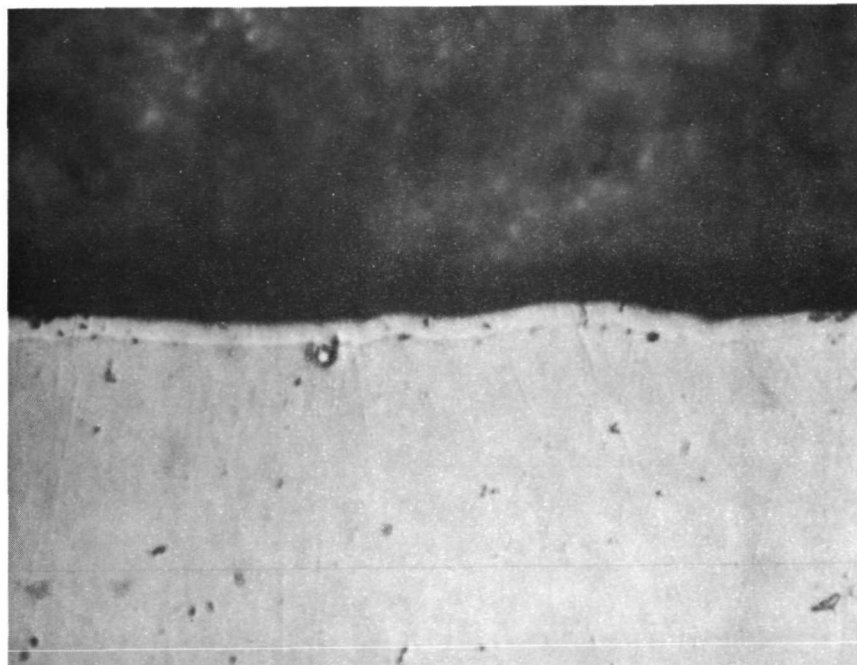
d. -1D/-2D After 400 Hours

Figure 4-3 (Cont'd). Photomicrographs of Electrolized-Inconel -1 Poppet and -2 Seat Interface as a Function of Time. 500°C Exposure in 10^{-6} Torr Magnification 1000X

4-11

5.0 ACOUSTIC SIGNATURE STUDY

5.1 INTRODUCTION

The transmittance of acoustic energy through a component provides a sensitive method of measurement and detection of discontinuities within a homogeneous structure. These discontinuities are defined at a surface interface or are inherent in the bulk material. The signature obtained from the vibrating acoustic wave can be used to characterize normal component performance. Change in the characterized or calibrated signature can be an indication of a degradation process or aging process or an indication of a defect or incipient failure.

It is the objective of this task to investigate acoustic techniques and the applicability of the test method to the measurement of the mechanical properties of a metal valve seat interface. These measurements in turn may provide a means of predicting leakage as a function of cycle life and provide a better understanding of the mechanisms of surface changes.

Materials may become anisotropic. Discontinuities may develop. The elements of the matrix of elastic constants may change in value. The changes may be detected from the measurement of mechanical transfer and impedance functions; or the impact response may indicate changes in the amplitude of various resonant frequencies of various elements.

An acoustic emission technique has been investigated at the University of Michigan to determine the irreversible changes such as dislocation motion, crack nucleation, and twinning[1]*. In the materials under test the model is used to predict the minimum dislocation, source length and the minimum slip region radius that is capable of producing detectable acoustic emission. The analytical results were confirmed experimentally on 99.99% pure aluminum and 2024 aluminum alloy.

---

*Numbers in parentheses refer to references listed at the end of this section.

The General Electric Company has developed techniques employing acoustic diagnosis of mechanical components including valves, motors and gyros[2]. Of specific interest was the GE work in acoustic signature analysis of a solenoid valve. The solenoid valve produces a distinct sound as the poppet moves along its stroke and when it impacts the valve seat. This sound (signature) is picked up using an accelerometer mounted on the valve body and recorded on an oscillograph. The detectable conditions and events utilizing a photographed time-amplitude display are as follows:

a) The opening and closing times of the valves

b) Scoring and particle generating conditions on the valve poppet guide bearing

c) Seating conditions of metal-to-metal contact of cone and seat.

Figure 5-1 depicts the GE test valve and signature trace. According to GE, the amplitude and shape of the peak at A_2 is dependent upon condition and seating of the "o" ring and orientation and velocity of the piston. A series of dry versus lubricated piston tests indicated that the amplitude A_1 of the signal during time T_1 represented scoring of the barrel. The presence of small particles of metal in the barrel was detectable in the same signature region.
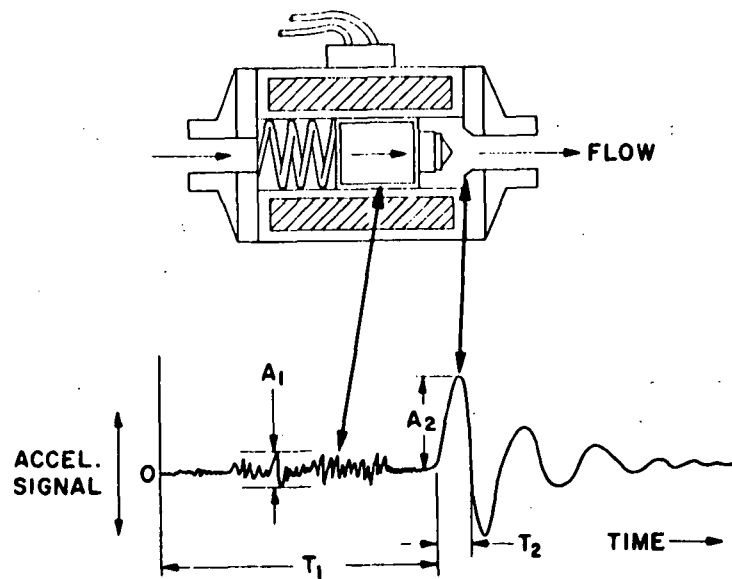
Figure 5-1. Typical Valve Closing Signature
(Taken from Reference 2)

5-2

5.1.1 Acoustic Signature Test Methods

The acoustic signature detected at a point can be in terms of acceleration, velocity, or displacement. Piezoelectric transducers are frequently employed in vibratory acceleration. The various types of acceleration, velocity and displacement transducers are:[3]

- Capacitance transducers
- Photoelectric transducers
- Potentiometric transducers
- Reluctance type transducers
- Strain gage transducers
- Servo acceleration transducers
- Piezoelectric acceleration transducers

The general characteristics of the piezoelectric transducer are given in the following:

- Mechanical energy is converted to electrical energy

- Signal conditioning circuitry is almost always required since the output impedance is too high

- High sensitivity

- Low weight and low volume

- Low frequency cutoff is a disadvantage.

For low frequency measurements the servo type or strain gage type sensors are recommended. However, in this program and based on the acoustic properties of the metals of interest, high frequency measurements are required. Therefore, piezoelectric type transducers were employed.

The change in the frequency transfer/impedance function can be the result of structural change (as compared to material change) or a loose particle, etc. By analogy to Fourier's work on electrical networks, it can be shown that the direct mobility of a linear passive structure with negligible damping is always expressible in the form:[4]

$$M = j\omega H \frac{(\omega^2 - \omega_1^2)(\omega^2 - \omega_3^2) \cdots (\omega^2 - \omega_{2n-1}^2)}{\omega^2(\omega^2 - \omega_2^2)(\omega^2 - \omega_4^2) \cdots (\omega^2 - \omega_{2n-2}^2)}$$

where: M = mechanical impedance dyne-sec/cm

H = constant dyne/cm

ω = variable frequency

$\omega_2, \omega_4 \cdots \omega_{2n-2}$ = resonant frequency

$\omega_1, \omega_3 \cdots \omega_{2n-1}$ = anti-resonant frequency

At these frequencies, force and velocity are in phase or force and acceleration differ in phase by 90°. Any change in the structure will necessarily effect one or more of the resonant or anti-resonant frequencies.

The acoustic signature is required to be processed for analysis and interpretation. Two major techniques employed are:

1. Determination of transfer or impedance function employing techniques such as fast Fourier transform algorithm.

2. Acousto-optic technique employing a matched filter concept.

The acousto-optic technique is described in Section 2.0. The elementary theory of the transfer/impedance function can be stated as follows:

Referring to the following figure:
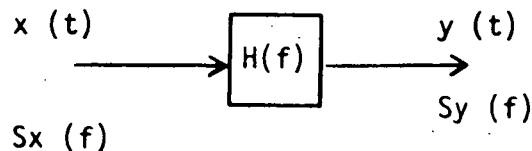
where: $x(t)$ = input function

$Sx(f)$ = $\int_{-\infty}^{\infty} x(f) e^{-j\omega t} dt$ Fourier transform

$Sy(f)$ = $\int_{-\infty}^{\infty} y(f) e^{-j\omega t} dt$ which is the Fourier transform of $x(f)$

$H(f)$ = $Sy(f)/Sx(f)$

$y(t)$ = output function

Note that if $x(t) = \delta(t)$ where $\delta(t)$ = impulse function, then $Sx(f) = 1$ and $H(f) = Sy(f)$.

Therefore, the impulse response defines the transfer function completely. A technique developed by Hewlett-Packard employs the power spectra function Gxx and Gyx to measure the transfer function; where

$$Gxx = SxSx^*$$

$$Gyx = SySx^*$$

$$Sx^* = \text{complex conjugate of } Sx$$

$$H = \frac{Gyx}{Gxx}$$

Employing power spectra technique, one second of data is needed to compute the transfer function with a resolution of 2Hz with the assumption that the signal to noise ratio is sufficiently high.

The impulse response can be divided into the amplitude and phase response as a function of frequency. The separated amplitude and phase response information is the same as the one obtained by measuring point by point amplitude and phase response of the system as a function of frequency. It should be noted that the amplitude response only may be adequate to determine the degradation characteristics of the components.

5.2 ACOUSTIC SIGNATURE PRELIMINARY TESTS

A series of tests were made using the acoustic energy transmissibility through the valve seat interface to determine the applicability of the method. These tests were preliminary, however, necessary to establish the range of change in acoustic signature output as a function of changing the seat surface topology.

5.2.1 Analytical Considerations

In an unbounded isotropic solid medium, there are longitudinal and shear waves propagated. When an elastic (acoustic) wave of either type reaches an interface between two media, in general four waves are generated, two of which are reflected from the boundary and two refracted into the second medium.

In a longitudinal wave of amplitude A, normal to the interface, the shear waves are zero. Reflected and transmitted longitudinal wave amplitudes are:[5]

$$A_2 = \frac{\rho_2 V_2 - \rho_1 V_1}{\rho_2 V_2 + \rho_1 V_1} A_1$$

$$A_3 = \frac{2\rho_1 V_1}{\rho_2 V_2 + \rho_1 V_1} A_1$$

where: A_1 = longitudinal wave amplitude input
A_2 = reflected wave amplitude
A_3 = transmitted wave amplitude
ρ_1 = density of medium 1
ρ_2 = density of medium 2
V_1 = acoustic wave velocity in medium 1
V_2 = acoustic wave velocity in medium 2
ρV = characteristic impedance of the medium

However, the conditions in the acoustic experiment considered here are different. The two media are almost identical $(\rho_1 V_1 \simeq \rho_2 V_2)$ while the

5-6

surface characteristic (roughness and waviness) will determine the contact area. If the contact area is very small, most of the power is reflected at the interface and very little transmitted since in this case the second medium is the gas (or vacuum) whose characteristic impedance is negligible compared to the characteristic impedance of medium one.

If the two surfaces are perfectly matching, the interface disappears, the contact area is 100%, the transmitted energy is near 100% and the wave amplitude remains the same on both sides of the interface.

Between these two extremes, the wave amplitude in the second medium will vary depending upon the surface characteristics.

It should be noted, however, that two other parameters —— frequency at which the acoustic wave is propagated and the valve seat/poppet bearing load —— are the factors determining the transmission of acoustic power. The frequency determines the amount of diffraction of sound waves while the valve seat loading determines the amount of real contact area from the apparent contact area; larger load yields asperities and increases the seal contact area. In most practical cases for all types and shapes of surface irregularities, the real contact area (A_r) is given by the following equation[6]:

$$A_r = \frac{1}{P} L$$

where: P = mean yield pressure of the asperities
        L = load

The reduction of the load may not reduce the contact area in proportion since yielding of asperities is an irreversible process.

5.2.2 Description of Test System

Initially, the leakage cycle life test fixture was employed (Figure 6-2, Section 6.0). Two drivers which were piezoelectric bimorph wafers, Clevite Part No. PZT-5A, were mounted one inside the cavity poppet close to the interface and one outside the test fixture. The bimorph wafers were bonded to the surface employing a silver impregnated conductive epoxy. The receiver sensor was an accelerometer, Endevco Model 2272, known for its excellent temperature characteristics (insensitive in the range of -452 to 500°F). Other equipment employed in the test are:

Power Oscilliator:	Optimation Inc.
	Model AC-104
	Regulation: Beter than 25 ppm
True RMS Differential Voltmeter:	Fluke 931B
	Accuracy: 0.01%
Charge Amplifier	Endevco 2710FM14
Oscilloscope:	Tektronix 545B

The accelerometer output as a result of driver frequency is given in Table 5-1.

Table 5-1. Acoustic Experiment Employing Leakage
Cycle Life Test Fixture

Noise Level: 12 m Volts

Driver Frequency HZ (48 Volts RMS)	Sensor Output mv Poppet in Contact	Sensor Output mv Poppet Not in Contact
1000	402 m volts	402 m volts
3000	404 " "	404 " "
10,000	529 " "	565 " "
20,000	591 " "	586 " "
30,000	373 " "	381 " "
40,000	365 " "	336 " "
50,000	284 " "	312 " "

It is apparent from the results that the change in the output is insignificant with and without poppet/seat contact. This is believed due to other wave propagation paths through the fixture housing. To avoid these paths, the poppet and the seat were removed from the test fixture and were compressed in a vice with a calibrated load cell (Kistler Model 912). The vice was acoustically isolated employing a foam rubber whose characteristic impedance is much smaller than that of the poppet and valve seat. Because of the characteristic impedance mismatch, a standing wave pattern is expected within the valve seat-poppet material. The block diagram of the test setup is shown in Figure 5-2. The design of the poppet and seat used for all the acoustic signature testing is shown in Figures 5-3 and 5-4.
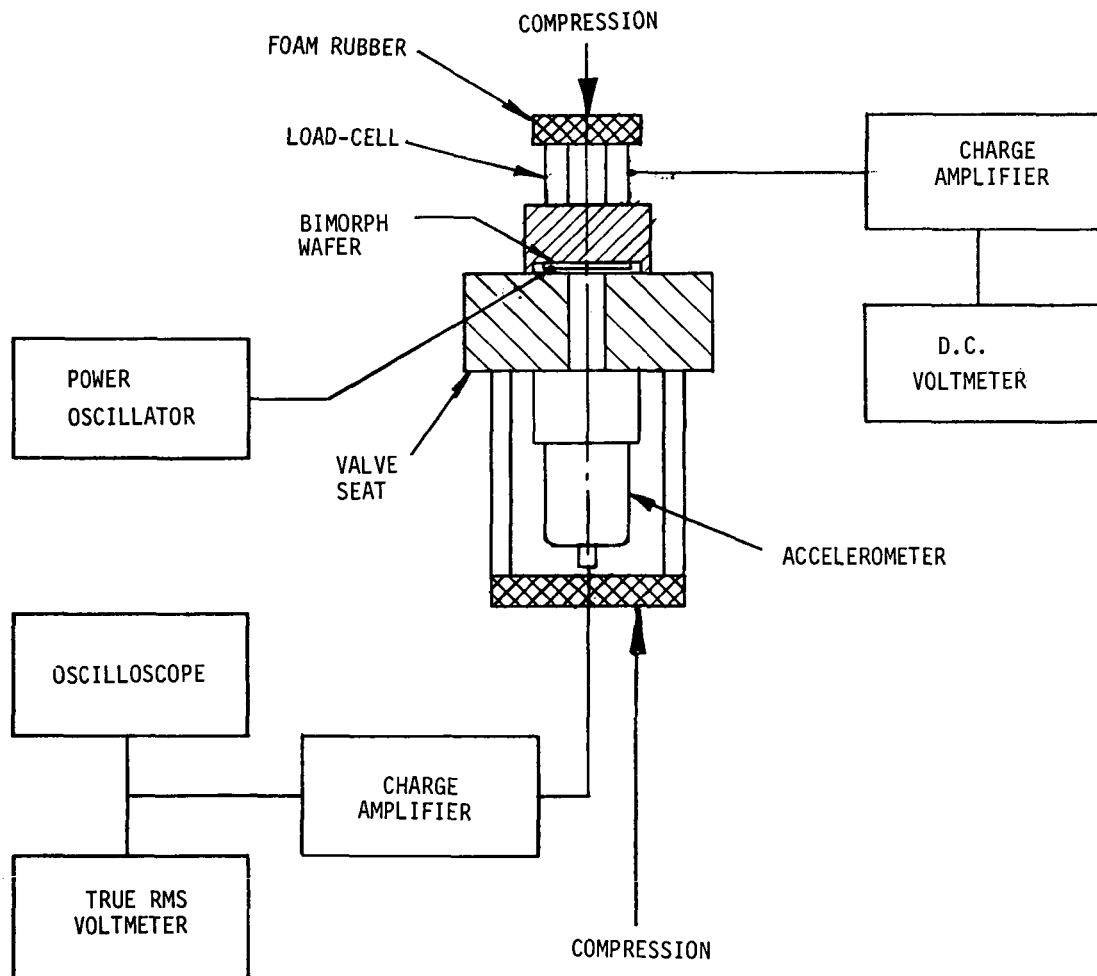
Figure 5-2. Acoustic Test System

#10-32 UNF-2B

1.000 Dia

.500

.065

.500 Dia

.060 +000 -002

.003 +000 -001
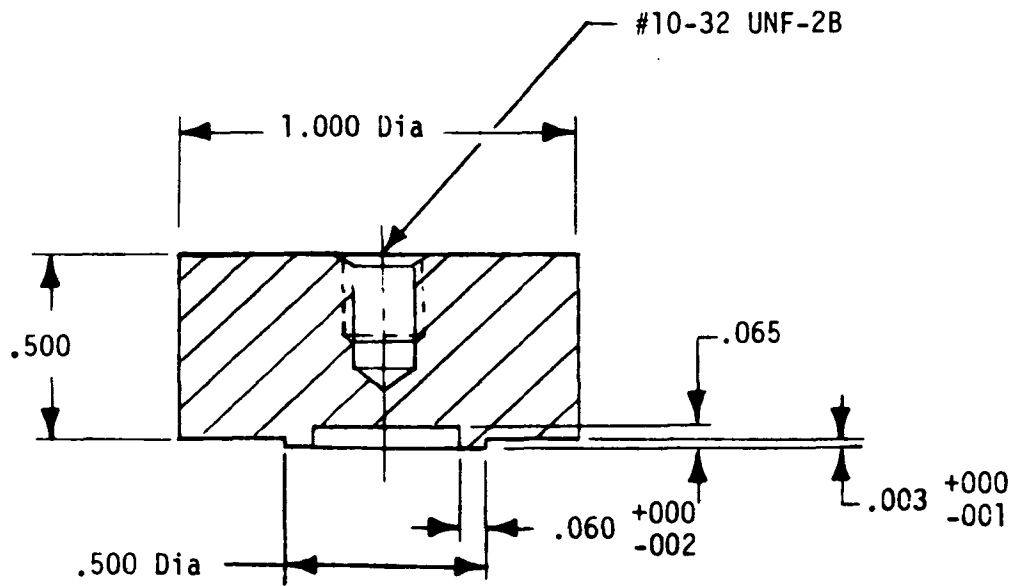
Figure 5-3. PN 16568 Poppet - Matl: Beryllium Copper
Alloy 172, Temp. H, QQC 530, 2X Size

.125 Dia

2.000 Dia

.750
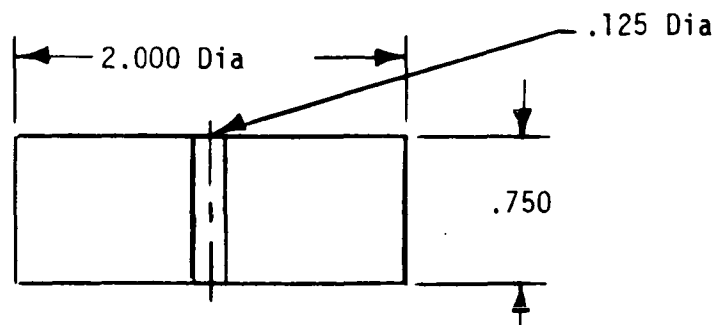
Figure 5-4. PN 254296 Seat - Matl: Alloy Steel

The poppet surface and the seat surface characteristics of each test specimen were varied in waviness and roughness. Three different surfaces were tested. Photographs of each of the three surfaces of the poppet are shown in Figures 5-5 through 5-7. Figure 5-8 represents the typical valve seat surface. The total roughness and waviness were measured in each case employing a Bendix Profi-corder Model RLC-4. Figures 5-9 through 5-11 are the reprints of typical Profi-corder chart outputs of each poppet surface. Figures 5-12 and 5-13 are reprints of typical Profi-corder chart recordings of each seat surface. The roughness and waviness of the three poppet surfaces are summarized as follows:

Poppet Surface	Peak-to-Peak Roughness Micro Inches	Peak-to-Peak Waviness Micro Inches	Total Micro Inches
16568-1A	25-50	75-100	100-150
16568-2A	15-25	25-50	40-75
16568-3A	1-5	100-250	100-250

The following figure illustrates the method in which the roughness and waviness were interpreted from the Profi-corder output. The peak-to-peak measurements taken from the Profi-corder charts and used above were average values.

PEAK-TO-PEAK TOTAL

PEAK-TO-PEAK WAVINESS

PEAK-TO-PEAK ROUGHNESS
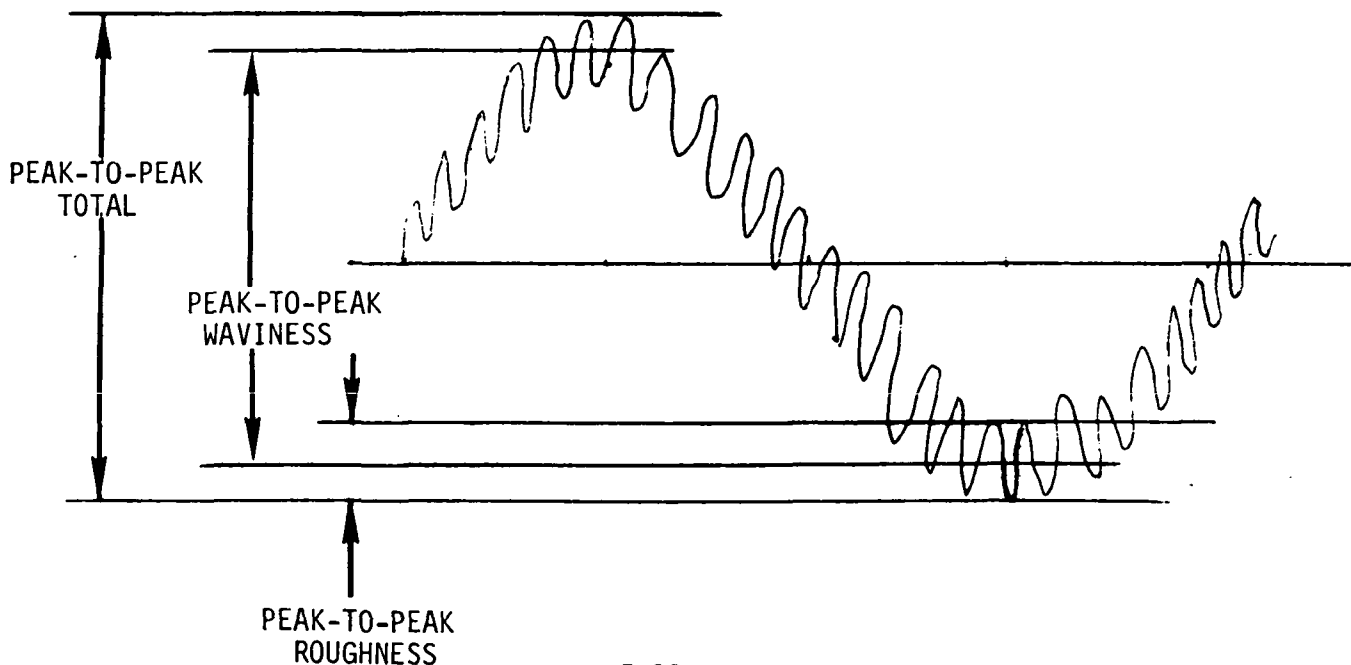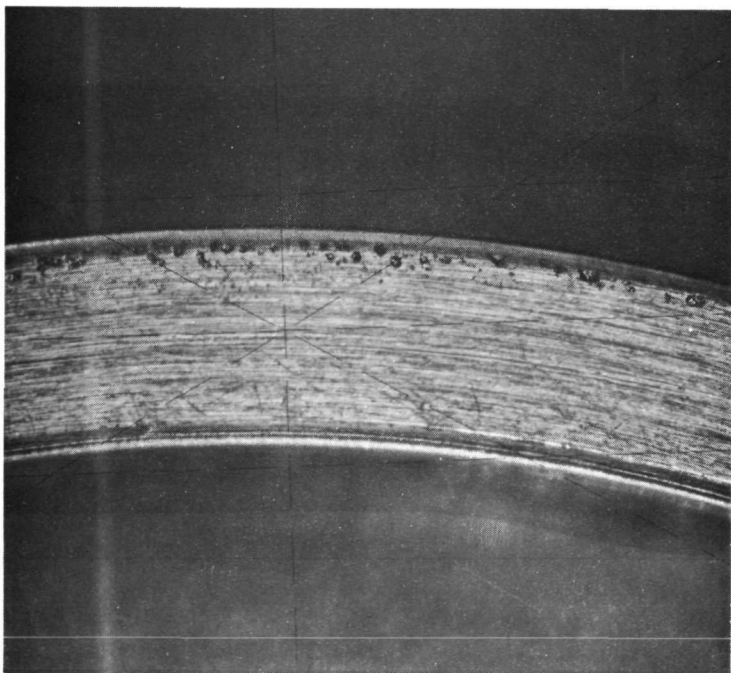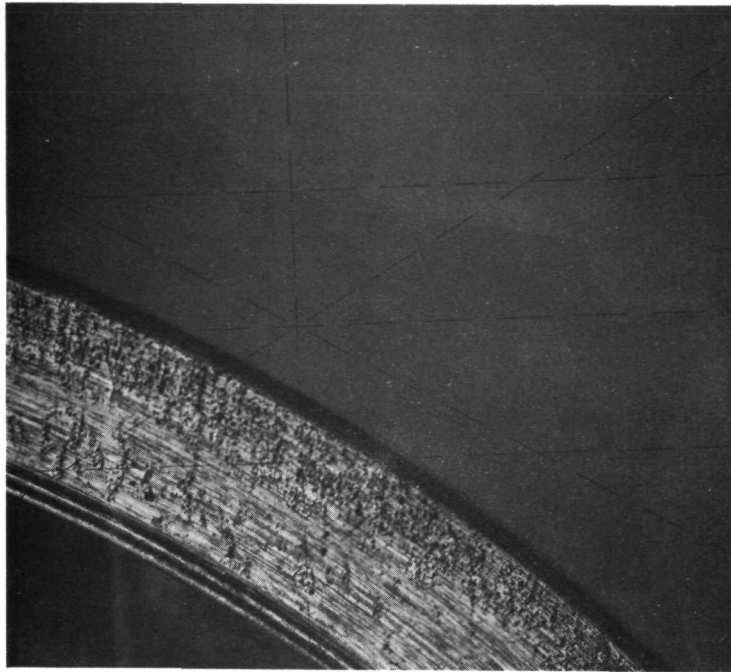
Figure 5-5. Poppet Surface: 16568-1 A
At Two Locations
Magnification 20X
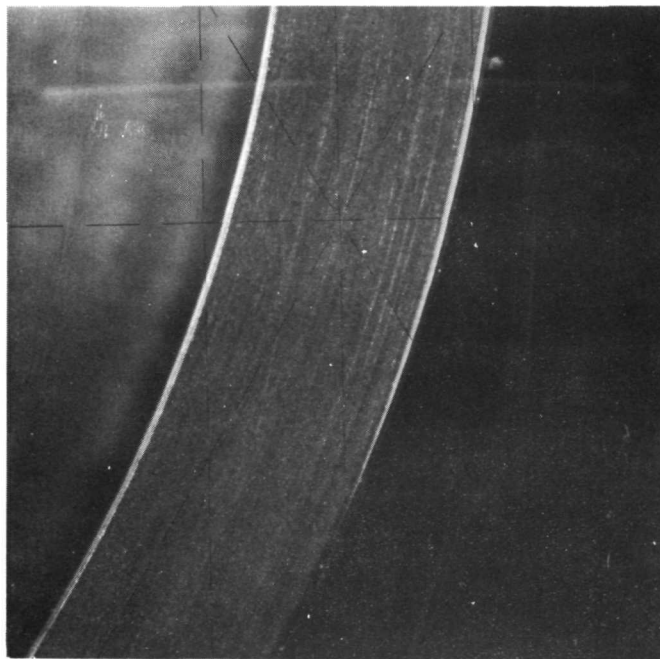
Figure 5-6.   Poppet Surface: 16568-2 A
             Magnification 20X
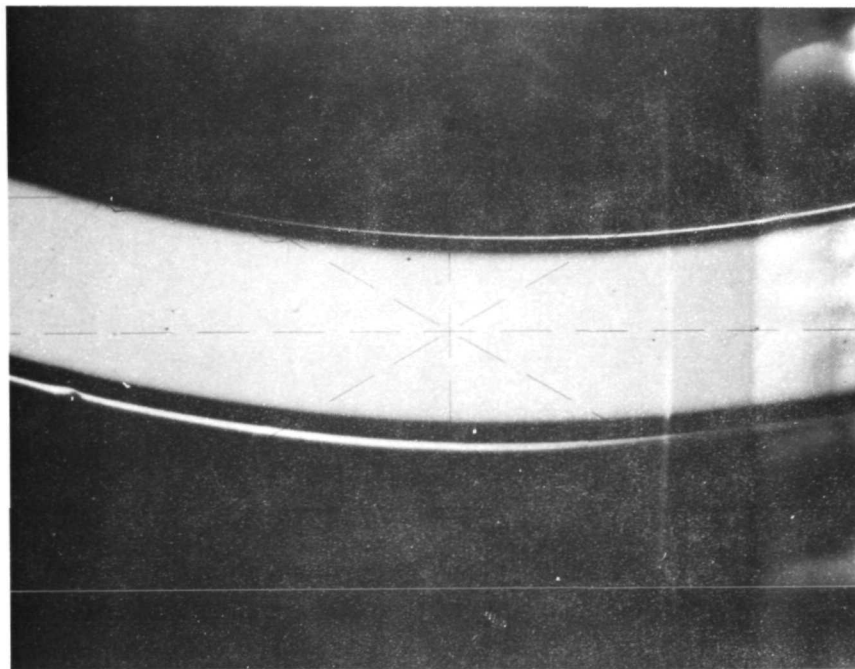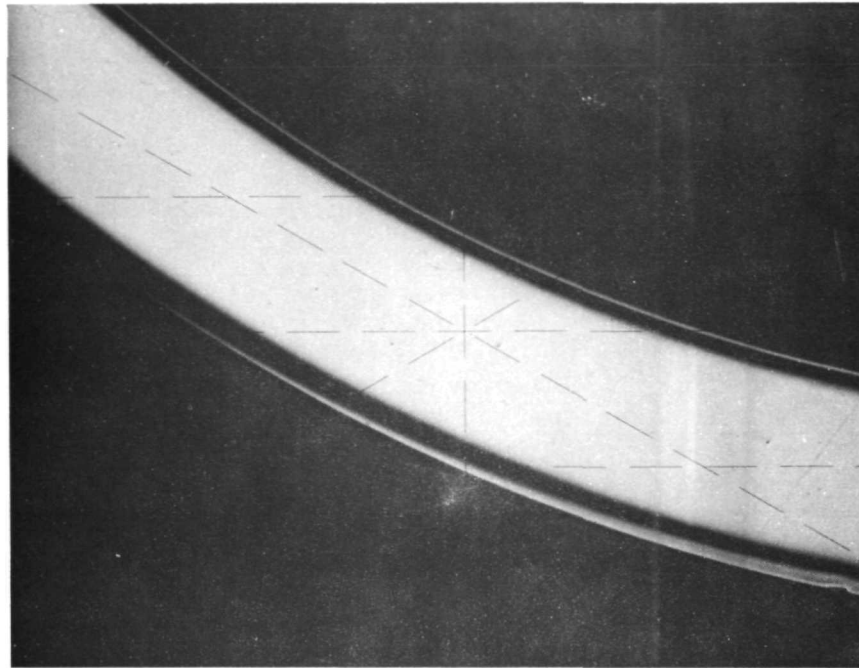
Figure 5-7. Poppet Surface: 16568-3 A
Magnification 20X
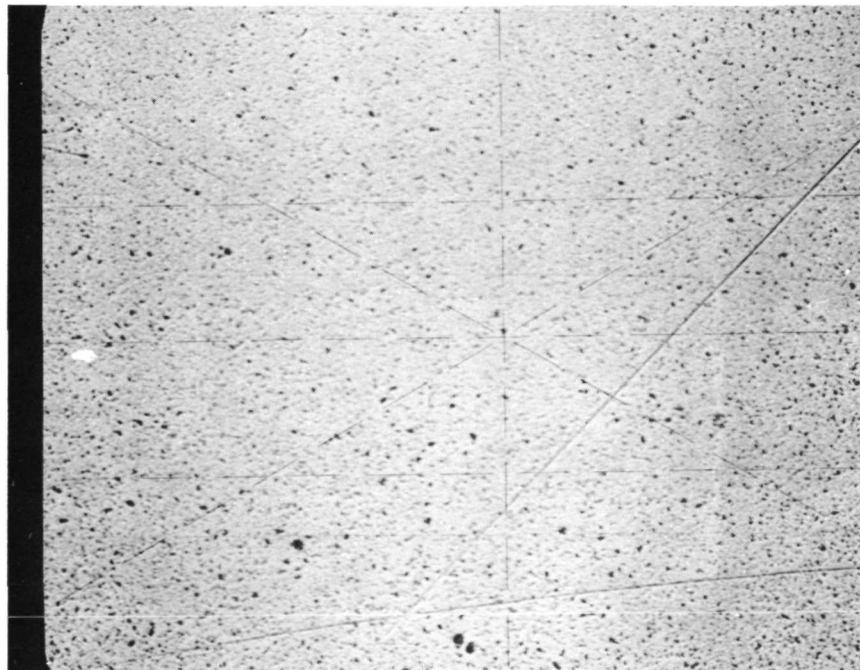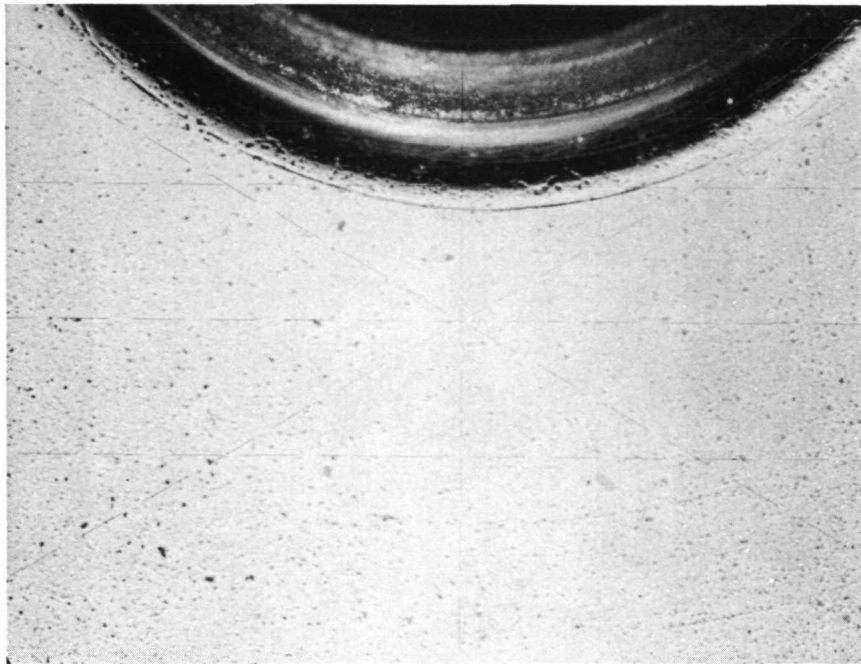
Figure 5-8. Valve Seat PN 254296 - Typical
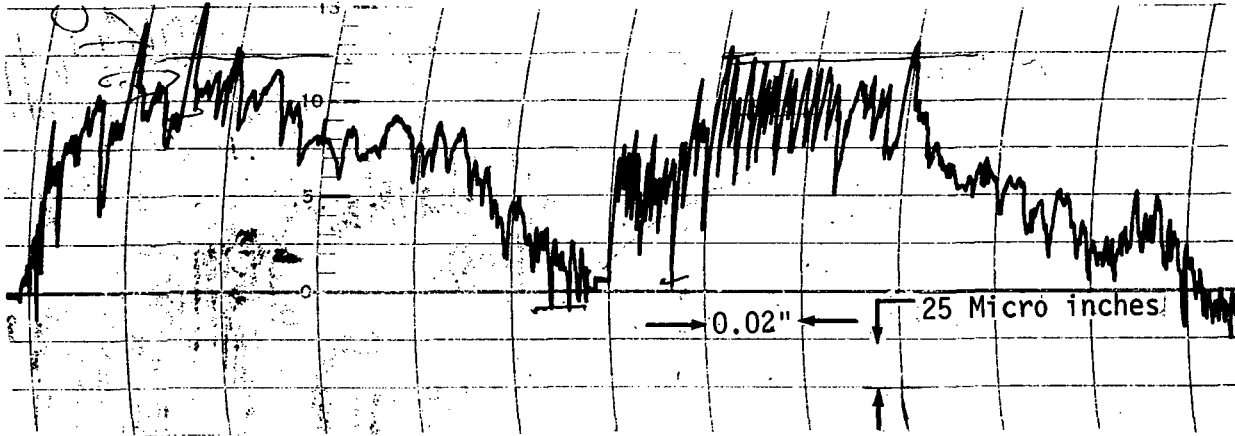Surface Magnification 20X

Figure 5-9. Typical Profile of Poppet Surface 16568-1A
Waviness: 100 μ inches
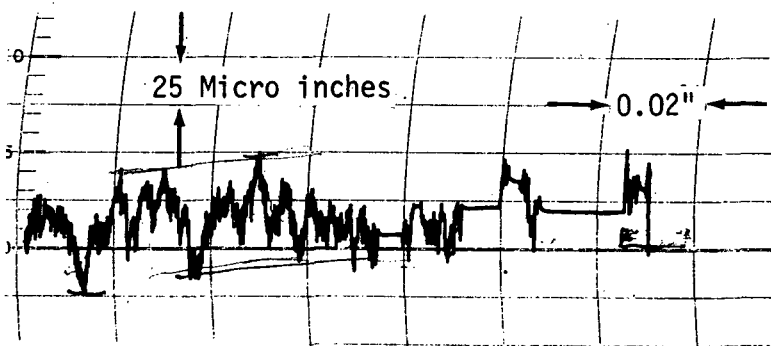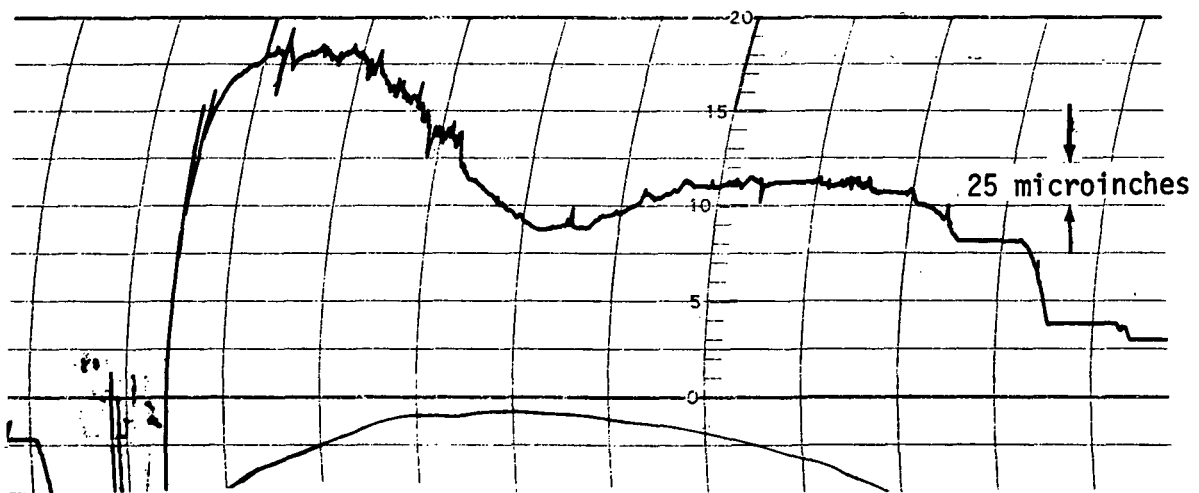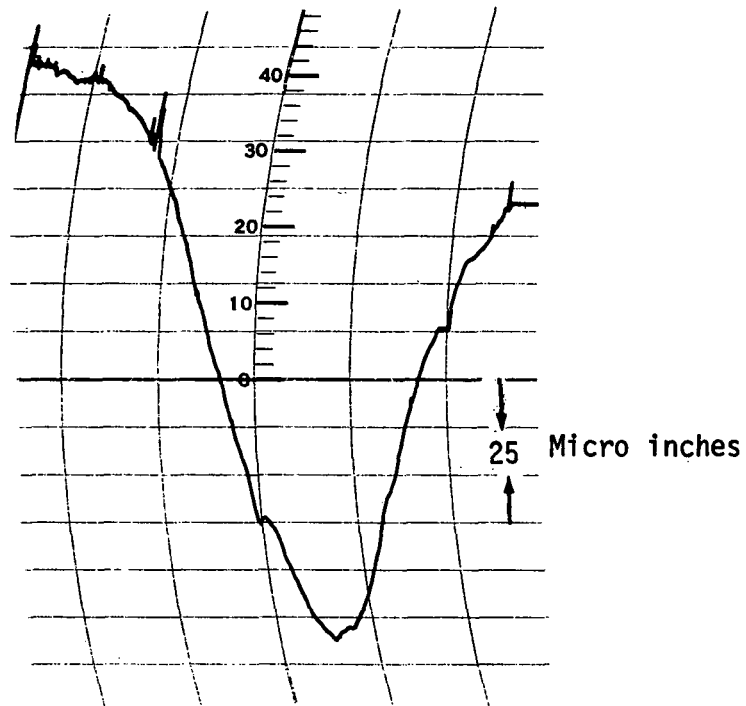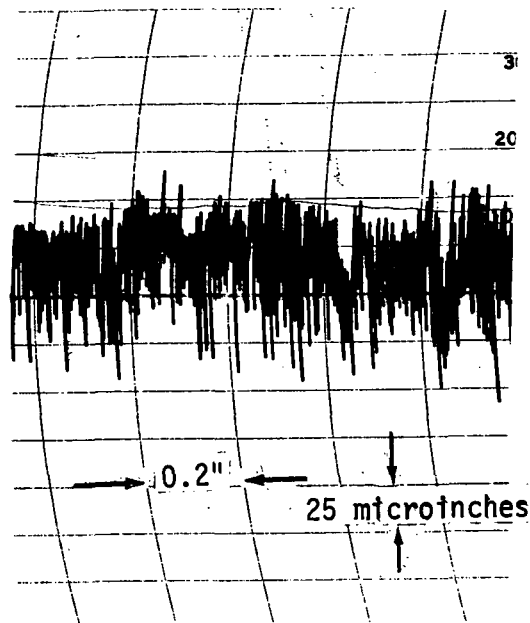Roughness: 25-50 μ inches
Stylus Radius = 500 μ inches

Figure 5-10. Typical Profile of Poppet Surface 16568-2A
Waviness: 50 μ inches
Roughness: 25 μ inches
Stylus Radius = 500 μ inches

25 Micro inches

25 microinches

Figure 5-11. Typical Profiles of Poppet Surface 16568-3A
Waviness: 100 to 250 micro inches
Roughness: 1 to 5 micro inches
Stylus Radius = 500 µ inches

Figure 5-12. Typical Profile of the Valve Seat PN 254296-1A
Waviness: 25 micro inches
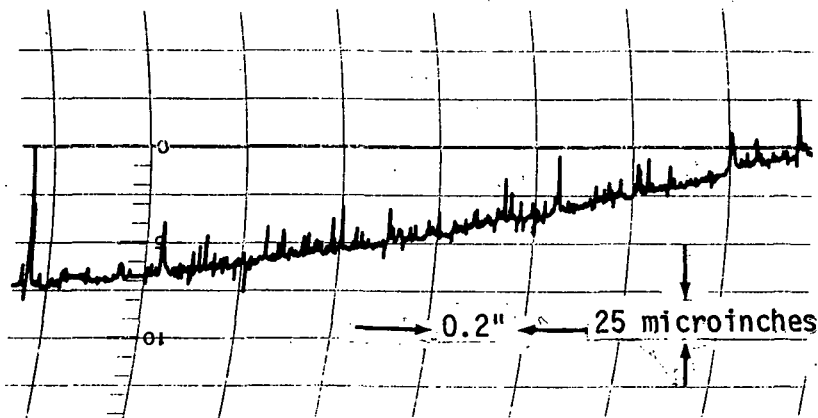Roughness: 30 to 50 micro inches
Stylus Radius = 500 µ inches

Figure 5-13. Typical Profile of the Valve Seat PN 254296-2A & -3A
Waviness: < 25 micro inches
Roughness: 10 to 25 micro inches
Stylus Radius = 500 µ inches

5.2.3 Test Results

The waviness was allowed to vary on all surfaces and was not controlled for these tests. Two types of tests were conducted, one with fixed frequency and varying seat load and the other with fixed load and varying frequency. The test data are given in Tables 5-2 and 5-3. The data of Table 5-2 (fixed frequency with varying seat load) were plotted on semilog papers with sensor output as an ordinate and seat load as an abscissa (Figures 5-14 through 5-17). The sensor output is in millivolts and represents true RMS acceleration, which can be converted to velocity and displacement. However, it requires to determine the sensor calibration beyond the manufacturer's specification and wave analysis of the output to determine the harmonics. This is not required since we are interested in measuring the relative changes in the output due to the changes in the surface characteristics.

The preliminary tests in the frequency range of 10 to 32 KHz indicated that the acoustic power transmission depends upon the roughness and waviness of the poppet/valve seat surfaces in contact and the seat loading (Tables 5-2, 5-3, Figures 5-14 to 5-17). The voltage output also changed as a result of cycling the valve poppet and seat at a given acoustic test frequency. This change in voltage output is interpreted to be due to a change in orientation of the mounting fixture and the hysteresis in the isolation pad. This offset was corrected by comparing the receiver output voltage at the standing wave maximum by changing the operating frequency. Note that the values with the super script M, Table 5-3, represent the standing wave maximum and m represents the standing wave minimum around 15, 23 and 31 KHz. The surface of poppet 16568-2A gave the largest transmission of acoustic power compared with the output with -1A and -3A surfaces. This result agrees with the analysis that smoother surface (smaller gap thickness) should transmit the largest acoustic power.

It is also observed from the data that voltage at standing wave maximum with larger loading is greater than that of smaller loading. This agrees with the preliminary analysis since larger loading gives larger real contact area than the smaller loading.

Table 5-2. Sensor Output (mv) as a Function of Seat Load

Piezoelectric Driven Voltage = 48 Volts RMS

Sensor Noise Level: 12 mv RMS

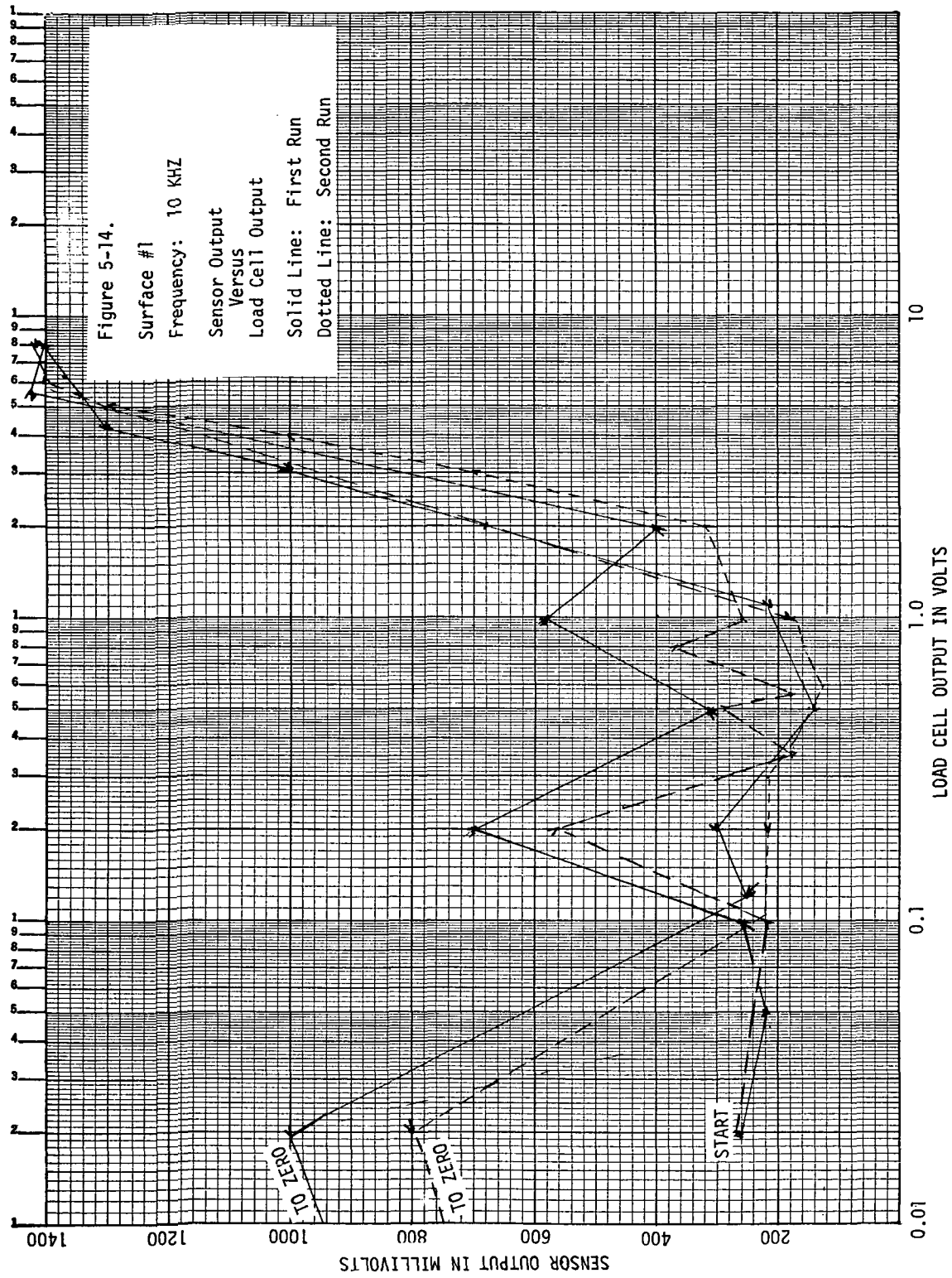| Load Cell Out - Volts	Load Lbs.	Sensor Output m Volts at 10 KHZ			Sensor Output in m Volts at 25 KHZ	
		Surf. #1*	Surf. #2	Surf. #3	Surf. #1	Surf. #2
000	000	192	---	140	000	000
0.02	1.0	260	---	820	90	---
0.05	2.5	220	---	440	360	---
0.10	5	260	---	340	100	800
0.20	10	700	---	520	70	1000
0.50	25	310	---	540	260	1850
1.00	50	580	---	520	760	2100
2.00	100	400	---	440	1100	2900
5.5	275	1600	---	480	500	2600
8.0	400	1600	800	---	460	---
4.3	215	1300	---	---	---	---
3.1	155	1000	---	---	---	---
2.0	100	---	1550	---	---	---
1.05	50	210	840	---	---	---
0.5	25	140	520	---	---	---
0.38	19	---	2000	---	---	---
0.28	14	310	830	---	---	---
0.11	5.5	250	520	---	---	---
0.02	1.0	1200	400	---	---	---
0.000	0.0	12 (noise)	300	---	---	---
0.02	1.0	270	---	---	---	---
0.10	5	220	860	---	---	---
0.2	10	560	1100	---	---	---
0.5	25	290	4400	---	---	---
0.7	35	---	1350	---	---	---
1.0	50	260	1150	---	---	---
2.0	100	320	1500	---	---	---
5.0	250	1300	1300	---	---	---
6.0	300	1450	1200	---	---	---
8.0	400	1450	---	---	---	---
1.0	50	175	---	---	---	---
0.80	40	160	---	---	---	---
0.10	5	220	---	---	---	---
0.02	1	800	---	---	---	---

*Surface number designates poppet and seat part numbers.
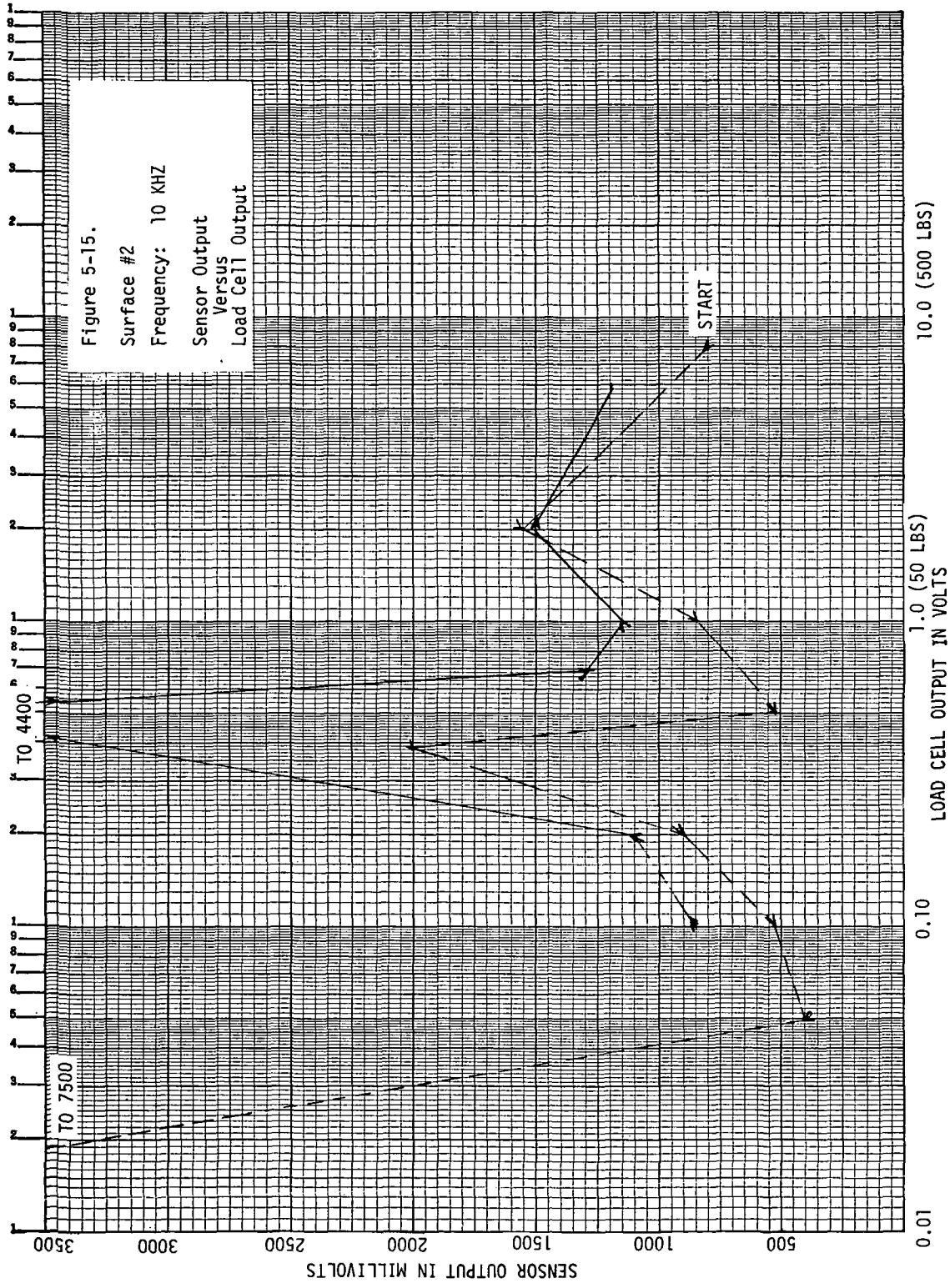Example: Surface #1 uses -1A poppet and -1A seat, etc.

Table 5-3. Sensor Output (m volts) Versus Driven Frequency (KHz) at Constant Seat Load
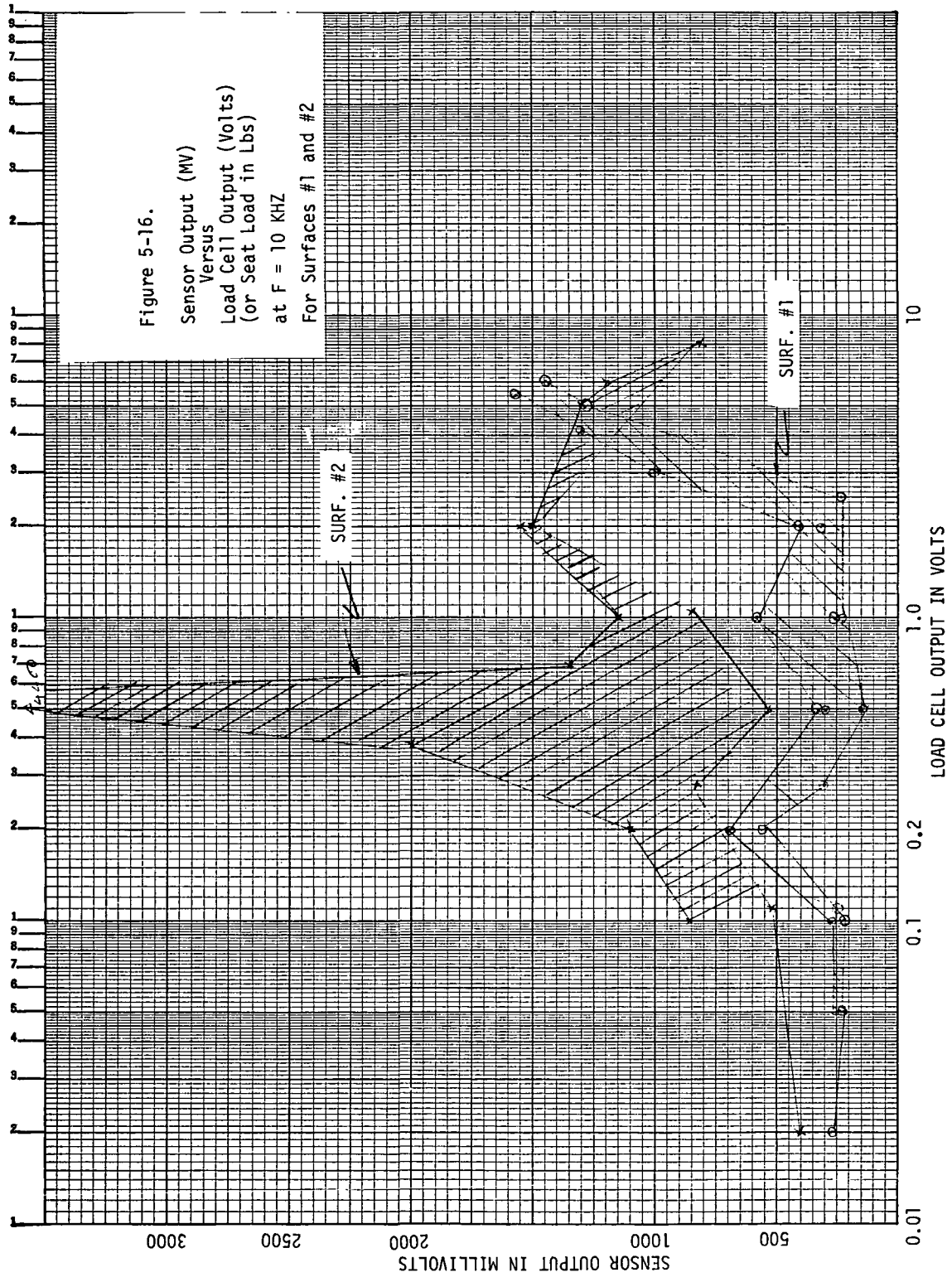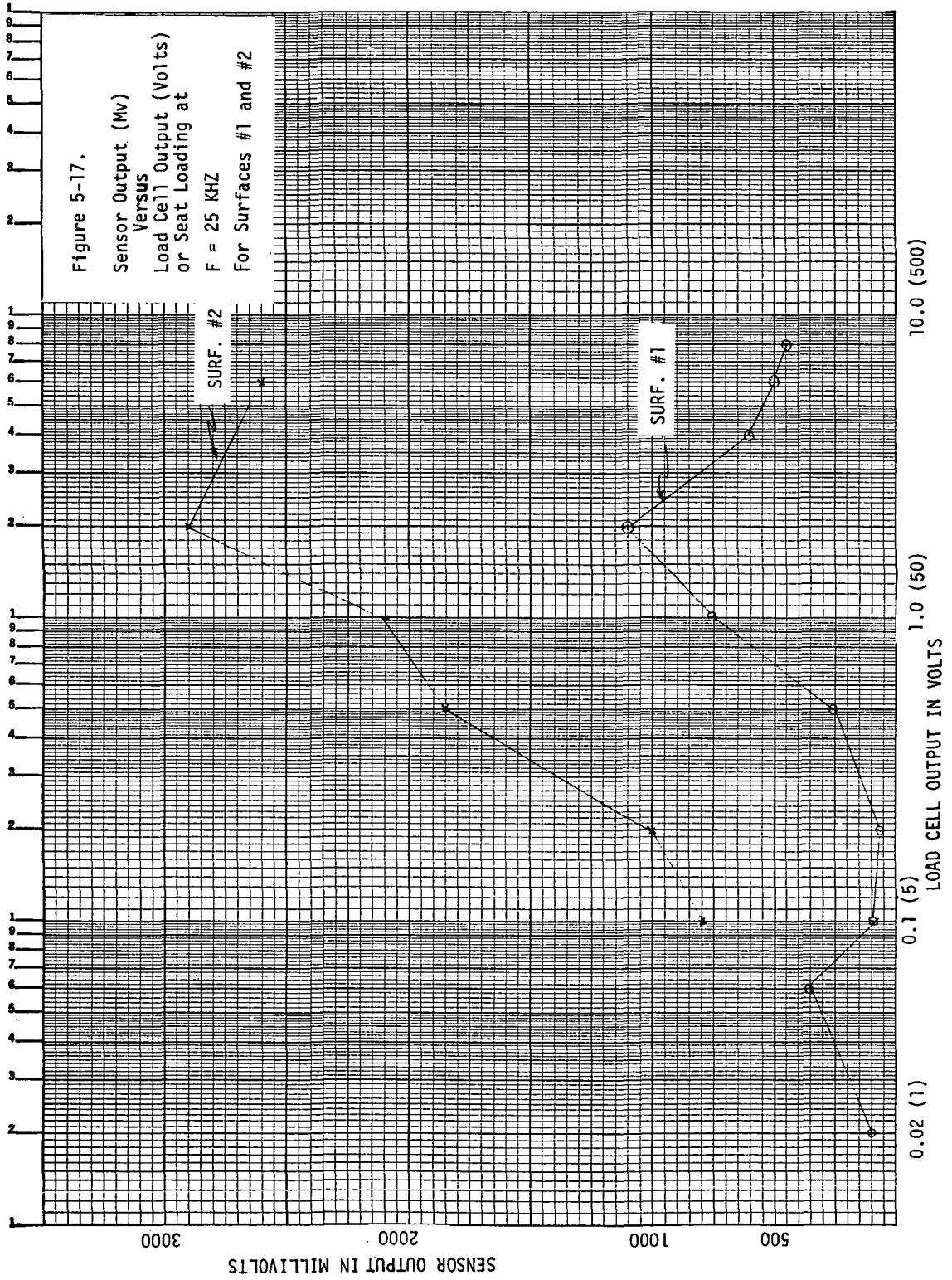
M: Maximum   m: Minimum

Driven Frequency KHz	Surf #1 Seat Load 300 Lbs	Surf #1 Seat Load 60 Lbs	Surf #1 Seat Load 20 Lbs	Surf #2 Seat Load 300 Lbs	Surf #2 Seat Load 60 Lbs	Surf #2 Seat Load 20 Lbs	Surf #2 Seat Load 300 Lbs	Surf #2 Seat Load 300 Lbs	Surf #3 Seat Load 300 Lbs	Surf #3 Seat Load 300 Lbs Vac. Grease	Surf #3 Seat Load 300 Lbs Vac. Grease Removed
10	2,500	330	170	800	700	300	560		480	600	260
10.4	1,500	130[m]		4,400[M]	1,050[M]		1,100[M]	980	260	1,500	280
11	160[m]	140	200	2,000[m]	1,050	540	760	1,000	230		
13	-	-		320	700	400	360[M]				
14	500	420	180	2,800	930	1,600	850	2,400	350	800	220
15	5,500[M]	870	230	4,000	3,800[M]	3,300[M]	2,600	2,100	640	2,900	280
15.5		-		18,000[M]	-				1,500[M]	14,000[M]	530[M]
16	400	130[m]	300	1,350	2,100	840	7,200[M]	2,300	660	3,900	250
17	220	140	500	2,300	600	400	400[M]		220	1,300	
17.5		-		680[m]		320[m]		4,300[M]			
18	170	180	420	1,200[M]	1,000	1,000	850	2,000		500	150
18.5				260[m]			340[m]			350[m]	
19	160[m]	220[m]	320	340	1,100	900	4,000	740		2,700	140
20	320	240	360	700	1,300	760	1,200	2,400			170
20.5									1,600[M]		
21	360	250	400	4,400	1,650	2,300	2,300	9,800[M]	1,200		500
21.5							7,000				
22	1,400[M]	520	460	7,600	3,000	6,400	6,600	4,300		11,000	900
23	580	700	350	18,000	16,000	7,000	6,000	5,300	5,400[M]	42,000[M]	2,800
23.4						9,400[M]					
24	380[m]	1,150	440	19,000[M]	5,400	3,000	18,000	21,000	1,600	780	510
25	580	2,400	500	3,100	1,450	1,300	2,800	3,300	400	400[M]	630
25.5							950				
26	1,300	4,700	640	1,100	800	1,350	1,200	1,100	350	520	1,900[M]
27	2,800	5,800	600	1,300	800	1,500	140	1,750	360	640	950
28	6,400	5,800	1,500	1,400	1,000	1,300	2,200	1,850	300	800	1,000
28.5										2,500	
29	12,000	6,900		2,100	1,500	3,500	4,200			2,000	700
30		8,000[M]	1,800[M]	4,600	2,750	3,800	8,000	6,400		3,800	600
30.7										13,000	
31	20,000[M]		1,350		14,000[M]	10,000[M]	15,000[M]	13,000[M]		12,000	650
31.4	15,000			21,000[M]							
32	1,600		660	17,000	9,400		5,100	5,000	2,500	22,000	650
33			1,100								

NOTE: Surface number designates poppet and seat part numbers.
Example: Surface #1 uses -1A poppet and -1A seat, etc.

5-21

Figure 5-14.

Surface #1

Frequency: 10 KHZ

Sensor Output
Versus
Load Cell Output

Solid Line: First Run
Dotted Line: Second Run

Figure 5-15.

Surface #2

Frequency: 10 KHZ

Sensor Output
Versus
Load Cell Output

Figure 5-16.

Sensor Output (MV)
Versus
Load Cell Output (Volts)
(or Seat Load in Lbs)
at F = 10 KHZ
For Surfaces #1 and #2

SURF. #1

SURF. #2

LOAD CELL OUTPUT IN VOLTS

SENSOR OUTPUT IN MILLIVOLTS

Figure 5-17.

Sensor Output (Mv)
Versus
Load Cell Output (Volts)
or Seat Loading at
F = 25 KHZ
For Surfaces #1 and #2

5.3 HIGH FREQUENCY TESTS

The previous section described the acoustic test and test results at lower frequency input. This section examines the use of higher frequency acoustic power at 4 and 12 MHz. The test sample transmitter and receiver were submerged in water during tests. This should eliminate dependence of the wave propagation on boundary conditions. Both continuous wave and pulsed wave transmission testing were examined. In addition, leakage volume is introduced. Leakage volume is defined as the void between the seat and poppet interface. The void volume is the sum of the leakage area times the path length.

A detailed analysis of the effect of interface on acoustic waves will be discussed with the following assumptions[6,7].

1. The interface or a gap between the poppet and the valve seat surfaces can be considered a disc of air or vacuum having much lower acoustic impedance.

2. The sound wave strikes the interface perpendicular to the interface.

3. The attenuation in the material of the poppet and the seat is insignificant and remains constant.

4. The acoustic wave train is infinitely long (compared to short wave trains or pulses).

The acoustic analysis gives the following expression for the reflectance R and transmittance D:

$$R = \left[\frac{\frac{1}{4}\left(m-\frac{1}{m}\right)^2 \sin^2\left(\frac{2\pi d}{\lambda}\right)}{1 + \frac{1}{4}\left(m-\frac{1}{m}\right)^2 \sin^2\left(\frac{2\pi d}{X}\right)} \right]^{1/2}$$

5-26

$$D = \frac{1}{\left[1 + \frac{1}{4}\left(m-\frac{1}{m}\right)^2 Sin^2\left(\frac{2\pi d}{\lambda}\right)\right]^{1/2}}$$

Where $m = \delta_1 V_1 / \delta_2 V_2$

d = thickness of the gap

λ = wavelength = V/f

Maxima of D and minima of R occur when

$\frac{d}{\lambda} = 0, \frac{1}{2}, 1, \frac{3}{2}$, etc.

Maxima of R and minima of D occur when

$\frac{d}{\lambda} = \frac{1}{4}, \frac{3}{4}, \frac{5}{4}$, etc.

Our interest lies in very thin gaps and this occurs at first transmittance maximum, i.e., when $\frac{d}{\lambda} = 0$ to $\frac{d}{\lambda} = 1/4$.

The transmittance D and reflection R for steel and aluminum with air gap and water gap are shown in Figures 5-18 and 5-19.

Note that the variable fd (product of frequency in MHz and the gap thickness in millimeter) is plotted on the absissa.

Our interest lies in determining the smallest gap thickness possible. Assume that a 5% change (based on overall instrumentation accuracies) are more reflected energy is detectable.

Referring to Figure 5-18, fd is less than 10^{-7}.

The following values were obtained as a function of frequency:

f(MHz)	d (mm)	d in microns
0.01	10^{-5}	10^{-2}
0.1	10^{-6}	10^{-3}
1.0	10^{-7}	10^{-4}
10.0	10^{-8}	10^{-5}

Figure 5-18. Transmittance D and Reflection R By Water Gap in Steel and Aluminum

d = Thickness of Gap (mm)
f = Frequency (MHz)

5-28

Figure 5-19. Transmittance D and Reflection R
By Air Gap in Steel and Aluminum

d = Thickness of the Gap (mm)

f = Frequency (MHz)
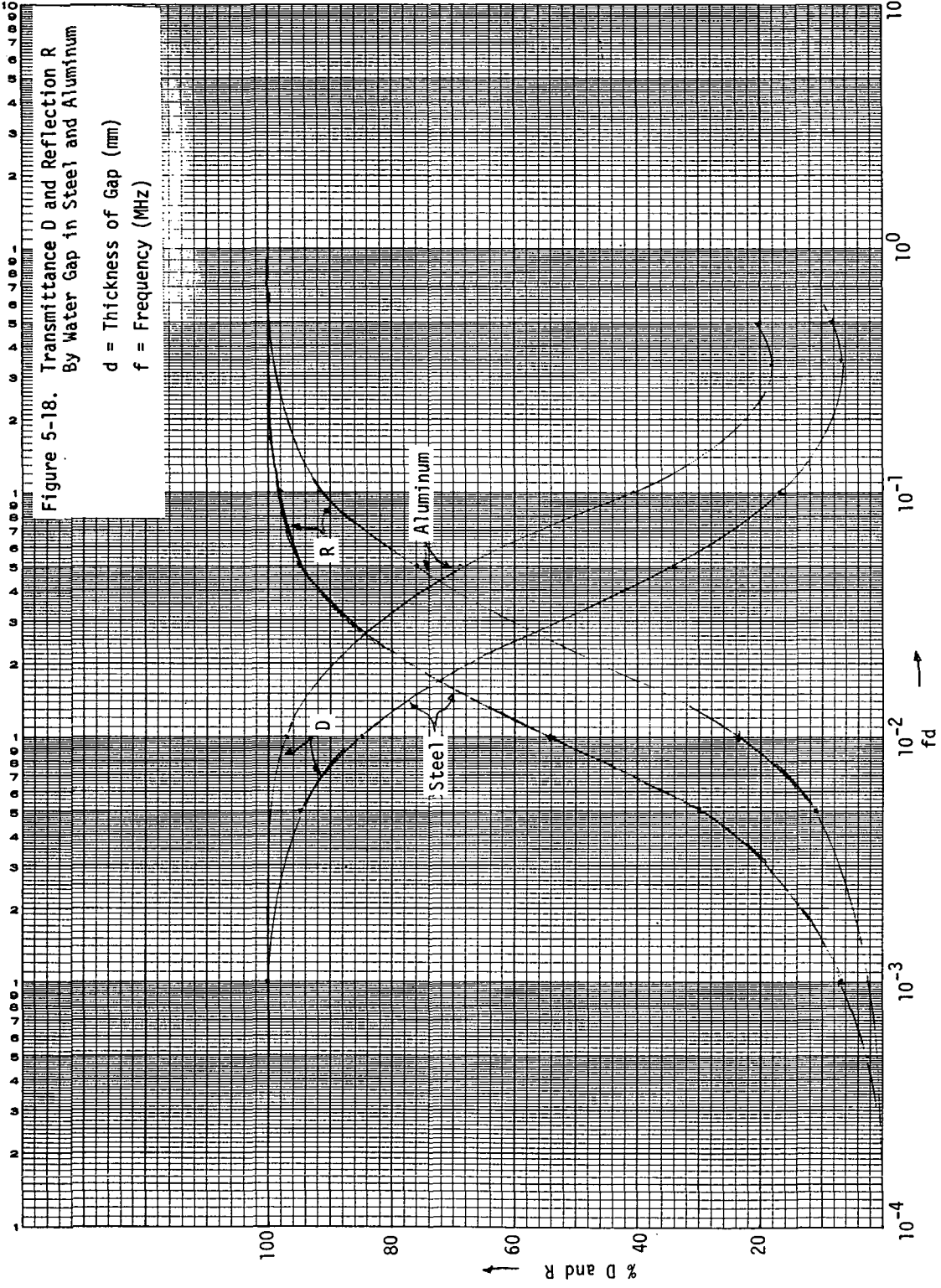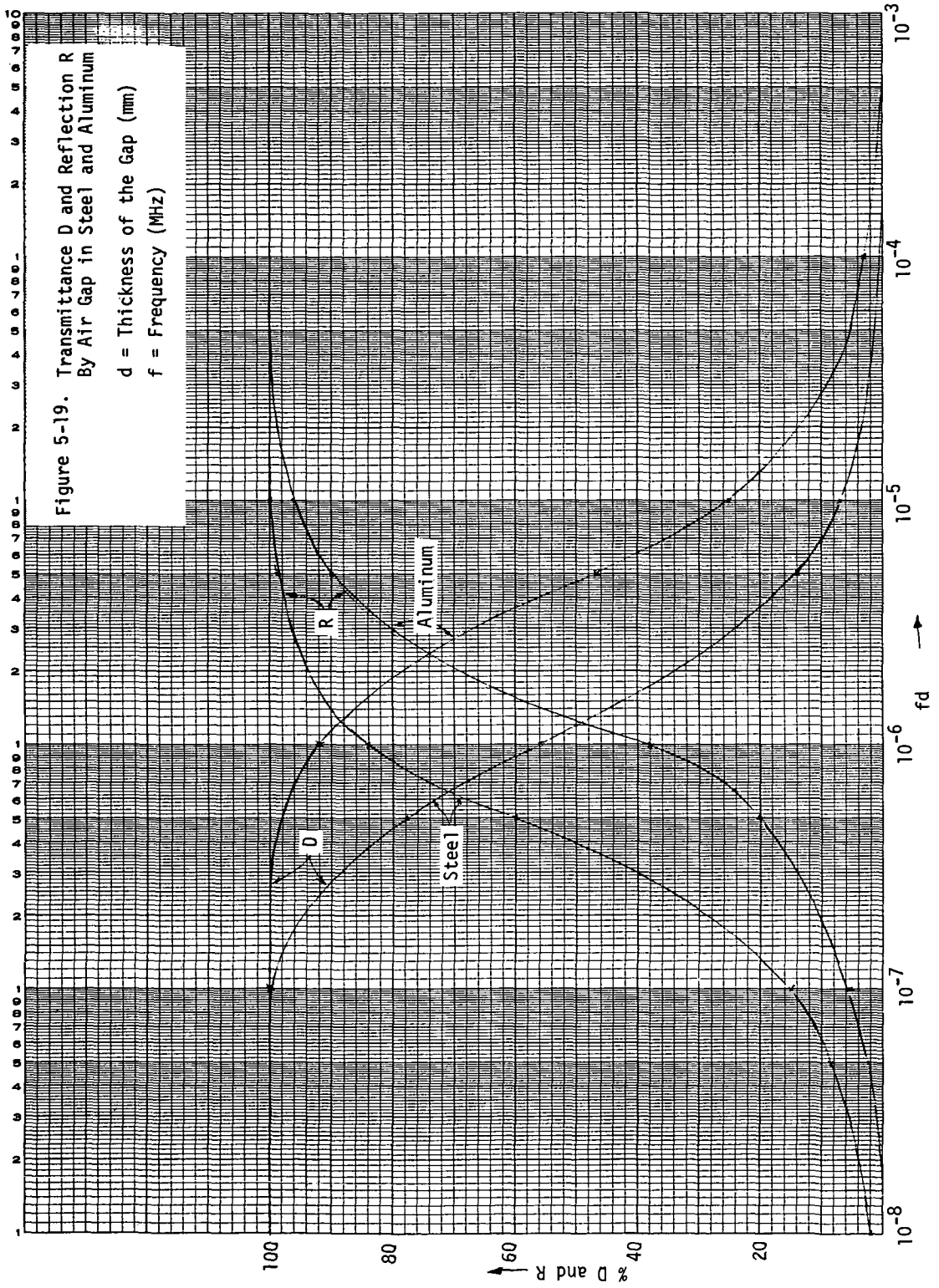
Note that the technique employing detection of transmitted wave is less sensitive than the one employing the detection of reflected wave since D does not change significantly as R at $fd = 10^{-7}$.

These computations are hypothetical since in actual practice the reflection is never 100% with an air gap of 10^{-5} mm because of the presence of foreign layer remaining on the surface even if cleaned most carefully which reduces the reflection and increases the transmission.

In case of a gap thickness in steel filled with water, the smallest detectable thickness as a function of frequency is given as follows:

f (MHz)	d (mm)	d (micron)
0.01	10^{-1}	100
.01	10^{-2}	10
1.0	10^{-3}	1
10.0	10^{-4}	0.1
100.0	10^{-5}	0.01

The duration of the acoustic wave depends upon the selection of technique. For reflection measurement the duration of the acoustic wave train should be sufficiently short so that interference pattern is not formed. For transmittance measurement technique employed in the test conducted previously, the wave train should be sufficiently long to form an interference pattern.

Determination of the smallest area of the air or water gap:

The echo wave produced by a circular disc or a gap can be analyzed with the following assumptions:

1. The gap area is located perpendicular to the axis of the radiator at a great distance so that near field interference is not present. It also means that the gap area is smaller than the beam and causes uniform illumination.

2. The air gap is of sufficient thickness to cause complete reflection.

3. The radiator diameter is much greater than the wave length.

4. The gap area is smaller than the area of cross section of the sound beam.

The sound pressure of the reflected wave on the axis can be calculated from the following equation:

$$H_f = \frac{P}{P_o} = \frac{A_s A_f}{a^2 \lambda^2} = 10 \frac{G^2}{X^2} \quad (A_f < A_{sound\ beam})$$

Where: P = reflected pressure wave amplitude

Po = initial pressure wave amplitude

A_s = radiator area

A_f = gap area

a = distance between the radiator and the gap

λ = wave length

$$G^2 = A_f/A_s = D_f^2/D_s^2 \quad (dimensionless)$$

$$N = A_s/\pi\lambda = \text{length of the near field}$$

$$X^2 = a^2/N^2 \quad (dimensionless)$$

If the gap area is greater than the sound beam cross sectional area, the expression for the sound pressure echo is:

$$H_r = \frac{P}{P_o} = \frac{A_s}{2a\lambda} = \frac{\pi}{2X} \quad (A_f > A_{sound\ beam})$$

The following observations are made from these equations and Figures 5-20 and 5-21.

1. The echo is larger if X is smaller. However, X is required to be as large or larger than the length of the near field N. Therefore, the poppet-seat interface should be approximately N, the length of the near field, away from the radiator.

2. The ratio G should be as large as possible. If an estimate of the range of gap diameter is obtained, the radiator diameter can be determined approximately.

5-31
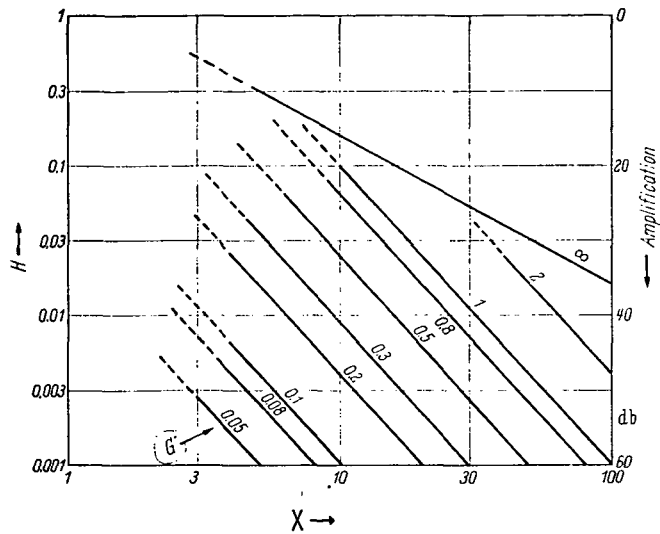
Figure 5-20.   Relation between distance of gap, height of
              echo H or amplification and size G of a flaw
              having the form of a circular disc in the
              far field.
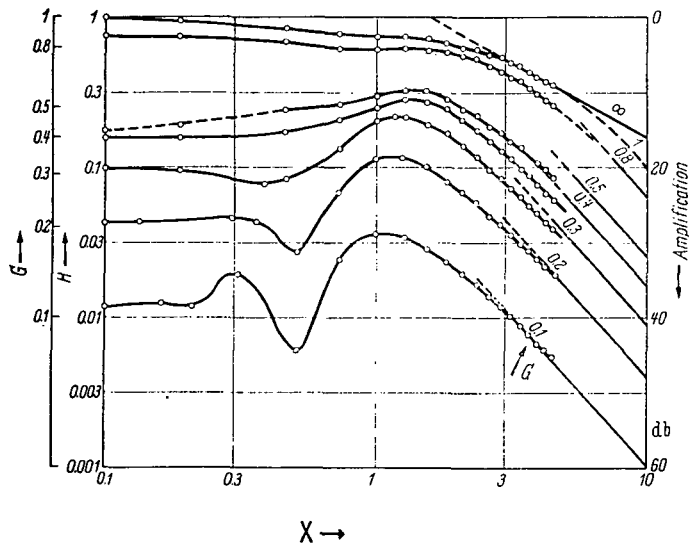
Figure 5-21.   Diagramm in the near field, measured in water
              with a 2 MHz radiator of 24 mm diameter.

It is known that the diffraction phenomena is an important factor in determining the gap if the gap diameter is smaller.than the wave length. However, it is possible to separate groups of small gaps (gap diameter smaller than wave length) from large gaps (gap diameter equal to a larger than the wave length).

Consider the shadow of a flaw in the form of a circular disc. The sound pressure at any given point in the shadow zone is:

$$P = P_o - P_s$$

where P_s is the sound pressure of the interfering wave and P expressed in the equation is a complex number and the phase change must be considered.

In the far field of the gap $(a \gg N_f)$

$$N_f = D_f{}^2/4\lambda$$

$$P = P_o \left(1 - \pi\frac{N_f}{a}\right)$$

At a very great distance a, the disturbance becomes negligible; that is, $P = P_o$. At distances shorter than 6 N_f, the phase change of the interfering wave will cause the sound pressure to vary in both directions. The sound pressure in a shadow zone as a function of distance in terms of N_f is shown in Figure 5-22. The distribution of sound pressure in the shadow zone of a circular flaw, calculated for a section transverse to the axis at a distance 6 N_f is shown in Figure 5-23. Note that the sound pressure variation shown in Figure 5-22 can be detected by small area receiver. A larger receiver would smooth out the differences by its averaging effect. Figure 5-22, indicates that at a = 30 N_f the sound pressure along the axis is 10% lower than the undisturbed sound pressure. However, in the zone from 0.5 N_f to 2 N_f, the sound pressure becomes greater and this zone is unsuitable for detection. The limits are drawn in Figure 5-24 for smaller flaw (gap) diameter of $\lambda/3$. As stated previously for diameters smaller than $1/3\lambda$ the sound pressure rapidly decreases to zero. The limitation imposed by the shaded area in Figure 5-24 can be bypassed by changing the frequency.
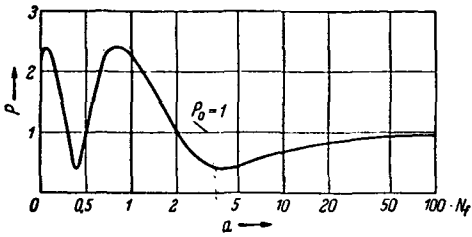
Figure 5-22. Sound pressure in the shadow zone of a circular disc gap, calculated for points along the axis.
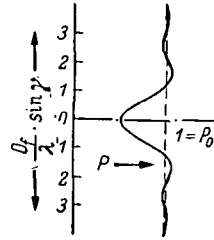

Figure 5-23. Distribution of sound pressure in the shadow zone of a circular disc flaw, calculated for a section transverse to the axis at distance $a = 6\ N_f$.
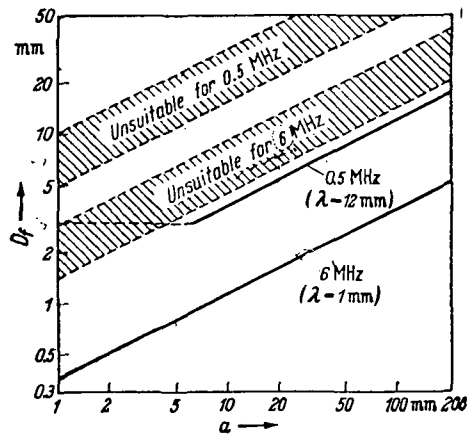

Figure 5-24. Minimum diameter of circular disc flaws, which can still be detected by a 10% reduction in sound pressure in their shadow zone at a distance a calculated for an incident, plane wave in steel or aluminum at 0.5 and 6 MHz, respectively.

Continuous and Pulsed Wave High Frequency Tests

The analysis showed that changes at the interface will result in changes in the acoustic transmittance provided the dimension of the void volume of the interface are larger than the limiting values based on frequency considerations. Also, as a result of the analysis the echo or reflectance measurement is more sensitive than the transmittance measured and that test frequencies should be in the range of from 0.1 MHz to 100 MHz.

Tests were conducted on the poppet and seat configuration at above 4 MHz. These tests consisted of continuous waves and pulsed wave transmission techniques. The smallest increment of void area that can be distinguished is of the order of $\lambda/3$. For f = 10 MHz considered here, diameter of the void area should be larger than 0.2 mm or .008 inch, for detection. The incremental void area is defined as the projected area of one asperity.

The test poppet and seat used in these tests are the same geometry as shown in Figures 5-3 and 5-4. The photographs and profiles of the surfaces of the test parts are shown in Figures 5-25 through 5-32. The peak-to-peak and rms values are estimated as shown in Table 5-4. Assume that the surface profile is approximated by a saw tooth wave. Then the maximum width of the incremental void area is of the order of a few microinches to tens of microinches which is much smaller than the 0.05 inch required to distinguish the void area. It is expected that the acoustic technique would detect variations in the thickness of the void (thickness d in previous analysis) but not the variations in the area. The transducer output should change in proportion to the roughness and waviness of the test sample surface.

Sample Preparation

Three samples, each consisting of a valve seat and a poppet of different surface finishes were prepared as follows:

1. The poppet was mounted on the valve seat so that they were concentric. The allowed eccentricity was of the order of ± 0.002 inch.
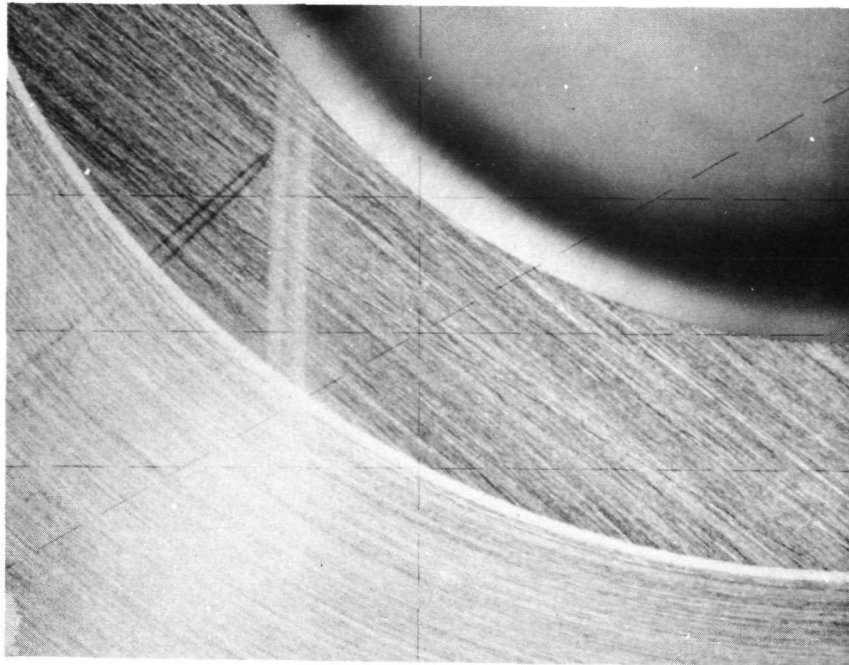
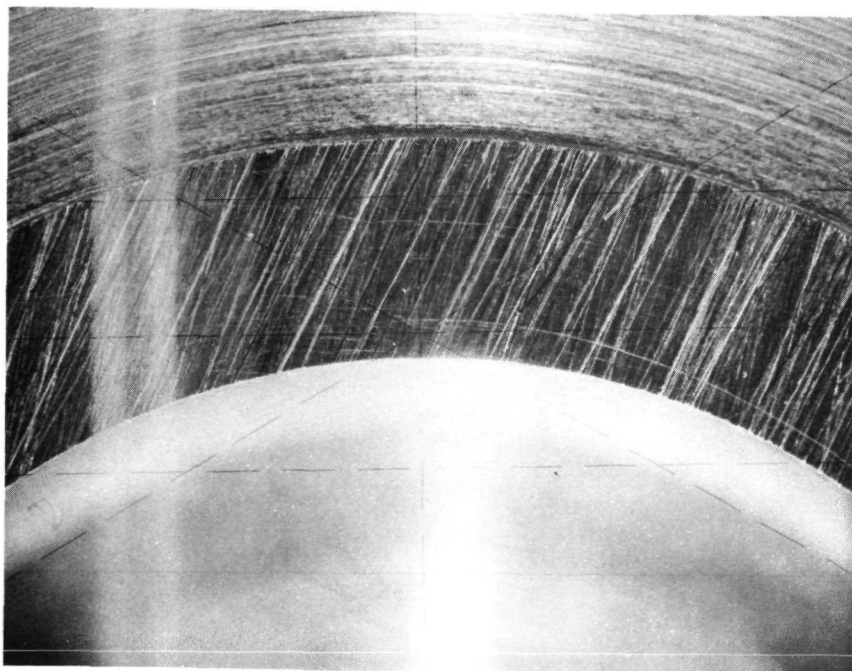Figure 5-25. PN 16568-1B Poppet Surface 20X

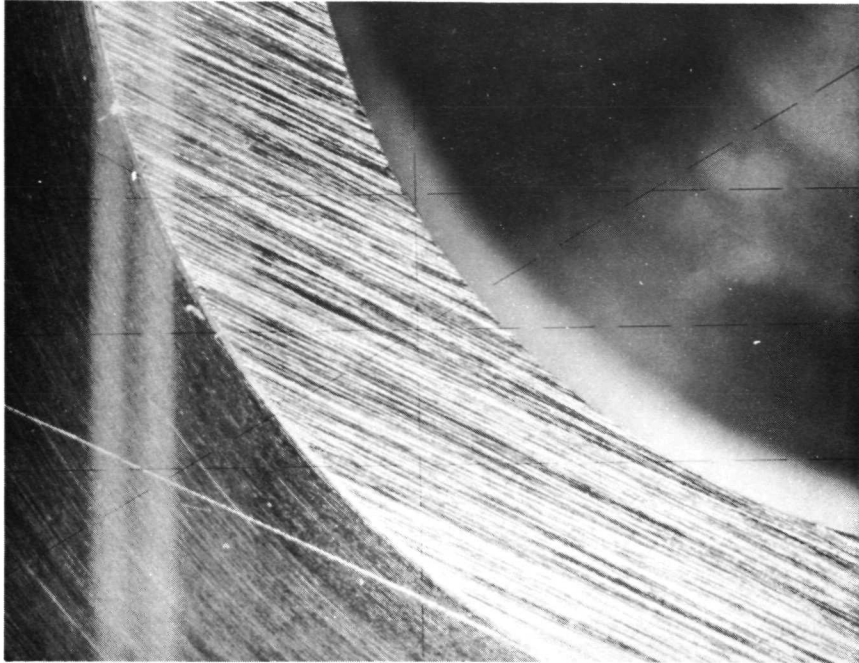Figure 5-26. PN 16568-2B Poppet Surface 20X

Figure 5-27. PN 16568-3B Poppet Surface 20X

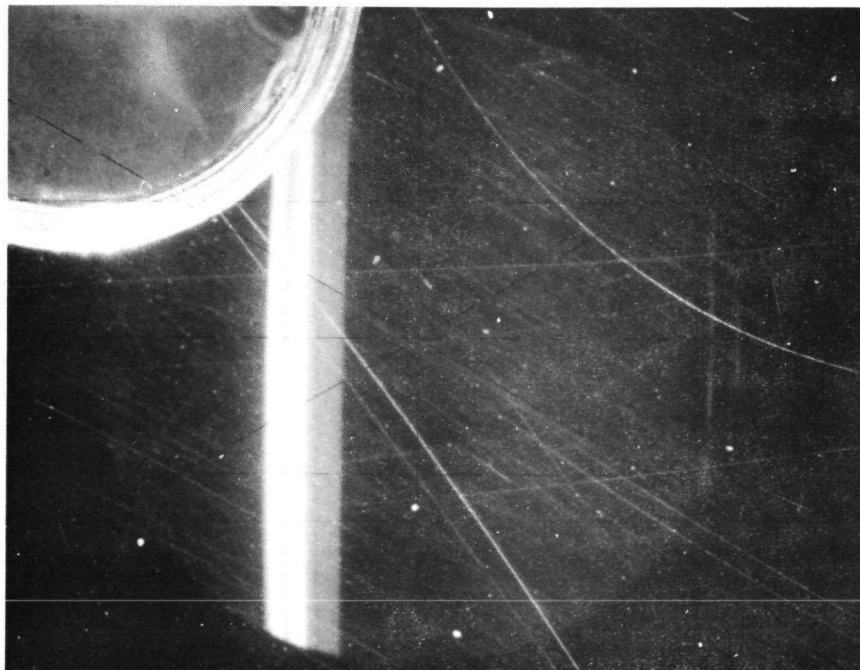Figure 5-28. PN 254296-1B Seat Surface 20X

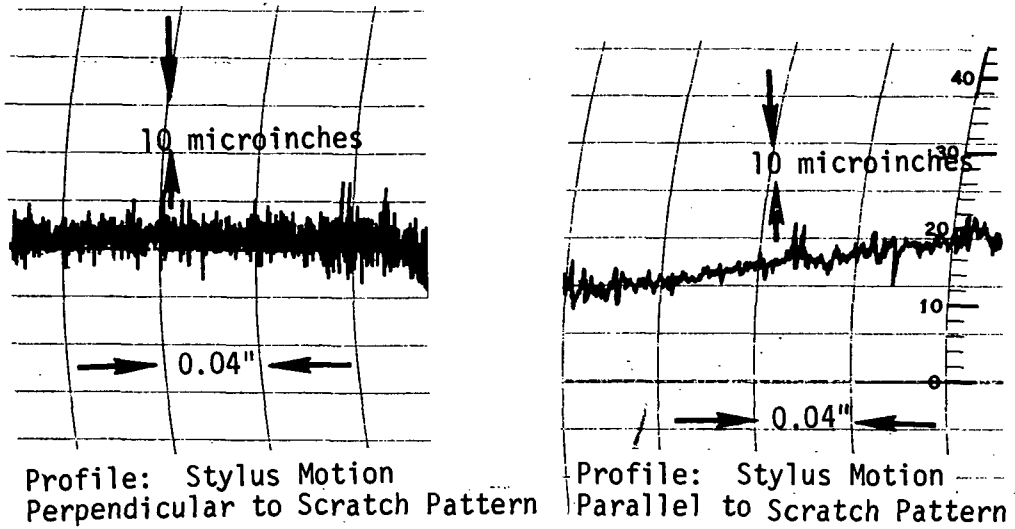Profile: Stylus Motion
Perpendicular to Scratch Pattern

Profile: Stylus Motion
Parallel to Scratch Pattern

Figure 5-29. Typical Profile of Poppet 16568-1B
Stylus Radius: 500 microinches

Profile: Stylus Motion
Perpendicular to Scratch Pattern

Profile: Stylus Motion
Parallel to Scratch Pattern
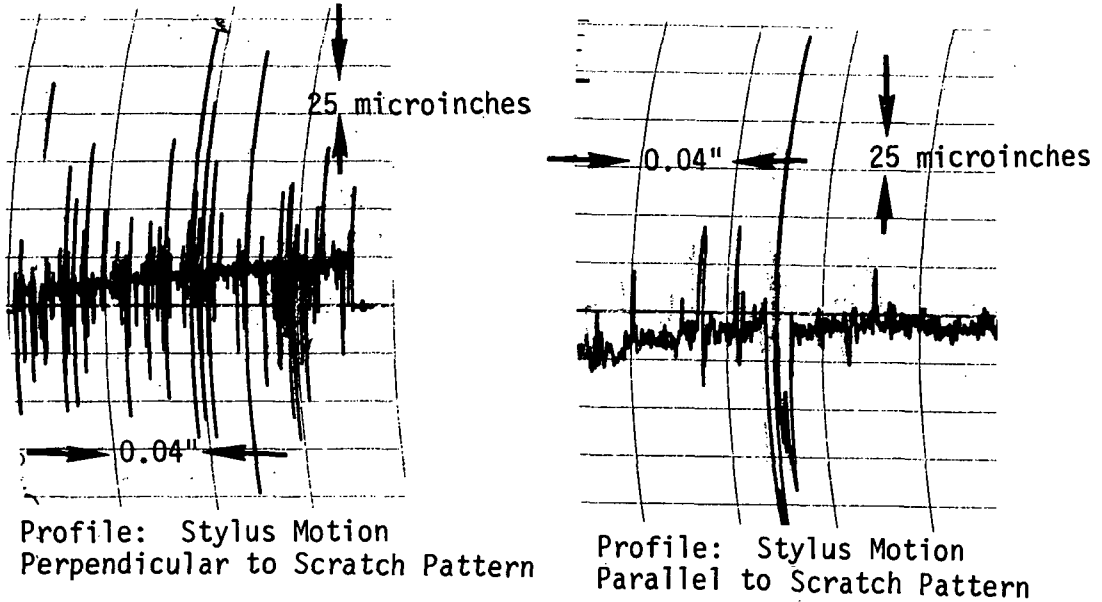
Figure 5-30. Typical Profile of Poppet 16568-2B
Stylus Radius: 500 microinches

Profile: Stylus Motion
Parallel to Scratch Pattern

Profile: Stylus Motion
Perpendicular to Scratch Pattern
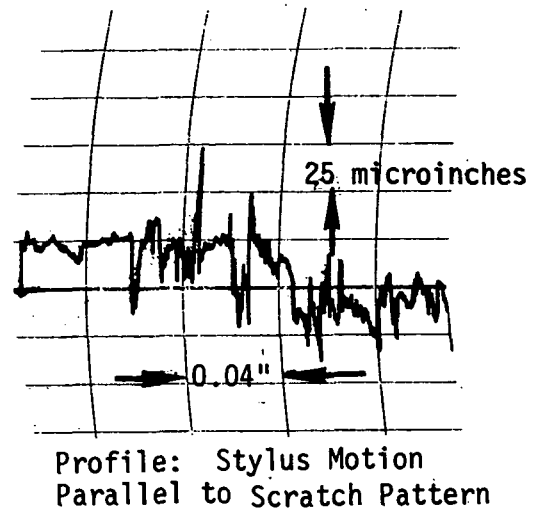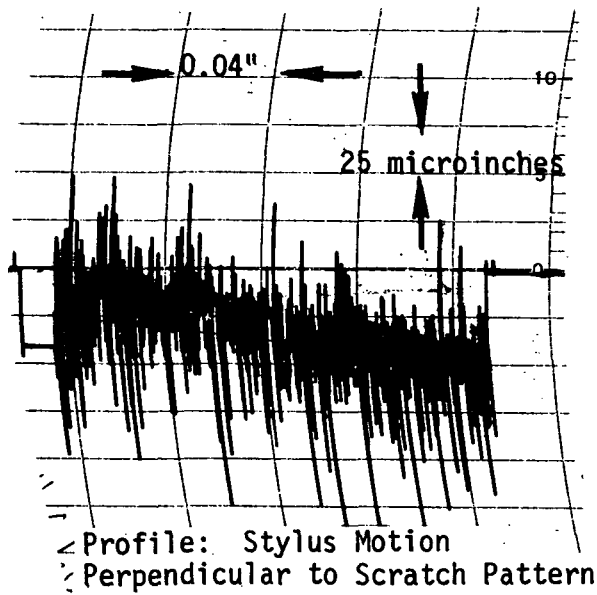
Figure 5-31. Typical Profiles of Poppet 16568-3B
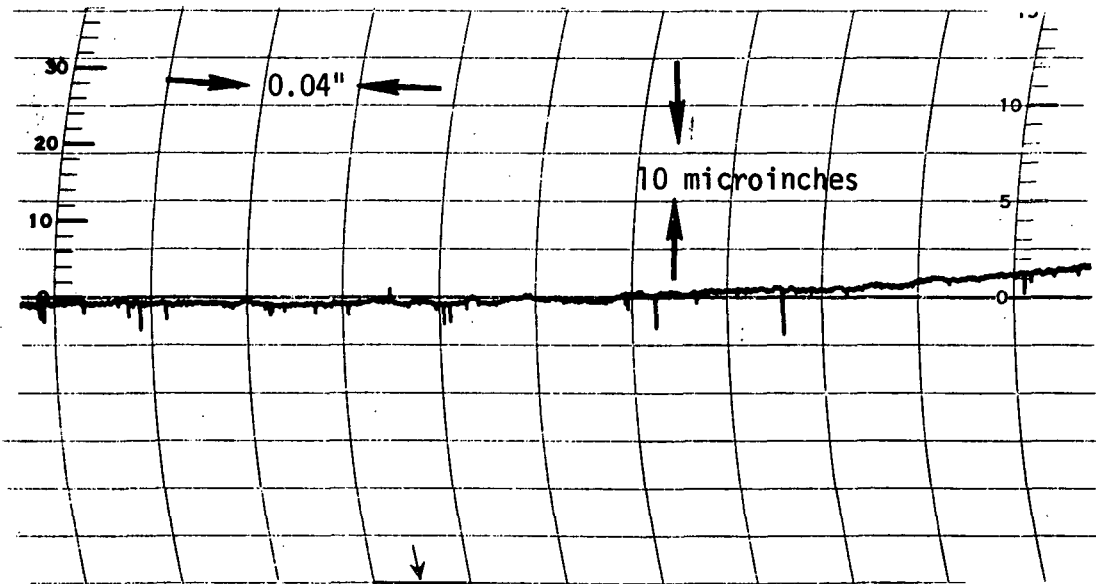Stylus Radius: 500 microinches

Figure 5-32. Typical Profile of a Valve Seat PN 254296-1B
Stylus Radius: 500 microinches
Waviness: 1 microinch rms
Roughness: 1 microinch rms

5-39

Table 5-4. Surface Topology Analysis

PART NO.	ROUGHNESS (0-2 mils Interval) Micro Inches		WAVINESS (20 mils or larger Interval) Micro Inches		TOTAL Micro Inches
16568-1B	8 Peak - Peak	3 R.M.S. (1)	4 Peak - Peak	1.5 R.M.S.	12 Peak-Peak
16568-2B	75 Peak - Peak	26 R.M.S.	38 Peak - Peak	12.8 R.M.S.	113 Peak-Peak
16568-3B	72 Peak - Peak	25 R.M.S.	38 Peak - Peak	12.8 R.M.S.	110 Peak-Peak

(1) RMS is obtained by multiplying the peak to peak value by .35.

2. The poppet and the seat were secured to each other by employing an adhesive tape. A thin layer of sealant (Dow Corning 731 RTV) was applied around the periphery of the poppet at the valve seat poppet interface. The sealant is an excellent sound absorber at high frequencies considered here. The objective of applying sealant is to make the interface cavity air tight.

3. A 20 pound weight was mounted on the assembly and the rubber was cured at room temperature in a 24 hour period. The valve seat hole was plugged with a 0.25 inch diameter dow-pin and sealed with Dow Corning 731 RTV sealant.

4. The assembly was cured at room temperature in a vacuum environment. The vacuum in the interface cavity gives a constant pressure of 14.7 psi across the interface. A photograph of three seat assemblies and a poppet is shown in Figure 5-33.
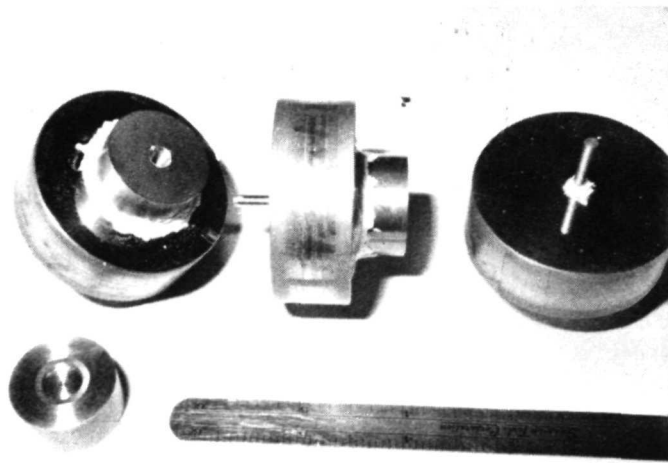

Figure 5-33. Seat and Poppet Samples Prepared For
Acoustic Signature Testing

Continuous Wave Transmission Test Description and Results

The previous test setup employing a Clevite PZT-5 crystal as a driver and the Endevco 2272 accelerometer cannot be employed at and beyond accelerometer resonant frequencies of 32 KHz. For the test at high frequences be beyond 4 MHz, an acoustic transmitter and a receiver were constructed employing quartz crystals manufactured by Valpey Corp., Hollister, Mass. The important specifications of the crystals are:

1. Dimensions: 1" x 1.25"

2. Surface Coating: Polished chrome gold coated sides with two leads, one on each side.

3. Flatness: 0.000020"

4. Parallelism: 0.000050"

5. Approximate Fundamental Resonant Frequency: 4 MHz

The transmitter and receiver assemblies are identical and can be interchanged. The detailed assembly drawing is shown in Figure 5-34.

The transmitting transducer is driven by a high voltage variable continuous wave frequency oscillator (Arenborg Ultrasonic Lab. Inc., Boston, Mass., Model PG 650). The receiving transducer output is measured by a high frequency voltmeter (Hewlett-Packard RF millivoltmeter, Model 411A)

The test setup diagram is shown in Figure 5-35. The acoustic output passes through a hole (aperture) in a 0.25" thick rubber plate. The rubber (Row-sec PC rubber) has the same acoustic characteristic impedance PC as that of water. The PC rubber is mounted on an epoxy base to provide a rigid support.

The function of the PC rubber is to absorb most of the acoustic power falling on its surface. The hole diameter is approximately the same as that of the poppet outer diameter. The center lines of the test sample, the aperture, the transmitter and the receiver are the same (Figure 5-35). The sample is positioned accurately between the receiver and the aperture employing a carrier, having a spherical coordinates (R, θ, ∅) movement.
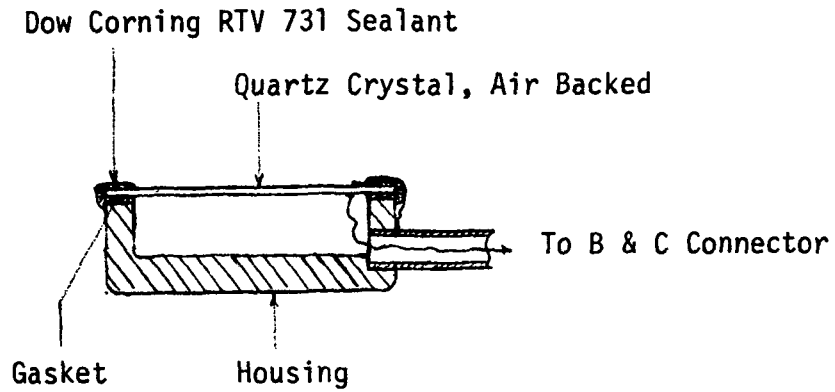
Dow Corning RTV 731 Sealant

Quartz Crystal, Air Backed

To B & C Connector

Gasket   Housing

Figure 5-34. Transducer Assembly

HP 411A
Volt-
Meter

ARULAB
PG 650
Power
Oscillator

Test
Sample

Aperture

Receiving
Transducer

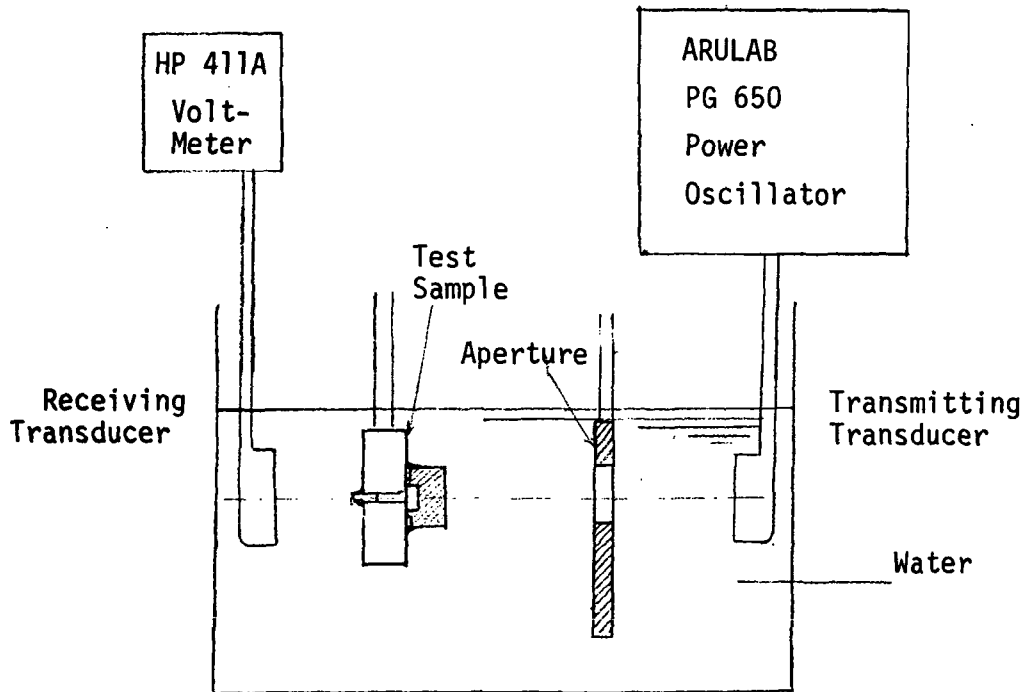Transmitting
Transducer

Water

Figure 5-35. Test Setup

The coordinates of the sample are adjusted such that the receiver output is maximum. The data taken with three samples is tabulated in Table 5-5. The initial data (Table 5-5, a, b) was taken with the adhesive tapes on the samples. The tapes were required only during the curing period of Dow Corning RTV 731 sealant. The results at 4 MHz (Table 5-5, a, c) indicate that the receiver output decreases with increase in surface roughness. The results at 12 MHz with the tape (Table 5-5b) are inconclusive.

With the adhesive tape removed, the results at both frequencies, 4 and 12 MHz (Table 5-5, c, d) indicate that the receiver output is higher with the smoother surfaces.

Pulsed Wave Transmission Test Description and Results

The results of the continuous wave transmission technique showed a standing wave pattern is formed and the receiver output is quite position dependent. Slight change due to a shock or vibration could change the output. However, in a pulsed wave transmission technique, the receiver output is expected to be much less position dependent since a standing wave pattern can be avoided. The tests were conducted employing a 4 MHz and 12 MHz, three micro-second wide pulses. The test setup was essentially the same as the one employed in continuous wave transmission technique. The frequency of the modulated wave was increased to 20 and 26 MHz which are the higher resonant frequencies of the quartz crystal. However, the receiver output was not detectable most likely due to the difference in these high resonant frequencies of the transmitting and receiving crystals.

The test results are given in Tables 5-6 and 5-7. The results at 4 MHz appear to be better than those at 12 MHz. This is believed due to the transmitter and receiver operating more efficiently at the first resonant frequency of 4 MHz.

Table 5-5. Continuous Wave Transmission Test Results
Oscillator Voltage Approximately 160V

Frequency: 4.1 MHZ
Interface Void Volume: Vacuum

SAMPLE	RECEIVER OUTPUT	SAMPLE WAVINESS AND ROUGHNESS MICROINCHES
None	3.4 volts	
16568-1	26.5 mv	12
None	3.65 Volts	
16568-1	25 mv	12
None	3.6 Volts	
16568-3	9.5 mv	110
None	3.5 Volts	
16568-3	10 mv	110
None	3.2 Volts	
16568-2	10 mv	113
None	2.9 Volts	
16568-1	25 mv	12

(a)

Frequency: 12 MHZ
Interface Void Volume: Vacuum

SAMPLE	RECEIVER OUTPUT IN MILLIVOLTS	SAMPLE WAVINESS AND ROUGHNESS MICROINCHES
None	160	
16568-1	8.5	12
None	160	
16568-1	7	12
None	100	
16568-1	8.5	12
None	150	
16568-3	32	110
None	160	
16568-1	16	12

(b)

Tape Removed

Frequency: 4 MHZ

Interface Void Volume: Vacuum

SAMPLE	RECEIVER OUTPUT	SAMPLE WAVINESS AND ROUGHNESS MICROINCHES
None	6.2 volts	
16568-1	210 mv	12
None	7.0 Volts	
16568-3	72 mv	110
None	5.3 Volts	

(c)

Tape Removed

Frequency: 12 MHZ

Interface Void Volume: Vacuum

SAMPLE	RECEIVER OUTPUT IN MILLIVOLTS	SAMPLE WAVINESS AND ROUGHNESS MICROINCHES
None	310	
16568-3	14	110
None	320	
16568-3	14	110
None	320	
16568-1	28	12
None	350	
16568-3	13	110
16568-1	26 max.	12

(d)

Table 5-6a. Pulsed Wave Transmission Test Results

Frequency: 4 MHz
Interface Void Volume: Vacuum

SAMPLE	ROUGHNESS & WAVINESS MICROINCHES	RECEIVER OUTPUT
No sample	-	1.7 volts
16568-1 poppet facing the sound source	12	10.0 m volts
No sample	-	2.0 volts
16568-1 poppet facing the sound source	12	12.0 m volts
No sample	-	2.0 volts
16568-3 poppet facing the sound source	110	2.0 m volts
No sample	-	2.1 volts
16568-2 poppet facing the sound source	113	2.0 m volts
No sample	-	1.55 volts
16568-1 valve seat facing the sound source	12	7.0 m volts
No sample	-	1.55 volts
16568-3 valve seat facing the sound source	110	1.8 m volts
No sample	-	1.55 volts
16568-2 valve seat facing the sound source	113	1.8 m volts

Table 5-6b.   Pulsed Wave Transmission Test Results

Frequency: 12 MHz

Interface Void Volume: Vacuum

SAMPLE (Poppet Facing The Source)	ROUGHNESS & WAVINESS MICROINCHES	RECEIVER OUTPUT IN MILLIVOLTS
No sample	-	44
16568-1	12	3.6
No sample	-	40
16568-2	113	2.4
No sample	-	42
16568-3	110	2.9
No sample	-	47
16568-1	12	2.8
16568-3	110	1.05

Table 5-6c.   Pulsed Wave Transmission Test Results

Frequency: 12 MHz

Interface Void Volume: Water

SAMPLE (Poppet Facing The Source)	ROUGHNESS & WAVINESS MICROINCHES	RECEIVER OUTPUT IN MILLIVOLTS
No sample	-	45
16568-1	12	6.6
No sample	-	46
16568-2	113	3.6
No sample	-	48
16568-3	110	4.6

5.4 SUMMARY OF TEST RESULTS AND CONCLUSIONS

Preliminary testing in the frequency range of 10 to 32 KHz indicated that the acoustic power transmission depends upon the roughness and waviness of the poppet/valve seat surfaces in contact. The preliminary tests also showed the voltage output at a given frequency changed as a result of cycling the valve poppet and seat. The reason for this change in voltage output is not known and is interpreted to be due to a change in orientation of the mounting fixture and changes in the isolation pads.

A more detailed analysis showed that the resolution of the acoustic technique increases with the test frequency; that is, the detectable interface void volume decreases with increase in the test frequency. The present state of the art in transducer technology is limited to about 100 MHz. The analysis indicates that at 100 MHz the detectable void thickness is 4 microinches and the minimum detectable void diameter is about .005 inches. The analysis also indicated that the frequency dependance (standing wave pattern) can be avoided by pulsed acoustic power transmission.

Based on the detailed analysis, a series of high frequency tests were planned. Twenty MHz and higher frequencies were tried. However, the tests were inconclusive because of the problem of matching of the available transmitter and receiver at multiple resonant frequencies. A 4 MHz transmitter and receiver set was assembled. The tests were conducted in water at 4 and 12 MHz. The reasons for conducting the test in a liquid medium is that the wave propagation from the transmitter to the liquid to the test specimen to the receiver should be independent of boundry conditions.

The test results of the continuous wave (CW) transmission technique showed that the receiver output is dependent on the seat interface characteristics, an order of magnitude change in surface topology resulted in about a 2.5 change in acoustic transmission.

The sensitivity of the pulsed technique at 4 MHz is better than that of the CW transmission. At the same frequency the pulsed technique gave an output ratio of 6:1 compared to the roughness ratio of 10:1 with an

uncertainty of about 20%. The CW technique resulted in an output ratio
of 2.5:1 for the same roughness ratio with about the same uncertainty.

The test data at 12 MHz indicate that the sensitivity is lower for both
the pulsed and CW technique than at 4 MHz. As indicated earlier the
transmitter and receiver used did not operate as efficiently at higher
harmonics as they did at fundamental frequencies. Also the measurement
in the range of millivolts at 12 MHz introduced instrumentation noise
errors (of the order of 20%).

The results of one test (sample 16568-3, Table 5-5b) showed a 4:1 increase
in acoustic output for a corresponding surface roughness increase of approxi-
mately ten. Comparing the data of Table 5-5d a 2:1 increase in acoustic
output corresponded to a 10:1 improvement in surface roughness. The differ-
ence between these tests was the addition of the tape mounting to the test
samples of Table 5-5b. The results of the tests of Table 5-5b are inconclusive.
There were believed two possible reasons for this anomaly, 1) the transducers
may not have been tuned to the same frequency, and 2) changes in the trans-
mission path may have occurred due to the tape method of mounting.

A problem developed in calibrating the transmitted wave between the trans-
mitter and receiver through the water medium (with no specimens in the
path). This is apparent from the data of Table 5-6 for the no sample
case where receiver voltage changed considerably. The reasons for this
are believed due to the stability of the system. A more rigid system
must be developed before any further testing.

Future work would require optimization of the test setup. This required
improved stability of the high frequency power oscillator and receiver.
Acoustic transmittance reflectance should be made in real time. The key
areas recommended for future work are given in the following:

1. Eliminating the formation of interference pattern in
    the test system.

2. Conduct test at higher frequencies above 12 MHz. This
    requires the design and fabrication of matched transmitting
    and receiving transducers.

3. Establish the interface void volume standardization for cali-
    bration purposes by providing several samples of different
    surface finishes.

4. Determine the effect of liquids on matching and dependence
    on environmental changes.

REFERENCES AND BIBLIOGRAPHIES

1. "An Investigation of the Behavior of the Acoustic Emission from the Metals and a Proposed Mechanism for its Generation", a PhD thesis by A.B.L. Agarwall, University of Michigan, Ann Arbor, Michigan, March 1968.

2. "Signature Analysis for Mechanical Devices", by L. F. Sturgeon, General Electric Company, in Volume 2 of Proceedings of the Symposium on Long Life Hardware for Space, March 17-19, 1969.

3. "Handbook of Transducers for Electronic Measuring Systems", by H.N. Norton, Jet Propulsion Laboratory, Prentice-Hall, 1969.

4. "Failure Detection by Mechanical Impedance Techniques", by R.B. Tatge, Journal of the Acoustical Society of America, Vol. 41, No. 5, p. 1196, 1967.

5. "Physical Acoustics and the Properties of Solids", D. Van Nostrand Company, 1958.

6. "Friction and Wear of Materials", by E. Rabinowicz, John Wiley and Sons, Inc., 1965.

7. "Ultrasonic Testing of Materials", by Krautkramer and Krautkramer, Springer-Verlag, New York, Inc., 1969.

8. "Nondestructive Testing Using TRW Acousto-Optical Imaging System", Semi-Annual Report, Contract DAAG46-70C-0103, prepared for Army Materials and Mechanics Research Center, Watertown, Massachusetts, January 1971.

9. "Surface Texture", American Society of Mechanical Engineers United Engineering Center, 345 E. 47th Street, New York. ASA B46.1-1962.

10. "Fourier Analyzers" Technical information note on determination of Transfer or Impedance Functions using Random Noise, Hewlett Packard, May 1970.

11. "Digital Fourier Analysis", by P. R. Roth, Hewlett Packard Journal, June 1970.

12. "Acoustic Emission", Material Research and Standards, ASTM's Magazine on Testing and Evaluation, March 1971.

13. "Use of Acoustic Emission in Nondestructive Testing", Published by J. R. Frederick, Department of Mechanical Engineering, University of Michigan, Ann-Arbor, U.S. Airforce, Aeronautical Systems Division, Contract No. F33615-68-C-1703, Wright-Patterson Air Force Base, Ohio ARPA Order No. 1244.

6.0 LEAKAGE-CYCLE TESTS

6.1 INTRODUCTION

Leakage cycle testing was performed for the purpose of determining the relationship between leakage and valve seat wear as a function of the number of cycles. The results of these tests were analyzed with the objective to determine valve seat surface topology during the wear process and its effect on leakage. Metal to metal seats were used in all testing. Leakage rates were monitored as a function of the number of cycles which in turn was monitored as a function of changes in surfaces. Two sets of valve seats (poppet and seat) were tested.

6.2 DESCRIPTION OF TEST SYSTEM

A schematic of the test system used for the leakage-cycle tests is illustrated in Figure 6-1. Figure 6-2 shows a cross section of the leakage test fixture. Referring to Figure 6-1, the test fixture is actuated by nitrogen gas regulated to 390 psig. The leakage test fluid used for all tests was nitrogen gas at ambient condition and at an inlet pressure of 50 psig.

Leakage is measured employing a volume displacement technique. The leakage measurement device is manufactured by Brooks Instrument Division of Emerson Electric Co., Hatfield, Pennsylvania. The leakage gas displaces a mercury wetted piston fitted in a calibrated tube.

6.3 TEST PROCEDURE

The test procedures are stated in the following:

A. Set the pressure regulator to 390 psig to load the poppet.

B. Set the fluid pressure to 50 psig.

C. Measure the leakage volume displacement and time to determine the leakage rate.

D. Close test fluid valve and vent test fluid circuit.

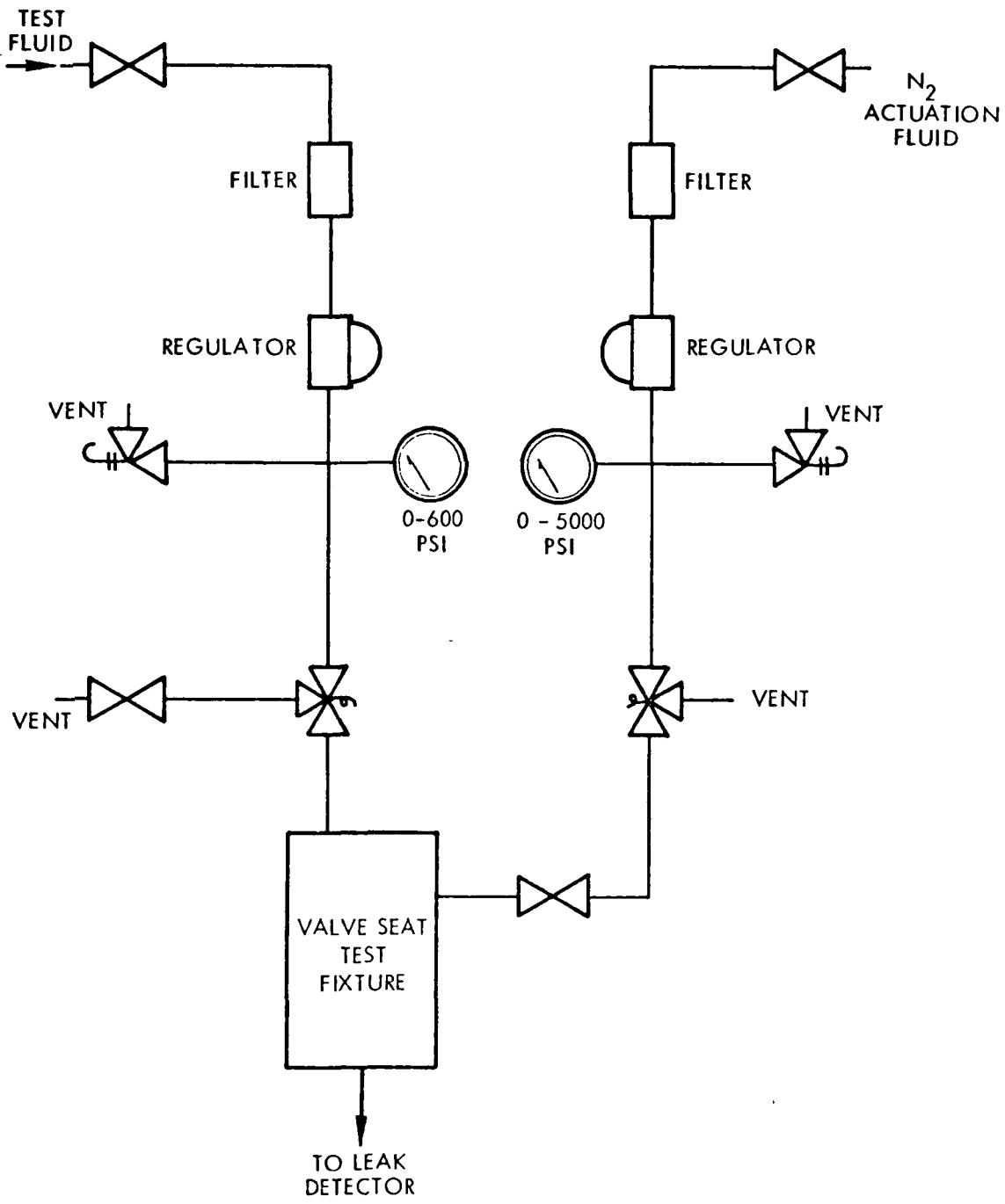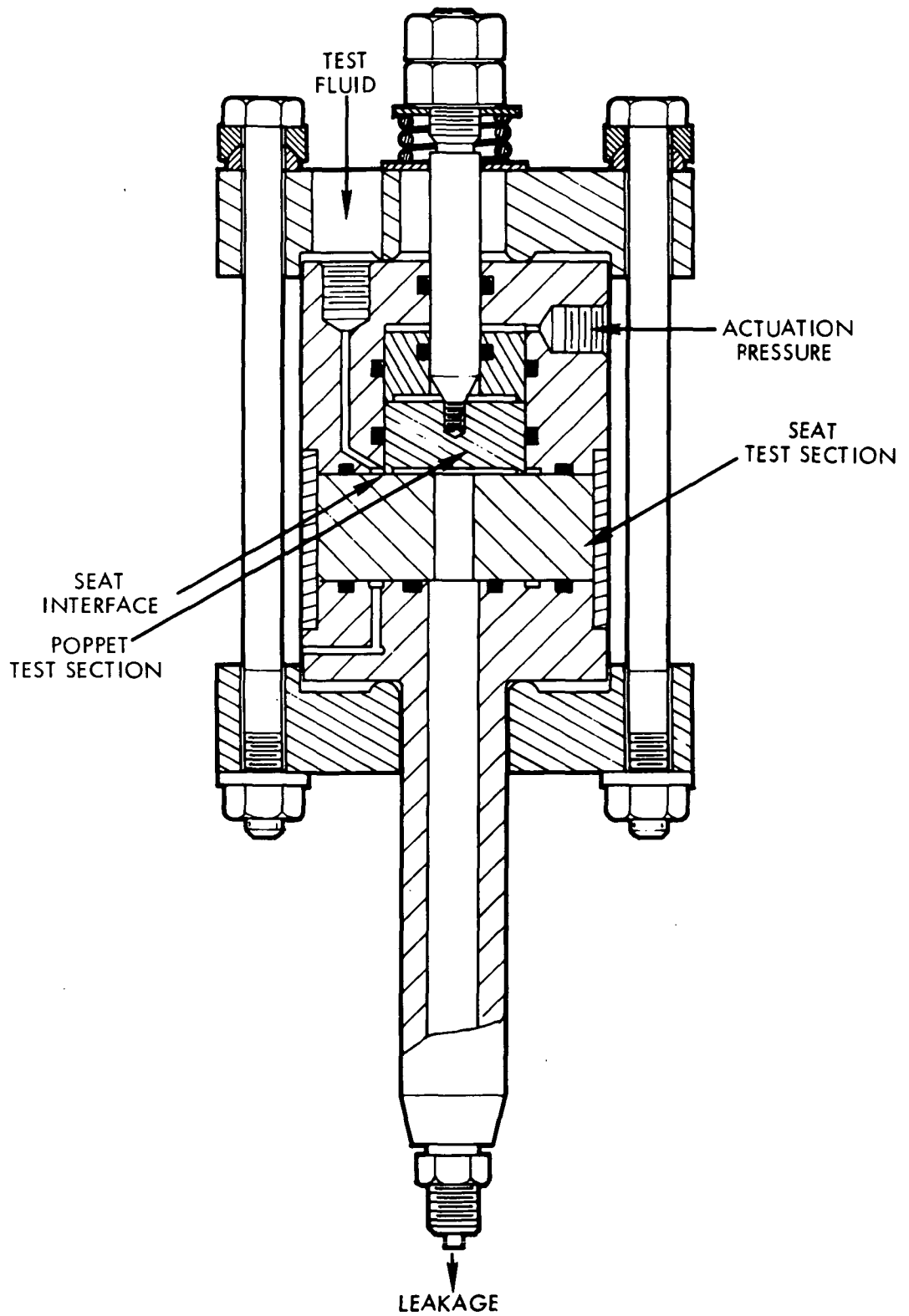Figure 6-1. Leakage Test Circuit Schematic

Figure 6-2. Leakage/Cycle Test Fixture

E. Close actuation fluid valve and vent.

F. To cycle valve close vent valves and open shutoff valve
    of actuation on circuit and then of fluid circuit.

G. After completing desired number of cycles repeat D and
    E and disassemble fixture and remove test poppet and
    seat.

H. Visually inspect surfaces.

I. Clean the surfaces of the poppet and seat with V-113
    degreaser Vatron TF manufactured by Baron Blackel Co.,
    Inc., Los Angeles.

J. Measure waviness and roughness of poppet and seat
    surface using the Bendix Profi-corder.

K. Repeat cleaning procedure of item I and assembly poppet
    and seat in test fixture. Orientation of the poppet and
    seat are to be within 0.01 inch.

L. Cycle test as above.

6.4 DESCRIPTION OF TEST SPECIMENS

The poppet and seat test specimens are identical to the specimens used in
the acoustic signature testing reported in Section 5.0, with the exception
of the surface finish and seat material. Figures 6-3 and 6-4 represent
the poppet and seat design and materials used on the cycle testing.

The surface finish and waviness at different cyclic levels are characterized
for both poppet and seat specimens using the Bendix Profi-corder Model RLC-4
to obtain the surface topology. The Profi-corder profiles are represented
and displayed in Figures 6-5 through 6-8. The rms values shown are obtained
by multiplying the average of the peak-to-peak values by 0.35.

The effective seat area is calculated to be 0.083 in^2. The effective
piston (poppet) area is calculated to be 0.675 in^2. At the piston loading
pressure of 390 psig the seat bearing stress under static load is:

$$\sigma_{brg} = (390 + 15) \frac{.675}{.083} = 3,300 \ lb_f/in^2$$

#10-32 UNF-2B

1.000 Dia

.500

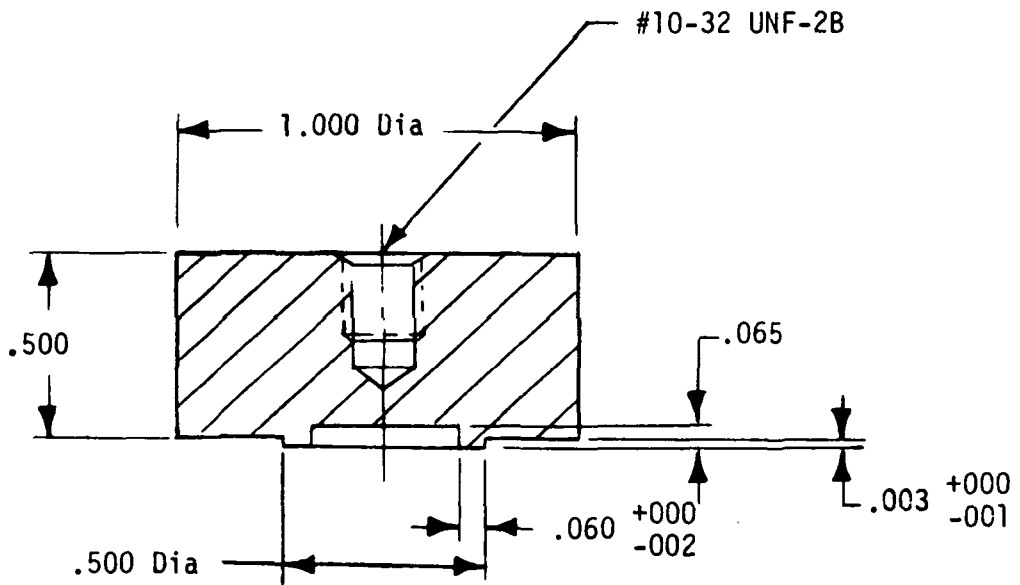.065

.500 Dia

.060 +000 -002

.003 +000 -001

Figure 6-3. 16568 Poppet - Matl: Beryllium Copper
Alloy 172, Temp. H, QQC 530, 2X Size
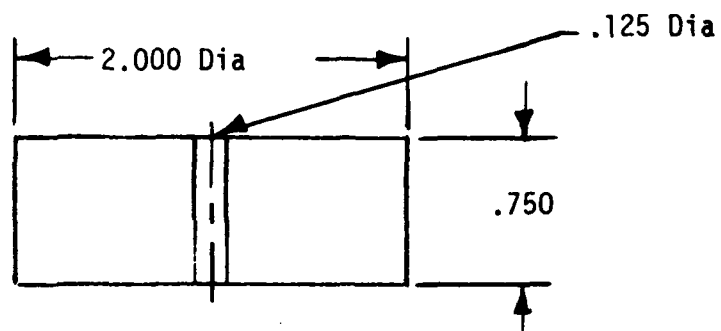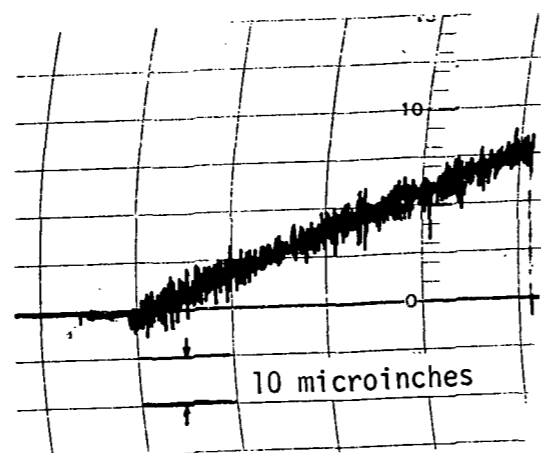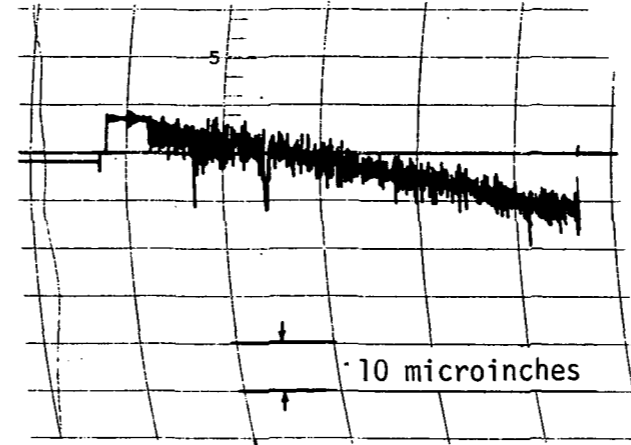
2.000 Dia

.125 Dia

.750

Figure 6-4. Seat - Matl: Inconel No. 718 Solution Annealed
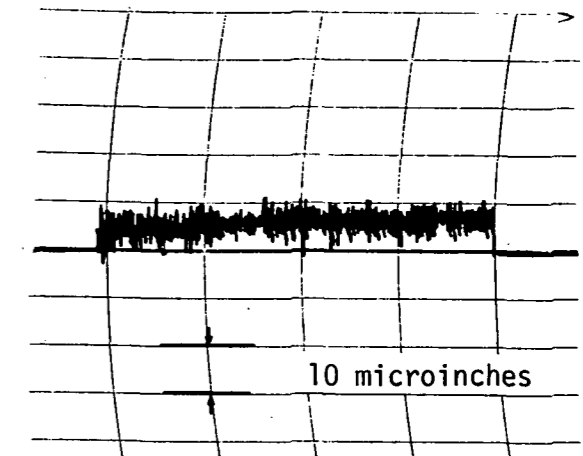and Age Hardened to Rc 42 Min., Electrolized
.0002 - .0003 Inch Thick

162586-1 Electrolized Surface as is
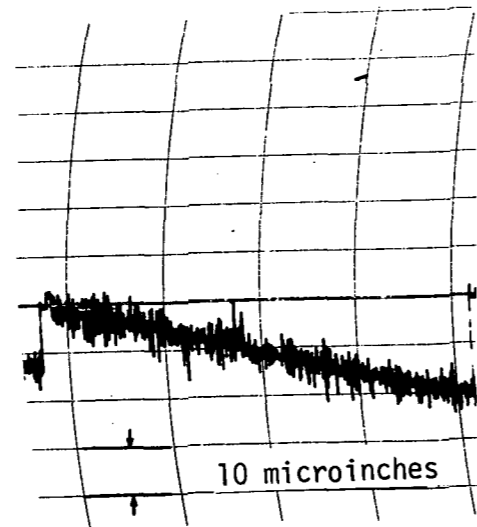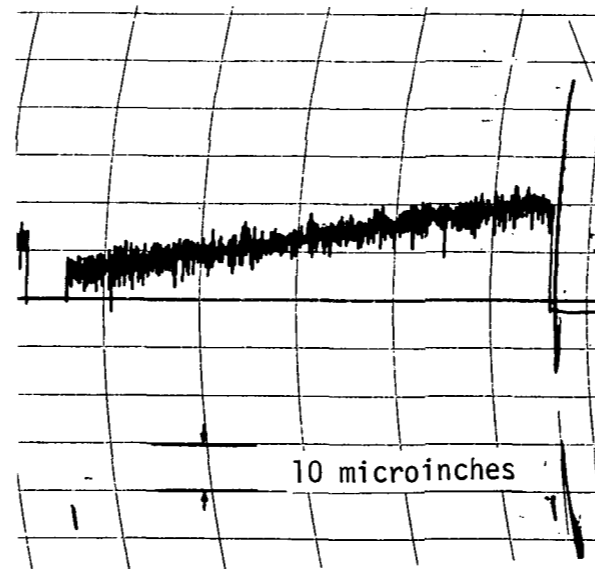162586-2 Electrolized Surface Polished

a. 1 cycle

10 microinches

b. 5 cycles

10 microinches

c. 20 cycles

10 microinches

d. 50 cycles

10 microinches

e. 102 cycles

10 microinches

f. 200 cycles

10 microinches   2.5 microinches

Figure 6-5.   Profiles of Poppet 16568-1 as a Function of Cycles
Bendix Profi-corder Stylus Radius: 500 microinches
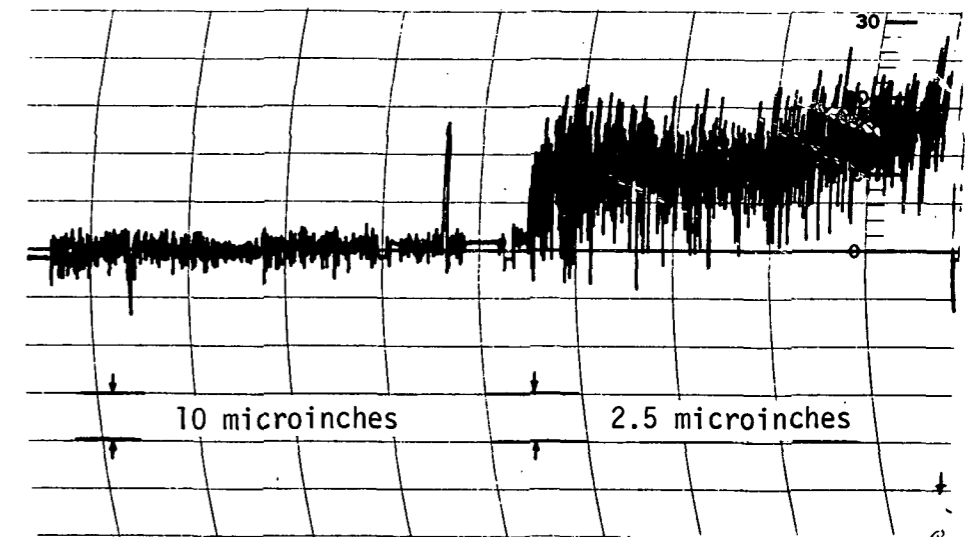Stylus Sweep Direction: Radial

a. 0 cycles

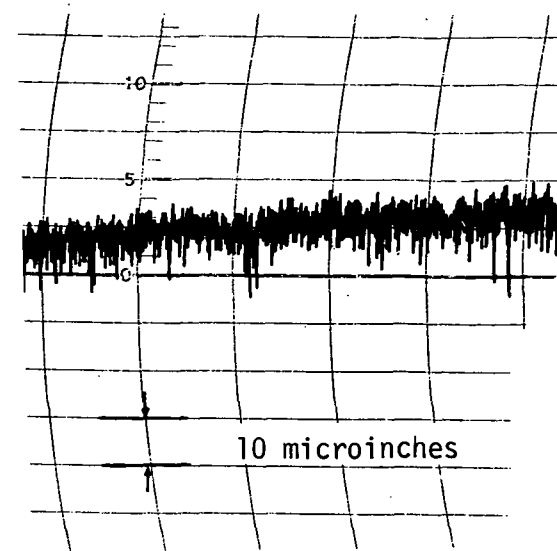b. 1 cycle

c. 5 cycles

d. 20 cycles

e. 50 cycles

f. 102 cycles

g. 200 cycles

Figure 6-6.   Profiles of Seat 16568-1 as a Function of Cycles
Bendix Profi-corder Stylus Radius: 500 microinches
Stylus Sweep Direction: Radial

a. 0 cycles　　　　　　b. 1 cycle　　　　　　c. 5 cycles　　　　　　d. 20 cycles
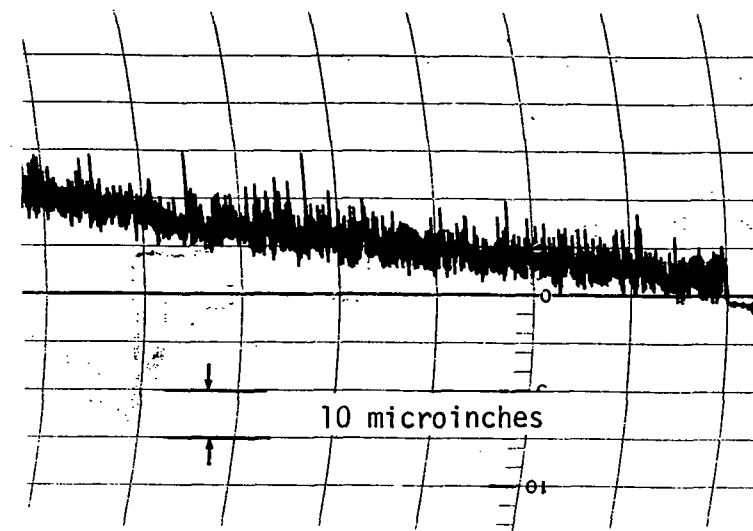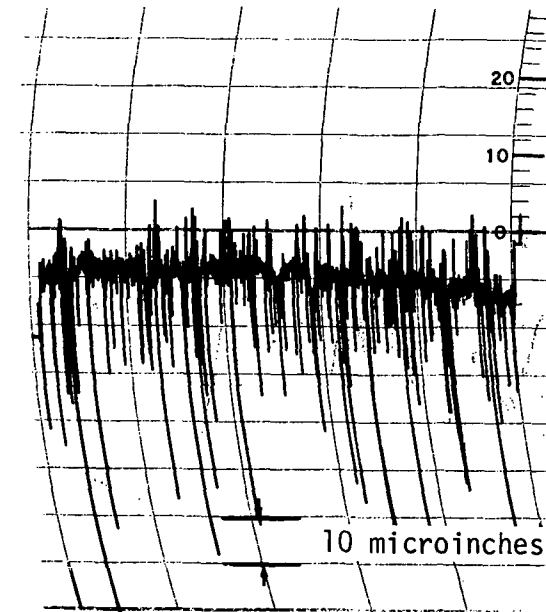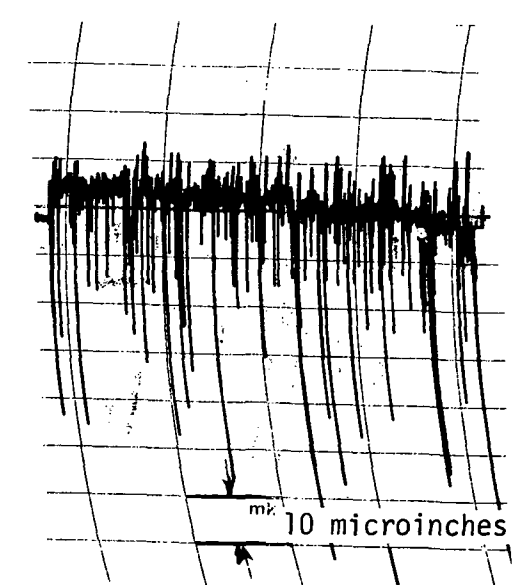
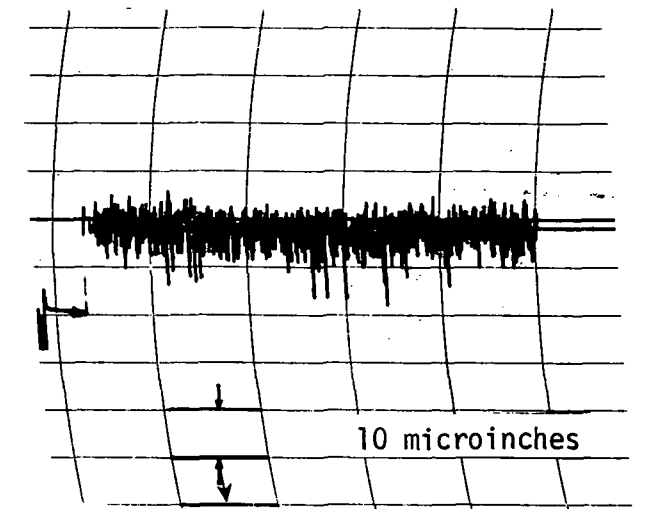e. 50 cycles　　　　　　f. 100 cycles　　　　　　g. 200 cycles　　　　　　h. 300 cycles

Figure 6-7.　Profiles of Poppet 16568-2 as a Function of Cycles
Bendix Profi-corder Stylus Radius:　500 microinches
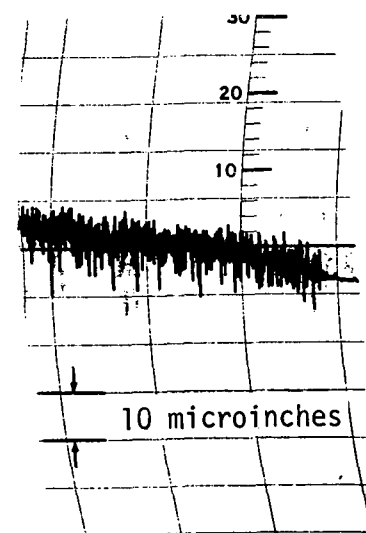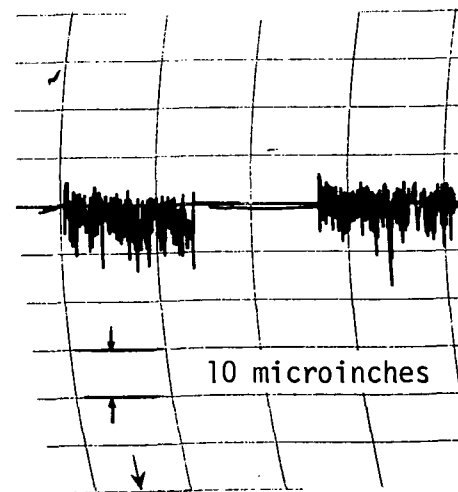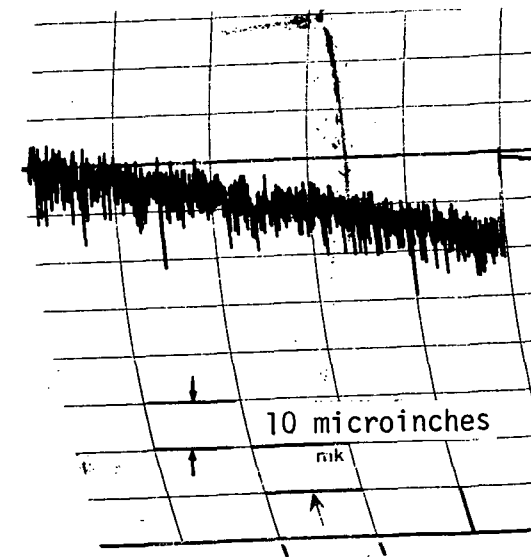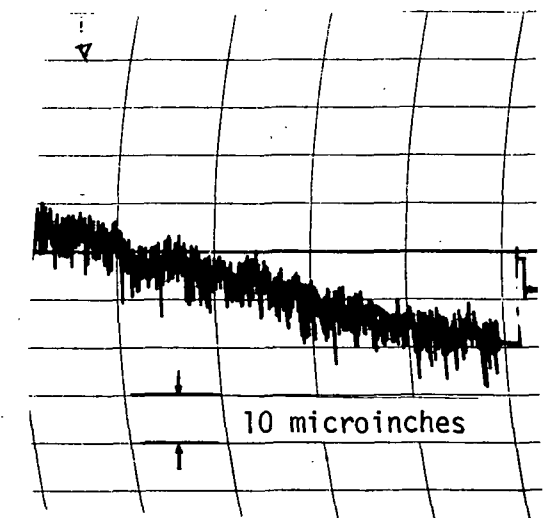Stylus Sweep Direction:　Radial
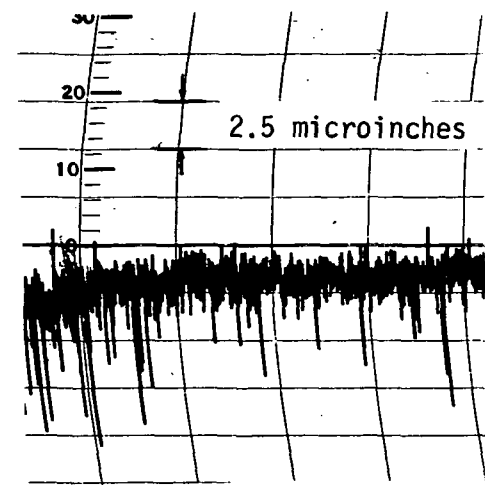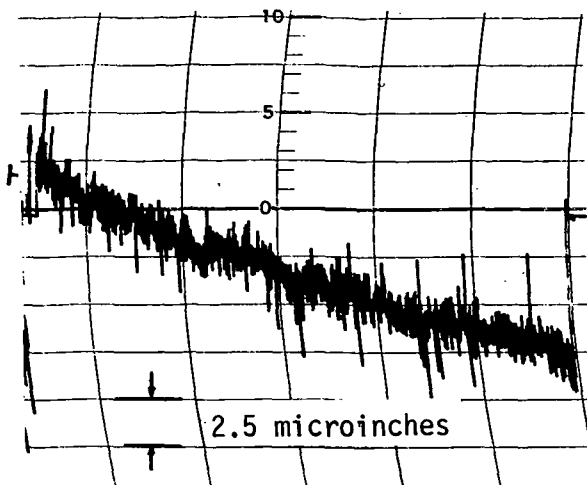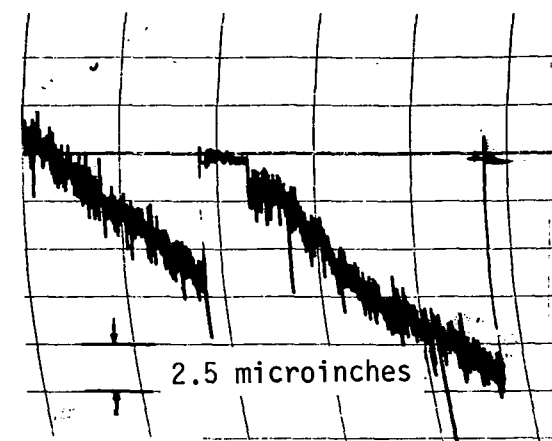
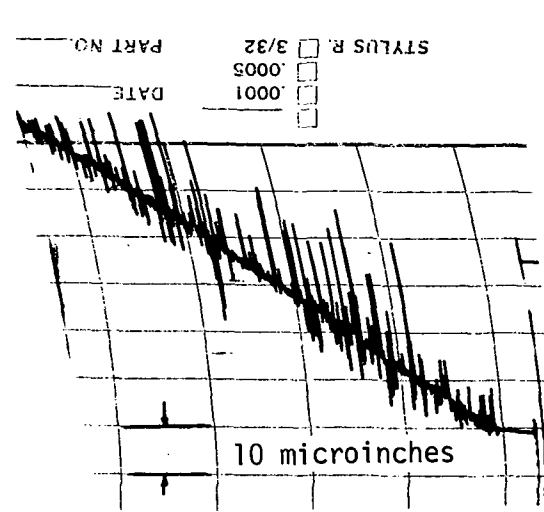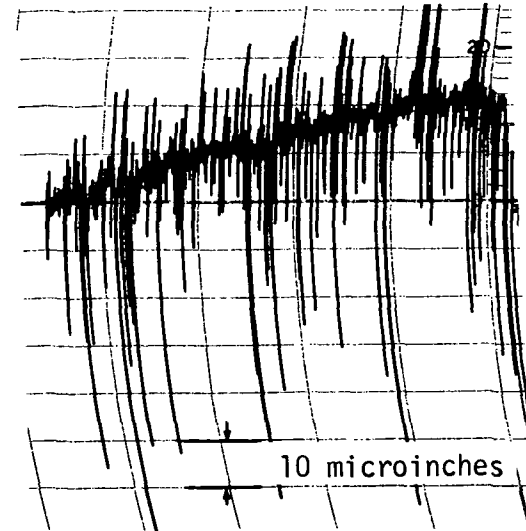a. 0 cycles   b. 1 cycle   c. 5 cycles   d. 20 cycles
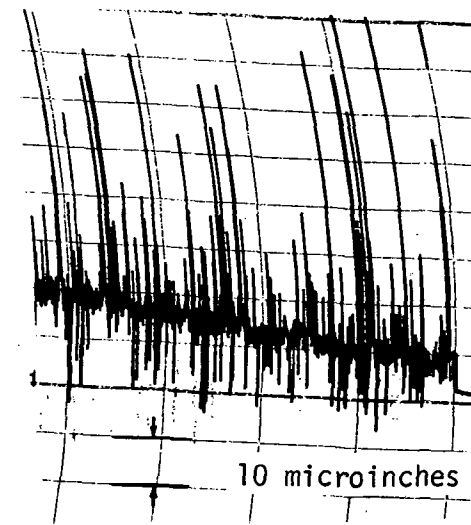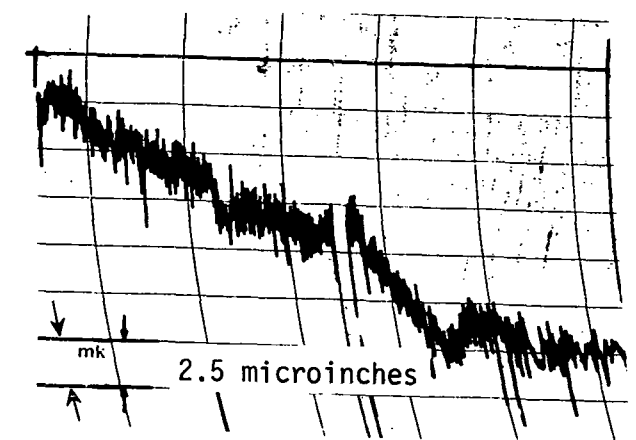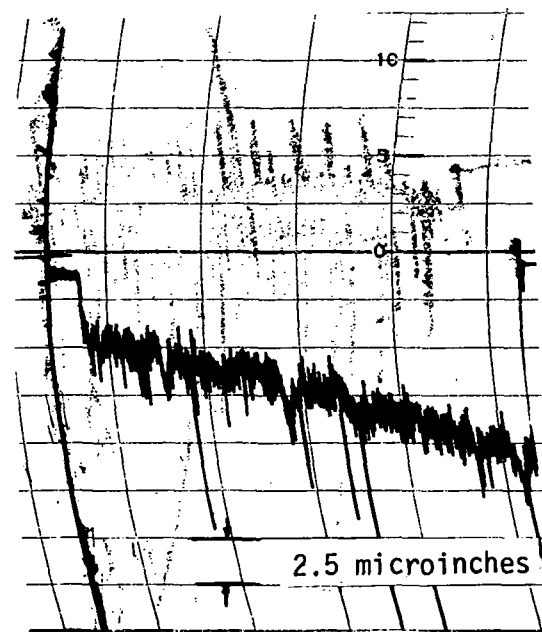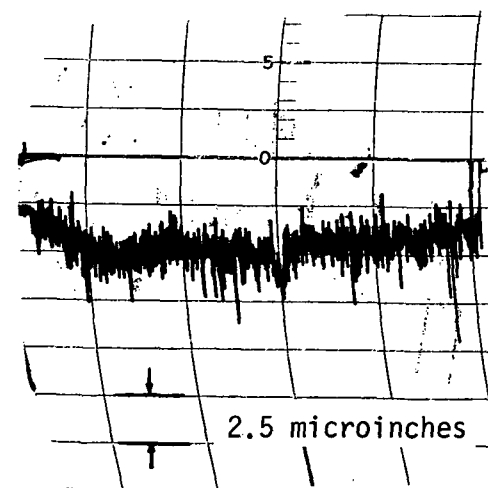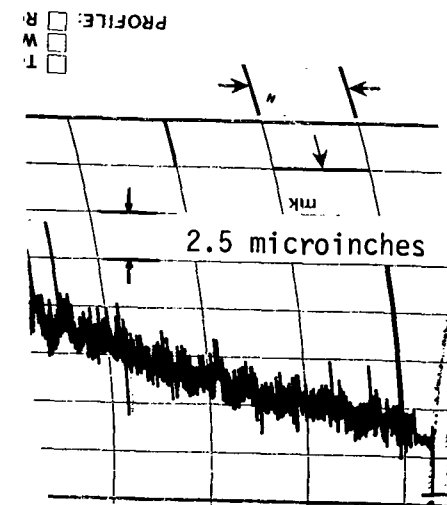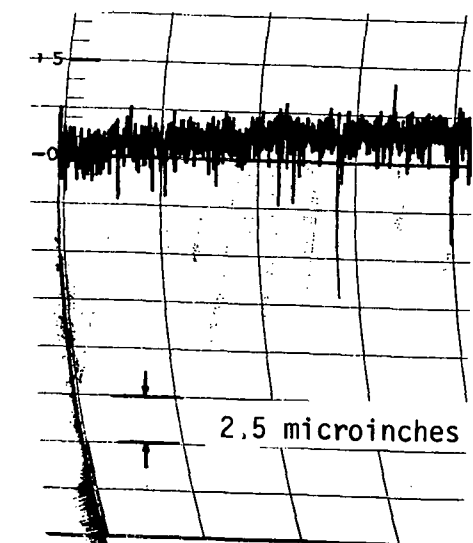
e. 50 cycles   f. 100 cycles   g. 200 cycles   h. 300 cycles

Figure 6-8. Profiles of Seat 162586-2 as a Function of Cycles
Bendix Profi-corder Stylus Radius: 500 microinches
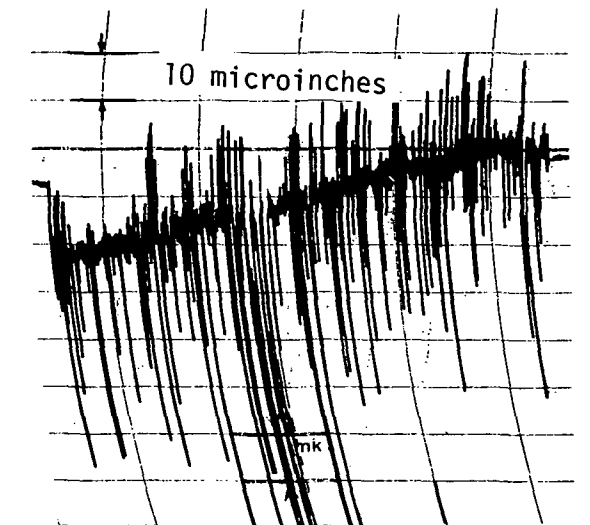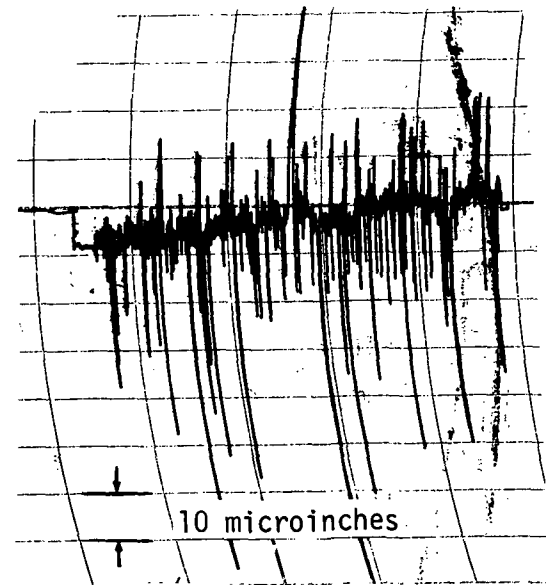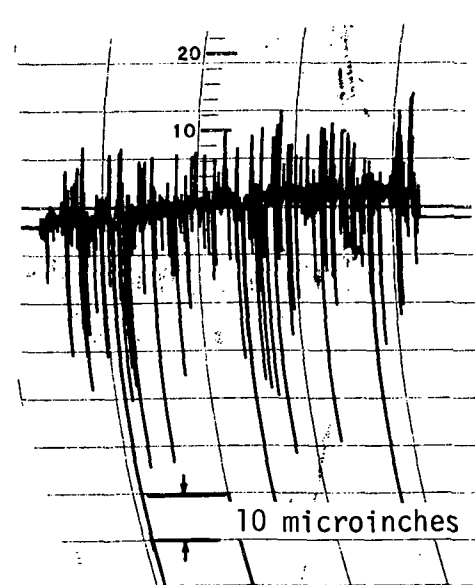Stylus Sweep Direction: Radial

6.5 TEST RESULTS

The test data results are given in Tables 6-1 and 6-2. Reported are the number of cycles, the corresponding surface (poppet and seat), roughness, and the leakage. Table 6-3 includes the penetration hardness of the surfaces.

6.5.1 Test I

In the first series of tests designated Test I the poppet experienced large change in roughness after the first cycle changing from 2.65 to 2.18 μ-inches or a change of about 20%. A constant roughness value was noted after 5 cycles and before 20 cycles. During this cycle testing no observed change in the seat surface was noted. The surface roughness on subsequent cycling improved going from approximately 2.2 μ-inches to 1.7 μ-inches at 200 cycles, a change of about 20%.

Leakage improved during the first and second cycles which would be expected due to the improvement in surface roughness. However, leakage varied within a factor of 10 throughout the cyclic testing. The reason for this is not known. In the two cases where leakage was higher (6 to 20 cycles and 100 to 200 cycles) particulate matter may have lodged between the sealing interface. Although orientation between the poppet and seat were maintained within 0.01 inches the effect of matching waviness also may be a factor. Microscopic examination of the -1 electrolized seat surface showed some adhesion had occurred. Particles as large as 30 μ-inches were noted on the -1 seat surface.

6.5.2 Test II

No significant changes in surface roughness or leakage was noted with the -2 poppet and seat. The roughness remained essentially constant at about 40 μ-inches rms. Leakage showed about a 20% improvement over the 300 cycle test range.

Examination of the -2 seat showed no adhesion occurred. The results of these tests showed no evidence of any wear or surface wear-in.

The difference between the -1 and -2 seat finish was that the -2 seat surface was polished after electrolizing whereas the -1 seat surface was not polished.

6.5.3 Conclusions

The results of the Test I and Test II indicated that the polished electro-lized coating exhibited no observable wear-in and no adhesion. It is, of course, possible that the -2 surfaces were at equilibrium at initial testing. However, this postulate is discounted on the basis of: 1) the absence of adhered particles on the polished surface, and 2) the wear-in process that developed for the -1 surfaces.

Based on the data, although limited, it would appear that the polished electrolized surface is preferred over the unpolished surface for the valve seat/beryllium copper poppet combination for use for long term missions.

Table 6-1. Test I Results

Cycle No.	Surface Roughness in Microinches - rms (1)		Leakage Rate in scc/sec
	Poppet PN 16568-1	Valve Seat PN 162586-1	
0	3.0 (2)	2.75	-
1	-	-	13.1×10^{-3}
Characterize poppet and seat	2.18	2.88	-
2	-	-	2.8×10^{-3}
5	-	-	1.74×10^{-3}
Characterize poppet and seat	2.18	2.83	
6	-	-	67×10^{-3}
10	-	-	120×10^{-3}
11	-	-	109×10^{-3}
20	-	-	53×10^{-3}
Characterize poppet and seat	1.77	2.80	-
21	-	-	4.95×10^{-3}
50	-	-	4.86×10^{-3}
Characterize poppet and seat	1.80	2.60	-
51	-	-	12.2×10^{-3}
60	-	-	7.3×10^{-3}
100	-	-	7.4×10^{-3}
102	-	-	5.67×10^{-3}
Characterize poppet and seat	1.85	2.80	-
103	-	-	43.5×10^{-3}
110	-	-	45.5×10^{-3}
150	-	-	46.0×10^{-3}
200	-	-	60.0×10^{-3}
Characterize poppet and seat	1.70	2.65	

(1) Surface rms values were obtained by multiplying the average peak to peak roughness profile by 0.35.

(2) The poppet, before this test, was employed in high frequency acoustic test of Section 5.0. The poppet was cycled twice at approximately 220 psi during the preparation of the test samples.

Table 6-2. Test II Results

Cycle No.	Surface Roughness in Microinches - rms (1)		Leakage Rate in scc/sec
	Poppet PN 16568-2	Valve Seat PN 162586-2	
0	40	1.5	-
1	-	-	87×10^{-3}
Characterize poppet and seat	40	1.5	-
2	-	-	75×10^{-3}
5	-	-	76.5×10^{-3}
Characterize poppet and seat	39	1.3	-
6	-	-	75×10^{-3}
10	-	-	77×10^{-3}
20	-	-	77×10^{-3}
Characterize poppet and seat	38	1.5	-
21	-	-	76.5×10^{-3}
50	-	-	78×10^{-3}
Characterize poppet and seat	38	1.6	-
51	-	-	76×10^{-3}
100	-	-	74×10^{-3}
Characterize poppet and seat	39	1.3	-
101	-	-	68×10^{-3}
110	-	-	67×10^{-3}
150	-	-	64×10^{-3}
200	-	-	61×10^{-3}
Characterize poppet and seat	39	1.3	-
201	-	-	63×10^{-3}
210	-	-	61×10^{-3}
250	-	-	59×10^{-3}
300	-	-	56.5×10^{-3}
Characterize poppet and seat	40	1.6	-

(1) Surface rms values were obtained by multiplying the average peak to peak roughness profile by 0.35.

Table 6-3. Surface Hardness Test of Poppet and Seat
Leitz Micro Hardness Tester Model 2120,
200 Gram Load

	Leitz Hardness in Microns	Knoop Hardness[1] in Kilograms/mm^2
16568-1 Poppet		
a.	118	205
b.	113	223
c.	117.5	206
16568-2 Poppet		
a.	113	223
b.	113	223
c.	112	227
162586-1 Seat		
a.	57	875
b.	59.5	795
c.	57	875
162586-2 Seat		
a.	58.5	832
b.	58	850
c.	55	945

[1] The Knoop hardness was calculated where $KH = \dfrac{14230 \times P}{L^2}$,
P is load in grams and L is Leitz hardness in microns (length of longest diagonal).

7.0 CONCEPTUAL STUDIES

7.1 VALVE SEAT SURFACE ENERGY STUDY

Recent investigations by Professor Roberts of the University of Bradford, England, have shown that contact angle measurements and surface tension data could be utilized to characterize the surfaces of thin polymeric films. This concept was extended to characterize bulk polymeric surfaces, and it was shown that preferential adsorption of butanol from butanol-water solutions occurred on surfaces of polystyrene and polymethyl methacrylate. This method of characterizing surfaces will be investigated to determine the compatibility and corrosion behavior of materials with propellants of interest. By observing the wetting behavior of a droplet of propellant on the surface of materials contemplated for use in valves, the interaction between the propellant and the materials may be elucidated. Since the wetting behavior of a liquid on a solid surface is exceedingly sensitive to the condition of the surface and the impurities present in the liquid, minute interactions between the surface and the contacting liquid will be readily observable as changes in the contact angle between the droplet and the solid surface as a function of time. Thus, by treating the metal surface, or by adding selected impurities to the propellant, the corrosion mechanism and compatibility behavior between the metal-propellant interface may be determined.

As a result of this work the University of Bradford was assigned a task under subcontract to further study surface energies of metal valve seats. The subcontract specific tasks are reproduced in the following.

7.1.1 Specific Tasks

For the purpose of meeting the objectives, the program should be designed to perform analysis, experimentation and technical demonstration. To be considered are:

    a. Metal valve seat materials of beryllium copper, tungsten carbide, Inconel and steel surfaces having a high quality surface finish.

    b. Liquid propellants are hydrazine, oxygen difluoride, diborane, fluorine and nitrogen tetroxide.

    c. Methods of cleaning and preparing the seats prior to exposure to the propellants.

Task I

The objectives of this task are to perform testing and experimentation to develop techniques to determine the long term performance of metal valve seats exposed to reactive propellants. This effort should provide a new method of measuring the rate processes of corrosion mechanisms. As a minimum the application of single or multiphase liquids to metal surfaces to determine compatibility and corrosion by measuring the time variations in contact angles (wettability) are to be accomplished. In addition, the percentage or ratio of sorption of a constituent of the two phase mixture should be done. Possible knowledge of surfaces may also be obtained by measuring the concentration of the metal or corrosion products in the liquid.

Task II

The objectives of this task are to develop a model and procedures based on the experimental data obtained under Task I which can be used to determine the long term compatibility of the components. The model and procedures should be constructed in a manner that is applicable to predicting long term performance of valve seats of varying geometries, materials and finishes which may require testing not performed under Task I.

Task III - Reporting Requirements

In connection with the work performed under this contract the contractor shall prepare and deliver within 15 calendar days after completion of the technical effort 5 copies and one reproducible copy of the final report. The final report shall include all technology and analyses necessary to fully assess the value and applications of methods and techniques developed under this contract. The final report should document recommendations and conclusions including continued efforts which would further advance the objectives of the program in the event additional funds become available.

7.1.2 Progress

The work carried out during the period June to August 1971, by the University of Bradford is reported in the following section.

Investigation of the Feasibility of Studying the Chemical
Nature of Metal Surfaces Using Contact Angle Techniques

The effect of hydrazine on smooth specular surfaces of brass, copper, stainless steel and gold was studied by following any change in the contact angle of aqueous butanol solutions on these surfaces before and after hydrazine treatment. It was believed a correlation between the contact angle and the surface tension of the aqueous butanol solutions, i.e., Zisman-type plots would be related to the chemical nature of the surface.

Brass, copper and stainless steel blocks were mechanically abraded to obtain highly polished surfaces. These were washed in detergent and used for contact angle studies. In all cases high contact angles (>40°) with deionized water were observed (see Table 7-1). Trevoy and Johnson[1]* obtained low contact angles (0 to 11°) using purified water on a variety of metal surfaces polished electrolytically, including the surfaces of brass, copper and stainless steel. They also reported the inadequacy of mechanical polishing and solvent-rinsing techniques in producing metal surfaces capable of showing near zero contact angles with water.

Specimens of copper block and copper plate were electropolished using similar handling techniques to Trevoy and Johnson. A 63 to 67% (w/w) aqueous ortho-phosphoric acid medium was employed using the potentiometric circuit of Tegart[2]. Copper block could not be electropolished satisfactorily. Specimens of copper plate were polished, however, with varying degrees of success; the polished surfaces did not show water wettability expected, i.e., near-zero contact angles. When the surfaces were washed in hot concentrated detergent, rinsed in deionized water and dried, contact angles <5° were observed.

Two specimens of stainless steel plate were polished in the orthophosphoric acid/sulphuric acid/water composition of Perryman[3]. Both specimens gave contact angles of <5° with deionized water immediately after polishing.

---

*Numbers in parenthesis refer to the references listed at the end of this section.

A 0.047 wt % aqueous butanol solution also spread over the surface. When the surface was subsequently rinsed with deionized water and dried, deionized water again gave contact angles <5°. <u>Storage ~3 hours in a dessicator under vacuum produced a tenfold increase in the contact angle of deionized water.</u> Water wettability was restored by either washing in hot concentrated detergent solution or by a 15 second dip in hot (ca 80°) chromic acid. The latter treatment did not appear to etch the steel surface.

One of the polished stainless steel plates was cleaned in chromic acid after storage, and immersed for 20 hours in hydrazine (obtained by distilling the monohydrate N_2H_4, H_2O, in chromic acid-cleaned glassware) kept in a dust-free container (also moisture-tight). The plate was subsequently rinsed with water and dried. Contact angles of water on this surface ranged from 18.5 to 29.5°. This is some evidence for a change in the chemical nature of the surface. (see Table 7-1, Run 10).

It was thought iron (which is known to react with hydrazine at elevated temperatures) would give clearer indications of reaction. The polishing characteristics of mild steel in orthophosphoric acid have been investigated. To date no polished surfaces have been obtained with this system, though Elmore[4] claims iron can be polished in orthophosphoric acid.

Discussion

Contact angle studies indicate quite clearly their usefulness in studying the nature of metal surfaces. The results obtained for the water wettability of mechanically abraded metal surfaces highlight the inadequacy of this method of preparation of surfaces, free from contamination. It has also been pointed out[5] that a mechanically polished surface does not reflect the true nature of the material. Thus, electropolishing is the most suitable technique that can be applied to this work to obtain reproducible metal surfaces.

That electropolished copper surfaces could not be obtained in an "uncontaminated" state after polishing (i.e., water did not form near-zero contact angles)

indicated that the surface became easily contaminated. Significant also was that a proprietary detergent removed contamination on the surface and that the detergent itself did not apparently adsorb on the surface to any measurable extent.

Both water and aqueous butanol solutions wetted polished stainless steel. Butanol adsorption on stainless steel appeared to be either reversible or negligible.

It was possible that the hydrazine reacted to some extent on the stainless steel surface or that the erratic contact angles of water on the treated surface were caused by organic contamination in the hydrazine or dust-tight container. Stainless steel has, however, been classified[6] as compatible with hydrazine.

The technique is clearly sensitive to changes in the chemical constitution of metal surfaces and therefore relevant to metal corrosion problems.

Table 7-1. The Water Wettability of Brass, Copper and Stainless Steel as a Variable of the Polishing Conditions and Subsequent Treatment of the Polished Metal Surfaces

Run	Metal	Type of Polish	Description of Polished Surface	Treatment of Polished Surface	Mean Contact Angle of Water($\theta°$)	Scatter of Contact Angles	Remarks
	Brass Block 3.7 x 2.5 x 2.5 cm	Mechanical	Smooth but slightly wavy	Washed in detergent	50.7	± 2.5°	Detergent used was "Tide"
	Copper Block 3.7 x 2.5 x 2.5 cm	"	"	"	79.1	± 4°	"
	"	"	"	Immersed in hydrazine 3.5 min. Rinsed in water and dried	70.0	± 5°	
1	Copper Plate 3 x 3.5 x 0.1 cm	Electrolytic (in orthophosphoric acid. 63 to 67% w/w) treatment	Smooth; lines from emergy just visible	A. Rinsed in 10% w/w H_3PO_4 and water	93.4	± 4°	Plate retained 72 hours in vacuo before contact angle measurements
1	"	"	"	B. Washed in hot detergent, rinsed and dried	<5°		Detergent used was "Tide"
4	Copper Plate 3 x 3.5 x 0.1 cm	Electrolytic	Smooth and specular. Shallow pits where O_2 was evolved	As for Run 1 A.	38.6	± 5°	
7	"	"	As for Run 1	As for Run 1 A.	40.5	± 4°	
8	"	"	Smooth and specular	As for Run 1 A.	39.2	± 5°	
8	"	"	"	As for Run 1 B.	24.3	± 3°	Detergent used was 50% Decon 75 to 50% de-ionized water
10	Stainless Steel Plate 2.5 x 2.5 x 0.1 cm	Electrolytic (in 67% w/w H_3PO_4, 10% w/w H_2SO_4, 23° H_2O)	Smooth and specular	As for Run 1 A.	4	± 1°	Angles measured immediately after polishing
10	Stainless Steel Plate	Electrolytic	Smooth and Specular	As for Run 1 A.	45.3	± 3°	Plate retained in vacuo 18 hrs
10	"	"	"	As for Run 1 B.	<5°		Detergent used was "Tide"
10	"	"	"	15s.dip in hot(80°) chromic acid; rinsed and dried	<5°		No visible etching of the surface by the chromic acid.
10	"	"	"	Immersed in freshly dis-tilled hydra-zine for 20 hours. Rinsed with water and dried	25.2	± 5°	Drops of water were unsymmet-rical
11	"	"	As for Run 4	As For Run 1 A.	<5°		Measured immed-iately after polishing

7.2 LEAKAGE MEASUREMENT

The use of the mass spectrometer as a generalized leak detector of components was investigated. A technological refinement in terms of standardized leak sources is necessary for the mass spectrometer to be utilized as a multi-functional instrument for detection of all the propellants and gases of interest.

The mass spectrograph is used presently to analyze and detect propellants and impurities. The instrument has a high sensitivity in that it can detect nanogram (10^{-9} g) quantities of material. Since it has wide mass range detection capabilities, it is uniquely capable of sensing and identifying very small amounts of propellants leaking from components. The primary drawback is that the precision of the mass spectrometer when used in its normal mode is only comparable to a gas chromatograph in terms of resolving differences in propellant concentration (e.g., ppm). Therefore, a standard leak source is needed in order to calibrate the mass spectrometer and allow it to be used as a leak detector for the propellants of interest.

The principle sources presently used in mass spectrograph leak detectors are helium and hydrogen, although they are not traceable to a primary NBS standard. The calibration of these sources is performed by determining the diffusion of helium through glass and hydrogen through palladium. Thus, if the mass spectrographic technique for leak detection is to be utilized with maximum efficiency for component evaluation, standardized leak sources for each propellant must be developed.

Several techniques for establishing a propellant leak source are available. Precision metering values, permeable membranes, porous structures, and plates with precisely bored holes (i.e., laser drilled) may be able to be used. As an example, TRW Systems performed a bladder permeation study for NASA[7] and determined that the permeation rate of N_2O_4 through TFE Teflon was $P \approx 6 \times 10^{-10}$ gm sec^{-1} cm^{-2} atm^{-1} cm at 0.6 atm over a temperature range of 25 to 90°C. This corresponds to a leak rate of approximately

8×10^{-8} std cc sec^{-1} for TFE Teflon of one cm^2 area, one cm thick, which is a leak rate range of interest. A major consideration in developing a leak source is the reactivity of some of the propellants (e.g., OF_2 and F_2). Thus, compatibility, passivation and preservation of the leak source must be considered.

After the leak source has been developed, it must be calibrated. ABLEAK[8] developed at TRW Systems under NASA contract may provide one method of calibration for establishing standardized leak sources for the various propellants.

Development work on miniaturized mass spectrometers for the Viking Project is being done by JPL[9]. The unit has a resolution of 1/200 - 1/330 over a mass range of 12 to 200 mass units, with a minimum net detection sensitivity of 4×10^{-4} nanogram/sec. The device weighs nine pounds and has a power consumption of 15 watts. Thus, if an on-board leak detector was desirable, refinement of this instrument as a propellant leak detector may be feasible.

The investigation included a leak rate analysis of the detection sensitivity required for various tank volumes for a 10 year mission life, the types of leak sources that may be utilized, and the calibration of the leak sources for use in conjunction with the mass spectrometer. Each of these topics are discussed below.

7.2.1 Leak Rate Analysis

Figure 7-1 summarizes the results from calculating the detection sensitivity as a function of tank volume. A ten year mission life was assumed. Three loss rates were utilized in the calculations; 10% during the mission life as an upper, intolerable bound, 1% a postulated acceptable figure, and 0.1%, a desirable level of loss. The system was assumed to be comprised of ten components (1 tank, 1 pressurant device, 4 lines and 4 valves), all leaking at the same rate. The measurement accuracy and error factors[10] were accounted for and the required tolerable leak rate measurement sensitivity was assumed to be one order of magnitude more precise. Thus, if the tank
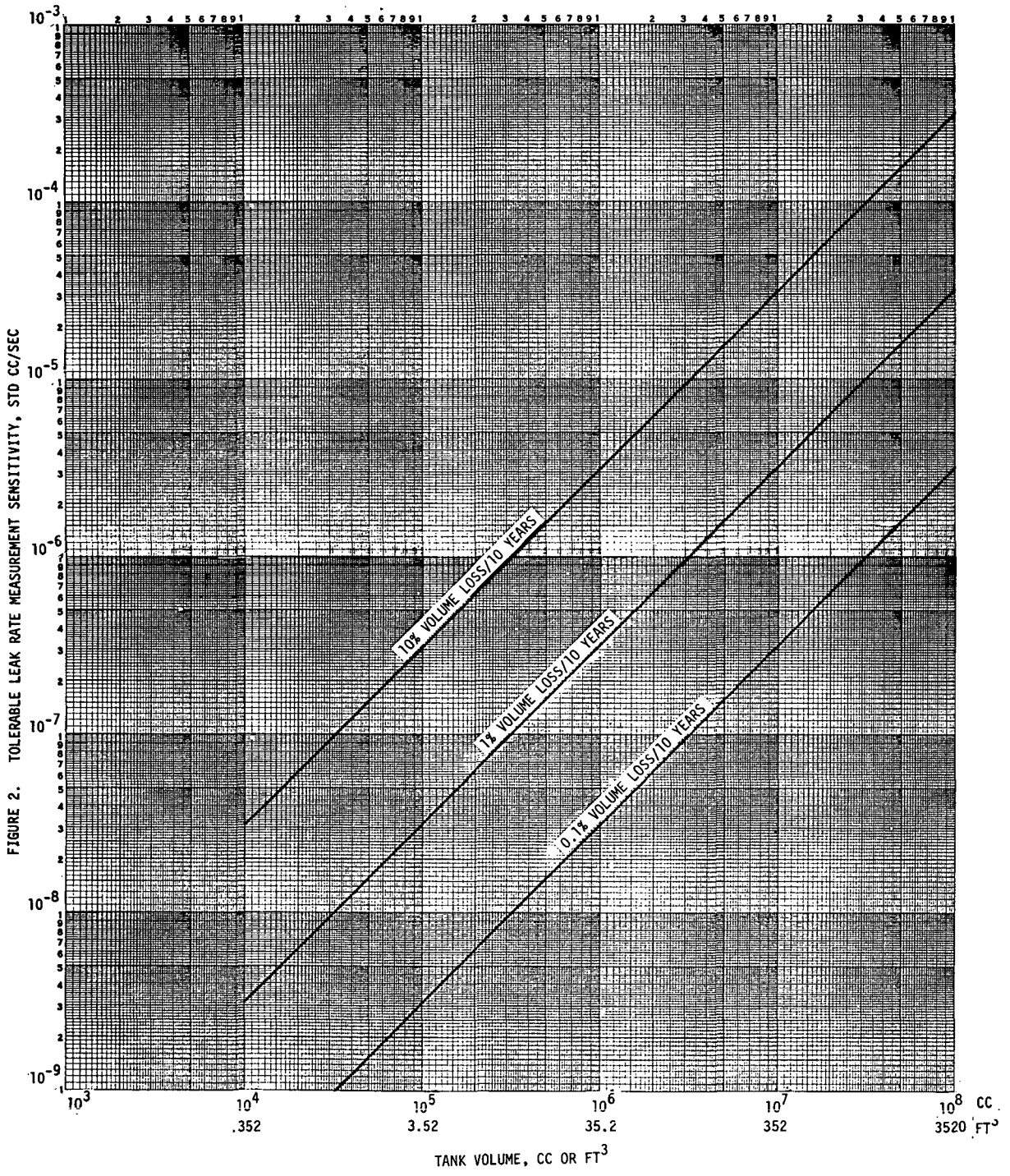
Figure 7-1. Tolerable Leak Rate Measurement Sensitivity Vs. Tank Volume for a 10 Year Mission Life

7-9

volume were 10^6 cc(35.2 ft^3), the leak source(s) for calibration of the mass spectrometer should have a leak range of $3x10^{-8}$ to $3x10^{-6}$ std cc/sec for testing each component in the system for determination of its acceptability. If fewer components are present, or if the total system can be leak checked after assembly, then the tolerable leak rate is increased and the standard leak source can have a higher leak rate range.

7.2.2 Types of Leak Sources

There are two broad classes of leaks: permeation leakage through a solid, and leakage through an open passage in a component[11].

The generalized process for a permeation type leak is as follows:

a. The material to be permeated is first adsorbed and dissolved in the surface layer on the high pressure side of the solid. Surface pretreatment may play an important role in this first step.

b. The material then diffuses through the solid, driven by the concentration gradient according to Fick's Law. The diffusion of the material may be as a dissociated molecule for metallic solids, or as molecules if the material is polymeric.

c. When the material reaches the low pressure surface of the solid, it undergoes a transition from a dissolved state to an absorbed state, reassociate if the diffusion was not molecular, and is desorbed at the surface. As in the first step, surface pretreatment may be important. The permeation process varies depending on the material. Norton[12] lists the generalities of permeation leaks between metals and polymers as follows:

Metals

● Rare gases do not permeate metals
● Hydrogen permeates many metals
● Oxygen permeates silver
● Permeation rates vary as the square root of the pressure

Polymers

- All gases permeate all polymers
- Many instances of permeation by specific materials
- Permeation rates vary directly with pressure

Leakage through an opening (i.e., small hole or crack) as contrasted to permeation is the passage of a material from one side to the other under a pressure or concentration differential existing across the opening. Since the leak path is usually a function of wear, geometry, corrosion, etc., the dimensions are generally unknown. Thus the leak is usually expressed as a leak rate in dimensions of volume or mass flow per unit time. In the leak rate regime of interest, the two dominant types of leaks are molecular flow or laminar flow. For leak rates of 10^{-5} std cc/sec or lower, molecular flow will predominate. For higher leak rates, transition to laminar flow may occur. If the type of flow could be accurately predicted for the leak, conversion to other conditions could be calculated and the leakage mechanism ascertained.

The above discussion illustrates the need to know the type of leak occurring in service (permeation or open path) and if the type of leak is important for calibration of the mass spectrometer. Examination of the propellants and pressurant gases of interest indicate that it is necessary for some materials to have a standardized leak source that is essentially identical to what would be expected in actual service use. Table 7-2 lists the propellants and pressurants of interest and the type of leak source which should be used. The rationale that was used is as follows: (1) ordinary gases have been used in permeation devices with good results and a number of permeation type leak sources have been developed[13]. Norton (Ref.12) has utilized a mass spectrometer to measure gas permeation through various materials and reports that the technique is extremely sensitive; (2) Teflon has been used for N_2O_4 permeation[7], however, corrosion may influence the leakage, thus other types of leaks must be investigated; (3) the mixed hydrazines and LPG, if leaking by molecular flow, may tend to separate. Thus, the same leak source must be used in order to determine compositional variations during leakage by the use of the mass spectrometer; (4) corrosion, decomposition, and subsequent deposition of reaction products indicate that the remainder of the propellants should use the same type of leak source that are encountered in service.

Table 7-2. Type of Leak Source for Calibration of
Mass Spectrometer Estimated for Use
With Various Propellants and Pressurants

Propellant/Pressurant	Same Type of Leak Source for Calibration	Other Types of Leak Source
Helium	N/C	Permeation
Hydrogen	N/C	Permeation
Nitrogen	N/C	Permeation
Oxygen	N/C	Permeation
Nitrogen Tetroxide	N/C - U	Permeation
Hydrazine	P	U
Hydrazine Mixes	P	None
LPG	P	None
Monomethyl Hydrazine	P	U
Fluorine	P	U
Oxygen Difluoride	P	U
Diborane	P	U

SYMBOLS: N/C - probably not critical
        P - probably critical
        U - unknown

Table 7-3 lists the types of leak sources of interest, and are discussed below.

Table 7-3. Types of Leak Sources

Fixed Leaks

    a. Porous Plug
    b. Orifice
    c. Permeation

Variable Leaks

    a. Variable Compacted Powder
    b. Needle Valve
    c. Labyrinth Path Capillary
    d. Deformable Capillary Tubing
    e. Temperature or Pressure Varied Leaks

7.2.2.1 Fixed Leaks

a. Porous Plug Leaks

This type of leak consists of a sintered metal, ceramic or glass plug which contains extremely fine connected pores. By altering the sintering conditions, the pore size can be varied and a wide range of leak rates can be obtained.

b. Orifice Leaks

These leaks consist of fine holes or cracks introduced into a disc by laser drilling, chemical etching, or thermal and chemical treatment of metals (e.g., thermal "sensitization" of stainless steel or hydrogen firing tough pitch copper). Another type is a long, fine capillary tube. One drawback to these leaks is that they can be easily clogged, or the leak rate changed by chemical reaction with the propellants.

c. Permeation Leaks

Permeation leaks are one of the more commonly used types, since they have a long life, can be built to deliver precise amounts of gas, and depending on the permeation membrane, can be used with a wide variety of gases[7, 13].

7.2.2.2 Variable Leaks

a. Variable Compacted Powder

Figure 7-2 illustrates this type of controllable leak. Fine metal or ceramic powder is contained in a threaded chamber. By varying the compaction pressure on the path length for gas flow is varied. Different leak rates can be obtained by utilizing powders of various fineness as well as by increasing or decreasing the compaction pressure.

b. Needle Valve

This type of variable leak depends on a precisely machined pintle-valve seat combination in which the opening is controlled by a multi-turned micrometer vernier handle. By adjusting the micrometer setting at zero for zero leak rate, the valve can be calibrated over a wide range of flow rates.
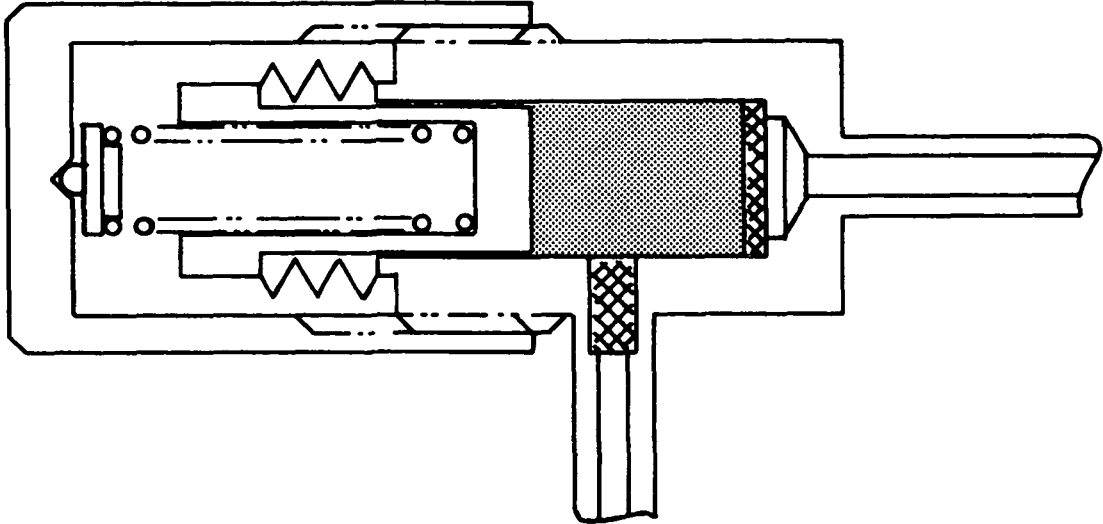
Figure 7-2. Compacted Powder Variable Leak

c. Labyrinth Path Capillary

The labyrinth path capillary variable leak consists of a long, fine threaded housing with a threaded plug inserted into the housing. The path length of the leak is adjusted by varying the amount of plug inserted into the housing.

d. Deformable Capillary Tubing

A mechanical plunger flexes the metal capillary to alter the area of the leak. Care must be taken in flexing the capillary so that the elastic limit of the metal is not exceeded, otherwise the leak rate range will not be reproducible.

e. Temperature or Pressure Varied Leaks

All leak sources are sensitive to the pressure of the gas source, and to the temperature of both gas and the leak device. These must be maintained at the same conditions that the device was calibrated in order to standardize the mass spectrometer.

If the calibration of the leak source is performed at several gas pressures and gas and leak source temperatures, the calibration range of the leak source can be increased, and thus increase the useful range of the mass

spectrometer. This method of extending the range of leak sources has been used commercially[10].

7.2.3 Leak Source Calibration

Each of the leak source devices that may be utilized for the propellants and pressurants of interest must be calibrated in order to correlate the leak rate to the mass spectrometer. Since the leak rates of interest may vary over a wide range depending on the size and complexity of the propulsion system, the method of calibration must be able to accommodate the leak rate ranges of interest. The calibration of a leak source is a difficult operation, and all methods have measurement errors associated with them[10]. These errors must be taken into account when calibrating the leak source so that the accuracy of the measurement can be calculated. There are two calibration methods which appear to be most applicable to these types of leak sources.

One such method of calibration is the ABLEAK[8] developed at TRW Systems under NASA contract. The operation of this device is based on measuring the buoyant change on a ball suspended in the leak media. The leaking gas will cause a buoyant force on the ball, which is measured. By knowing the chamber and ball volumes, and the force exerted on the buoyant member by the leaking gas, the mass flow per unit time can be calculated and converted to a standard leak rate. The present ABLEAK instrument can measure leakage in the range above 10^{-3} scc/sec. A modified design of the present apparatus should be capable of detecting leak rates of 10^{-7} to 10^{-8} scc/sec.

The other method is the isobaric volume change measurement technique utilized by Haywood[14]. A gas reservoir of known pressure and volume is attached to one end of the leak source, which is evacuated on the other end by a vacuum system. As gas leaks through the source from the reservoir, the pressure drop in the reservoir is compensated by the use of the piston to reduce the volume and maintain the original reservoir pressure. By measuring the volume displacement as a function of time, leak rates as low as 10^{-6} scc/sec have been detected, with an accuracy of $\pm$ 5%. By using longer measurement times, it should be possible to measure even lower leak rates.

7.3 MASS GAUGING IN ZERO-G ENVIRONMENT

Several approaches to mass gauging have been studied such as radiation sensors, acoustic sensors and measurements applied to the thermodynamic relationship of fluids.

A concept discussed here uses the concentration of a tracer gas to the propellant ullage to determine the volume of the ullage gas in the storage tank, thereby knowing the volume of the tank the liquid level may be determined.

By the addition of a tracer gas, say helium, to a propellant tank storing liquid hydrogen the ullage volume may be measured. Assuming a tank volume of 10^8 cm^3 filled with liquid hydrogen at a pressure of approximately 30 psia and taking the two extremes, 1) a full tank, 2) an empty tank, and adding Q amount of helium, the ullage volume can be determined. A full tank having an ullage volume of .01% would contain 10^5 cc of hydrogen vapor.

Then $vf_{He} = \dfrac{V_{He}}{V}$, $vf_{H_2} = \dfrac{V_{H_2}}{V}$ where V is the total volume of the mixture and vf is the volume fraction of either hydrogen or helium.

The addition of 1 cc of He to the ullage would give:

$$vf_{He} = \frac{1}{10^5} = 10^{-5} \frac{cc}{cc}$$

For a completely empty tank the volume fraction of He would be for 1 cc of He added

$$vf_{He} = \frac{1}{10^8} = 10^{-8} \frac{cc}{cc}$$

Concentration of the tracer gas depends on its partial pressure

$$vf_{He} = \frac{P_{He}}{P} = \frac{P_{He}}{P_{He} + P_{H_2}}$$

where P_{He} and P_{H_2} are partial pressures.

By adding a known increment of He to the tank ullage at any given tank condition and measuring the concentration, the ullage of the tank can be determined.

Helium was selected here because a well known sensitive technique for determining helium concentration is the helium leak detector, using a mass spectrometer as the analyzer. The pre-calibrated mass spectrometer can be used to determine most tracer gases that may be considered for this application. The partial pressure analysis may also be a candidate instrument.

Diffusion of the tracer gas must be considered. The time constant to reach equilibrium of the mix may be longer than desired. A method of stirring the mixture may be necessary if response requirements are relatively short.

The addition of radioactive species in known incremental amounts may also be applicable. The advantages of pre-calibration of the ullage volume may apply to any volume sampling method.

A complete survey in the area of propellant gauging has not been done and it is possible that this technique has been documented by earlier investigators. However, in conforming to the NASA New Technology contractual requirements, the concept is reported.

REFERENCES

1. D. J. Trevoy and H. Johnson Jr., J. Phys. Chem., 62, 833 (1958)

2. J. W. McG. Tegart, "Electrolytic and Chemical Polishing of Metals," Permagon Press, London, 2nd Edition, p. 42.

3. E. C. Perryman, Metallurgia, 46, 55, (1952).

4. W. C. Elmore, J. Appl. Physics, 724, (1939).

5. P. A. Jacquet, Met. Finish, 47 (7), 58, (1949).

6. E. Suarez-Alfonco, A. E. Chambers, "Hydrazine Handling Manual," U. S. Dept. Commerce, Office of Technical Services, AD266, 145, (1961).

7. "A Study to Analyze the Permeation of High Density Gases and Propellant Vepors Through Single Layer Teflon or Teflon Structure Materials and Lamination," (Design Guide) Contract NAS 7-705, 15 August 1969.

8. "Advanced Valve Technology," TRW Systems Interim Report No. 06641-6004-R000, Contract NAS 7-436, November 1966.

9. P. L. Levins and J. E. Oberholtzer, "Study of Long Term Atmospheric Trace Contaminant Monitoring and Control," A. D. Little, Contract NAS 9-10434, May 24, 1970.

10. "Leakage Testing Handbook," Revised Edition, General Electric Report No. S-69-1117, Prepared for JPL, NASA under Contract NAS 7-396, July 1969.

11. R. C. Elwell and A. J. Bialous, "Study of Dynamic and Static Seals for Liquid Rocket Engines," General Electric Co., NASA Contract NAS 7-102, NASA No. CR-50662, March 1963.

12. F. J. Norton, J. Appl. Phy. 28, 34 (1957).

13. NASA Tech. Brief No. 68-10142 "Device Provides Controlled Gas Leaks," April 1968.

14. W. H. Haywood and R. L. Jysen, Vacuum Symposium Transactions, 1962, p. 459.

COPIES	RECIPIENT
	NASA Headquarters Washington, D. C. 20546
1	Contracting Officer
1	Patent Office
	NASA Lewis Research Center 21000 Brookpark Road Cleveland, Ohio 44135
1	Office of Technical Information
	NASA Manned Spacecraft Center Houston, Texas 77058
1	Office of Technical Information
	NASA Marshall Space Flight Center Huntsville, Alabama 35812
2	Office of Technical Information, MS-IP
1	Technical Library
1	Dale Burrows S+E-ASTN-PJ
	NASA Ames Research Center Moffet Field, Calif. 94035
1	Patents and Contracts Management
	Jet Propulsion Laboratory 4800 Oak Grove Drive Pasadena, California 91103
2	G. A. Yankura
3	Manager, Liquid Rocket Propulsion Tech., Code RPT
3	Manager, Space Storable Propulsion Technology, Code RPI Office of Advanced Research and Technology NASA Headquarters Washington, D. C. 20546
1	Director, Technology Utilization Division Office of Technology Utilization NASA Headquarters Washington, D. C. 20546
25	NASA Scientific and Technical Information Center P.O. Box 33 College Park, Maryland 20740
1	Director, Launch Vehicles and Propulsion, SV Office of Space Science and Applications NASA Headquarters Washington, D. C. 20546

COPIES	RECIPIENT	
1	Director, Advanced Manned Missions, MT Office of Manned Space Flight NASA Headquarters Washington, D. C. 20546	
1	Mission Analysis Division NASA Ames Research Center Moffett Field, California 24035	

NASA FIELD CENTERS

2	Ames Research Center Moffett Field, California 94035	Hans M. Mark
1	Goddard Space Flight Center Greenbelt, Maryland 20771	Merland L. Moseson Code 620
2	Jet Propulsion Laboratory California Institute of Technology 4800 Oak Grove Drive Pasadena, California 91103	Henry Burlage, Jr. Propulsion Div. 38
2	John F. Kennedy Space Center, NASA Cocoa Beach, Florida 32931	Dr. Kurt H. Debus
2	Langley Research Center Langley Station Hampton, Virginia 23365	Ed Cortwright Director
2	Lewis Research Center 21000 Brookpark Road Cleveland, Ohio 44135	Bruce Lundin Director
2	Marshall Space Flight Center Huntsville, Alabama 35812	Hans G. Paul Code R-P+VED
2	Manned Spacecraft Center Houston, Texas 77058	J. G. Thibodaux, Jr. Chief, Prop. & Power Div. H. Pohl

GOVERNMENT INSTALLATIONS

1	Headquarters, U. S. Air Force Washington 25, D. C. 20546	Col. C. K. Stambaugh AFRST
1	Arnold Engineering Development Center Arnold Air Force Station Tullahoma, Tennessee 37388	Dr. H. K. Doetsch

COPIES	RECIPIENT	
2	Air Force Rocket Propulsion Laboratory Research and Technology Division Air Force Systems Command Edwards, California 93523	RPRPD/Mr. H. Main
1	Air Force Missile Test Center Holloman Air Force Base, New Mexico 45433	Library
1	Air Force Missile Test Center Patrick Air Force Base, Florida	L. J. Ullian
1	Aeronautical Systems Division Air Force Systems Command Wright-Patterson Air Force Base Dayton, Ohio 45433	D. L. Schmidt Code ASRCNC-2
1	Space and Missile Systems Organization Air Force Unit Post Office Los Angeles 45, California 90045	Col. Clark Technical Data Center
1	Defense Documentation Center Headquarters Cameron Station, Building 5 5010 Duke Street Alexandria, Virginia 22314 Attn: TISIA	
1	Bureau of Naval Weapons Department of the Navy Washington, D. C. 20546	J. Kay RTMS-41
1	U. S. Naval Ordnance Test Station China Lake California 93557	Code 4562 Chief, Missile Propulsion Div.
1	Picatinny Arsenal Dover, New Jersey 07801	I. Forsten, Chief Liquid Propulsion Lab.
1	U. S. Army Missile Command Redstone Arsenal Alabama 35809	Mr. Walter Wharton

CPIA

COPIES	RECIPIENT	
1	Chemical Propulsion Information Agency Applied Physics Laboratory 8621 Georgia Avenue Silver Spring, Maryland 20910	Tom Reedy

INDUSTRY CONTRACTORS

COPIES	RECIPIENT	
1	Aerojet-General Corporation P. O. Box 296 Azusa, California 91703	W. L. Rogers
1	Aerojet-General Corporation P. O. Box 1947 Technical Library, Bldg. 2015, Dept. 2410 Sacramento, California 95809	R. Stiff
1	Aerojet-General Corporation Space Division 9200 East Flair Drive El Monte, California 91734	S. Machlawski
1	Aerospace Corporation 2400 East El Segundo Boulevard P. O. Box 95085 Los Angeles, California 90045	John G. Wilder MS-2293
1	AVCO Systems Division Wilmington, Massachusetts	Howard B. Winkler
1	Beech Aircraft Corporation Boulder Division Box 631 Boulder, Colorado	J. H. Rodgers
1	Bell Aerosystems Company P. O. Box 1 Buffalo, New York 14240	W. M. Smith
1	Bellcomm 955 L-Enfant Plaza, S. W. Washington, D. C.	H. S. London
1	Bendix Systems Division Bendix Corporation 3300 Plymouth Road Ann Arbor, Michigan 48105	John M. Brueger
1	Boeing Company P. O. Box 3999 Seattle, Washington 98124	Library
1	Boeing Company P. O. Box 1680 Huntsville, Alabama 35801	Ted Snow

COPIES	RECIPIENT	
1	Missile Division Chrysler Corporation P. O. Box 2628 Detroit, Michigan 48231	Mr. John Gates
1	Wright Aeronautical Division Curtiss-Wright Corporation Wood-Ridge, New Jersey 07075	G. Kelley
1	Research Center Fairchild Hiller Corporation Germantown, Maryland	Ralph Hall
1	Republic Aviation Corporation Fairchild Hiller Corporation Farmingdale, Long Island, New York	Library
1	General Dynamics, Convair Division P. O. Box 1128 San Diego, California	Library
1	Missile and Space Systems Center General Electric Company Valley Forge Space Technology Center P. O. Box 8555 Philadelphia, Pa.	F. Mezger F. E. Schultz
1	Grumman Aircraft Engineering Corp. Bethpage, Long Island New York 11714	Joseph Gavin
1	Honeywell, Inc. Aerospace Div. 2600 Ridgway Road Minneapolis, Minn.	Mr. Gordon Harms
1	Hughes Aircraft Co. Aerospace Group Centinela and Teale Streets Culver City, California 90230	E. H. Meier V. P. and Div. Mgr., Research & Dev. Div.
1	Reliability Analysis Center ITT Research Institute 10 West 35th Street Chicago, Illinois 60616	H. A. Lauffenburger Program Manager
1	Walter Kidde and Company, Inc. Aerospace Operations 567 Main Street Belleville, New Jersey	R. J. Hanville Dir. of Research Engr.

COPIES	RECIPIENT	
1	Ling-Temco-Vought Corporation P. O. Box 5907 Dallas, Texas, 75222	Library
1	Arthur D. Little, Inc. 20 Acorn Park Cambridge, Massachusetts 02140	Library
1	Lockheed Missiles and Space Co. Attn: Technical Information Center P. O. Box 504 Sunnyvale, California 94088	J. Guill
1	Lockheed Propulsion Company P. O. Box 111 Redlands, California 92374	Library
1	The Marquardt Corporation 16555 Saticoy Street Van Nuys, California 91409	Library
1	Baltimore Division Martin Marietta Corporation Baltimore, Maryland 21203	Mr. John Calathes (3214)
1	Denver Division Martin Marietta Corporation P. O. Box 179 Denver, Colorado 80201	Dr. Morganthaler A. J. Kullas
1	Orlando Division Martin Marietta Corporation Box 5837 Orlando, Florida	J. Ferm
1	McDonnell-Douglas Corporation P. O. Box 516 Municipal Airport St. Louis, Missouri 63166	R. A. Herzmark
1	Space & Information Systems Division North American Rockwell 12214 Lakewood Boulevard Downey, California 90241	Library
1	Rocketdyne (Library 586-306) 6633 Canoga Avenue Canoga Park, California 90250	Dr. R. J. Thompson S. F. Iacobellis
1	Aeroneutronic Corporation Philco Corporation Ford Road Newport Beach, California 92663	Library

COPIES	RECIPIENT	
1	Astro-Electronics Division Radio Corporation of America Princeton, New Jersey 08540	Y. Brill
1	Rocket Research York Center Redmond, Washington 98052	F. McCullough, Jr.
1	Scientific Service Bureau, Inc. P. O. Box 375 Morrisplains, New Jersey 07950	T. F. Seamans
1	Stanford Research Institute 333 Ravenswood Avenue Menlo Park, California 94025	Dr. Gerald Marksman
1	Sunstrand Aviation 2421 11th Street Rockford, Illinois 61101	R. W. Reynolds
1	TRW Systems Group TRW Incorporated One Space Park Redondo Beach, Calif. 90278	G. W. Elverum
1	Tapco Division 23555 Euclid Avenue Cleveland, Ohio 44117	P. T. Angell
1	Thiokol Chemical Corp. Aerospace Services Elkton Division Bristol, Pennsylvania	Library
1	Thiokol Chemical Corporation Huntsville Division Huntsville, Alabama 35807	John Goodloe
1	Research Laboratories United Aircraft Corp. Windsor Locks, Connecticut 06906	Erle Martin
1	United Technology Center 587 Methilda Avenue P. O. Box 358 Sunnyvale, California 94088	Dr. David Altman

COPIES	RECIPIENT	
1	Florida Research and Dvelopment Pratt and Whitney Aircraft United Aircraft Corporation P. O. Box 2691 West Palm Beach, Florida 33402	R. J. Coar
1	Vickers, Inc. Box 302 Troy, Michigan	Library
1	McDonnell-Douglas Astronautics 5301 Bolsa Avenue Huntington Beach, California 92647	J. L. Waisman
1	Battelle 505 King Avenue Columbus, Ohio 43201	Reports Library (HAMI)